Author: C. Keith Scott

Title: Nuclear Spectra Calculations Using Realistic Interactions and Realistic Single-Particle Wavefunctions.

Department: Physics

Degree: Ph.D.

ABSTRACT

Nuclear spectra of A = 14, 18, 38, 42, 206 and 208 nuclei were calculated using free reaction matrices as effective interactions and Woods-Saxon single-particle wavefunctions. The calculations show that, in most of the cases considered, realistic single-particle wavefunctions must be used in the determination of realistic effective interaction matrix elements. The results are especially interesting in the A = 18 nuclei where it is found that the use of realistic single-particle wavefunctions produce changes in spectra comparable to those introduced by core-polarization. In heavier nuclei it appears that a simple harmonic oscillator calculation is out of the question at least for states involving both neutrons and protons. Wavefunctions deduced for a single value of the oscillator parameter $\hbar\omega$ cannot adequately describe the states in nuclei such as Pb^{206} and Pb^{210} possessing a large neutron excess.

SCOTT: NUCLEAR SPECTRA CALCULATIONS

Nuclear Spectra Calculations Using Realistic Interactions and Realistic Single-Particle Wavefunctions

C. Keith Scott

A thesis submitted to the Faculty of Graduate Studies and Research in partial fulfilment of requirements for the degree of Doctor of Philosophy.

Institute of Theoretical Physics
McGill University
Montreal 2, Quebec

October 30, 1968

ACKNOWLEDGEMENTS

I am indebted to Professor S. Kahana for suggesting this research topic and his continued interest and guidance.

I gratefully acknowledge a continuously stimulating dialogue with H-C. Lee concerning most aspects of the research. In addition I would like to thank H-C. Lee for assisting in checking several computations and other computational assistance.

I would like to thank: N. de Takacsy, for many useful discussions and for making available computer codes; B. Buck, E.K. Warburton, J. Weneser and A. Zuker, for their interest and discussions of various aspects of this research; E.H. Auerbach, for making available his code ABACUS; K.T.R. Davies, for a useful communication concerning his code BRAKET; Mrs. P. Towey, for her assistance in preparing the manuscript, and; the staff of Brookhaven National Laboratory for their hospitality during 1967-68.

This thesis was made possible by the continued financial assistance of the National Research Council of Canada and assistance from Brookhaven National Laboratory during 1967-68.

The computational work was performed on the IBM 7044 computer at McGill University and the CDC 6600 computer at Brookhaven National Laboratory.

ABSTRACT

Nuclear spectra of A=14, 18, 38, 42, 206 and 208 nuclei were calculated using free reaction matrices as effective interactions and Woods-Saxon single-particle wavefunctions. The calculations show that, in most of the cases considered, realistic single-particle wavefunctions must be used in the determination of realistic effective interaction matrix elements. The results are especially interesting in the A=18 nuclei where it is found that the use of realistic single-particle wavefunctions produce changes in spectra comparable to those introduced by core-polarization. In heavier nuclei it appears that a simple harmonic oscillator calculation is out of the question at least for states involving both neutrons and protons. Wavefunctions deduced for a single value of the oscillator parameter $\hbar\omega$ cannot adequately describe the states in nuclei such as Pb^{206} and Pb^{210} possessing a large neutron excess.

TABLE OF CONTENTS

TABLE OF CONTENTS (continued)

CHAPTER 1

INTRODUCTION

Since the nuclear shell model was proposed by Mayer and Jensen[1] it has become a sophisticated and powerful tool[2] for understanding many aspects of the structure of finite nuclei. In what is termed phenomenological shell model theory the residual interaction is parametrized and the parameters determined by fitting experimental data. The usual practice in this model is to include the minimum number of configurations required to fit the data and at the same time give "reasonable" two-body matrix elements. For example, the low-lying positive parity states in O^{18} would be described by two interacting valence particles confined to the (1s,0d) shell outside an inert closed shell O^{16} core. The effects of neglected configurations are absorbed in the residual interaction parameters. The model dependent interaction obtained in this manner is referred to as an effective interaction. As a result of the model dependence, effective interaction matrix elements may not have much resemblance to the same matrix elements evaluated with the free space nucleon-nucleon interaction. In the past few years much research[/] has been done in efforts to obtain effective interaction matrix elements from the free nucleon scattering data. Much of this work has been discussed in a lecture series by Baranger.[7]

/ The realistic interactions most often used in the literature are those of Kallio and Kolltveit,[3] Kuo and Brown,[4,5] and Tabakin.[6]

Since effective interaction matrix elements are model dependent it is important that all aspects of the model dependence are examined. In previous calculations of effective interaction matrix elements from realistic interactions the shell model single-particle wavefunctions have been taken to be eigenfunctions of an infinitely deep harmonic oscillator potential. If a shell model single-particle potential exists, it must be finite with a diffuse surface. Wavefunctions for states near the surface of a finite potential well will differ considerably from wavefunctions for an infinitely deep well. In this thesis we have investigated the effects of using more realistic single-particle wavefunctions in evaluations of effective interaction matrix elements. To obtain wavefunctions for a finite single-particle potential we assumed that the shell model potential could be represented by a Woods-Saxon[8] potential with a Thomas[9] spin-orbit term. To study more complicated effects (for example, non-locality) a more sophisticated model would be required. There have been earlier calculations to investigate the effect of using Woods-Saxon wavefunctions. Flowers and Wilmore[10] considered the spectra of O^{18} and F^{18} and Stamp and Mayer[11] considered the structure of the collective octupole states in O^{16} and Ca^{40}. These authors used phenomenological interactions and found significant changes in matrix elements compared to the values obtained using harmonic oscillator wavefunctions. However, in phenomenological calculations a large part of the wavefunction dependence can be absorbed in the parameters of the interaction. On the other hand, in calculations of effective interaction

it is imperative to include the wavefunction dependence.

We have used free reaction matrices developed by Kahana and co-workers [12-17] as realistic effective interactions in our study of the effects of more realistic wavefunctions. Calculations were performed with harmonic oscillator wavefunctions as well as with Woods-Saxon wavefunctions. In most of the nuclei considered the free reaction matrices had not been used as effective interactions even with harmonic oscillator wavefunctions. As a result we also considered properties of the free reaction matrix itself as an effective interaction.

In Chapter 2 Green's function techniques [18] are used to define the lowest order shell model effective interactions for two-particle, two-hole and particle-hole states. The lowest order realistic effective interaction in the nuclear reaction matrices is discussed. The method for obtaining a nuclear reaction matrix from a free reaction matrix is discussed briefly. Lee [17] has considered this problem in detail.

In Chapter 3 we present a standard particle-hole model [20] calculation of the odd-parity states in O^{16}. This calculation was performed to study the effective particle-hole interaction obtained from free reaction matrices. Only harmonic oscillator single-particle wavefunctions were used in this calculation. The local velocity dependent free reaction matrices [16] were used as the effective interaction.

In Chapter 4 Woods-Saxon wavefunctions for A=15,17,39,41,207

and 209 nuclei are determined. For convenience in shell model calculations the Woods-Saxon wavefunctions are tabulated as expansions in terms of harmonic oscillator wavefunctions.

In Chapters 5 and 6 we present calculations of the spectra of N^{14}, O^{18}, F^{18}, Ca^{38}, Ca^{42}, Sc^{42}, Pb^{206} and Pb^{210} using Woods-Saxon wavefunctions. Two forms of the free reaction matrix are used as effective interactions: a local velocity dependent representation for realtive S states only and free reaction matrices obtained from a non-local separable potential. For comparison the spectra were also calculated with harmonic oscillator wavefunctions. The shell model technology required to calculate the various spectra is standard. In Appendix A we give the expressions for the various types of matrix elements used and the phase conventions used throughout the thesis are defined.

In Chapter 7 we conclude by summarizing the most significant results from each chapter.

CHAPTER 2

SHELL MODEL EFFECTIVE INTERACTIONS AND THE FREE REACTION MATRIX

2-A Introduction

We use Green's function techniques[18] to arrive at a consistent formalism for defining an effective shell model Hamiltonian. The particular cases considered are those of two-particle, two-hole and particle-hole Hamiltonians. The derivation is based on the assumption of a Hartree-Fock ground state that would be obtained from Brueckner theory.[19] The derivation is used to show the relationships among the nuclear reaction matrices for the cases considered and to examine differences in various nuclei. Once the effective interaction is defined within the framework of a model, a realistic interaction is then used to calculate the effective interaction. In our case we use a free reaction matrix to determine the nuclear reaction matrix. Lee[17] has discussed, in detail, the procedure for determining the effective interaction from a free reaction matrix.

2-B Green's Functions

We define one and two-particle Green's functions to be

$$G_{\rho\sigma}(t_\rho,t_\sigma) \equiv (-i)\langle N|T\{a_\rho(t_\rho)a_\sigma^+(t_\sigma)\}|N\rangle \qquad (2\text{-}1a)$$

and

$$G_{\rho\sigma\kappa\lambda}(t_\rho,t_\sigma,t_\kappa,t_\lambda) \equiv (-i)^2\langle N|T\{a_\rho(t_\rho)a_\sigma(t_\sigma)a_\lambda^+(t_\lambda)a_\kappa^+(t_\kappa)\}|N\rangle \qquad (2.1b)$$

respectively. Other Green's functions are defined in a similar manner. The operators $a_\sigma^+(t_\sigma)$ and $a_\rho(t_\rho)$ are the usual Heisenberg representation

of the fermion creation and annihilation operators. The Greek subscripts denote the full set of quantum numbers that label a single-particle state and $|N>$ is the fully interacting ground state of the N fermion system

$$H|N> = E_N^{o}|N> \quad . \tag{2.2}$$

The one-particle Green's function may be written in the form

$$\begin{aligned} G_{\rho\sigma}(t_\rho,t_\sigma) &= \theta(t_\rho-t_\sigma)(-i) < N|a_\rho(t_\rho)a_\sigma^{+}(t_\sigma)|N> \\ &\quad -\theta(t_\sigma-t_\rho)(-i) < N|a_\sigma^{+}(t_\sigma)a_\rho(t_\rho)|N> \\ &= G_{\rho\sigma}^{+}(t_\rho-t_\sigma)+G_{\rho\sigma}^{-}(t_\rho-t_\sigma) \end{aligned} \tag{2.3}$$

where

$$\begin{aligned} \theta(t_\rho-t_\sigma) &= 0 \qquad t_\rho < t_\sigma \\ &= 1 \qquad t_\rho > t_\sigma \quad . \end{aligned}$$

In (2.3) and the following discussion G is used to denote the Green's function with the discontinuity at $t_\rho=t_\sigma$ subtracted. G^{+} is a particle propagator and G^{-} is a hole propagator. Introducing the Fourier transform

$$G_{\rho\sigma}^{+}(\omega) = \int_{-\infty}^{+\infty} dt\, e^{i\omega t}\, G_{\rho\sigma}^{+}(t) \tag{2.4}$$

it follows that the spectral representation for G^{+} is

$$G_{\rho\sigma}^{+}(\omega) = \sum_{\alpha} \frac{< N|a_\rho|N+1,\alpha > < N+1,\alpha|a_\sigma^{+}|N>}{[\omega-(E_{N+1}^{\alpha}-E_N^{0})+i\eta]} \quad . \tag{2.5}$$

The summation in (2.5) is over all states of the (N+1)-particle nucleus. Similarly, for the hole propagator we have

$$G_{\rho\sigma}^{-}(\omega) = -\sum_{\alpha} \frac{\langle N|a_{\sigma}^{+}|N-1,\alpha\rangle\langle N-1,\alpha|a_{\rho}|N\rangle}{[\omega+(E_{N-1}^{\alpha}-E_{N}^{0})-i\eta]} . \qquad (2.6)$$

Both G^{+} and G^{-} have a series of poles on the real axis corresponding to the single-particle and single-hole energies of the (N+1) and (N-1)-particle nuclei, respectively. The problem of determining the self-consistent single-particle (hole) energies relative to the ground state of the N-particle system is the problem of determining the poles of $G^{\pm}(\omega)$. However, we are interested in calculating the spectra of the closed shell nucleus $|N>$ and the $|N\pm2>$ nuclei rather than the self-consistent potential which would determine the single-particle (hole) energies. To do this we make the usual assumption of nuclear spectroscopy; a Hartree-Fock ground state for the nucleus exists and $G_{\rho\sigma}^{\pm}(\omega)$ are diagonal in the Hartree-Fock representation. That is, we demand that our formalism be consistent in principle rather than in practice for calculating the Hartree-Fock energies. We will return to this point later.

To determine the spectra of the N and $(N\pm2)$-particle nuclei, the two-particle and particle-hole Green's functions are required. The two-particle Green's function may be written in the form

$$\begin{aligned} G_{\rho\sigma\kappa\lambda}(t_\rho,t_\rho,t_\lambda;t_\lambda) &= \theta(t_\rho-t_\lambda)(-i)^2\langle N|a_\rho(t_\rho)a_\sigma(t_\rho)a_\lambda^{+}(t_\lambda)a_\kappa^{+}(t_\lambda)|N\rangle + \\ &+ \theta(t_\lambda-t_\rho)(-i)^2\langle N|a_\lambda^{+}(t_\lambda)a_\kappa^{+}(t_\lambda)a_\rho(t_\rho)a_\sigma(t_\rho)|N\rangle \\ &= G_{\rho\sigma\kappa\lambda}^{+}(t_\rho-t_\lambda) + G_{\rho\sigma\kappa\lambda}^{-}(t_\rho-t_\lambda) \qquad (2.7) \end{aligned}$$

where G^{+} and G^{-} are the propagators for two-particles and two-holes,

respectively. The spectral representations are

$$G^{+}_{\rho\sigma\kappa\lambda}(\omega) = (-i)\sum_{\alpha} \frac{\langle N|a_\rho a_\sigma|N+2,\alpha\rangle\langle N+2,\alpha|a_\lambda^{+}a_\kappa^{+}|N\rangle}{[\omega-(E_{N+2}^{\alpha}-E_N^{0})+i\eta]} \qquad (2.8a)$$

and

$$G^{-}_{\rho\sigma\kappa\lambda}(\omega) = (-i)\sum_{\alpha} \frac{\langle N|a_\lambda^{+}a_\kappa^{+}|N-2,\alpha\rangle\langle N-2,\alpha|a_\rho a_\sigma|N\rangle}{[\omega+(E_{N-2}^{\alpha}-E_N^{0})-i\eta]} . \qquad (2.8b)$$

$G^{-}_{\rho\sigma\kappa\lambda}(\omega)$ and $G^{-}_{\rho\sigma\kappa\lambda}(\omega)$ have series of poles on the real axis corresponding to the spectra of the $(N\pm2)$-particle nuclei. The particle-hole Green's function is the special case of (2.1b) where $t_\rho=t_\lambda$ and $t_\sigma=t_\kappa$ which leads to the spectral representation.

$$G_{\rho\sigma\kappa\lambda}(\omega) = (+i)\sum \frac{\langle N|a_\lambda^{+}a_\rho|N,\alpha\rangle\langle N,\alpha|a_\kappa^{+}a_\sigma|N\rangle}{[\omega-(E_N^{\alpha}-E_N^{0})+i\eta]}$$

$$+(-i)\sum \frac{\langle N|a_\kappa^{+}a_\sigma|N,\alpha\rangle\langle N,\alpha|a_\lambda^{+}a_\rho|N\rangle}{[\omega+(E_N^{\alpha}-E_N^{0})-i\eta]} . \qquad (2.9)$$

The particle-hole Green's function has a series of poles on the real axis corresponding to excitation energies of the N-particle system.

In nuclear spectroscopy the problem of determining the excitation energies of the systems under consideration is that of determining the poles of the Green's functions (2.8) and (2.9). To perform such a calculation without approximations is entirely unfeasible. The first approximation made is an assumption about the structure of the ground

state wavefunctions for the N,(N+1) and (N-1) particle nuclei. We consider cases where $|N>$ is a closed shell nucleus and make the shell model assumption that the ground states may be represented by single-particles moving in a self-consistent Hartree-Fock potential. Equations (2.1) may be used to write down equations of motion for the propagators. The result is a hierarchy of coupled equations which can only be solved in various approximations.[15] We will work from the following set of approximate equations for the propagators:

<u>one-particle</u>

$$G_{\rho\sigma}^{+}(t_\rho - t_\sigma) = G_{\rho\sigma}^{o+}(t_\rho - t_\sigma) + i\sum_{\sigma_1\sigma_2}\int dt_{\sigma_1} dt_{\sigma_2}\, G_{\rho\sigma_1}^{o+}(t_\rho - t_{\sigma_1}) \times \Lambda_{\sigma_1\sigma_2}^{p}(t_{\sigma_1} - t_{\sigma_2}) G_{\sigma_2\sigma}^{+}(t_{\sigma_2} - t_\sigma) \qquad (2.10a)$$

<u>one-hole</u>

$$G_{\rho\sigma}^{-}(t_\rho - t_\sigma) = G_{\rho\sigma}^{o-}(t_\rho - t_\sigma) + i\sum_{\sigma_1\sigma_2}\int dt_{\sigma_1} dt_{\sigma_2}\, G_{\rho\sigma_1}^{o-}(t_\rho - t_{\sigma_1}) \times \Lambda_{\sigma_1\sigma_2}^{h}(t_{\sigma_1} - t_{\sigma_2}) G_{\sigma_2\sigma}^{-}(t_{\sigma_2} - t_\sigma) \qquad (2.10b)$$

<u>two-particle</u>

$$G_{\rho\sigma\kappa\lambda}^{+}(t_\rho - t_\lambda) = G_{\rho\kappa}^{+}(t_\rho - t_\lambda) G_{\sigma\lambda}^{+}(t_\rho - t_\lambda) - G_{\rho\lambda}^{+}(t_\rho - t_\lambda) G_{\sigma\kappa}^{+}(t_\rho - t_\lambda) + (i)\sum_{\substack{\rho_1\sigma_1 \\ \rho_2\sigma_2}}\int dt_{\rho_1} dt_{\rho_2}\, G_{\rho\rho_1}^{+}(t_\rho - t_{\rho_1}) G_{\sigma\sigma_1}^{+}(t_\rho - t_{\rho_1}) \times \Gamma_{\rho_1\sigma_1\rho_2\sigma_2}^{2P}(t_{\rho_1} - t_{\rho_2}) G_{\rho_2\sigma_2\kappa\lambda}(t_{p_2} - t_\lambda) \qquad (2.10c)$$

two-hole

$$G_{\rho\sigma\kappa\lambda}^{-}(t_\rho - t_\lambda) = G_{\rho\kappa}^{-}(t_\rho - t_\lambda)G_{\sigma\lambda}^{-}(t_\rho - t_\lambda) - G_{\rho\lambda}^{-}(t_\rho - t_\lambda)G_{\sigma\kappa}^{-}(t_\rho - t_\lambda)$$
$$+ i\sum_{\substack{\rho_1\sigma_1\\ \rho_2\sigma_2}}\int dt_{\rho_1} dt_{\rho_2} G_{\rho\rho_1}^{-}(t_\rho - t_{\rho_1})G_{\sigma\sigma_1}^{-}(t_\rho - t_{\rho_1})$$
$$\times \Gamma^{2h}_{\rho_1\sigma_1\rho_2\sigma_2}(t_{\rho_1} - t_{\rho_2})G_{\rho_2\sigma_2\kappa\lambda}^{-}(t_{\rho_2} - t_\lambda) \quad (2.10d)$$

particle-hole

$$G_{\rho\sigma\kappa\lambda}^{ph}(t_\rho - t_\sigma) = G_{\rho\kappa}^{+}(t_\rho - t_\kappa)G_{\sigma\lambda}^{-}(t_\kappa - t_\rho)$$
$$+ i\sum_{\substack{\rho_1\sigma_1\\ \rho_2\sigma_2}}\int dt_{\rho_1} dt_{\rho_2} G_{\rho\rho_1}^{+}(t_\rho - t_{\rho_1})G_{\sigma\sigma_1}^{-}(t_\kappa - t_{\rho_1})$$
$$\times \Gamma^{ph}_{\rho_1\sigma_1\rho_2\sigma_2}(t_{\rho_1} - t_{\rho_2})G_{\rho_2\sigma_2\kappa\lambda}^{ph}(t_{\rho_2} - t_\kappa). \quad (2.10e)$$

In (2.10) the self-energy operators Λ^P and Λ^h and the interaction operators Γ^{2P}, Γ^{2h} and Γ^{ph} are as yet unspecified functions of the two-nucleon interaction. Equations (2.10) contain no direct coupling among the various two-particle propagators. Since the equations are, in fact, coupled, the self-energy and interaction operators should be chosen consistently for all equations. We start by defining a representation in which the particle propagator is diagonal and then obtain solutions for the two-particle equations in the same approximation.

2-C The Hartree-Fock Energies

The Hartree-Fock approximation for (2-10a) would be to take the

self-energy operator to be

$$\Lambda_{\rho_1\rho_2}{}^{P}(t_{\rho_1}-t_{\rho_2}) = \sum_{\delta < \epsilon_F} (v_{\rho_1\delta\rho_2\delta}\text{-exch.})\,\delta(t_{\rho_1}-t_{\rho_2}) \quad (2.11)$$

where v is the two-nucleon interaction. It is well known that the strong, short-range, repulsive nature of the nucleon-nucleon interaction makes a Hartree-Fock calculation with (2.11) impossible. In the Brueckner theory of finite nuclei[19] the Hartree-Fock single-particle states and the Brueckner reaction matrix are determined self-consistently simultaneously. The single-particle energies are

$$\epsilon_i = T_i + \sum_{j < k_F} (K_{ijij}\text{-exch.}) \quad (2.12)$$

where T_i is the kinetic energy of the particle. The Brueckner reaction matrix is

$$K_{ijk\ell} = v_{ijk\ell} + \sum_{mn} \frac{v_{ijmn}K_{mnk\ell}}{\epsilon_k+\epsilon_\ell-\epsilon_m-\epsilon_n-\Delta} \quad (2.13)$$

where only unoccupied intermediate states are included in the summation and Δ is a parameter to modify the denominator for off-the-energy-shell propagation in the intermediate states.

Taking the Fourier transform of (2.10a) we have

$$G_{\rho\sigma}{}^{+}(\omega) = G_{\rho\sigma}{}^{0+}(\omega) + \sum_{\rho_1\rho_2} G_{\rho\rho_1}{}^{0+}(\omega)\Lambda_{\rho_1\rho_2}{}^{P}(\omega)G_{\rho_2\sigma}{}^{+}(\omega) \quad . (2.14)$$

In Brueckner theory the self-energy operator is

$$\Lambda_{\rho_1\rho_2}{}^{P}(\omega) = \sum_{\delta < k_F} (K_{\rho_1\delta\ \rho_2\delta} - \text{exch.}) \quad . \tag{2.15}$$

Determining the poles of $G_{\rho\sigma}{}^{+}(\omega)$ defines the reaction matrix (2.13) at the single-particle energies (2.12) of the diagonal representation. In the diagonal representation

$$G_{\rho\sigma}(t) = (-i)[(1-f_\rho)\theta(t)-f_\rho\theta(-t)]e^{-i\epsilon_\rho t}\,\delta_{\rho\sigma} \tag{2.16}$$

where

$$\begin{aligned} f_\rho &= 0 \qquad \epsilon_\rho > \epsilon_F \\ &= 1 \qquad \epsilon_\rho < \epsilon_F \end{aligned}$$

and ϵ_F is the Fermi energy. For the (N+2)-particle system the Hamiltonian

$$H = T+v \tag{2.17}$$

becomes

$$\begin{aligned} H &= H_0+H_1 \\ &= \sum_k \epsilon_k a_k{}^{+}a_k + \frac{1}{2}\sum_{\substack{\alpha\beta \\ \gamma\delta}} v_{\alpha\beta\gamma\delta}\ a_\alpha{}^{+}a_\beta{}^{+}a_\delta a_\gamma \quad . \end{aligned} \tag{2.18}$$

The single-particle energies are those defined in (2.12) and the perturbation is the two-nucleon interaction for two-particles in the states of the (N+1)-particle nucleus.

2-D The Two-Particle Propagator

To determine the poles of the two-particle propagator we make the approximation

$$\Gamma_{\rho_1\sigma_1\rho_2\sigma_2}{}^{2p}(t_{\rho_1}-t_{\rho_2}) = v_{\rho_1\sigma_1\rho_2\sigma_2}\,\delta(t_{\rho_1}-t_{\rho_2}) \quad . \quad (2.19)$$

Taking the Fourier transform of (2.10c) we have that

$$G_{\rho\sigma\kappa\lambda}{}^{+}(\omega) = \frac{(1-f_\rho)(1-f_\sigma)}{[\omega-\epsilon_\rho-\epsilon_\sigma+in]}\left\{\delta_{\rho\kappa}\,\delta_{\sigma\lambda} - \delta_{\rho\lambda}\,\delta_{\sigma\kappa} + \right.$$

$$\left. + \sum_{\rho_1\sigma_1} v_{\rho\sigma\rho_1\sigma_1} G_{\rho_1\sigma_1\kappa\lambda}{}^{+}(\omega)\right\} \quad . \quad (2.20)$$

Equation (2.20) may put in the matrix form

$$(\omega-H_0-v)G^{+}(\omega) = (-i)I \quad . \quad (2.21)$$

From (2.21) it follows that finding the poles of $G^{+}(\omega)$ is equivalent to diagonalizing the Hamiltonian

$$H = H_0+v \quad (2.22)$$

in the Hilbert space of two-particle states above the Fermi sea. Equation (2.20) is represented in terms of diagrams in Fig. 2-1. Iteration of the equation leads to a ladder series in the interaction v.

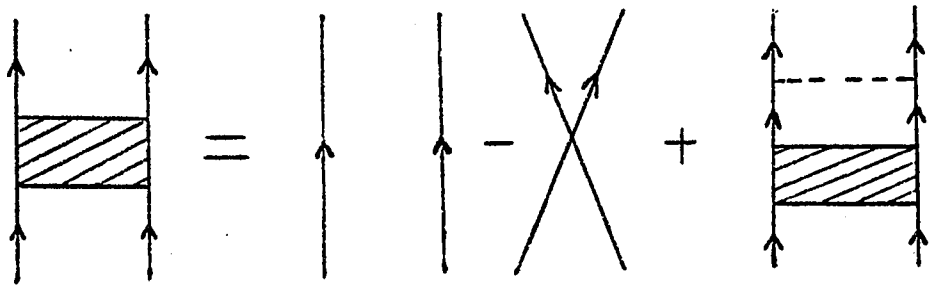

Fig. 2-1. The two-particle propagator in the "ladder" approximation.

With the bare nucleon-nucleon interaction as the two-particle perturbation it would be necessary to diagonalize (2.22) in the entire

Hilbert space of two-particle states above the Fermi sea. This difficulty can be removed by introducing a reaction matrix which permits diagonalization of the Hamiltonian within a subspace of the two-particle configurations. For a subspace M we define the reaction matrix by

$$\sum_{\substack{\rho_1\sigma_1 \\ \text{in M}}} K_{\rho\sigma\rho_1\sigma_1}(\omega) G_{\rho_1\sigma_1\kappa\lambda}^{+}(\omega) = \sum_{\rho_1\sigma_1} v_{\rho\sigma\rho_1\sigma_1} G_{\rho_1\sigma_1\kappa\lambda}^{+}(\omega) \quad . \quad (2.23)$$

From (2.23) and (2.20) it follows that

$$K_{\rho\sigma\rho_1\sigma_1}(\omega) = v_{\rho\sigma\rho_1\sigma_1} + \sum_{\substack{\rho_2\sigma_2 \\ \text{outside M}}} v_{\rho\sigma\rho_2\sigma_2} \frac{(1-f_{\rho_2})(1-f_{\sigma_2})}{[\omega-\epsilon_{\rho_2}-\epsilon_{\sigma_2}+i\eta]} K_{\rho_2\sigma_2\rho_1\sigma_1}(\omega) \quad (2.24a)$$

and

$$K_{\rho\sigma\sigma_1\rho_1}(\omega) = v_{\rho\sigma\sigma_1\rho_1} + \sum_{\substack{\rho_2\sigma_2 \\ \text{outside M}}} v_{\rho\sigma\rho_2\sigma_2} \frac{(1-f_{\rho_2})(1-f_{\sigma_2})}{[\omega-\epsilon_{\rho_2}-\epsilon_{\sigma_2}+i\eta]} K_{\rho_2\sigma_2\sigma_1\rho_1}(\omega) . \quad (2.24b)$$

It is more convenient to write (2.24) in the matrix form

$$K(\omega) = v + v\,\mathcal{G}(\omega) Q\, K(\omega) \quad (2.25)$$

where Q is a projection operator restricting the intermediate states to states not contained in M. The operator $(1-f_{\rho_2})(1-f_{\sigma_2})$ projects out the occupied core states. $K(\omega)$ is a regular function in the upper half-plane and

$$K(\omega) \to v$$
$$\omega \to \infty \quad .$$

The form of (2.24) implies a discrete spectrum of intermediate states which is not a necessary assumption. For the purposes of the present discussion the nature of the intermediate states is not important.

For shell model calculations in a convenient subspace of two-particle configurations $(\rho_1\sigma_1)$ the two-particle Green's function is

$$G^{+}_{\rho\sigma\kappa\lambda}(\omega) = \frac{(1-f_\rho)(1-f_\sigma)}{[\omega-\epsilon_\rho-\epsilon_\sigma+i\eta]}\left\{\delta_{\rho\kappa}\,\delta_{\sigma\lambda} - \delta_{\rho\lambda}\,\delta_{\sigma\kappa} + \sum_{\rho_1\sigma_1} K_{\rho\sigma\rho_1\sigma_1}(\omega) G^{+}_{\rho_1\sigma_1\kappa\lambda}(\omega)\right\} \tag{2.26}$$

and the effective Hamiltonian is

$$H(\omega) = H_0 + K(\omega) \quad . \tag{2.27}$$

Determining the poles of $G^{+}(\omega)$ in (2.26) is not a simple eigenvalue problem as in (2.20). Equation (2.26) is a self-consistent equation; the poles of $G^{+}(\omega)$ can be determined by diagonalizing the effective Hamiltonian (2.27) which in turn is defined by the positions of the poles. It will be seen later that with a suitable choice of the subspace of configurations the reaction matrix is essentially the same for all states α, consequently we take the Hamiltonian to be

$$H(\omega) = H_0 + K(\bar{\omega}_\alpha) \quad . \tag{2.28}$$

With (2.28) finding the poles of $G^{+}(\omega)$ is a self-consistent eigenvalue problem. This point will be discussed later. Equations (2.25) and (2.26) are expressed in terms of diagrams in Fig. 2.2. When drawing diagrams a wavy line is used to denote a reaction matrix interaction and a dashed line denotes a v interaction. It should be noted that although K is a sum over many nucleon-nucleon interactions occuring in a finite time interval it is treated as an instantaneous interaction

when used as a perturbation.

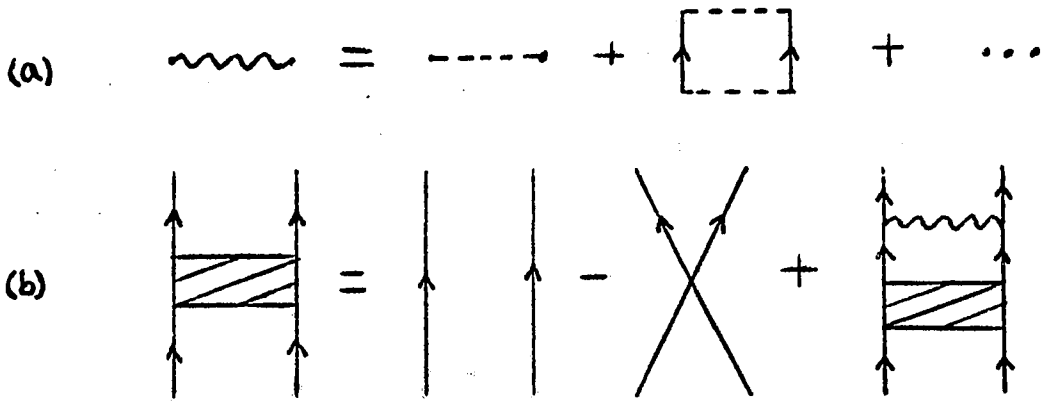

Fig. 2-2. The two-particle propagator as a ladder series in the reaction matrix. In (a) the intermediate states are outside the subspace of diagonalization. In (b) the intermediate states are in the subspace of diagonalization.

From the definition (2.24) it can be seen that $K(\omega)$ contains all of the effects of two-particle correlations outside the chosen subspace while the diagonalization of $H(\omega)$ includes all correlations within the subspace. Consequently, (2.26) contains all of the two-body correlations above the Fermi sea without any double counting of diagrams. Finding the poles of the Green's function (2.26) gives the same eigenvalues as would have been obtained for (2.20), however, only a set of the eigenvalues can be determined. On the other hand, only the piece of the wavefunction in the subspace is determined by diagonalization. From the eigenvalue problem (2.22) one obtains the amplitudes of the unperturbed configurations in the state α

$$X_{\rho\sigma}^{\alpha} = \langle N | a_\rho a_\sigma | N+2, \alpha \rangle \qquad (2.29)$$

where the configurations (ρ,σ) are in the entire Hilbert space above the Fermi sea. From the eigenvalue problem (2.28) one obtains the amplitudes

$$\tilde{X}_{\rho\sigma}{}^{\alpha} = \langle N|a_{\rho}a_{\sigma}|N+2,\alpha\rangle \tag{2.30}$$

where the configuration (ρ,σ) are within the subspace. The full set of amplitudes can be calculated in a straight forward manner. Substituting the spectral representation (2.8a) into (2.23) and finding the residues, we have

$$\sum_{\substack{\rho_1\sigma_1 \\ \text{in M}}} K(\omega_{\alpha})\tilde{X}_{\rho_1\sigma_1}{}^{\alpha} = \sum_{\rho_1\sigma_1} v_{\rho\sigma\rho_1\sigma_1} X_{\rho_1\sigma_1}{}^{\alpha} \quad . \tag{2.31}$$

In matrix notation (2.31) is

$$K(\omega_{\alpha})\varphi^{\alpha} = v\,\psi^{\alpha} \tag{2.32}$$

where φ^{α} is the wavefunction (uncorrelated) in the subspace and ψ^{α} is the wavefunction (correlated) for the entire space of two-particle configurations. To obtain ψ^{α} from φ^{α} we define a wave matrix by

$$\psi^{\alpha} = M(\omega_{\alpha})\varphi^{\alpha} \quad . \tag{2.33}$$

From (2.32) it follows that

$$K(\omega_{\alpha}) = vM(\omega_{\alpha}) \tag{2.34}$$

and

$$M(\omega_{\alpha}) = 1+\not{g}(\omega_{\alpha})QK(\omega_{\alpha}) \quad . \tag{2.35}$$

Equations (2.26), (2.33), (2.34) and (2.35) give the complete solution for the problem of determining the low-lying levels of the (N+2)-particle nucleus with the interaction operator (2.19).

2-E The Two-Hole Propagator

The Fourier transform of (2.10d) is

$$G^{-}_{\rho\sigma\kappa\lambda}(\omega) = \frac{f_\rho f_\sigma}{[\omega+\epsilon_\rho+\epsilon_\sigma-i\eta]} \left\{ \delta_{\rho\kappa}\delta_{\sigma\lambda} - \delta_{\rho\lambda}\delta_{\sigma\kappa} + \sum_{\rho_1\sigma_1} \Gamma^{2h}_{\rho\sigma\rho_1\sigma_1}(\omega) G^{-}_{\rho_1\sigma_1\kappa\lambda}(\omega) \right\} . \qquad (2.36)$$

The poles of $G^{-}(\omega)$ are at the energies of the states in the (N-2)-particle nucleus relative to the ground state of the N-particle nucleus. When two particles are removed from the N-particle nucleus creating two-hole states the residual interaction is the effective interaction between the two particles in the N-particle nucleus. From our definition of the ground state the two-hole interaction operator is

$$\Gamma^{2h}_{\rho\sigma\rho_1\sigma_1}(\omega) = K^{2h}_{\rho\sigma\rho_1\sigma_1}(\omega) \qquad (2.37)$$

where

$$K^{2h}_{\rho\sigma\rho_1\sigma_1}(\omega) = v_{\rho\sigma\rho_1\sigma_1} + \sum_{\rho_2\sigma_2} v_{\rho\sigma\rho_2\sigma_2} \frac{(1-f_{\rho_2})(1-f_{\sigma_2})}{[\omega-\epsilon_{\rho_2}-\epsilon_{\sigma_2}]} K^{2h}_{\rho_2\sigma_2\rho_1\sigma_1}(\omega) . \qquad (2.38)$$

That is, the interaction operator is the particle-particle reaction matrix evaluated at the poles of the two-hole propagator. The Green's function is

$$G^{-}_{\rho\sigma\kappa\lambda}(\omega) = \frac{f_\rho f_\sigma}{[\omega+\epsilon_\rho+\epsilon_\sigma-i\eta]} \left\{ \delta_{\rho\kappa}\delta_{\sigma\lambda} - \delta_{\rho\lambda}\delta_{\sigma\kappa} + \sum_{\rho_1\sigma_1} K^{2h}_{\rho\sigma\rho_1\sigma_1}(\omega) G^{-}_{\rho_1\sigma_1\kappa\lambda}(\omega) \right\} . \qquad (2.38)$$

The two-hole propagator and a hole-hole reaction matrix element are given in terms of diagrams in Fig. 2-3. The hole-hole interaction matrix element is shown as an insertion of a ladder series on particle

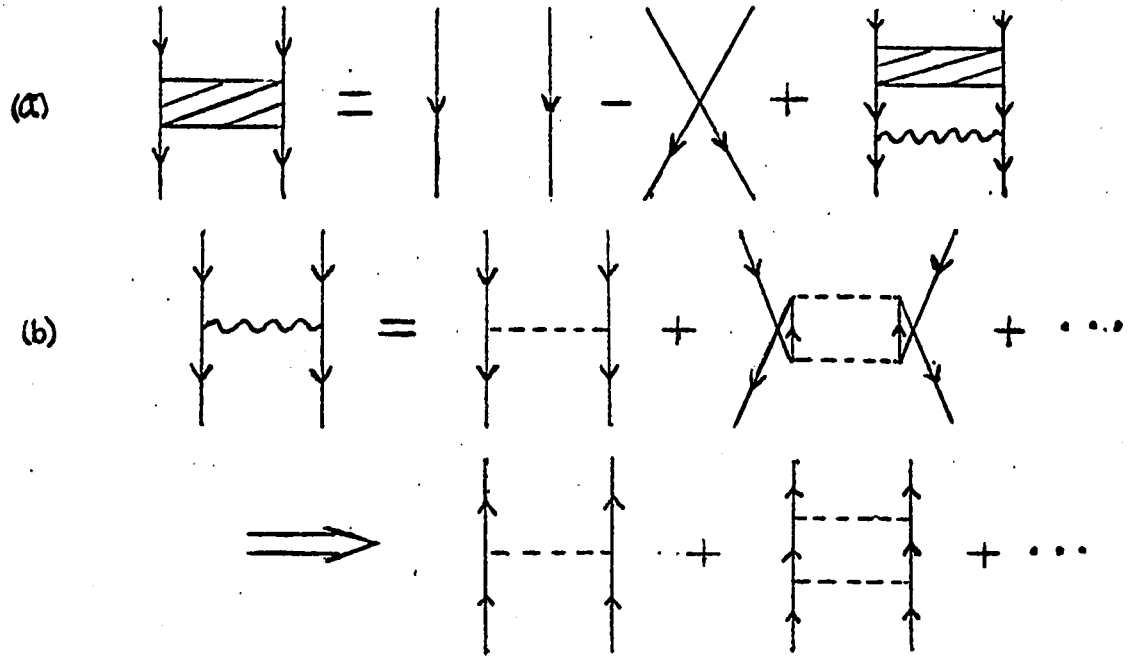

Fig. 2-3. (a) The two-hole propagator as a ladder series in the two-hole reaction matrix. (b) A hole-hole interaction matrix element as a ladder series in the interaction v.

lines. Diagrams drawn in this manner can be misleading; the hole-hole interaction does not contain any four-hole two-particle interactions. For example, the matrix element of the second order term in Fig. 2-3b is just the conjugate of the particle-particle matrix element.

The effective Hamiltonian for the two-hole states is

$$H(\omega) = H_0 + K^{2h}(\omega) \quad . \tag{2.39}$$

The problem of finding the poles of the two-hole Green's function is a self-consistent problem as it was for the case of two-particles. If

the reaction matrix does not depend on the various eigenvalues of the states with the same quantum numbers, the poles of (2.38) can be determined by diagonalizing the Hamiltonian

$$H(\omega) = H_0 + K^{2h}(\bar{\omega}_\alpha) \quad . \tag{2.40}$$

There are several differences between the two-particle and two-hole reaction matrices. For two particles the subspace of configurations which defined the reaction matrix could be chosen arbitrarily. In the case of two holes the reaction matrix is defined by the subspace of occupied states. The two-particle correlations of (2.33) are contained in the Hartree-Fock single-particle states in the case of two holes.

2-F The Particle-Hole Propagator

The Fourier transform of (2.10e) is

$$G_{\rho\sigma\kappa\lambda}^{ph}(\omega) = \frac{(1-f_\rho)f_\sigma - (1-f_\sigma)f_\rho}{[\omega - \epsilon_\rho + \epsilon_\sigma \mp i\eta]} \left\{ \delta_{\rho\kappa}\,\delta_{\sigma\lambda} + \right.$$

$$\left. + \sum_{\rho_1\sigma_1} \Gamma_{\rho\sigma\rho_1\sigma_1}^{ph}(\omega) G_{\rho_1\sigma_1\kappa\lambda}^{ph}(\omega) \right\} . \tag{2.41}$$

The poles of $G^{ph}(\omega)$ are at the excitation energies of particle-hole states relative to the ground state of the N-particle nucleus. In calculations of particle-hole structure the unperturbed single-particle (hole) energies are taken to be the energies of the states in the (N+1) and (N-1) nuclei. With this definition of the unperturbed states the residual interaction is the interaction between a particle in a state of the (N+1)-particle system and the particles in the N-particle

nucleus.[20] The particle-hole interaction operator is then the reaction matrix for these states evaluated at the excitation energy of the particle-hole system

$$\Gamma_{\rho\sigma\rho_1\sigma_1}^{ph}(\omega) = K_{\rho\sigma\rho_1\sigma_1}^{ph}(\omega) - K_{\rho\sigma_1\sigma\rho_1}^{ph}(\omega) \quad . \tag{2.42}$$

There are two terms in (2.42) because the direct and exchange particle-hole matrix elements are different. Particle-hole matrix elements are just linear combinations of the particle-particle matrix elements for the same states. A particle-hole reaction matrix is a linear combination of the particle-particle reaction matrices for the same configurations but evaluated at the particle-hole excitation energies. The particle-particle reaction matrices for the particle-hole matrix elements (2.42) are

$$K_{\rho\sigma\rho_1\sigma_1}^{ph}(\omega) = v_{\rho\sigma\rho_1\sigma_1} + \sum_{\rho_2\sigma_2} v_{\rho\sigma\rho_2\sigma_2} \frac{(1-f_{\rho_2})(1-f_{\sigma_2})}{[\omega-\epsilon_{\rho_2}-\epsilon_{\sigma_2}]} K_{\rho_2\sigma_2\rho_1\sigma_1}^{ph}(\omega) \tag{2.43a}$$

and

$$K_{\rho\sigma_1\sigma\rho_1}^{ph}(\omega) = v_{\rho\sigma_1\sigma\rho_1} + \sum_{\rho_2\sigma_2} v_{\rho\sigma_1\rho_2\sigma_2} \frac{(1-f_{\rho_2})(1-f_{\sigma_2})}{[\omega+\epsilon_{\rho_2}-\epsilon_{\sigma_2}]} K_{\rho_2\sigma_2\sigma\rho_1}^{ph}(\omega) \quad . \tag{2.43b}$$

Although we have used the same notation in (2.42) and (2.43), the matrix elements (2.43) are particle-particle coupled matrix elements.

The particle-hole Green's function is

$$G_{\rho\sigma\kappa\lambda}{}^{ph}(\omega) = \frac{(1-f_\rho)f_\sigma-(1-f_\sigma)f_\rho}{[\omega-\epsilon_\rho+\epsilon_\sigma\pm i\eta]}\left\{\delta_{\rho\kappa}\delta_{\sigma\lambda} + \sum_{\rho_1\sigma_1}{}' [K_{\rho\sigma\rho_1\sigma_1}{}^{ph}(\omega)-K_{\rho\sigma_1\sigma\rho_1}{}^{ph}(\omega)]G_{\rho_1\sigma_1}{}^{ph}(\omega)\right\} \quad (2.44)$$

It can be shown[21] that finding the poles of (2.44) is equivalent to solving the eigenvalue problem

$$(\epsilon_\rho-\epsilon_\lambda-\omega_\alpha)X_{\rho\lambda}{}^{\alpha}+\sum_{\delta\beta}\left\{K_{\rho\beta\lambda\delta}{}^{ph}(\omega)-K_{\rho\beta\ \delta\lambda}{}^{ph}(\omega)\right\}X_{\delta\beta}{}^{\alpha} + \sum_{\delta\beta}\left\{K_{\rho\ \delta\lambda\beta}{}^{ph}(\omega)-K_{\rho\ \delta\beta\lambda}{}^{ph}(\omega)\right\}Y_{\delta\beta}{}^{\alpha}=0 \quad (2.45a)$$

$$(\epsilon_\rho-\epsilon_\lambda+\omega_\alpha)\bar{Y}_{\rho\lambda}{}^{\alpha}+\sum_{\delta\beta}\left\{K_{\rho\beta\lambda\delta}{}^{ph}(\omega)-K_{\rho\ \delta\beta\lambda}{}^{ph}(\omega)\right\}\bar{Y}_{\delta\beta}{}^{\alpha} + \sum_{\delta\beta}\left\{K_{\rho\ \delta\lambda\beta}{}^{ph}(\omega)-K_{\rho\ \delta\beta\lambda}{}^{ph}(\omega)\right\}\bar{X}_{\delta\beta}{}^{\alpha}=0 \quad . \quad (2.45b)$$

Equations (2.45) are the eigenvalue problem for the particle-hole states in the random phase approximation. The various matrix elements in (2.45) are shown in Fig. 2-4. The amplitudes of the particle-hole configurations contained in a particle-hole state are

$$X_{\rho\lambda}{}^{\alpha}(1-f_\rho)f_\lambda+Y_{\rho\lambda}{}^{\alpha}(1-f_\lambda)f_\rho = \langle N|a_\rho a_\lambda{}^{+}|N,\alpha\rangle \quad . \quad (2.46)$$

The bar on the amplitudes in (2.45b) denotes the complex conjugate. $X_{\rho\lambda}{}^{\alpha}$ is the amplitude of a configuration (ρ,λ) in the state α arising from excitation of a particle from the core. $Y_{\rho\lambda}{}^{\alpha}$ is the amplitude of a configuration in the state α arising from particle-hole configurations

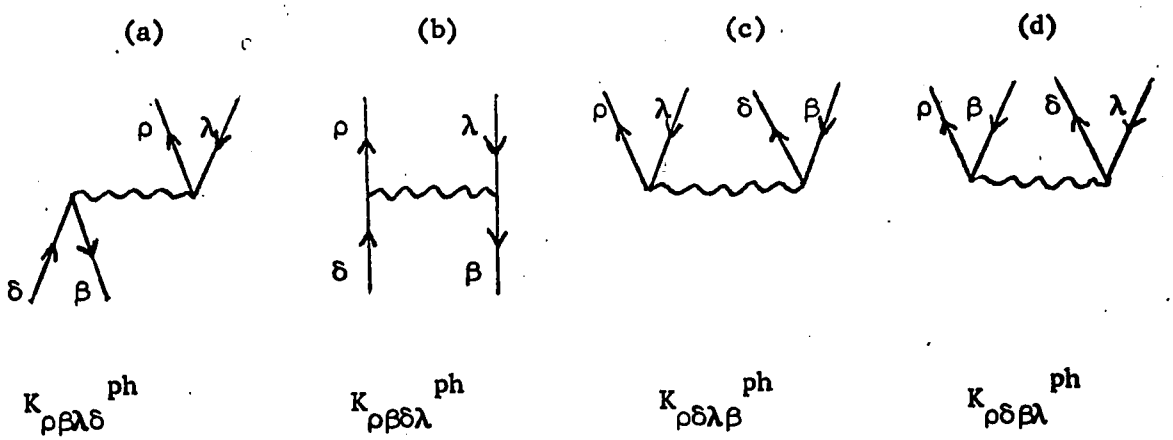

Fig. 2-4. The particle-hole interaction matrix elements.

already present in the ground state. The Tamm-Dancoff approximation is obtained from (2.45) by setting Y^{α} equal to zero

$$(\epsilon_\rho - \epsilon_\lambda - \omega_\alpha) X_{\rho\lambda}^{\alpha} + \sum_{\delta\beta}' \left\{ K_{\rho\beta\lambda\delta}^{ph}(\omega) - K_{\rho\beta\,\delta\lambda}^{ph}(\omega) \right\} X_{\delta\beta}^{\alpha} = 0 \qquad (2.47)$$

The eigenvalue equations (2.45) and (2.47) are self-consistent equations in the same way the eigenvalue problems for two particles and two holes were. The particle-hole reaction matrix is similar to the two-hole reaction matrix in that the subspace of configurations defining the reaction matrix is partly the space of occupied states.

2-G The Free Reaction Matrix

To perform shell model calculations with the effective Hamiltonians of the previous sections the nuclear reaction matrices must be determined from the nucleon-nucleon interaction. A free reaction matrix [12] deduced from the nucleon-nucleon scattering data can be

used to determine the nuclear reaction matrices. The free reaction matrix is defined by the integral equation

$$K_F(e) = v+v\not{g}_F(e)PK_F(e) \tag{2.48}$$

where

$$\not{g}_F(e) = \frac{1}{e-T} \quad .$$

P is the principal value operator and T is the total kinetic energy operator. On the energy shell e becomes the total kinetic energy and, in general, may be treated as a complex parameter. The nuclear reaction matrices of the previous sections were all of the form

$$K(\omega) = v+v\not{g}(\omega)QK(\omega) \quad . \tag{2.49}$$

Solving (2.48) for v in terms of K_F and substituting in (2.49) we have

$$K(\omega) = K_F(e)+K_F(e)[\not{g}(\omega)Q-\not{g}_F(\epsilon)P]K(\omega) . \tag{2.50}$$

When fitting a representation of K_F to the free nucleon-nucleon scattering data, translational invariance of the two-nucleon potential is required; therefore, the propagator in (2.48) is replaced by the propagator

$$\not{g}_F(\epsilon) = \frac{1}{\epsilon-t} \quad . \tag{2.51}$$

In (2.51) t is the relative kinetic energy operator and on the energy shell ϵ is the relative kinetic energy of the two nucleons. In fact, $K_F(\epsilon)$ is related to the two-body scattering data through on the energy shell matrix elements

$$\langle \underline{k}|K_F(\epsilon = \frac{\hbar^2k^2}{M})|\underline{k}'\rangle \quad .$$

With K_F known the nuclear reaction matrix can be obtained from

$$K(\omega) = K_F(\epsilon)+K_F(\epsilon)[\not{g}(\omega)Q-\not{g}_F(\epsilon)P]K(\omega) \quad . \tag{2.52}$$

The determinaton of K_F and K has been discussed in detail by Lee.[17] In finite nuclei the nucleon-nucleon interaction need not be on the energy shell; however, in an exact calculation of (2.52) the nuclear reaction is independent of ϵ. On the other hand, it is often useful to make the approximation

$$K(\omega) = K_F(\epsilon) \tag{2.53}$$

by choosing an appropriate value of ϵ. For $\epsilon < 0$ the choice (2.53) is equivalent to the lowest order reference spectrum approach of Bethe, et al.[22].

2-H Correction Terms

In first order the nuclear reaction matrix is the free reaction matrix. The higher order terms contain the corrections arising from the fact that $K(\omega)$ is determined by nucleons scattering in bound states whereas $K_F(\epsilon)$ is determined by free nucleon scattering. We examine briefly the second order correction terms for the various nuclear reaction matrices. When drawing diagrams a solid line is used to denote a free reaction matrix interaction and p and h are used to designate states above and below the Fermi sea, respectively.

a) Two-particle

The two-particle reaction matrix element (2.25) is

$$K_{p_3p_4p_1p_2}(\omega) \equiv$$

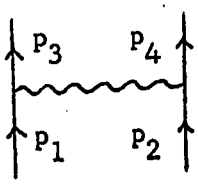

(2.54)

As an expansion in K_F (2.54) is

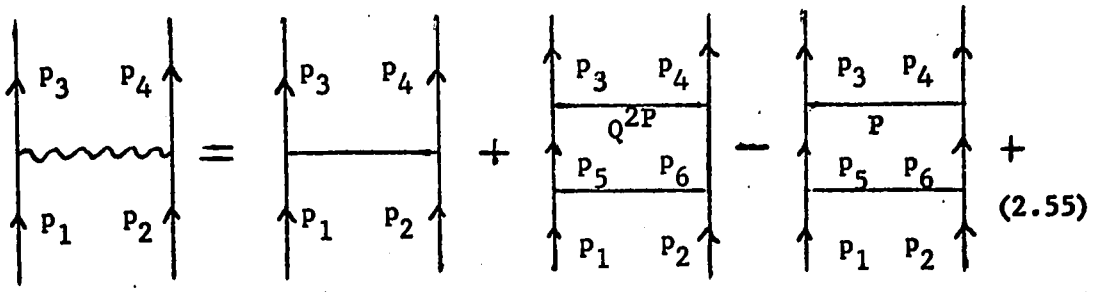

(2.55)

The projection operator Q^{2p} restricts the intermediate states to configurations in which p_5 and p_6 are not both in the subspace of configurations used to diagonalize the effective Hamiltonian.

b) Two-hole

The two-hole reaction matrix element (2.37) is

$$K_{h_3h_4h_1h_2}^{2h}(\omega) \equiv$$

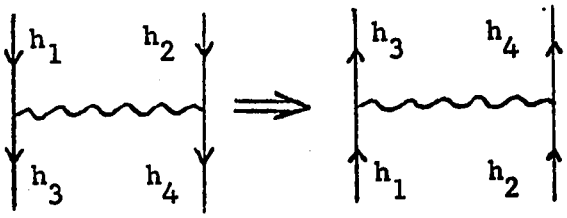

(2.56)

As an expansion in K_F (2.56) is

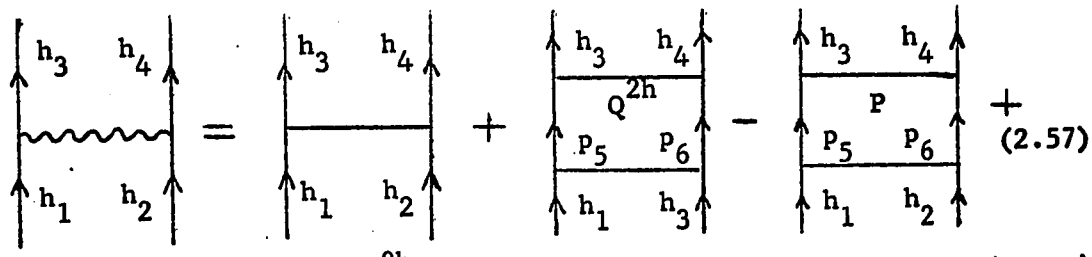

(2.57)

The projection operator Q^{2h} restricts the intermediate states (p_5, p_6) to all possible two-particle configurations above the Fermi sea.

c) Particle-Hole

The particle-hole reaction matrix elements (2.45) are

$$K_{p_2h_1h_2p_1}^{ph}(\omega) \equiv$$

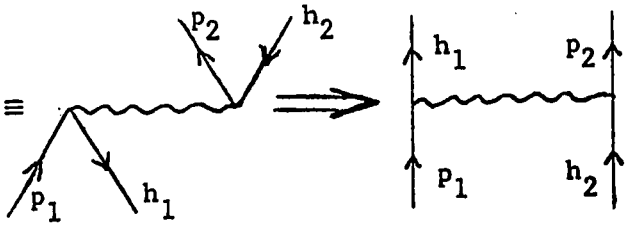

(2.58a)

$K_{p_2h_1p_1h_2}{}^{ph}(\omega) \equiv$ 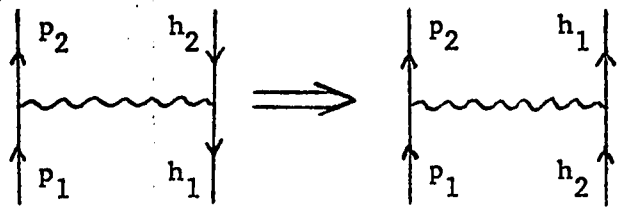 (2.58b)

$K_{p_2p_1h_2h_1}{}^{ph}(\omega) \equiv$ 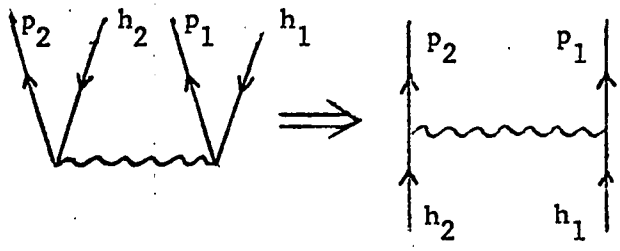 (2.58c)

$K_{p_2p_1h_1h_2}{}^{ph}(\omega) \equiv$ 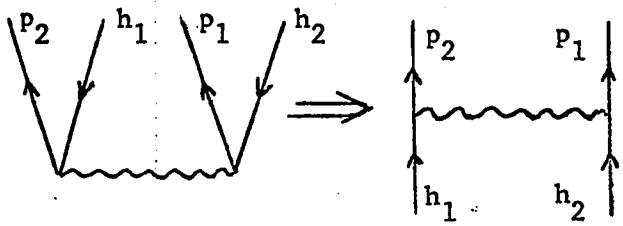 (2.58d)

As expansions in K_F (2.58a) and (2.58c) are

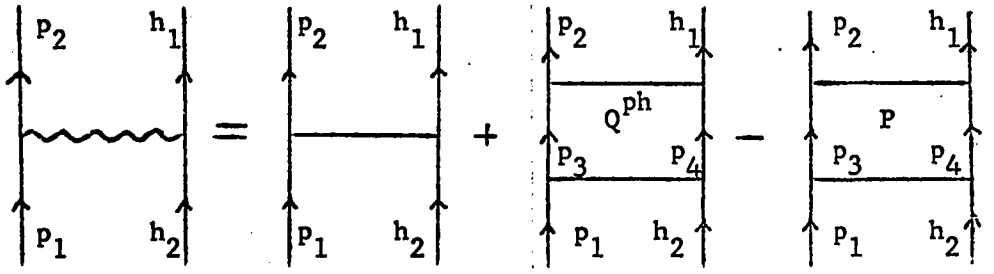 (2.59a)

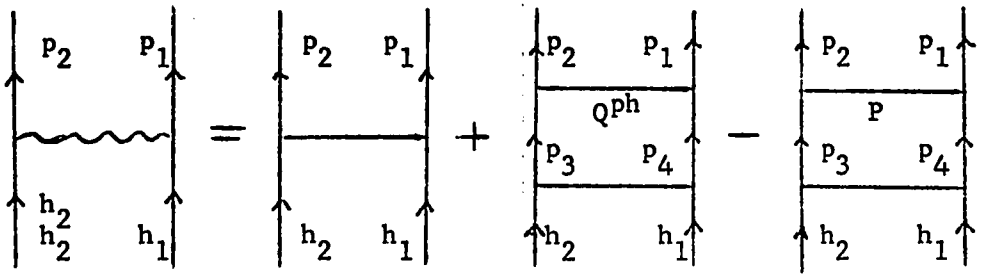 (2.59b)

The diagrams (2.58b) and (2.58d) are exchange diagrams. The projection operator Q^{ph} restricts the intermediate states (p_3,p_4) to all possible two-particle configurations above the Fermi sea. The diagrams (2.58a) and (2.58b) are the Tamm-Dancoff approximation and the ground state correlation diagrams (2.58c) and (2.58d) are included in the random phase approximation. From (2.59) it can be seen that, if the particle-holes states have negative parity, Q^{ph} is different for (2.59a) and (2.59b). That is, the effective interaction would be different for the Tamm-Dancoff diagrams and the ground state correlation diagrams.

2-I Energy Dependence of $K(\omega)$

In all the cases discussed the effective shell model Hamiltonian was energy dependent and the determination of the eigenvalues involved a self-consistent calculation of the reaction matrix. If $K(\omega_\alpha)$ is state dependent for states with the same quantum numbers, the eigenvalues and eigenvectors cannot be determined by a simple diagonalization of the effective Hamiltonian. This difficulty can be avoided by reducing the subspace of configurations to only the dominant configuration of the state under consideration. In general, such a procedure is not necessary. Some insight into the energy dependence of $K(\omega)$ can be gained by considering the correction terms in the previous section. The energy dependence enters via the propagator $\frac{Q}{\omega - QHQ}$. In the following discussion we assume that harmonic oscillator states are used to evaluate the matrix elements.

a) Two-particle: With a judicious choice of the subspace for

diagonalization most of the energy dependence in (2.55) can be removed. For example, by choosing the subspace to be an entire shell, the first intermediate state contribution is $2\hbar\omega$ away in energy. In general, the spread in eigenvalues for a set of states is not large and a good approximation[17] is to evaluate the reaction matrix at the mean excitation energy.

b) Two-hole: For the two-hole matrix elements (2.57) the intermediate states are not related to the choice of the subspace for diagonalization. However, the lowest intermediate state is always at $2\hbar\omega$. Again, a good approximation is to use the average excitation energy.

c) Particle-hole: For the particle-hole matrix elements (2.59) there are two cases to consider: 1) negative parity particle-hole states, and 2) positive parity particle-hole states. For negative parity states with oscillator shell spacings the lowest intermediate state energies in (2.59a) and (2.59b) are $3\hbar\omega$ and $2\hbar\omega$, respectively. In heavy closed shell nuclei, such as Pb^{208}, the spin-orbit splitting gives mixed parity shells. With mixed parity shells there can be both positive and negative parity low-lying particle-hole states. For mixed parity shells the lowest energy intermediate states are at $2\hbar\omega$ for both (2.59a) and (2.59b). In practice the single particle states are not degenerate and in heavy nuclei intermediate state energies may be near the excitation energy. The difficulty of small denominators, if it does exist, has not been considered. In the random phase approximation it is possible to have imaginary eigenvalues.

If an eigenvalue becomes imaginary, the effective interaction also becomes imaginary. In terms of the model a complex eigenvalue means that the interaction used would not have yielded the Hartree-Fock solution assumed for the ground state.[21] In the present case this appears directly in terms of the interaction. The particle-hole reaction matrix is the reaction matrix assumed to give the ground state but evaluated at a different energy. The inability to find a self-consistent solution for a real interaction means that the interaction is inconsistent with the assumption of the Hartree-Fock ground state.

2-J Summary

A formalism for defining the effective shell model Hamiltonian was derived using Green's functions. The integral equations for the Green's functions were solved in the approximations that give the usual shell model eigenvalue problems. In all the cases considered the effective interaction is a nuclear reaction matrix defined self-consistently by the excitation energies of the states being considered. For the one-particle case the reaction matrix is the Brueckner reaction matrix and the single-particle states are the Brueckner Hartree-Fock states. The one-particle, two-hole and particle-hole reaction matrices are defined by the subspace of occupied states. The two-particle reaction matrix is defined by the subspace of configurations chosen for diagonalization. The nuclear reaction matrices can be evaluated from an expansion in terms of a free reaction matrix.

CHAPTER 3

ODD-PARITY PARTICLE-HOLE STATES IN O^{16}

3-A Introduction

We present in this chapter a standard shell model calculation of the odd-parity states in O^{16} using the relative S state phenomenological free reaction matrix[16] as an effective interaction. The particle-hole structure was calculated in both the Tamm-Dancoff and the random phase approximations. Since the original work of Elliott and Flowers[23] there have been many calculations of the particle-hole states in O^{16}. Gillet and Vinh Mau[24] carried out a detailed phenomenological calculation and since then there have been several calculations using realistic interactions.[3,25-27] The work presented here is similar to that of Kallio and Kolltveit[3] in that only the relative S state part of the nucleon-nucleon interaction is included. The method for obtaining an effective interaction from a free reaction matrix is quite different from the Scott-Moszkowski separation method.[28] To examine the difference the effective interaction, obtained from the free reaction matrix, is compared to the Kallio-Kolltveit interaction which was obtained by the Scott-Moszkowski separation method. The dependence of the particle-hole spectra on the higher energy components contained in the free reaction matrix is discussed.

3-B Particle-Hole States

We make the usual shell model assumption that the nuclear Hamiltonian consists of a diagonal part and a two-body perturbation

$$H = H_0 + v_1$$
$$= \sum_k \epsilon_k a_k^+ a_k + \tfrac{1}{2} \sum_{\substack{\alpha\beta \\ \gamma}} v_{\alpha\beta\gamma\delta}\, a_\alpha^+ a_\beta^+ a_\delta a_\gamma \quad . \qquad (3.1)$$

Presumably, the single-particle energies ϵ_k would be obtained from a self-consistent calculation of the ground state. It was shown in Chapter 2 that an appropriate effective Hamiltonian for shell model calculations is

$$H(\omega) = H_0 + K(\omega) \quad . \qquad (3.2)$$

$K(\omega)$ is the two-nucleon reaction matrix defined by

$$K(\omega) = v + v\,\mathcal{G}(\omega)\,QK(\omega) \qquad (3.3)$$

where

$$\mathcal{G}(\omega) = \frac{1}{\omega - H_0} \quad .$$

Q is the projection operator to be chosen so that diagonalization of (3.2) does not lead to double counting of ladder diagrams.

With (3.3) as the effective Hamiltonian, the particle-hole excitation energies and wavefunctions are given by the solution of the eigenvalue problem[15]

$$(\epsilon_p - \epsilon_h - \omega_\alpha) X_{ph}^{\alpha} + \sum_{p'h'} \{K_{ph'hp'}(\omega_\alpha) - K_{ph'p'h}(\omega_\alpha)\} X_{p'h'}^{\alpha}$$
$$+ \sum_{p'h'} \{K_{pp'hh'}(\omega_\alpha) - K_{pp'h'h}(\omega_\alpha)\} Y_{p'h'}^{\alpha} = 0 \qquad (3.4a)$$

$$(\epsilon_p - \epsilon_h + \omega_\alpha) \bar{Y}_{ph}^{\alpha} + \sum_{p'h'} \{K_{ph'hp'}(\omega_\alpha) - K_{pp'h'h}(\omega_\alpha)\} \bar{Y}_{p'h'}^{\alpha}$$
$$+ \sum_{p'h'} \{K_{pp'hh'}(\omega_\alpha) - K_{pp'h'h}(\omega_\alpha)\} \bar{X}_{p'h'}^{\alpha} = 0 \qquad (3.4b)$$

X_{ph}^{α} and Y_{ph}^{α} are the Tamm-Dancoff and ground state correlation amplitudes, respectively. The bar on the amplitudes in (3.4b) denotes the complex conjugate. The eigenvalue problem (3.4) was determined in the well known random phase approximation (RPA). The Tamm-Dancoff approximation (TDA) is obtained from (3.4) by setting Y_{ph}^{α} equal to zero, whence the eigenvalue problem

$$(\epsilon_p-\epsilon_h-\omega_\alpha)X_{ph}^{\alpha}+\sum_{p'h'}\{K_{ph'hp'}(\omega_\alpha)-K_{ph'p'h}(\omega_\alpha)\}X_{p'h'}^{\alpha}=0 \quad . (3.5)$$

The properties of the particle-hole eigenvalue problems have been discussed in detail by Thouless.[21] The matrix elements required in (3.4) and (3.5) are defined in Appendix A.

In Chapter 2 the calculation of $K(\omega)$ from an expansion in terms of a free reaction matrix K_F was discussed. The expansion is

$$K(\omega) = K_F(\epsilon)+K_F(\epsilon)[\mathcal{U}(\omega)Q-\mathcal{U}_F(\epsilon)P]K(\omega) \quad . \qquad (3.6)$$

The eigenvalue problems (3.4) and (3.5) are self-consistent determinations of the spectra and reaction matrices. We calculated the spectra in the first order approximation

$$K(\omega) \doteqdot K_F(\epsilon) \quad . \qquad (3.7)$$

In the approximation (3.7) the eigenvalue problems are no longer self-consistent. In an exact calculation of $K(\omega)$ there is no dependence on ϵ; however, in the approximation (3.7) ϵ is essentially a free parameter. The ϵ dependence can be used to advantage by using

the dependence to compensate for the neglect of the correction terms.

The reaction matrix elements included in our calculation are given in (2.58) and (2.59). We diagonalized the residual interaction in the subspace of configurations consisting of 0p-shell holes and (0d,1s)-shell particles. In this case the lowest energy intermediate states in (2.59a) and (2.59b) are $(p_3,p_4) \equiv (0d,1s;0f,1p)$ and (0d,1s;0d,1s), respectively. The large spin-orbit splitting ($\approx 1\hbar\omega$) of the unperturbed particle-hole configurations gives a significant variation in $\mathcal{M}(\omega)$ for a set of states with the same quantum numbers. It is interesting to note that the contribution of nearby states in the correction terms has the largest effect on the high T=1 states and the least effect on the low-lying T=0 states. Apart from the state and matrix element dependence, the correction terms contribute differently to different isotopic spin states. If the isotopic spin coupling is performed explicitly (Appendix A), there are different linear combinations of the T=0 and T=1 particle-particle matrix elements for T=0 and T=1 particle-hole matrix elements. For the direct particle-hole matrix element (2.58a) the coupling is

$$T_{ph} = 0: \quad < \left| \frac{\{3K(T=1)+K(T=0)\}}{2} \right| >$$

$$T_{ph} = 1: \quad < \left| \frac{\{K(T=1)-K(T=0)\}}{2} \right| > .$$

We calculated the particle-hole spectra for various values of ϵ to obtain some information about the dependence of the spectra on the correction terms.

3-C The Free Reaction Matrices

In this calculation we used the relative S state phenomenological free reaction matrices discussed by Kahana.[16] Since the dominant contributions to the free reaction matrices are the relative S state reaction matrices, we included only relative S state components in the effective interaction. In the coordinate space representation K_F is non-local; accordingly we have used local but velocity dependent representations of the form

$$^{1,3}K_0(\epsilon) = \lambda(\epsilon)\left\{-g_1\left(\frac{\epsilon}{\epsilon_0}+b_1\right)e^{-\alpha_1 r}+\tfrac{1}{2}g_2\left(\frac{\epsilon}{\epsilon_0}+b_2\right)\left[\left(\frac{p}{mc}\right)^2 e^{-\alpha_2 r}+e^{-\alpha_2 r}\left(\frac{p}{mc}\right)^2\right]\right\} \qquad (3.8)$$

where

$$\lambda^{-1}(\epsilon) = \frac{\epsilon}{\epsilon_0} + \delta_{T1} - \delta_{T0} \qquad (3.9)$$

We use $^1K_0$ and $^3K_0$ to denote the T=1 and T=0 relative S state free reaction matrices, respectively. It should be noted that $^3K_0(\epsilon)$ contains a pole which is a consequence of the existence of the deuteron bound state. The parameters in (3.8), which were determined by fitting the Hamada-Johnston phase shifts,[29] are given in Table 3.1.

Table 3.1

Parameters for the free reaction matrices

	$^1K_0$(T=1,S=0,ℓ=0)	$^3K_0$(T=0,S=1,ℓ=0)
ϵ_0(MeV)	1.7	8.6
g_1(MeV)	53.827	103.297
g_2(MeV)	2,442.2	1,697.0
α_1(fm^{-1})	0.897	1.115
α_2(fm^{-1})	3.072	2.670
b_1	4.72	1.50
b_2	4.40	2.28

3-D The Odd-Parity Particle-Hole States

Particle-hole states were constructed as eigenstates of total angluar momentum J and total isotopic spin T. The j-j coupling scheme used is described in Appendix A. The particle-hole interaction was diagonalized in both the TDA and RPA in the subspace of configurations consisting of 0p-shell holes and (0d,1s)-shell particles. The unperturbed energies and configurations are given in Table 3.2. The unperturbed energies used were the neutron configuration energies given by Gillet and Vinh Mau.[24] Harmonic oscillator wavefunctions were used with a size parameter corresponding to $\hbar\omega$ = 13.4 MeV.

Table 3.2

The unperturbed neutron particle-hole configurations.

Configuration	Energy (MeV)
$0p_{3/2}^{-1}, 0d_{5/2}$	17.65
$0p_{3/2}^{-1}, 1s_{1/2}$	18.52
$0p_{3/2}^{-1}, 0d_{3/2}$	22.73
$0p_{1/2}^{-1}, 0d_{5/2}$	11.51
$0p_{1/2}^{-1}, 1s_{1/2}$	12.38
$0p_{1/2}^{-1}, 0d_{3/2}$	16.59

As mentioned earlier, with the approximations made, ϵ is essentially a free parameter. The dependence of the spectra on ϵ was examined and it was found that only the highest $J^{\pi},T = 1^{-},1$ states and the lowest $3^{-},0$ state were appreciably ϵ dependent. The ϵ dependence of these levels is shown in Fig. 3.1. From Fig. 3.1 it can be seen that all of the levels are nearly ϵ independent for $\epsilon > 80$ MeV. This follows from the ϵ dependence of the free reaction matrices. ${}^{1}K_{0}(\epsilon)$ and ${}^{3}K_{0}(\epsilon)$ are relatively insensitive to variations in ϵ when ϵ is greater than 80 MeV; furthermore, for ϵ less than 80 MeV, varying ϵ is to a good approximation only altering the strength of the interaction. It is well known [20] that the collective particle-hole states shown in Fig. 3.1 are sensitive to the strength of the interaction. We present our calculations with

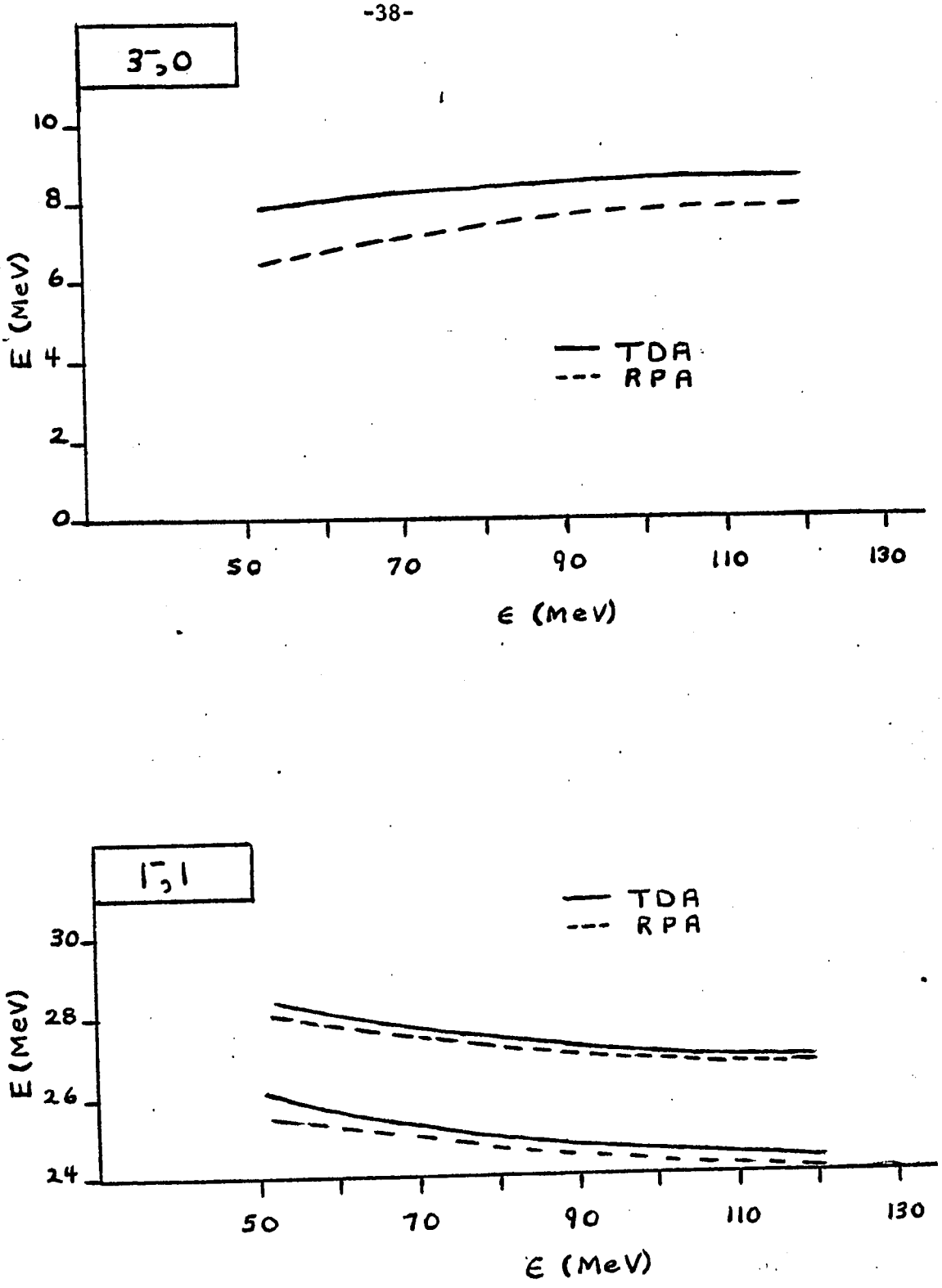

Fig. 3-1. The ϵ dependence of the collective particle-hole states in O^{16}.

ϵ = 86 MeV. This value was chosen since the same value gives reasonable agreement with the spectra of neighboring nuclei.[16]

The required radial integrals of the free reaction matrices are given in Table 3.3. In Fig. 3.2 the results of the present calculation in the RPA are compared with experiment and the spectra for the Kallio-Kolltveit interaction.[27,30] The energy levels and wavefunctions in both the TDA and RPA are tabulated in Table 3.4. In the particle-hole model one of the $1^-,0$ states is a spurious state. In the RPA the spurious state should be at zero energy, however, in the present calculation it is imaginary. The spurious state is very sensitive to the strength of the interaction; consequently, with the present approximations there is no reason why it should be at zero energy.

Comparing the calculated spectra with experiment it can be seen that there is very little agreement with experiment. The structure of the low-lying T=0 states is not well determined. Brown and Green[31] proposed that the structure be explained by the coexistence of spherical and deformed ground states in O^{16}. More recently, Zuker, Buck and McGrory[32] have calculated the structure of the low-lying states in a many-particle configuration model. The calculated particle-hole states should be compared with their unperturbed positions which cannot be obtained from experiment. The giant dipole states are too high; again, the structure of the giant dipole states is not well known. The giant dipole states and lowest $3^-,0$ state have the proper collective behavior in both the TDA and RPA in the present calculation.

Table 3.3

Radial integrals of the free reaction matrices with

$\hbar\omega$ = 13.4 MeV and ϵ = 86 MeV

n	n'	$< n\|\|^1K_0\|\|n' >$	$< n\|\|^3K_0\|\|n' >$
0	0	-7.034	-11.079
0	1	-4.021	-7.799
0	2	-2.234	-5.116
1	1	-4.193	-7.557
1	2	-2.722	-5.746
2	2	-2.374	-5.164

Fig. 3-2. The odd-parity states in O^{16} calculated in the random-phase approximation. The columns labeled K_F is the present calculation and the columns labeled KK are for the Kallio-Kolltveit interaction.[27]

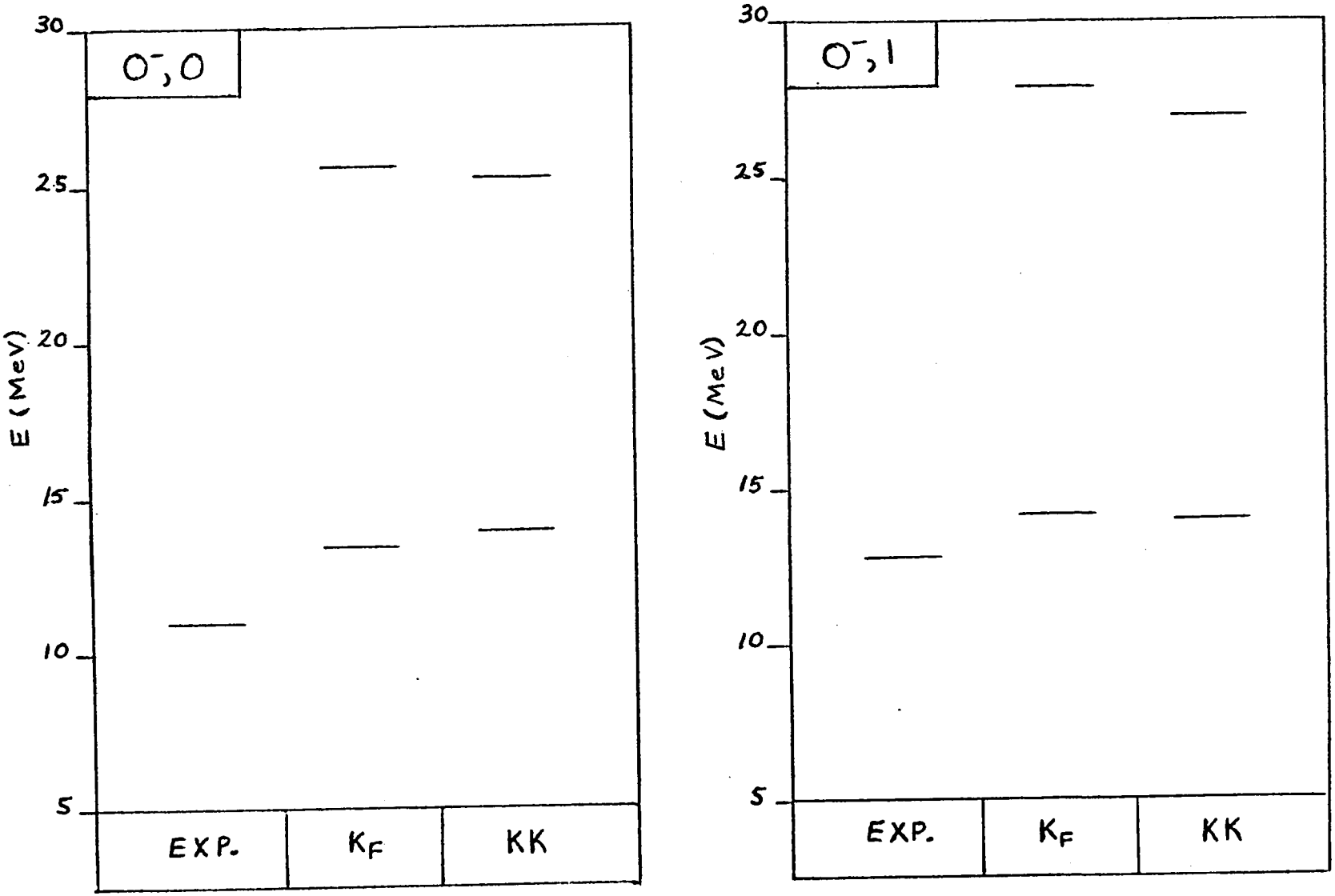

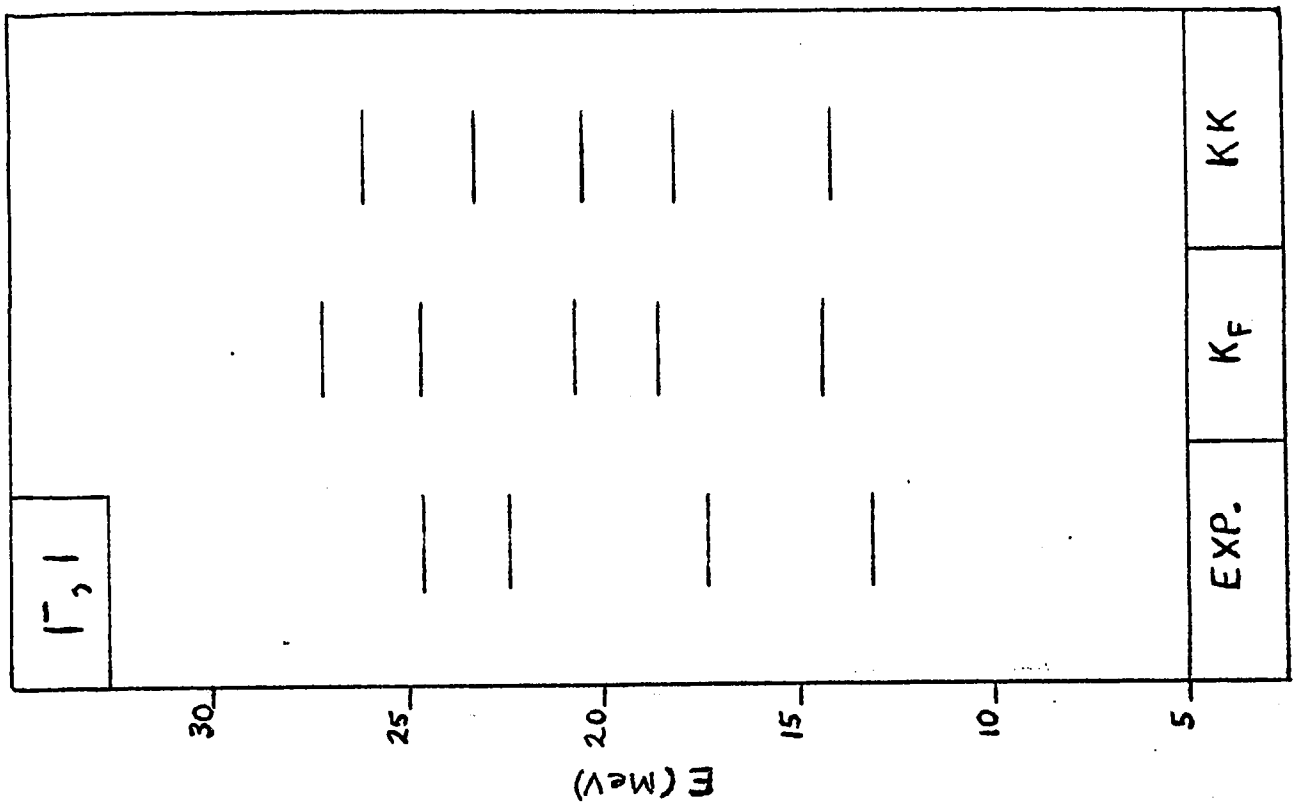
$1^-,1$
EXP.
K_F
KK
30
25
20
15
10
5
E (MeV)

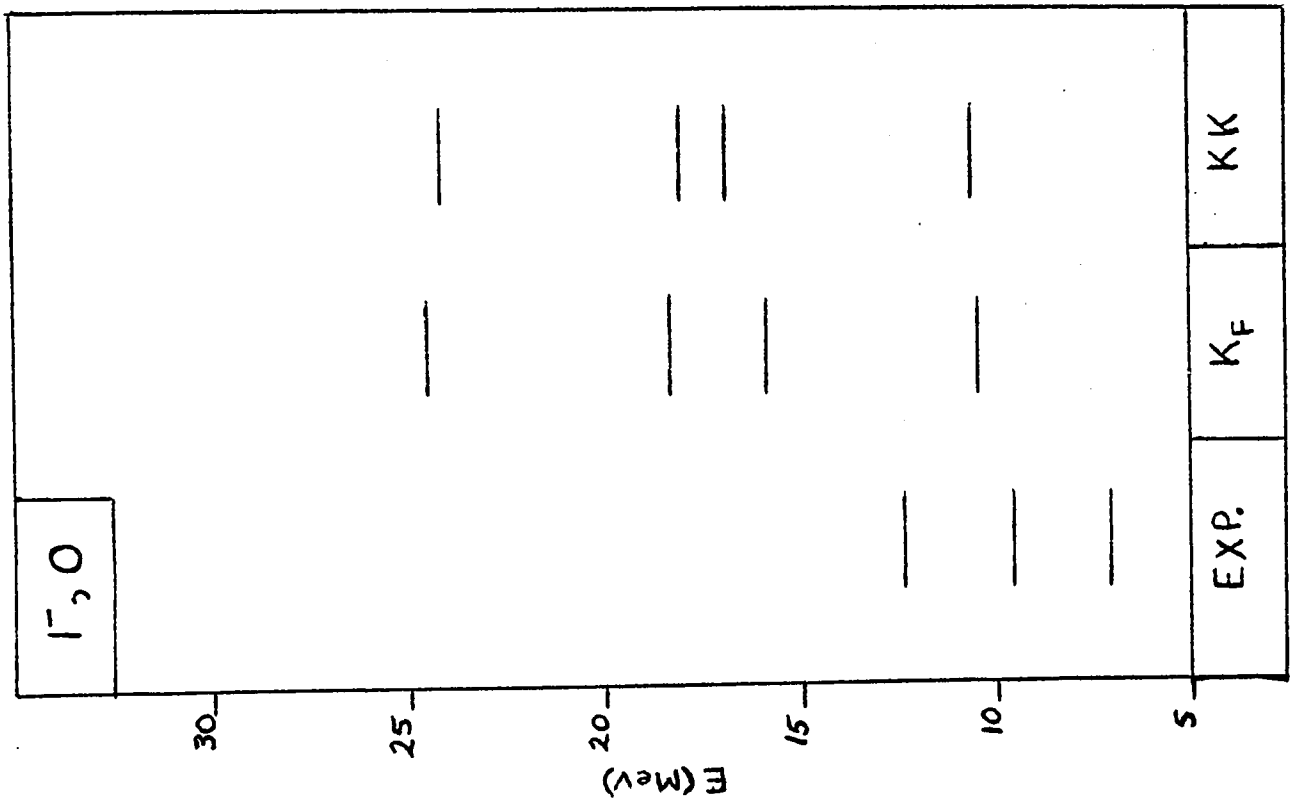
$1^-,0$
EXP.
K_F
KK
30
25
20
15
10
5
E (MeV)

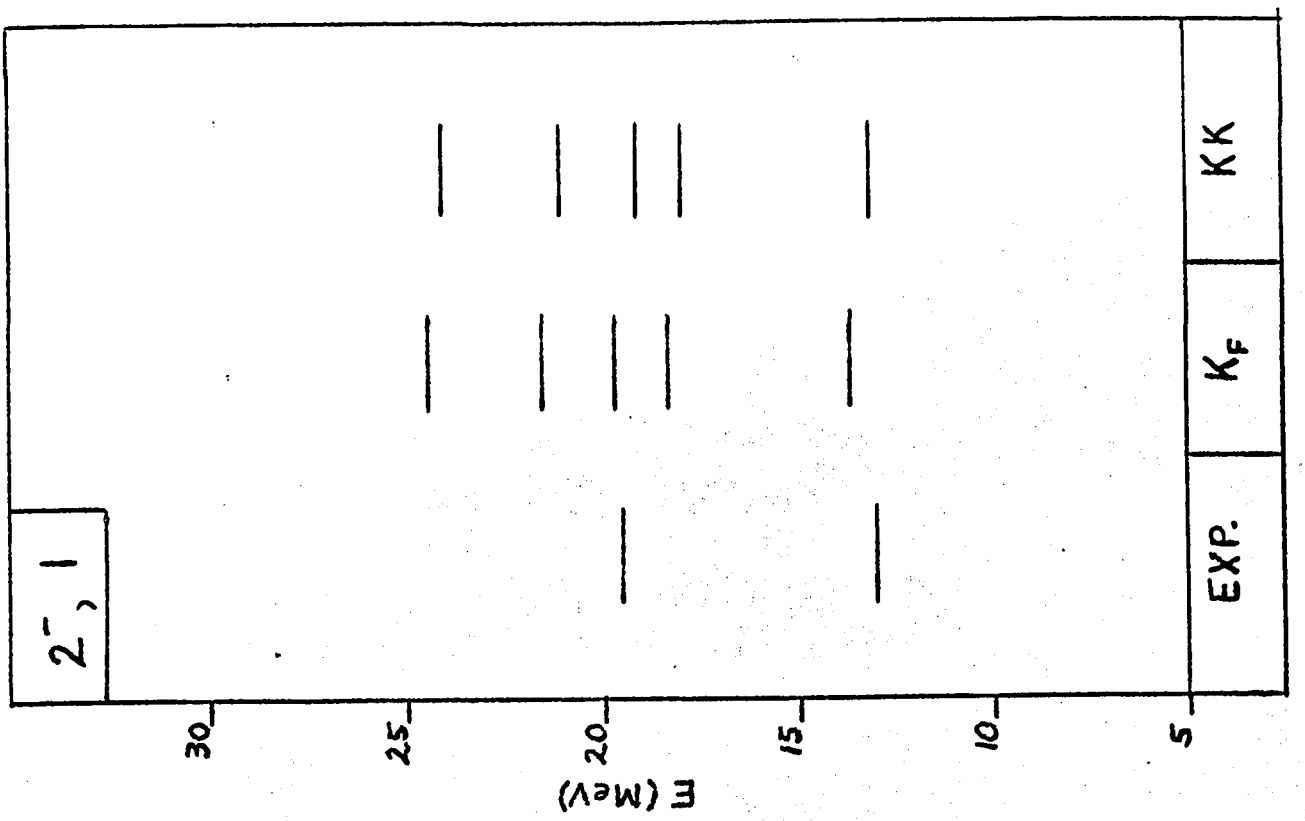
2⁻, 1
EXP.
K_F
KK
30
25
20
15
10
5
E (MeV)

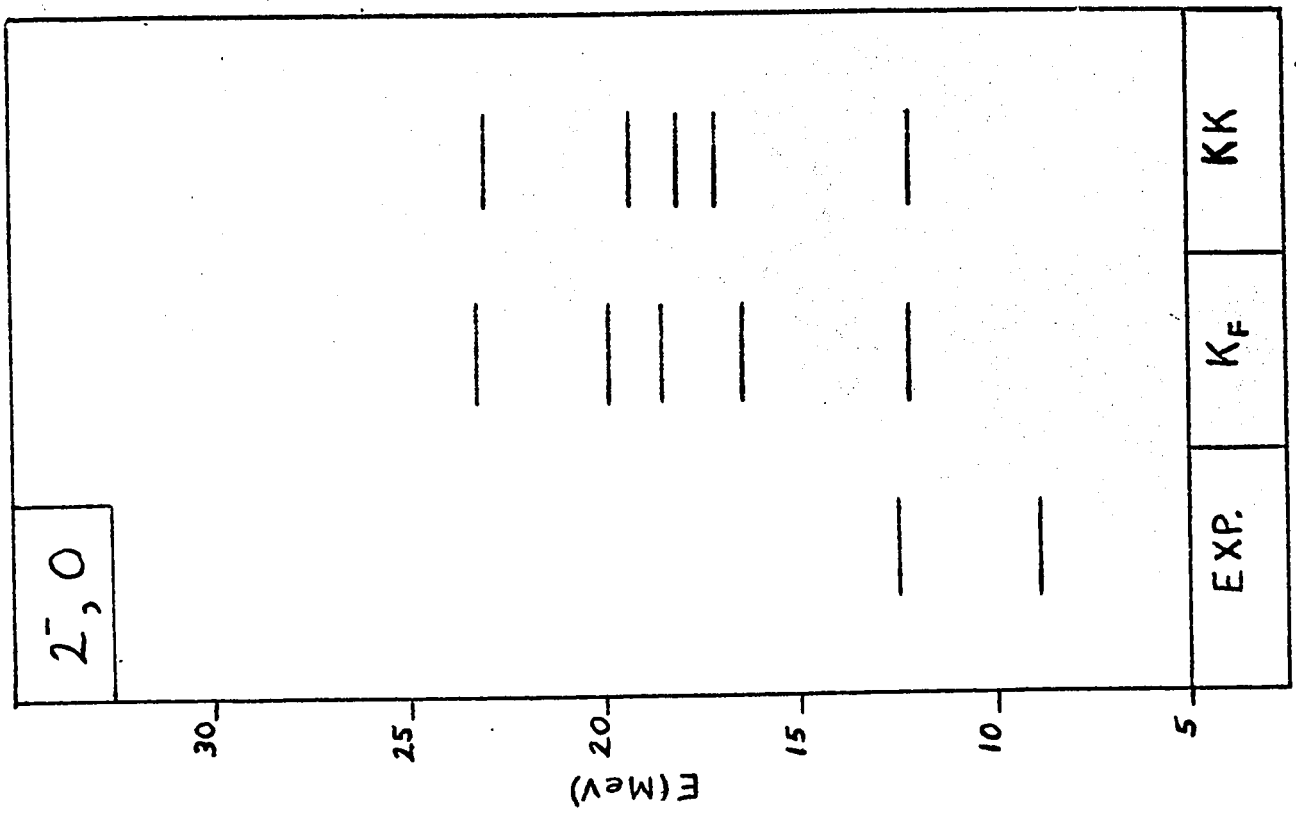
2⁻, 0
EXP.
K_F
KK
30
25
20
15
10
5
E (MeV)

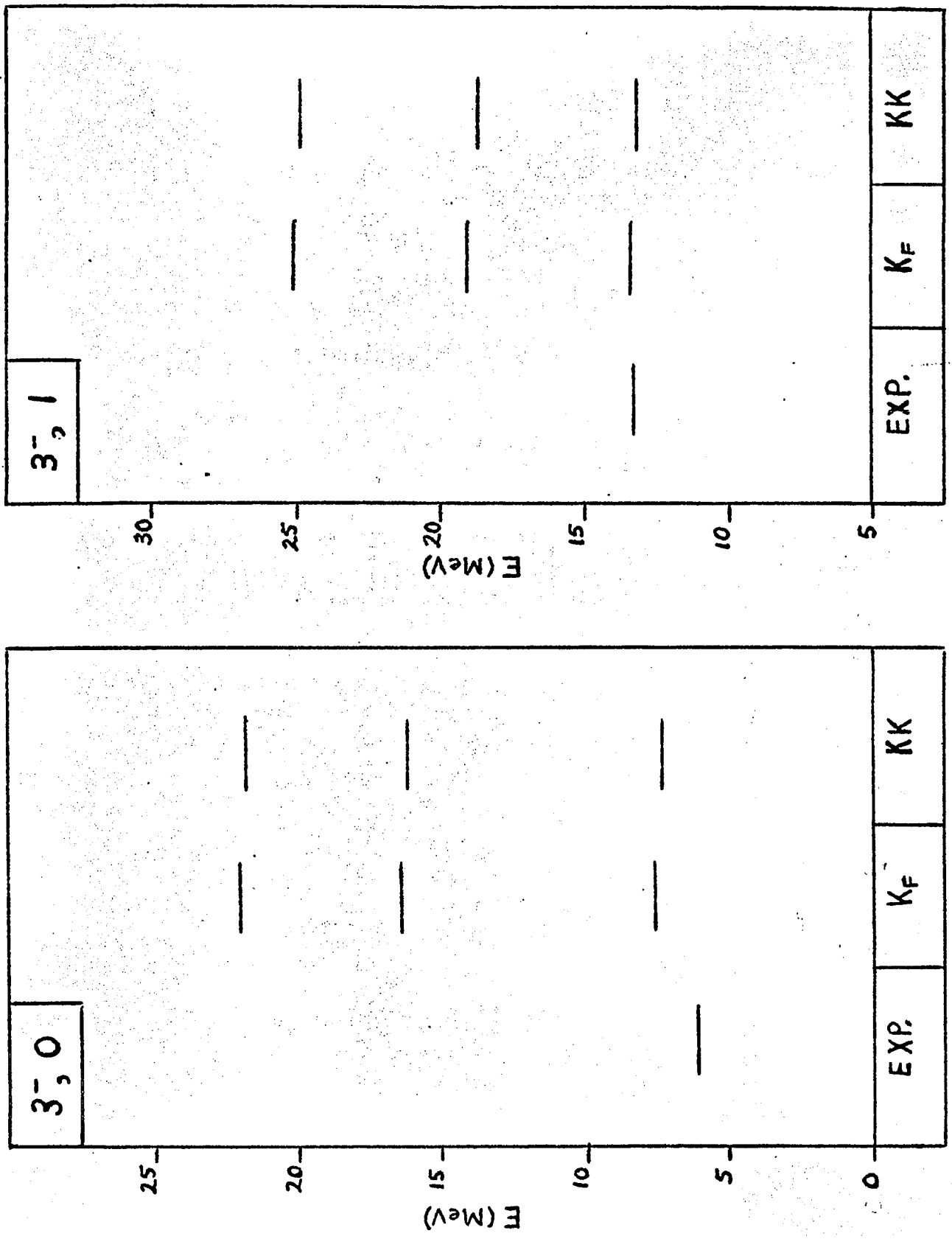
3⁻, 1
3⁻, 0
EXP.
K_F
KK
E (MeV)
0
5
10
15
20
25
30

Table 3.4

The energy levels and wavefunctions for the odd-parity states from the present calculation (ϵ = 86.0 MeV, $\hbar\omega$ = 13.4 MeV). The phases of the wavefunctions are defined in Appendix A. The last columns in the table are the ground state correlation amplitudes

$J^\pi, T = 0^-, 0$

E	Approx	$0p_{3/2}^{-1} 0d_{3/2}$	$0p_{1/2}^{-1} 1s_{1/2}$	$0p_{3/2}^{-1} 0d_{3/2}$	$0p_{1/2}^{-1} 1s_{1/2}$
13.41	TDA	0.064	0.998		
13.41	RPA	0.064	0.998	-0.003	0.001
25.56	TDA	0.998	-0.064		
25.54	RPA	0.998	-0.064	0.019	-0.004

$J^\pi, T = 0^-, 1$

E	Approx	$0p_{3/2}^{-1} 0d_{3/2}$	$0p_{1/2}^{-1} 1s_{1/2}$	$0p_{3/2}^{-1} 0d_{3/2}$	$0p_{1/2}^{-1} 1s_{1/2}$
14.22	TDA	0.097	0.995		
14.21	RPA	0.096	0.995	0.005	-0.012
27.93	TDA	0.995	-0.097		
27.80	RPA	0.996	-0.096	-0.046	0.010

$J^{\pi},T = 1^{-},0$

E	Approx	$0p_{3/2}^{-1}\,0d_{5/2}$	$0p_{3/2}^{-1}\,1s_{1/2}$	$0p_{3/2}^{-1}\,0d_{3/2}$	$0p_{1/2}^{-1}\,1s_{1/2}$	$0p_{1/2}^{-1}\,0d_{3/2}$	$0p_{3/2}^{-1}\,0d_{5/2}$	$0p_{3/2}^{-1}\,1s_{1/2}$	$0p_{3/2}^{-1}\,0d_{3/2}$	$0p_{1/2}^{-1}\,1s_{1/2}$	$0p_{1/2}^{-1}\,0d_{3/2}$
0.65	TDA	0.702	0.274	-0.185	0.285	0.562					
i(7.70)	RPA	*									
10.67	TDA	-0.299	0.369	0.039	0.850	-0.225					
10.50	RPA	-0.251	0.394	0.030	0.870	-0.183	-0.072	0.005	0.022	0.005	-0.057
16.88	TDA	0.105	0.843	0.017	-0.416	-0.325					
16.88	RPA	0.107	0.843	0.017	-0.418	-0.321	-0.006	0.009	0.003	0.007	-0.006
18.29	TDA	-0.571	0.277	0.228	-0.140	0.724					
18.28	RPA	-0.565	0.276	0.226	-0.140	0.731	-0.020	0.001	-0.006	-0.002	-0.009
24.54	TDA	0.283	-0.043	0.955	0.061	-0.049					
24.51	RPA	0.287	-0.043	0.954	0.061	-0.045	0.000	-0.005	0.015	0.001	-0.018

* Eigenvalue is imaginary.

$J^{\pi}, T = 1^{-}, 1$

E	Approx	$0p_{3/2}^{-1}\,0d_{5/2}$	$0p_{3/2}^{-1}\,1s_{1/2}$	$0p_{3/2}^{-1}\,0d_{3/2}$	$0p_{1/2}^{-1}\,1s_{1/2}$	$0p_{1/2}^{-1}\,0d_{3/2}$	$0p_{3/2}^{-1}\,0d_{5/2}$	$0p_{3/2}^{-1}\,1s_{1/2}$	$0p_{3/2}^{-1}\,0d_{3/2}$	$0p_{1/2}^{-1}\,1s_{1/2}$	$0p_{1/2}^{-1}\,0d_{3/2}$
14.39	TDA	-0.149	-0.053	-0.038	0.986	0.017					
14.38	RPA	-0.148	-0.053	-0.038	0.987	0.016	-0.002	0.011	-0.001	-0.002	0.002
18.50	TDA	-0.319	-0.206	0.264	-0.064	0.884					
18.47	RPA	-0.314	-0.204	0.257	-0.062	0.889	-0.021	-0.002	0.014	0.002	0.006
20.69	TDA	-0.306	0.929	0.203	0.011	0.046					
20.67	RPA	-0.316	0.926	+0.201	0.009	0.043	-0.006	0.004	0.009	0.011	-0.010
24.87	TDA	0.873	0.204	0.305	0.150	0.283					
24.59	RPA	0.879	0.225	0.269	0.150	0.296	0.036	0.014	-0.035	0.005	0.054
21.31	TDA	-0.142	-0.223	0.891	0.007	-0.368					
27.13	RPA	-0.107	-0.217	0.906	0.013	-0.351	-0.056	-0.003	-0.014	-0.012	-0.007

$J^{\pi}, T = 2^{-}\ 0$

E	Approx	$0p_{3/2}^{-1}\ 0d_{5/2}$	$0p_{3/2}^{-1}\ 1s_{1/2}$	$0p_{3/2}^{-1}\ 0d_{3/2}$	$0p_{1/2}^{-1}\ 0d_{5/2}$	$0p_{1/2}^{-1}\ 0d_{3/2}$	$0p_{3/2}^{-1}\ 0d_{5/2}$	$0p_{3/2}^{-1}\ 1s_{1/2}$	$0p_{3/2}^{-1}\ 0d_{3/2}$	$0p_{1/2}^{-1}\ 0d_{5/2}$	$0p_{1/2}^{-1}\ 0d_{3/2}$
12.22	TDA	0.288	0.052	-0.026	0.949	0.115					
12.20	RPA	0.288	0.052	-0.027	0.949	0.116	-0.023	-0.002	0.001	0.002	-0.008
16.46	TDA	0.453	-0.073	-0.157	-0.239	0.841					
16.45	RPA	0.456	-0.073	-0.157	-0.241	0.839	-0.009	0.001	0.014	-0.016	-0.002
18.54	TDA	0.728	-0.450	-0.095	-0.140	-0.489					
18.53	RPA	0.730	-0.443	-0.095	-0.140	-0.492	0.005	0.002	0.002	-0.013	-0.013
19.88	TDA	0.369	0.884	-0.161	-0.142	-0.192					
19.87	RPA	0.364	0.887	-0.160	-0.140	-0.190	0.005	0.002	0.003	-0.010	-0.008
23.29	TDA	0.214	0.093	0.969	-0.051	0.059					
23.28	RPA	0.213	0.092	0.970	-0.050	0.060	0.009	0.002	0.001	-0.009	0.007

$J^{\pi}, T = 2^{-}, 1$

E	Approx	$0p_{3/2}^{-1}\,0d_{5/2}$	$0p_{3/2}^{-1}\,1s_{1/2}$	$0p_{3/2}^{-1}\,0d_{3/2}$	$0p_{1/2}^{-1}\,0d_{5/2}$	$0p_{1/2}^{-1}\,0d_{3/2}$	$0p_{3/2}^{-1}\,0d_{5/2}$	$0p_{3/2}^{-1}\,1s_{1/2}$	$0p_{3/2}^{-1}\,0d_{3/2}$	$0p_{1/2}^{-1}\,0d_{5/2}$	$0p_{1/2}^{-1}\,0d_{3/2}$
13.68	TDA	0.252	0.093	0.076	0.960	-0.021					
13.64	RPA	0.243	0.091	0.074	0.963	-0.021	0.017	0.004	0.018	-0.028	-0.002
18.26	TDA	0.270	-0.025	-0.089	-0.041	0.958					
18.23	RPA	0.264	-0.022	-0.084	-0.037	0.960	-0.001	0.000	-0.010	0.004	-0.030
19.66	TDA	-0.608	0.763	0.027	0.088	0.198					
19.64	RPA	-0.627	0.749	0.029	0.090	0.196	0.018	-0.002	-0.001	-0.014	-0.011
21.59	TDA	0.658	0.614	-0.320	-0.211	-0.208					
21.52	RPA	0.652	0.633	-0.304	-0.207	-0.200	-0.029	-0.010	-0.002	0.023	0.016
24.45	TDA	0.247	-.177	0.940	-0.156	0.015					
24.39	RPA	0.234	0.172	0.946	-0.149	0.017	-0.013	-0.006	-0.011	0.031	-0.008

$J^{\pi},T = 3^{-},0$

E	Approx	$0p_{3/2}^{-1}\ 0d_{5/2}$	$0p_{3/2}^{-1}\ 0d_{3/2}$	$0p_{1/2}^{-1}\ 0d_{5/2}$	$0p_{3/2}^{-1}\ 0d_{5/2}$	$0p_{3/2}^{-1}\ 0d_{3/2}$	$0p_{1/2}^{-1}\ 0d_{5/2}$
8.50	TDA	0.306	-0.263	0.915			
7.59	RPA	0.351	-0.304	0.918	0.118	-0.113	0.177
16.48	TDA	0.898	-0.237	-0.369			
16.36	RPA	0.884	-0.245	-0.402	0.029	-0.039	0.042
22.03	TDA	0.314	0.935	0.164			
21.96	RPA	0.331	0.929	0.170	-0.022	0.032	-0.020

$J^{\pi},T = 3^{-},1$

E	Approx	$0p_{3/2}^{-1}\ 0d_{5/2}$	$0p_{3/2}^{-1}\ 0d_{3/2}$	$0p_{1/2}^{-1}\ 0d_{5/2}$	$0p_{3/2}^{-1}\ 0d_{5/2}$	$0p_{3/2}^{-1}\ 0d_{5/2}$	$0p_{3/2}^{-1}\ 0d_{5/2}$
13.50	TDA	-0.161	0.009	0.987			
13.44	RPA	-0.151	+0.007	+0.989	+0.009	-0.040	+0.004
19.07	TDA	0.981	0.113	0.159			
19.02	RPA	0.983	0.106	0.151	0.020	-0.025	+0.009
25.25	TDA	-0.110	0.994	-0.026			
25.15	RPA	-0.104	0.996	-0.024	-0.022	0.006	-0.044

Among the remaining levels, the most pronounced discrepancy is with the 0^- levels. It is known[25] that the tensor force contributes with opposite sign to the central force shifting the 0^- levels down towards the experimental positions. The 1^-,1 spectrum has nearly the correct relative spacing of levels but the levels are shifted upwards relative to the experimental spectrum. One should not attribute too much significance to the relative spacing of levels since the positions of the states, which are believed to be described by the particle-hole model, are largely determined by the unperturbed energies of the dominant configurations. This can be seen from the data in Table 3.5. The lowest T=1 levels are nearly pure configurations and the energy shifts are small. These levels, apart from the role of the tensor force, are not sensitive to the interaction. The 17.3 (1^-,1) and 19.5 (2^-,1) MeV states do contain significant configuration mixing since there are three relatively close spaced unperturbed configurations at 16.59, 17.65 and 18.52 MeV.

Comparing the present results with the spectra for the Kallio-Kolltveit interaction it can be seen that amongst the levels which are known experimentally only the giant dipole states differ significantly. There are several differences for the other states. It can be seen by comparing Tables 3.1 and 3.6 that there are real differences between K_F and the Kallio-Kolltveit interaction. $^1K_0$ and $^3K_0$ are more attractive in the n'=n=0 state and less attractive in the other states.

Table 3.5

The positions of the particle-hole states relative to the unperturbed energies of the dominant configuration

J^{π},T	Exp. (MeV)	Unpert. Energy (MeV)	ΔE_{exp}	Unperturbed Configuration	Calc. Energy (MeV)	ΔE_{calc}	Calculated Configuration
$0^-,0$	10.95	12.38	-1.43	$0p_{1/2}^{-1},1s_{1/2}$	13.41	+1.03	$0.998(0p_{1/2}^{-1},1s_{1/2})$
$0^-,1$	12.78	12.38	$\pm$0.40	$0p_{1/2}^{-1},1s_{1/2}$	14.21	+1.83	$0.995(0p_{1/2}^{-1},1s_{1/2})$
$1^-,1$	13.10	12.38	+0.72	$0p_{1/2}^{-1},1s_{1/2}$	14.38	+2.00	$0.987(0p_{1/2}^{-1},1s_{1/2})$
$1^-,1$	17.3	16.59	+0.71	$0p_{1/2}^{-1},0d_{3/2}$	18.47	+1.88	$0.889(0p_{1/2}^{-1},0d_{3/2})$
$2^-,0$	12.52	11.51	+1.01	$0p_{1/2}^{-1},0d_{5/2}$	12.20	+0.69	$0.949(0p_{1/2}^{-1},0d_{5/2})$
$2^-,1$	12.96	11.51	+1.45	$0p_{1/2}^{-1},0d_{5/2}$	13.64	+2.13	$0.963(0p_{1/2}^{-1},0d_{5/2})$
$2^-,1$	19.5	18.52	+0.98	$0p_{3/2}^{-1},1s_{1/2}$	19.64	+0.14	$0.749(0p_{3/2}^{-1},1s_{1/2})$
$3^-,1$	13.26	11.51	+1.75	$0p_{1/2}^{-1},0d_{5/2}$	13.44	+1.93	$0.987(0p_{1/2}^{-1},0d_{5/2})$

Table 3.6

Radial integrals for the Kallio-Kolltveit interaction taken from reference 7

n	n'	$^1S_0$	$^3S_1$
0	0	-6.07	-9.15
0	1	-5.34	-9.71
0	2	-4.30	-7.12
1	1	-5.01	-8.28
1	2	-4.18	-7.18
2	2	-3.68	-6.67

That the corresponding spectra do not reflect these differences is because the positions of the levels are mainly determined by the unperturbed energies.

It is instructive to examine the role of the higher energy components of K_F in determining the particle-hole spectra. It has been found that the low energy properties of the nucleon-nucleon interaction are dominant in determining the spectra of O^{18} and F^{18}.[16] This is because the contributions of the repulsive terms to the n=n'=0 matrix element is small. In Table 3.7 the separate contributions of attractive and repulsive terms in K_F to the matrix elements required for the particle-hole spectra are listed. The longer range attractive terms, which are mainly determined by the low energy

scattering data, are more like the Kallio-Kolltveit interaction. The off-diagonal integrals n=0; n'=1,2 are still smaller but the others are more or less uniformly larger. The shorter range repulsive terms make an almost negligible contribution to the n=n'=0 integrals and the contribution increases with n and n'. Bhaduríe and Tomusiak[33] and Mavromatis, Markiewicz and Green[27] have found that using a state dependent separation distance for the Kallio-Kolltveit interaction also decreases the radial integrals for higher n quantum numbers. If the particle-hole spectra are sensitive to the higher energy components of the nucleon-nucleon interaction, the sensitivity will be manifested in a dependence on the higher n and n' radial integrals. To examine this dependence we used only the attractive terms of $^1K_0$ and $^3K_0$ as an effective interaction. The results are compared with those of the correct K_F in Table 3.8. Most of the levels are only slightly affected while the lowest $3^-,0$ state is shifted by 1.4 MeV.

Table 3.7

The contributions of the attractive and repulsive parts of the free reaction matrices to the radial integrals

n	n'	$\langle n \| {}^1K_0 \| n' \rangle$		$\langle n \| {}^3K_0 \| n' \rangle$	
		-	+	-	+
0	0	-7.480	+0.446	-11.673	+0.574
0	1	-5.035	+1.013	-8.890	+1.091
0	2	-3.423	+1.189	-6.632	+1.516
1	1	-5.506	+1.313	-9.244	+1.687
1	2	-4.450	+1.728	-7.930	+2.184
2	2	-4.566	+2.192	-7.895	+2.731

Table 3.8

Comparison of the particle-hole spectra calculated with K_F and K_F (no repulsion) in the RPA

J^π,T	K_F	K_F(no repulsion)
0^-,0	13.41, 25.54	13.50, 25.76
0^-,1	14.21, 27.80	14.34, 28.07
1^-,0	10.50, 16.88, 18.28, 24.51	10.07, 16.85, 18.28, 24.66
1^-,1	14.38, 18.47, 20.67, 24.59, 27.13	14.52, 18.47, 20.82, 24.86, 27.35
2^-,0	12.20, 16.45, 18.53, 19.87, 23.28	12.31, 16.63, 18.72, 19.98, 23.36
2^-,1	13.63, 18.23, 19.64, 21.52, 24.39	13.66, 18.35, 19.79, 21.66, 24.48
3^-,0	7.59, 16.36, 21.96	6.15, 16.18, 22.00
3^-,1	13.44, 19.02, 25.15	13.61, 19.12, 25.45

3-E Electromagnetic Transitions in O^{16}

The formulae for calculating transition probabilities in the particle-hole model are given in Appendix A. In Table 3.9 the reduced transition probabilities for transitions to the ground state are tabulated. The transition probabilities were calculated in the TDA with no effective charge. Transition probabilities are not given for the $1^-,0$ states since $\Delta T=0$ dipole transitions are forbidden by isospin selection rules.[34] There is very little data available for levels above 10 MeV.

The octupole and giant dipole transition strengths are enhanced as predicted by the schematic model.[20] Experimentally, the B(E3) for the 6.13 MeV $(3^-,0)$ transition is 209.5 e^2fm^6. In the present calculation the B(E3) is 67.8 and 120.9 e^2fm^6 in the TDA and RPA, respectively. The dipole strength is almost completely concentrated in the two highest states which are in the region of the giant dipole resonance.[35] It is well known that the shell model gives too large a contribution to the dipole sum rule. Shakin and de Providencia[36] have shown that the correlations in the RPA ground state give Pauli corrections which decrease considerably the dipole transitions strength.

The $2^-,1$ states indicate the existence of a giant magnetic quadrupole resonance. The magnetic resonance has been observed in inelastic electron scattering.[37] The Saskatchewan group[38] have assigned the 19.08 MeV state $J^\pi = 2^-,1$. Unfortunately, the spin-parity assignment can only be made by a model dependent analysis of

Table 3.9

The reduced transition probabilities B(E-M,1) for the transition $J^{\pi},T \rightarrow$ g.s. in the TDA

J^{π},T	E	B(E-M,L)	Exp†	J^{π},T	E	B(E-M,L)
$2^-,0$	12.22	0.01	0.600	$1^-,1$	14.39	0.024
$2^-,0$	16.46	5.26		$1^-,1$	18.50	0.013
$2^-,0$	18.54	3.47		$1^-,1$	20.69	0.008
$2^-,0$	19.88	6.83		$1^-,1$	24.87	0.941
$2^-,0$	23.29	0.74		$1^-,1$	27.31	0.438
$3^-,0$	8.50	67.83	209.5	$2^-,1$	12.22	37.45
$3^-,0$	16.48	14.97		$2^-,1$	16.46	3.75
$3^-,0$	22.03	10.44		$2^-,1$	18.54	8.36
				$2^-,1$	19.88	193.2
				$2^-,1$	23.29	88.4
				$3^-,1$	13.50	21.58
				$3^-,1$	19.07	25.91
				$3^-,1$	25.25	45.78

† reference 39

the transverse magnetic form factor. The present calculation indicates that the resonance would be in the vicinity of 20 MeV and split between the $(p_{3/2}^{-1},d_{5/2})$ and $(p_{3/2}^{-1},d_{3/2})$ configurations as in the case of the giant dipole resonance.

The $2^-,0$ states at 8.88 MeV and 12.52 MeV decay to the ground state by M2 radiation with reduced transition probabilities of 0.55 $\mu_0^2 fm^2$ and 0.60 $\mu_0^2 fm^2$, respectively.[39] The lowest $2^-,0$ state (12.22 MeV) in the present calculation has a $B(M^2)$ of 0.01 $\mu_0^2 fm^2$.

In this transition there is a very sensitive cancellation between the $(p_{3/2}^{-1}, d_{5/2})$ and $(p_{1/2}^{-1}, d_{5/2})$ components. All of the calculations with realistic forces have the lowest $2^-,0$ state in the vicinity of 12 MeV. The phenomenological calculations of Elliott and Flowers and Gillet and Vinh Mau have the lowest state near 10.5 MeV. Recently, Gill et al.[40] have concluded that the particle-hole state in Elliott and Flower's calculation is in reasonable agreement with the decay properties of the 8.88 MeV state. On the other hand, the $O^{16}(p,p')$ experiments of Hasselgren et al.[41] indicate that the 8.88 MeV state does not contain an appreciable one-particle-one-hole component. The theoretical and experimental evidence favor assigning the 12.52 MeV state the structure of the lowest particle-hole state.

3-F Electromagnetic Transitions in N^{16}

The quartet of lowest T=1 states in O^{16} are unstable against particle emission and contain isobaric spin mixing from nearby T=0 states. The analogue states in N^{16} are stable against particle emission and do not contain T=0 admixtures. An analysis of electromagnetic transitions among the levels in N^{16} provides a test of the wavefunctions calculated in O^{16} assuming isotopic spin as a good quantum number. In the absence of Coulomb effects the amplitudes of the neutron particle-proton hole configurations in the N^{16} states are the same as those calculated for O^{16}. Coulomb effects are present and result in a relative shifting of the analogue states in the A=16 multiplet. The Coulomb shifts have been discussed by Elliott and Flowers and Tombrello. We have used the calculated O^{16} ampli-

tudes to calculate the transition probabilities in N^{16}. The states are nearly the pure particle-hole configurations given in Fig. 3-4. The decay scheme of the states is shown in Fig. 3-3 and the experimental branching[30] is given in Table 3.10.

Table 3.10

Experimental gamma-branching in N^{16}

γ	Mode	Branching (%)
γ_1	E2	100
γ_2	E2+M1	100
γ_3	M3	< 2
γ_4	E2+M1	25
γ_5	M1	75
γ_6	E2	< 2

The experimental[39] B(E2) for the $0^- \rightarrow 2^-$ transition is 4.1 e^2fm^4. With no effective charge the calculated B(E2) was 0.074 e^2fm^4. The transition probability can be expressed in terms of the single-particle transitions of the neighboring nuclei N^{15} and O^{17}. The main contribution is from the $s_{1/2} \rightarrow d_{5/2}$ neutron particle transition with a small amplitude for the $p_{1/2} \rightarrow p_{3/2}$ proton hole transition.[39] With the experimental values for the single-particle

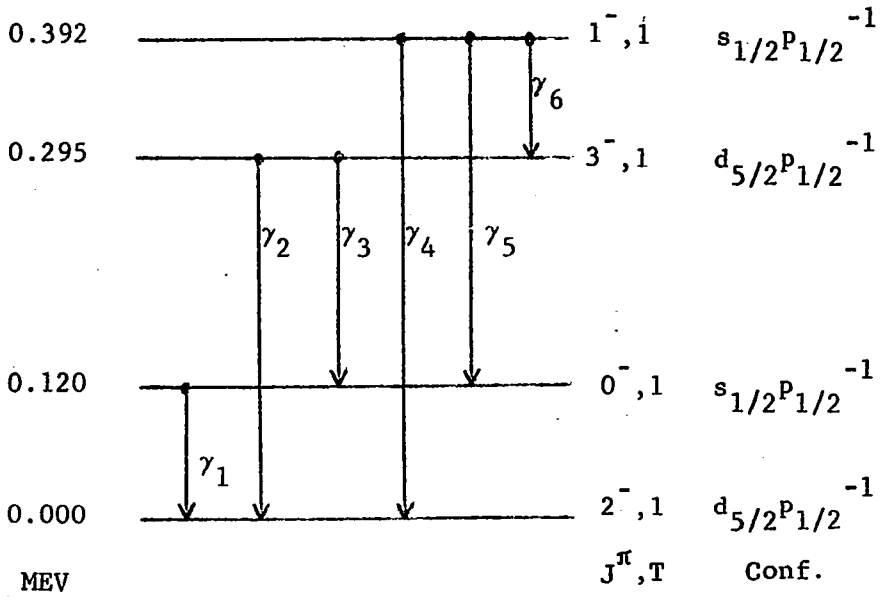

Fig. 3-3. The electromagnetic transitions in N^{16}.

transitions the N^{16} B(E2) is 7.1 e^2fm^4. The proton hole transition probability is not well known experimentally, however, it enters with an amplitude of 0.092 whereas the neutron particle transition has an amplitude of 0.955. Assuming that the O^{17} neutron effective charge arises from a polarization of the charged core and is proportional to Z, the N^{16} B(E2) is reduced to 5.7 e^2fm^4. A similar treatment of the γ_2, γ_4 and γ_6 E2 decay modes does not enhance them sufficiently to compete with the M1 decay modes.

In the last column of Table 3.11 the decay widths of the levels are given. The widths were calculated using the experimental energies of the levels. The calculated widths are in agreement with the experimental results for the γ_2, γ_3 and γ_6 branching of the decay scheme. The branching ratio γ_5/γ_4 is 3 while the calculated value is 0.9. The γ_4 M1 decay is very sensitive to small amplitudes in the wavefunctions since the dominant configurations $|s_{1/2},p_{1/2}^{-1}> \rightarrow |d_{5/2},p_{1/2}^{-1}>$ cannot contribute to the transition.

3-G Summary

The particle-hole spectra calculated with the relative S state free reaction matrices is in reasonable agreement with experiment. The positions of the levels that are predicted by the particle-hole model are mainly determined by the unperturbed energies of the dominant configurations. These particle-hole levels are fairly insensitive to the structure of the interaction. On the other hand, the collective octupole and giant dipole states are very sensitive to the interaction and the model used. Only the collective octupole

state is sensitive to the higher energy components in K_F. This sensitivity is not unique since the octupole state is sensitive to all aspects of the interaction and model.

Table 3.11

Calculated gamma decay widths in N^{16}

Trans	Mode	$B(L,\pi)$ $e^2 f_m^{2L} - \mu_0^2 f_m^{2L-2}$	$\Gamma^n_{L,\pi}/B(L,\pi)$	$\Gamma^n_{L,\pi}$ (eV)
γ_1	E2	0.074	0.201×10^{-10}	1.49×10^{-12}
γ_2	M1	0.548	0.297×10^{-3}	1.63×10^{-4}
	E2	0.053	0.180×10^{-8}	9.54×10^{-11}
γ_3	M3	571	0.209×10^{-19}	1.19×10^{-17}
γ_4	M1	0.085	0.696×10^{-3}	6.75×10^{-5}
	E2	0.006	0.746×10^{-8}	4.48×10^{-11}
γ_5	M1	0.258	0.232×10^{-3}	5.92×10^{-5}
γ_6	E2	0.044	0.695×10^{-11}	3.06×10^{-13}

CHAPTER 4

SINGLE-PARTICLE POTENTIALS AND WAVEFUNCTIONS FOR SHELL MODEL CALCULATIONS

4-A Introduction

Shell model calculations with realistic forces are usually performed for either closed or nearly closed shell nuclei. It is clearly of interest to learn the additional effect of using more realistic single-particle wavefunctions than the conventional harmonic oscillator field. To this end Woods-Saxon potentials with a Thomas spin-orbit term have been fitted to the experimentally observed single-particle energies. Potentials and wavefunctions have been determined for nuclei with A = 15, 16, 17, 39, 40, 41, 207, 208 and 209. It seems best to perform shell model calculations by expanding Woods-Saxon wavefunctions in terms of harmonic oscillator functions. Obvious modifications in the wavefunctions are produced by introducing a finite well. It is vital to see that the nuclear radius is correctly described by the more realistic single particle wavefunctions. The size of the valence orbits plays a large role in determining the energy scale for the inter-valence-nucleon interaction. The only direct experimental information on nuclear sizes comes from measurement of the r.m.s. radius of the nuclear charge distribution. In a shell model description of nuclei the single-particle potential radius for protons can be determined by requiring the r.m.s. radius, calculated using single-particle wavefunctions,

to be consistent with the observed r.m.s. radius of the charge distribution. There is very little experimental information on the neutron distribution in nuclei. However, some information can be obtained about the size of valence neutron orbits by appealing to the Coulomb energy shift deduced from the positions of analogue states. This method has been used by Nolen et. al.[43] for nuclear size determinations in the calcium region. The above methods were used to determine well radii in the calculations presented in this chapter.

4-B The Potential and Wavefunctions

For a harmonic oscillator (HO) potential the single-particle Hamiltonian is

$$H_{ho} = \frac{p^2}{2m} + \frac{1}{2} m\omega^2 r^2 \qquad (4.1)$$

which satisfies the Schrodinger equation

$$H_{ho}\, \varphi_{n\ell m}(\underline{r}) = \epsilon_{n\ell}\, \varphi_{n\ell m}(\underline{r}) \qquad (4.2)$$

where

$$\epsilon_{n\ell} = (2n+\ell+3/2)\hbar\omega$$

$$\varphi_{n\ell m}(\underline{r}) = R_{n\ell}(r) Y_{\ell m}(\theta,\varphi)$$

and

$$\int \varphi^{*}_{n\ell m}(\underline{r})\varphi_{n\ell m}(\underline{r})\, d\underline{r} = 1 \quad .$$

The radial oscillator function $R_{n\ell}(r)$ is defined in Appendix B. Since the HO potential doesn't contain a spin-orbit term, the single-particle energies are taken from experiment and states of total angular momentum (j,m) are constructed from HO wavefunctions with an appropriate size parameter

$$\alpha = \left(\frac{m\omega}{\hbar}\right)^{\frac{1}{2}} \quad . \tag{4.3}$$

The wavefunctions are then

$$\psi_{n\ell jm}(\underline{r}) = \sum_{\substack{m' \\ m_s}} < \ell\tfrac{1}{2}m'm_s | jm > \varphi_{n\ell m'}(\underline{r})\chi_{m_s}^{\frac{1}{2}} \quad . \tag{4.4}$$

For finite potentials we take a Woods-Saxon (WS) shape with a Thomas spin orbit† term,

$$V(r) = -V_o f(r) + V_{so}\left(\frac{\hbar}{m_\pi c}\right)^2 \frac{2}{r}\frac{d}{dr} f(r)\ell\cdot\sigma + V_c(r) \tag{4.5}$$

where

$$f(r) = \left[1+\exp\left(\frac{r-R}{a}\right)\right]^{-1} \tag{4.6}$$

and

$$\begin{aligned} V_c(r) &= \frac{Ze^2}{2R_u}\left[3-\left(\frac{r}{R_u}\right)^2\right] && r \leq R_u \\ &= \frac{Ze^2}{r} && r \geq R_u \end{aligned} \quad . \tag{4.7}$$

The Coulomb potential (4.7) is that of an equivalent uniform charged sphere of the same r.m.s. radius as the actual nuclear charge distribution. With this potential the single-particle Hamiltonian is

$$H_{WS} = \frac{p^2}{2m} + V(r) \tag{4.8}$$

which defines the Schrödinger equation

$$H_{WS}\,\psi_{\nu\ell jm}(\underline{r}) = \epsilon_{\nu\ell j}\psi_{\nu\ell jm}(r)$$

---

† In the calculations $\left(\frac{\hbar}{m_\pi c}\right)^2 = 2.0\ \text{fm}^2$.

where

$$\psi_{\nu\ell jm}(\underline{r}) = \sum_{\substack{m' \\ m_s}} < \ell \tfrac{1}{2} m' m_s | jm > y_{\nu\ell j}(r) Y_{\ell m}(\theta,\varphi) \chi_{m_s}^{\frac{1}{2}} \qquad (4.9)$$

and

$$\int \psi_{\nu\ell jm}^{*}(\underline{r}) \psi_{\nu\ell jm}(\underline{r}) d\underline{r} = 1 \quad .$$

The radial wavefunction $y_{\nu\ell j}(r)$ is the solution of the equation

$$\left\{ -\frac{\hbar^2}{2m}\left[\frac{1}{r}\frac{d^2}{dr^2} r - \frac{\ell(\ell+1)}{r^2}\right] + V(r) - \epsilon_{\nu\ell j} \right\} u_{\nu\ell j}(r) = 0 \qquad (4.10)$$

Making the substitution

$$y_{\nu\ell j}(r) = r\, u_{\nu\ell j}(r) \qquad (4.11)$$

Eq. (4.10) becomes

$$\left\{ -\frac{\hbar^2}{2m}\frac{d^2}{dr^2} + \frac{\hbar^2}{2m}\frac{\ell(\ell+1)}{r^2} - V_o f(r) + V_{so}\left(\frac{\hbar}{m_\pi c}\right)^2 \frac{2}{r}\frac{d}{dr} f(r)\, \underline{\ell}\cdot\underline{\sigma} + V_c(r) - \epsilon_{\nu\ell j} \right\}$$

$$y_{\nu\ell j}(r) = 0 \quad . \qquad (4.12)$$

The eigenvalues of the operator $\underline{\ell}\cdot\underline{\sigma}$ are

$$< \underline{\ell}\cdot\underline{\sigma} > = \ell \quad , \quad j = \ell + \tfrac{1}{2}$$

$$= -\ell - 1 \quad , \quad j = \ell - \tfrac{1}{2} \quad . \qquad (4.13)$$

The radial function $y_{\nu\ell j}(r)$ was obtained by numerical integration of (4.12). The solution is in units of $fm^{-\frac{1}{2}}$ and is normalized in the fashion

$$\int_0^\infty |y_{\nu\ell j}(r)|^2 dr = 1 \quad . \qquad (4.14)$$

For tabulating the $y_{\nu\ell j}(r)$ and for calculations with (4.9) as basis states it is useful to expand $y_{\nu\ell j}(r)$ in terms of the functions $R_{n\ell}(r)$. The oscillator functions of Eq. (4.2) are dimensionless and are an orthonormal set of functions in the principal quantum number n,

$$\int_0^\infty \alpha^3 R_{n\ell}(r) R_{m\ell}(r) r^2 dr = \delta_{mn} \quad . \tag{4.15}$$

It is convenient to write the size parameter α as

$$\alpha^2 = 0.0241145\hbar\omega \quad . \tag{4.16}$$

The expansion of $y_{\nu\ell j}(r)$ is

$$y_{\nu\ell j}(r) = \sum_{n=0}^{\infty} a_{n\ell j}(\hbar\omega)\alpha^{3/2} r\, R_{n\ell}(r) \tag{4.17}$$

where α is a free parameter. The coefficients $a_{n\ell j}(\hbar\omega)$ are dimensionless and are determined by overlap integrals,

$$a_{n\ell j}(\hbar\omega) = \int_0^\infty \alpha^{3/2} r\, R_{n\ell}(r)\, y_{\nu\ell j}(r) dr \quad . \tag{4.18}$$

From the normalizations (4.14) and (4.15) we have

$$\int_0^\infty |y_{\nu\ell j}(r)|^2 dr = 1 = \sum_{n=0}^{\infty} |a_{n\ell j}(\hbar\omega|^2 \quad . \tag{4.19}$$

In practice the number of terms required in the expansion (4.17) is not large; in fact, the number of terms is minimized by choosing

a value of $\hbar\omega$ to maximize the overlap of the term $n = \nu$. This point is discussed further in the following sections. Using (4.17) we immediately have the single-particle states (4.90) as an expansion in oscillator states (4.4),

$$\psi_{\nu\ell j}(\underline{r}) = \sum_{n=0}^{\infty} a_{n\ell j}(\hbar\omega)\psi_{n\ell j}(\underline{r}) \quad . \tag{4.20}$$

4-C Nuclear Sizes

Experiments such as electron scattering are able to determine the size of the nuclear charge distribution $\rho_c(\underline{r})$.[44] For spherical nuclei the quantity measured is the root-mean-square radius defined by

$$< r^2 >_c^{\frac{1}{2}} = \left[\int \rho_c(r) r^2 d\underline{r}\right]^{\frac{1}{2}} = \left[4\pi \int_0^{\infty} \rho_c(r) r^4 dr\right]^{\frac{1}{2}} \quad . \tag{4.21}$$

A uniform charge distribution which gives the same low energy scattering as the actual nuclear charge distribution will have the same r.m.s. radius. The equivalent uniform charge distribution

$$\begin{aligned} \rho_c(r) &= \frac{3}{4\pi R_u^3} && r \leq R_u \\ &= 0 && r \geq R_u \end{aligned} \tag{4.22}$$

has an r.m.s. radius

$$< r^2 >_c^{\frac{1}{2}} = \left(\frac{3}{5}\right)^{\frac{1}{2}} R_u \quad . \tag{4.23}$$

The "equivalent radius" is then

$$R_u = \left(\frac{5}{3}\right)^{\frac{1}{2}} < r^2 >_c^{\frac{1}{2}} \tag{4.24}$$

where $< r^2 >_c^{\frac{1}{2}}$ is the measured r.m.s. radius of the charge distribution. Measured r.m.s. radii and equivalent radii for some of the nuclei we will consider are given in Table 4.1.

Table 4.1

Charge radii for various nuclei

Nucleus	$< r^2 >_c^{\frac{1}{2}}$ (fm)	R_u	Experiment	Ref.
N^{14}	2.46	3.18	Elect. Scatt.	a
O^{16}	2.71	3.50	Elect. Scatt.	a
O^{18}	2.77	3.58	Elect. Scatt.	a
Ca^{40}	3.50	4.51	Elect. Scatt.	a
Ca^{42}	3.53	4.56	Elect. Scatt.	a
Tl^{207}	5.480	7.07	Muonic X-ray	b
Pb^{206}	5.489	7.09	Muonic Xoray	b
Pb^{208}(nat)	5.493	7.09	Muonic X-ray	b
Bi^{209}	5.513	7.12	Muonic X-ray	b

a) H.R. Collard, L.R.B. Elton and R. Hofstadter, Nuclear Radii, Numerical Relationships in Science and Technology, New Series, Group 1, Vol. 2, ed. H. Schopper, Landolt-Bornstein, Springer-Verlag, 1967.

b) H.L. Acker, G. Backenstoss, C. Daum, J.C. Sens and S.A. De Witt Nucl. Phys. 87, 1 (1966).

We assume that the nuclei we consider are well described by neutrons and protons moving independently in average spherical potentials. With this assumption the charge distribution and the distribution of particle centres (matter distribution) can be obtained from the single-particle wavefunctions. For the potential (4.5) the proton and neutron matter distributions are, respectively,

$$\rho_p(r) = \frac{1}{4\pi}\frac{1}{Z}\sum_{(\nu\ell j)} (2j+1)\left|u_{\nu\ell j}^{\,p}(r)\right|^2 \qquad (4.25a)$$

and

$$\rho_n(r) = \frac{1}{4\pi}\frac{1}{N}\sum_{(\nu\ell j)} (2j+1)\left|u_{\nu\ell j}^{\,n}(r)\right|^2 \quad . \qquad (4.25b)$$

The total matter distribution is then

$$\rho(r) = \frac{Z}{A}\rho_p(r) + \frac{N}{A}\rho_n(r) \quad . \qquad (4.25c)$$

The proton matter distribution does not coincide with the charge distribution. To obtain the charge distribution the charge distribution of the proton itself must be folded into the matter distribution. The proton charge distribution is fitted by [44,45]

$$\rho_{prot}(r) = \frac{1}{\pi^{3/2} a_p^{\,3}} e^{-r^2/a_p^{\,2}} \qquad (4.26)$$

with $$a_p = 0.65 \text{ fm} \quad .$$

From (4.21) we have that

$$\langle r^2 \rangle_{prot.} = \frac{3}{2} a_p^{\,2}$$

$$= 0.63 \text{ fm}^2 \quad . \qquad (4.27)$$

The r.m.s. radius of the charge distribution is

$$\langle r^2 \rangle_c = \langle r^2 \rangle_p + \langle r^2 \rangle_{prot} \qquad (4.28)$$

where $\langle r^2 \rangle_p$ is obtained from (4.25a).

The gross behaviour of nuclear radii, as a function of mass number, can be represented by the well known "$A^{1/3}$ law". Recently, Elton[44] has reviewed the A dependence of matter and charge radii. Along the valley of maximum stability, the charge radius varies somewhat less than $A^{1/3}$. For isotopes and isotones the departures from an $A^{1/3}$ variation are large. The quantity used to measure deviations of the charge radius R_c from the $A^{1/3}$ law is

$$\gamma = \frac{3A}{R_c} \frac{dR_c}{dA} \quad .$$

If R_c is proportional to $A^{1/3}$ then $\gamma = 1$. For isotopes of spherical nuclei $\gamma \doteqdot 0.65$, while $\gamma \doteqdot 1.5$ for isotones. It has been suggested[45,47] that in a microscopic description of nuclei the deviation of γ from unity can be ascribed to the binding energy of the valence particles. Elton also points out that for mass radii the experimental evidence is not in conflict with an $A^{1/3}$ dependence.

4-D Harmonic Oscillator Potentials

When a HO potential is used as a single-particle potential the size parameter must be determined for each nucleus. One method of determining the size parameter is to require consistency with the observed r.m.s. radii discussed in the preceding section. For the purpose of comparison in later sections we determined HO potentials for O, Ca and Pb.

With HO function basis states all orbitals in the same shell have the same r.m.s. radius which we denote by

$$\begin{aligned} \langle r^2 \rangle_s^{\frac{1}{2}} &= \langle n\ell \| r^2 \| n\ell \rangle^{\frac{1}{2}} \\ &= \frac{(2n+\ell+3/2)^{\frac{1}{2}}}{\alpha} \\ &= \frac{n_s^{\frac{1}{2}}}{\alpha} \end{aligned} \tag{4.29}$$

where α is the size parameter (4.3). Denoting the number of neutrons and protons in an oscillator shell by N_s^n and N_s^p, the r.m.s. radii of neutrons and protons are

$$\langle r^2 \rangle_n^{\frac{1}{2}} = \left[\sum_s \frac{N_s^n n_s}{N\alpha} \right]^{\frac{1}{2}} \tag{4.30a}$$

and

$$\langle r^2 \rangle_p^{\frac{1}{2}} = \left[\sum_s \frac{N_s^p n_s}{Z\alpha} \right]^{\frac{1}{2}} \tag{4.30b}$$

respectively. For a nucleus consisting of A nucleons (A=N+Z) we have

$$\langle r^2 \rangle^{\frac{1}{2}} = \left[\sum_s \frac{(N_s^n + N_s^p)}{A\alpha} n_s \right]^{\frac{1}{2}} . \tag{4.30b}$$

In (4.30b) we assumed that the neutrons and protons were in wells of the same radius. The generalization to wells of different radii is obvious. The oscillator size parameters can be determined from (4.30) by using experimental values of the r.m.s. radii. We have

$$\hbar\omega_p = \frac{1}{\langle r^2 \rangle_p} \left(\frac{\hbar^2}{Zm} \right) \sum_s N_s^p n_s \tag{4.31a}$$

$$\hbar\omega_n = \frac{1}{< r^2 >_n} \left(\frac{\hbar^2}{Nm}\right) \sum_s N_s^n n_s \qquad (4.31b)$$

and

$$\hbar\omega = \frac{1}{< r^2 >} \left(\frac{\hbar^2}{Am}\right) \sum_s (N_s^n + N_s^p) n_s \ . \qquad (4.31c)$$

In Table 4.2 the occupied orbitals of the closed shell nuclei O^{16}, Ca^{40} and Pb^{208} are listed. Equations (4.31) were used to obtain $\hbar\omega$ values with proton matter radii deduced from the charge radii of Table 4.1. The results, assuming that the neutron and proton r.m.s. radii are the same, are listed in Table 4.3. With $< r^2 >_n = < r^2 >_p$ the N=Z nuclei, O^{16} and Ca^{40}, have the same HO potential for both neutrons and protons. However, for Pb^{208}, which has a neutron excess, the HO potentials have different radii for neutrons and protons. From Table 4.2 it can be seen that higher oscillator shells weight the r.m.s. radius heavily. Imposing the condition $< r^2 >_n = < r^2 >_p$ requires a neutron potential with a smaller radius. This immediately implies that in a single-particle representation isospin is no longer a good quantum number. This point will be discussed in the following sections.

Table 4.2

The Shell Model Single-Particle States

$2n+\ell$	$n\ell j$	$\Sigma n_s N_s$	ΣN_s	Nuclei
0	$0s_{1/2}$	3.0	2	
1	$0p_{3/2}$ $0p_{1/2}$	18.0	8	-------- N=8, Z=8; O^{16}
2	$0d_{5/2}$ $1s_{1/2}$ $0d_{3/2}$	60.0	20	-------- N=20, Z=20;Ca^{40}
3	$0f_{7/2}$ $1p_{3/2}$ $1p_{1/2}$ $0f_{5/2}$	150.0	40	
4	$0g_{9/2}$ $1d_{5/2}$ $2s_{1/2}$ $1d_{3/2}$ $0g_{7/2}$	315.0	70	
5	$0h_{11/2}$ $0h_{9/2}$ $1f_{7/2}$ $2p_{3/2}$ $2p_{1/2}$ $1f_{5/2}$	588.0	82 112	N=126, Z=82;Pb^{208}
6	$0i_{13/2}$ $1p_{9/2}$ $0i_{11/2}$ $2d_{5/2}$ $3s_{1/2}$ $2d_{3/2}$ $1g_{7/2}$	1008.0	126 168	
7	$0j_{15/2}$	1136.0	184	

Table 4.3

Harmonic Oscillator potential parameters assuming the neutron and proton matter radii to be the same

Nucleus	$\hbar\omega_p$	$\hbar\omega_n$
O^{16}	13.90	13.90
Ca^{40}	10.71	10.71
Pb^{208}	6.73	7.72

On the other hand, if one takes the neutron potential to be identical to the proton potential then $< r^2 >_n^{\frac{1}{2}} = 5.82$ fm. and for the nucleus $< r^2 >^{\frac{1}{2}} = 5.67$ fm. That is, both the neutron and the total matter distributions would be outside the charge distribution. For the charge distribution $< r^2 >_c^{\frac{1}{2}} = 5.493$ fm. (Table 4.1). Another relevant quantity in later discussions is the r.m.s. radius of the neutron excess in Pb^{208} with neutrons and protons in the same potentials $< r^2 >_{ne}^{\frac{1}{2}} = 6.48$ fm. and when the neutrons and protons have the same r.m.s. radii $< r^2 >_{ne}^{\frac{1}{2}} = 6.05$ fm.

4-E Isobaric Spin and Analogue States

In the absence of the Coulomb interaction the nucleon-nucleon interaction is very nearly charge independent.[48] Neglecting the Coulomb interaction it is useful to introduce the isobaric spin (isospin) quantum numbers and treat the neutron and proton as different

isospin states of the same particle. It is well known that the isospin operator $\vec{t}$ is a spherical tensor operator of rank one with components t_+, t_- and t_3. The components of $\vec{t}$ satisfy the same commutation relations as those of the spin operator $\vec{\sigma}$. First we briefly review the notation that will be used. The isospin part of the nucleon wavefunction is denoted by the ket $|t,t_3>$ and we define

$$|\text{proton}> \equiv |\tfrac{1}{2}+\tfrac{1}{2}>$$
$$|\text{neutron}> \equiv |\tfrac{1}{2}-\tfrac{1}{2}> \quad . \tag{4.32}$$

The isospin states are eigenstates of the operator t_3

$$t_3|\tfrac{1}{2} \pm \tfrac{1}{2}> = \pm\tfrac{1}{2}|\tfrac{1}{2}, \pm\tfrac{1}{2}> \tag{4.33a}$$

and t_+ and t_- satisfy

$$t_+|\tfrac{1}{2}+\tfrac{1}{2}> = 0 \ , \quad t_-|\tfrac{1}{2}-\tfrac{1}{2}> = 0$$
$$t_+|\tfrac{1}{2}-\tfrac{1}{2}> = |\tfrac{1}{2}+\tfrac{1}{2}> \ , \quad t_-|\tfrac{1}{2}+\tfrac{1}{2}> = |\tfrac{1}{2}-\tfrac{1}{2}> \ . \tag{4.33b}$$

For a many nucleon system the corresponding operators are

$$T_\pm = \sum_{i=1}^{A} t_\pm(i), \qquad T_3 = \sum_{i=1}^{A} t_3(i) \tag{4.34a}$$

and the total isospin is

$$\vec{T} = \sum_{i=1}^{A} \vec{t}(i) \quad . \tag{4.34b}$$

For a state $|T',T_3'>$ of the A nucleon system

$$T_\pm|T',T_3'> = [(T'\mp T_3')(T'\pm T_3+1)]^{\frac{1}{2}}|T', T_3'\pm 1> \ . \tag{4.35}$$

The eigenstates of the system are eigenfunctions of the operators T^2 and T_3 where

$$T^2 = T_+T_- + T_3{}^2 - T_3 \quad . \tag{4.36}$$

The eigenvalues are

$$< T^2 > \; = \; T'(T'+1)$$

and

$$< T_3 > = T_3' = \frac{(Z-N)}{2} \quad . \tag{4.37}$$

With the above definition of the isospin states we write the total wavefunctions for neutrons and protons as

$$|\text{neutron} > \equiv \psi_{\nu \ell j}{}^{n}(\underline{r}) \left|\tfrac{1}{2}-\tfrac{1}{2}\right>$$

and

$$|\text{proton} > \; \equiv \psi_{\nu \ell j}{}^{p}(\underline{r}) \left|\tfrac{1}{2}+\tfrac{1}{2}\right> \quad . \tag{4.38}$$

The necessary condition for isospin to be a valid quantum number is* that the space-spin parts of the wavefunctions be identified, i.e.,

$$\psi_{\nu \ell j}{}^{n}(\underline{r}) \; \equiv \; \psi_{\nu \ell j}{}^{p}(\underline{r}) \quad . \tag{4.39a}$$

In terms of the raising and lowering operators the condition is

$$< \text{neutron}|t_-|\text{proton} > = < \text{proton}|t_+|\text{neutron} > = 1 \; . \tag{4.39b}$$

The eigenfunctions of the charge independent nuclear Hamiltonian form multiplets of states with total isospin T and $-T \leq T_3 \leq T$. These eigenfunctions correspond to the states of different nuclei with the same number of nucleons but differing in the number of neutrons and protons. That is, the states differ only in their charge number and are called analogue states.[49] Analogue states are defined by introducing modified isospin raising and lowering operators.

---

* One should point out that the average field in which nucleons move could itself be isotopic spin dependent without destroying isospin invariance.

$$\mathcal{T}_+ = T_+ \frac{1}{[T^2-T_3^2-T_3]^{\frac{1}{2}}}$$

and (4.40)

$$\mathcal{T}_- = (\mathcal{T}_+)^+ = \frac{1}{[T^2-T_3^2-T_3]^{\frac{1}{2}}} T_-$$

where

$$[T^2-T_3^2-T_3]^{-\frac{1}{2}}|T'T_3'> = [(T'-T_3')(T'+T_3'+1)]^{-\frac{1}{2}}|T'T_3'> .$$

The state $|N-1,Z+1> \equiv |TT_3+1>$ which is the analogue of the state $|N,Z> \equiv |TT_3>$, is obtained by

$$|T\ T_3+1> = \mathcal{T}_+|T,T_3> \quad .$$

In the case of a nucleus the Hamiltonian is not charge independent because of the presence of the charge dependent Coulomb force

$$V_c(i,j) = \frac{e^2}{r_{ij}} (\tfrac{1}{2}-t_3(i))(\tfrac{1}{2}-t_3(j)) \quad . \tag{4.41}$$

Including the Coulomb force displaces the members of an isopsin multiplet in energy. The energy shift is readily calculated in perturbation theory using the eigenstates of isospin,[50]

$$M(T,T_3) = a+bT_3 + cT_3^2 \quad . \tag{4.42}$$

Equation (4.42) is the well known isobaric mass formula. In the absence of nuclear structure effects the mass difference of neighbouring members of a multiplet are related to the Coulomb energy shift ΔE_c,

$$\begin{aligned} M(T,T_3+1)-M(T,T_3) &= \Delta E_c - \delta \\ &= (b+c)+2cT_3 \end{aligned} \tag{4.43}$$

where δ is the neutron-proton mass difference. In addition to shifting the energy levels the Coulomb force introduces two other effects: (1) dynamic distortion of the spacial part of the nucleon wavefunction; and (2) mixing of states of different isopin. The wavefunction for a state of isospin T is then

$$\varphi_0 = \varphi_0(t) + \sum_{\mu\neq 0}' \alpha_\mu(T)\varphi_\mu(T) + \sum_{\substack{\nu \\ T'\neq T}}' \beta_\nu(T')\varphi_\nu(T') \quad . \quad (4.44)$$

The second term is the mixing of states of the same spin and parity through dynamic distortion effects[51] while the third is the mixing of different isospin states through the Coulomb force,[50]

$$\beta_\nu(T') = \frac{<\varphi_\nu|V_c|\varphi_0>}{(E_0-E_\nu)} \quad . \quad (4.45)$$

Even though the mixing of states of different isospin may be small, rigorous validity of the isospin quantum number requires that the space-spin parts of the neutron and proton wavefunctions be identical. Departures from isospin invariance can be estimated by calculating the deviation of (4.39b) from unity. For the purpose of discussing these deviations we use (4.38) and (4.39) to define

$$\begin{aligned} \chi(\nu'\ell'j';\nu\ell j) &= 1 - <\text{proton}|t_+|\text{neutron}> \\ &= 1 - \int_0^\infty u_{\nu'\ell'j'}^{p}(r)\, u_{\nu\ell j}^{n}(r)\, r^2 dr \quad . \end{aligned} \quad (4.46)$$

When $\chi(\nu'\ell'j' = \nu\ell j) = 1$ and $\chi(\nu'\ell'j' \neq \nu\ell j) = 0$, the spatial parts of the wavefunctions are identical and isospin is a valid quantum

number. To calculate the isospin impurity in the ground state of a nucleus one has to sum over products of the overlap integrals occuring in (4.46).

To calculate the Coulomb energy shift in perturbation theory one needs the structure of the analogue state. These states are quite different for nuclei with N=Z and nuclei with N≠Z. If we assume the ground states of closed shell nuclei to be states of good isospin then N=Z nuclei are generally T=0 states and N≠Z nuclei are states with $T = |T_3|$ and $T_3 = \frac{(Z-N)}{2}$. We are primarily interested in the Coulomb energy shifts of analogue single-particle states. The analogue states of O^{17} and Ca^{41} are states in F^{17} and Sc^{41}, respectively,

$$|F^{17}\text{s.p.}> = \mathcal{T}_+|O^{17}\text{s.p.}>$$

$$|Sc^{41}\text{s.p.}> = \mathcal{T}_+|Ca^{41}\text{s.p.}> \quad .$$

The only effect of the operator $\mathcal{T}_+$ is to change the valence neutron into a proton. In perturbation theory the Coulomb energy shift is then that of the single-particle interacting with the charged particles of the closed shell core. The analogue states of the single-particle states in Pb^{209} are states in Bi^{209}. However, the analogue states are not single-particle states since there is a neutron excess. The analogue state is

$$\begin{aligned} |Bi^{209}A> &= \mathcal{T}_+|Pb^{209}\text{s.p.}> \\ &= T_+ \frac{1}{[T^2-T_3{}^2-T_3]^{\frac{1}{2}}}|Pb^{209}\text{s.p.}> \\ &= \frac{1}{(45)^{\frac{1}{2}}} \sum_{i=1}^{N} t_+(i)|Pb^{209}\text{s.p.}> \end{aligned} \qquad (4.47)$$

where we have used the fact that Pb^{209} is a state of isospin $T = 45/2$ and $T_3 = -45/2$. In (4.47) the operator t_+ gives zero for all states which are filled with both neutrons and protons but gives a non-zero result for the neutron excess. The analogue state wavefunction contains a term in which the valence neutron is changed to a proton but also contains terms in which the valence neutron remains unchanged while proton particle-neutron hole states are created in the Pb^{208} neutron excess. The analogue state wavefunctions for O^{17}, Sc^{41} and Bi^{209} are represented pictorially in Fig. 4.1. The Coulomb energy shift of the Bi^{209} analogue states is that from particles in all the neutron excess orbitals interacting with the charge Z=82 core and weighted by the amplitudes in (4.47).

4-F Single-Particle Energies

The low-lying states in A=15 and A=17 nuclei with their shell model assignments are given in Table 4.4. The lowest states having the same spin and parity as would be expected on the basis of the shell model are usually taken to be the single-particle (hole) states. Naquib and Green[52] have recently shown that the $O^{16}(d,p)O^{17}$ experiment gives spectroscopic factors consistent with unity for the (0d;1s) states. The amount of configuration mixing in the O^{16} ground state and the degree to which the single-particle (hole) strength is spread over several states is still an unsolved problem. Shukla[53] has calculated transition strengths in A=15 nuclei by introducing configuration mixing. In our calculations we take the experimentally observed energies in Table 4.5 to be the single-particle energies in A=15 and A=17 nuclei.

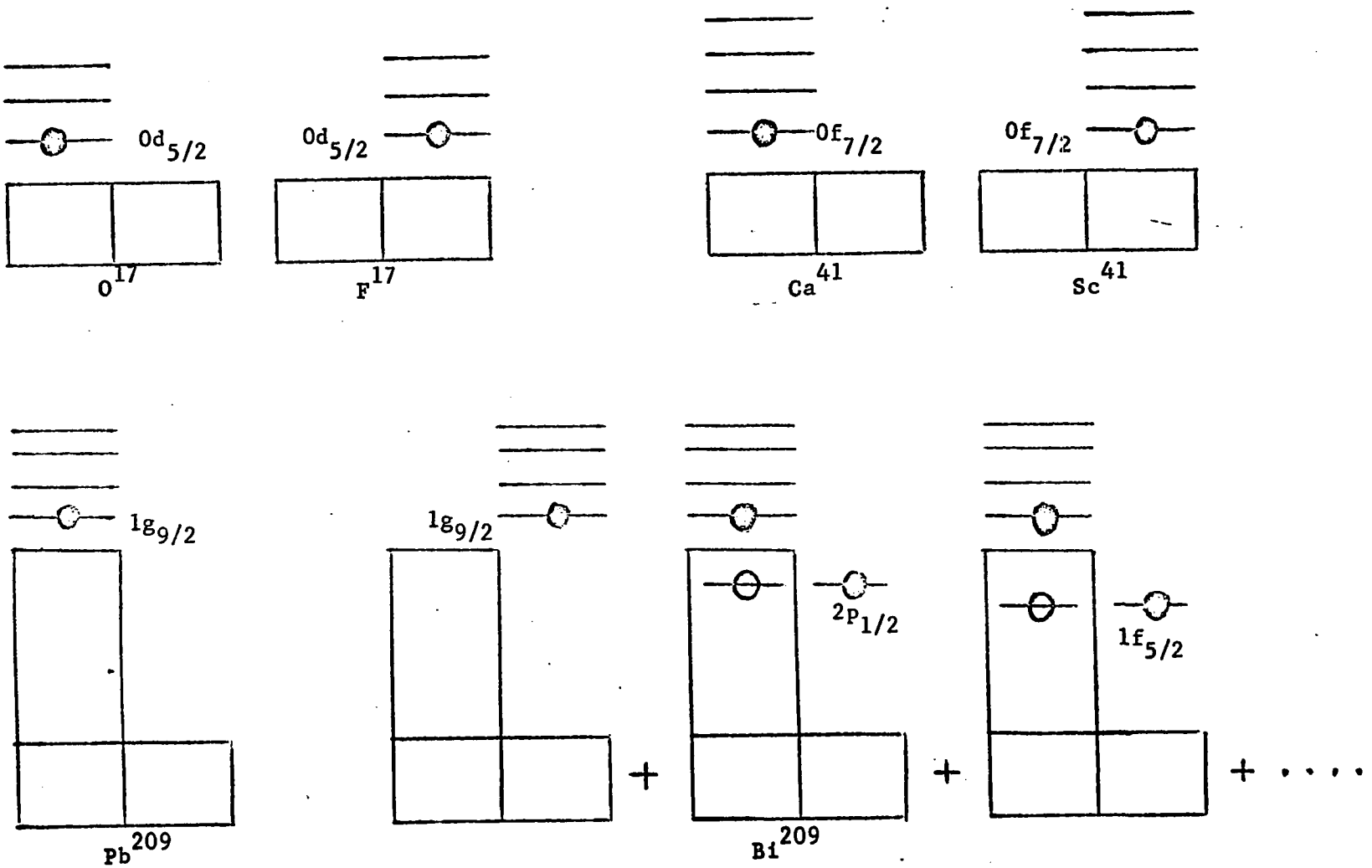

Fig. 4-1. Isobaric Analogue States

Table 4.4

Low-lying levels in A=15 and A=17 nuclei [30]

O^{15}			N^{15}		
E_x (MeV)	$n\ell j$	3π	E_x (MeV)	$n\ell j$	3π
0.00	$0p_{1/2}$	$\frac{1}{2}^-$	0.00	$0p_{1/2}$	$\frac{1}{2}^-$
5.19		$\frac{1}{2}^+$	5.27		$5/2^+$
5.24		$5/2^+$	5.30		$\frac{1}{2}^+$
6.16	$0p_{3/2}$	$3/2^-$	6.33		$3/2^-$
6.79		$3/2^+$	7.15		$5/2^+$
6.86		3/2,5/2	7.31		$3/2^+$

O^{17}			F^{17}		
E_x (MeV)	$n\ell j$	3π	E_x (MeV)	$n\ell j$	3π
0.00	$0d_{5/2}$	$5/2^+$	0.00	$0d_{5/2}$	$5/2^+$
0.87	$1s_{1/2}$	$\frac{1}{2}^+$	0.50	$1s_{1/2}$	$\frac{1}{2}^+$
3.06		$\frac{1}{2}^-$			
3.85		$5/2^-$			
4.56		$3/2^-$			
5.08	$0d_{3/2}$	$3/2^+$	5.10	$1d_{3/2}$	$3/2^+$
5.22					
5.38		$3/2^-$			
5.71		$7/2^-$			
5.73					
5.87		$\geq 3/2$			

Table 4.5

Single-particle binding energies for A=16 and A=17 nuclei

O^{15}		N^{15}		O^{17}		F^{17}	
$n\ell j$	E_b (MeV)	$n\ell j$	E_B (MeV)	$n\ell j$	E_B (MeV)	$n\ell j$	E_B (MeV)
$0p_{1/2}$	-15.65	$0p_{1/2}$	-12.11	$0d_{5/2}$	-4.14	$0d_{5/2}$	-0.60
$0p_{3/2}$	-21.81	$0p_{3/2}$	-18.44	$1s_{1/2}$	-3.27	$1s_{1/2}$	-0.10
				$0d_{3/2}$	+0.94	$0d_{3/2}$	+4.50

In contrast to the A=15 and A=17 nuclei, analysis of nucleon transfer reactions for A=39 and A=41 nuclei show that the single-particle (hole) strength is badly fragmented. For A=41 there are approximately 80 levels below 6 MeV, while for A=39 there are approximately 25 below 6 MeV. With such a high density of states it is natural that there should be considerable mixing. The (0f,1p) shell single-particle states would have spins and parities $7/2^-$, $3/2^-$, $1/2^-$ and $5/2^-$. The known negative parity states below 5.76 MeV in Sc^{41} are given in Table 4.6. The levels listed are from (p,γ) and (p,p) experiments.[54] Bock, Duhm and Stock[55] have analysed the $Ca^{40}(He^3,d)Sc^{41}$ stripping reactions to obtain spectroscopic factors for the 0.00, 1.71 and 2.42 MeV states. The results are given in Table 4.7. Belote, Sperduto and Buechner[56] have studied the level structure of Ca^{41} using the $Ca^{40}(d,p)Ca^{41}$ stripping reaction. Their

Table 4.6

Low-lying states in Sc^{41} (ref. 54)

E_x(MeV)	J^π	J^π (provisional)	E_x(MeV)	J^π	J^π (provisional)
0.00	$7/2^-$		4.808	$5/2^-, (7/2^-)$	
1.714	$3/2^-$		4.950	$5/2^-$	
2.409	$3/2^-$		5.008	$7/2^-$	
2.584	$5/2^-$		5.067	$1/2^-$	
2.663	$5/2^\mp$, $9/2^+$		5.139	$3/2^-$	
2.879	$7/2^-$ $(7/2^+, 5/2^-)$		5.392		$1/2^-$
2.969	$7/2^-$ $(7/2^+)$		5.490		$1/2^-$
3.182	$5/2^-$, $9/2^+$		5.521		$\geq 5/2^+$
3.467	$1/2^-$		5.530		$3/2^-$
3.692	$5/2^-$, $7/2^\pm$		5.650	$5/2^-, 7/2^-$	
3.729		$1/2^-$	5.690		$\geq 5/2^\pm$
3.769		$1/2^-$	5.698		$1/2^-$
4.018	$7/2^-$		5.706	$5/2^-, 7/2^-$	
4.027	$5/2^-, 7/2^\pm$		5.755		$1/2^-$
4.437	$3/2^-, 5/2^\pm, 7/2^\pm$				
4.511	$5/2^-, 9/2^+$				
4.532	$3/2^-$				
4.639	$1/2^-$				

Table 4.7

Spectroscopic factors and single-particle excitation energy in Sc^{41} (ref. 55)

E_x(MeV)	J^π	$n\ell j$	No. of Levels	S	ΣS	$E_x(n\ell j)$
0.0	$7/2^-$	$0f_{7/2}$	1	0.92	0.92	0.00
1.71	$3/2^-$	$0p_{3/2}$		0.91		
2.42	$3/2^-$		2	0.09	1.00	1.77

analysis to obtain spectroscopic factors and shell model identifications is given in Table 4.8. Only the $0f_{7/2}$ single-particle state corresponds to a single state in both the $Ca^{40}(He^3,d)Sc^{41}$ and the $Ca^{40}(p,d)Ca^{41}$ experiments. Both experiments also give consistent results for the $0p_{3/2}$ single-particle state. The single-particle strength is mostly in the lowest $3/2^-$ state with the remainder in the second $3/2^-$ state. In Ca^{41} the $0p_{\frac{1}{2}}$ strength is spread over five states while only 50% of the $0f_{5/2}$ strength is contained in the states observed. To obtain unperturbed positions for the single-particle states we define the single-particle excitation energy to be

$$E_x(n\ell j) = \frac{1}{\Sigma S} \sum_{i=1}^{m} S(i)E_x(i) \quad .$$

The single-particle energies for Ca^{41} and Sc^{41} are given in the last columns of Tables 4.7 and 4.8. Hinds and Middleton[57] have used the $Ca^{40}(t,\alpha)K^{39}$ and $Ca^{40}(He^3,\alpha)Ca^{39}$ pick up reactions to locate the single-hole states in K^{39} and Ca^{39}. Their identification is given in Table 4.9. Recently, Kozub[58] has analyzed the $Ca^{40}(p,d)Ca^{39}$ experiment to obtain spectroscopic factors for the states containing the single-particle strength. The spectroscopic factors are given in Table 4.10 and the unperturbed single-particle energies are given in the last column of the same table. The (t,α) and (p,d) experiments both indicate that most of the $0d_{5/2}$ strength is concentrated in the states at 5.13, 5.48, and 6.15 MeV. The single-particle binding energies for A=39 and A=41 are listed in Table 4.11.

Table 4.8

Spectroscopic factors and single-particle excitation energies in Ca^{41} (ref. 56)

E_x(MeV)	J^π	$n\ell j$	No. of levels	S	ΣS	$E_x(n\ell j)$
0.00	$7/2^-$	$0f_{7/2}$	1	1.00	1.00	0.00
1.95	$3/2^-$	$0p_{3/2}$		0.94		
2.47	$3/2^-$		2	0.28	1.22	2.07
3.62	$1/2^-$	$0p_{1/2}$		0.11		
3.95	$1/2^-$			0.73		
4.20	$1/2^-$			0.01		
4.62	$1/2^-$			0.11		
4.76	$1/2^-$		5	0.21	1.17	4.13
4.89	$5/2^-$			0.12		
5.66	$5/2^-$			0.25		
5.81	$5/2^-$		3	0.11	0.48	5.50

Table 4.9

Single-hole states in A=39 nuclei (ref. 57)

Ca^{39}			K^{39}		
E_x(MeV)	J^π	$n\ell j$	E_x(MeV)	J^π	$n\ell j$
0.00	$3/2^+$	$0d_{3/2}$	0.00	$3/2^+$	$0d_{3/2}$
2.47	$1/2^+$	$1s_{1/2}$	2.53	$1/2^+$	$1s_{1/2}$
5.13	$5/2^+$	$0d_{5/2}$	5.28	$5/2^+$	$0d_{5/2}$
5.49	$5/2^+$	$0d_{5/2}$	5.62	$5/2^+$	$0d_{5/2}$
6.15	$5/2^+$	$0d_{5/2}$	6.35	$5/2^+$	$0d_{5/2}$

Table 4.10

Spectroscopic factors and excitation energies for the single-hole states in Ca^{39} (ref. 58)

E_x(MeV)	J^π	$n\ell j$	S a	S b	ΣS a	ΣS b	$E_x(n\ell j)$ a	$E_x(n\ell j)$ b
0.00	$3/2^+$	$0d_{3/2}$	1.78	0.92	1.78	0.92	0.00	0.00
2.47	$1/2^+$	$1s_{1/2}$	1.16	0.91	1.16	0.91	2.47	2.47
5.13	$(5/2)^+$	$0d_{5/2}$	0.36	0.24				
5.48	$(3/2,5/2)^+$	$0d_{5/2}$	0.16	0.11				
6.15	$(5/2)^+$	$0d_{5/2}$	0.36	0.25	0.88	0.60	5.61	5.62

a) Neutron well radius r_0 = 1.11 fm.

b) Neutron well radius r_0 = 1.35 fm.

Table 4.11

Single-particle binding energies in A=39 and A=40 nuclei

Ca^{39}		K^{39}		Ca^{41}		Sc^{41}	
E_B(MeV)	$n\ell j$	E_B(MeV)	$n\ell j$	E_B(MeV)	$n\ell j$	E_B(MeV)	$n\ell j$
-15.64	$0d_{3/2}$	-8.33	$0d_{3/2}$	-8.36	$0f_{7/2}$	-1.08	$0f_{7/2}$
-18.11	$1s_{1/2}$	-10.86	$1s_{1/2}$	-6.29	$1p_{3/2}$	+0.71	$0p_{3/2}$
-21.25	$0d_{5/2}$			-4.23	$1p_{1/2}$		
				-2.86	$0f_{5/2}$		

The binding energies were determined from the excitation energies from Tables 4.7-4.10 and the neutron and proton separation energies.[59]

A distorted-wave-approximation analysis[60] of the single-nucleon transfer reactions $Pb^{208}(d,p)Pb^{209}$ and $Pb^{208}(d,t)Pb^{207}$ demonstrated that the shell model single-particle (hole) states can be identified with single states in Pb^{209} and Pb^{207}. The single-particle (hole) binding energies are listed in Table 4.12. The single proton states in Bi^{209} have been studied by the $Pb^{208}(He^3,d)Bi^{209}$[61,62] and the $Pb^{208}(\alpha,t)Bi^{209}$[63] reactions and the distorted wave analysis of the results indicate that most of the single-particle strength is concentrated in one state. However, the $2p_{\frac{1}{2}}$ strength is fragmented. Bardwick and Tickle[64] have studied the $Pb^{208}(He^3,d)Bi^{209}$ reaction and found that the $2p_{\frac{1}{2}}$ strength was split between levels at E_x = 3.64 MeV (60%) and E_x = 4.42 MeV (40%). With this result the unperturbed position of the $2p_{\frac{1}{2}}$ state would be unbound by 0.18 MeV. Hinds et al.[65] have used the $Pb^{208}(t,\alpha)$ reaction to excite the single-hole states in Tl^{207}. Apart from the $0g_{7/2}$ level, analysis of the experiment showed that the spectroscopic factors for the states observed were consistent with unity. The level at 3.48 MeV excitation energy was tentatively assigned a $0g_{7/2}$ character; however, if the assignment is correct the level contains only 25% of the single-particle strength.

Table 4.12

Single-particle binding energies in A=208

and A=209 nuclei

Pb^{207}		Pb^{209}		Tl^{207}		Bi^{209}	
$n\ell j$	E_B (MeV)	$n\ell j$	E_B (MeV)	$n\ell j$	E_B (MeV)	$n\ell j$	E_B (MeV)
$2p_{1/2}$	-7.38	$2d_{3/2}$	-1.42	$2s_{1/2}$	-8.03	$2p_{1/2}$	+0.18
$1f_{5/2}$	-7.95	$1g_{7/2}$	-1.45	$1d_{3/2}$	-8.38	$2p_{3/2}$	-0.57
$2p_{3/2}$	-8.27	$3s_{1/2}$	-1.91	$0h_{11/2}$	-9.37	$1f_{5/2}$	-0.94
$0i_{13/2}$	-9.01	$2d_{5/2}$	-2.36	$1d_{5/2}$	-9.70	$0i_{13/2}$	-2.16
$1f_{7/2}$	-9.72	$0j_{15/2}$	-2.53	$0g_{7/2}$	-11.51(?)	$1f_{7/2}$	-2.87
$0h_{9/2}$	-10.85	$0i_{11/2}$	-3.15			$0h_{9/2}$	-3.77
		$1g_{9/2}$	-3.94				

4-G Coulomb Displacement Energies

The general behaviour of Coulomb displacement energies of nuclear ground states and their analogue states is reproduced by the semi-empirical formula of Anderson, Wong and McClure[66]

$$\Delta E_c = 1.444\ \bar{Z}\ A^{1/3} - 1.13\ (\text{MeV}) \quad . \qquad (4.48)$$

The formula (4.48) does not reproduce nuclear structure effects. Excited states, particularly valence particle states, could not be expected to be fitted by (4.48) because of Thomas-Ehrman[67,68] shifts arising from the proximity of the two-body threshold. For example, the $0d_{5/2}$-$1s_{1/2}$ splitting in O^{17} and F^{17} is 0.87 MeV and 0.50 MeV, respectively. Nuclear structure effects can be reproduced by

performing a shell model calculation with the Coulomb interaction (4.41). Harchol et al.[69] have calculated the displacement energies of the analogues of ground states in the region $28 < A < 65$. In the calculation the oscillator size parameter was varied to fit the data. We have used the nuclear size dependence of the Coulomb energy shift to determine the single-particle potential radius while the other parameters were varied to fit the single-particle energies. In such a parameter search, calculation of the two-body matrix elements of the Coulomb interaction (4.41) at each stage in the search would be excessively time consuming.

The Coulomb energy shifts were calculated assuming that the particles moved in the average Coulomb potential of the charged core nucleus. The potential was taken to be that of a uniformly charged sphere of the same r.m.s. radius as the actual nucleus. In this approximation only the direct Coulomb interaction terms are included. The exclusion principle has the effect of keeping the protons apart; hence the exchange terms decrease the Coulomb energy. Sood and Green[70] calculated the exchange contributions for nuclei up to A=41 using HO wavefunctions. They found that including the exchange effects decreased the Coulomb energy by 6% for A=15 and 17 and by 4% for A=39 and 41. Nolen, Schiffer and Williams[71] have estimated the exchange effects to be 3.5% for Pb^{208}. Calculating Coulomb energies by the above procedure does not give structure effects e.g., pairing,[72] but it does give Thomas-Ehrman shifts.

4-H Method of Determining Potentials

Woods-Saxon potentials were fitted to the experimental single-

particle energies given in Tables 4.5, 4.11, and 4.12. The eigenvalues and eigenvectors were calculated by numerical integration of (4.12) using the code ABACUS II.[73] In the calculations we were only able to consider bound states.

The procedure followed for A=17 and A=41 nuclei was the following: 1) Neutron wells were determined for O^{17} and Ca^{41} by adjusting V_0, a and V_{so} to reproduce the experimental single-particle spectra. Simultaneously the potential radius was largely determined by requiring the Coulomb energy displacement to be correctly predicted by including the Coulomb potential in perturbation theory, i.e.

$$\Delta E_c = \langle \psi^n | V_c | \psi^n \rangle \quad .$$

2) The proton single-particle eigenvalues and eigenvectors were calculated using the nuclear potential deduced for neutrons but with the Coulomb potential included in the numerical solution of (4.12). It was found in this way that the Coulomb energy shift ΔE_c calculated in perturbation theory agreed for the $0d_{5/2}$ or $0f_{7/2}$ levels with that obtained from including V_c to all orders.

The procedure followed for A=15 and A=39 nuclei was the following: 1) The potential radii obtained for the A=17 and A=41 nuclei were parametrized in the form $R = r_0 A^{1/3}$. 2) Apart from an $A^{1/3}$ change, the neutron potentials for A=15 and A=39 were assumed to be the same as those for A=17 and A=41. Calculating the single-hole energies it was found that the potentials did not give sufficient binding. The diffusivity was kept fixed while V and V_{so} were varied

to reproduce the single-hole spectra. 3) To check the consistency of the results the Coulomb displacement energies were calculated in perturbation theory and the proton energies were calculated by including the Coulomb potential in the solution of (4.12).

The procedure for fitting the hole spectra requires some clarification. It should be emphasized that the basic assumption in the fitting procedure is that the experimental states can be assigned a single-particle character. A self-consistent Hartree-Fock calculation of the type discussed in Chapter 2 would give the single-particle states and an average single-particle potential. The Woods-Saxon potentials obtained for the A=17 and A=41 nuclei are then representations of the Hartree-Fock potentials for these nuclei. The potentials for the hole states should be representations of the Hartree-Fock potentials for A=16 and A=40 nuclei since an experimental single-hole energy is that of a particle in the closed shell nucleus. Initially it was assumed that the particle and hole potentials differed only by a radius change of $A^{1/3}$. In Sec. 4.C the A dependence of nuclear sizes was discussed. The empirical evidence is that isotopes and isotones increase less and more rapidly than $A^{1/3}$, respectively. Perey and Schiffer[47] have suggested that these variations can be ascribed to changes in wavefunctions as a function of binding energy. In view of the fact that it is useful to consider neutrons and protons as identical particles in shell model calculations, it is a good approximation to assume an average behaviour of an $A^{1/3}$ dependence. This model does not take into account rearrangement energy effects.

In general, the Brueckner Hartree-Fock single-particle potential is non-local[74] or, alternatively, local but energy dependent. The energy dependence of single-particle potentials for nuclei with $A \leq 40$ has been discussed by Elton and Swift.[45] They found that the assumption of a linear relationship between the strength of the potential for nuclei with N=Z and the proton kinetic energy was sufficient to explain the experimental data. We followed the same procedure and changed only V_0 and V_{so} to fit the single-hole spectra. With local and energy dependent potentials states differing only in the number of nodes in the radial wavefunction are not orthogonal. In shell model calculations one normally works with a subspace of configurations such that the non-orthogonality does not enter into the calculations.

When the fitting procedures described above were applied to nuclei with A=207 and A=209 it was found that there were ambiguities in the potentials. The methods used for the heavy nuclei are discussed with the results for those nuclei.

4-I Results for A=15 and A=17 Nuclei

A problem in A=17 nuclei is that the $0d_{3/2}$ level is unbound whereas one normally includes the state in shell model calculations. In O^{17} the $0d_{3/2}$ state is seen as a narrow resonance at 0.94 MeV in neutron elastic scattering on O^{16}. Since the resonance is narrow, a reasonable approximation to obtain the effects of a finite nuclear potential is to calculate a wavefunction for the state with a small binding energy. In shell model calculations using the O^{17} single-

particle states as unperturbed configurations this is equivalent to adding a term $\Delta V(r)$ to the single-particle Hamiltonian and removing it from the two-body perturbation.

The WS potential for O^{17} was determined by the method discussed in the previous section. To determine the spin-orbit strength the binding energy of the $0d_{3/2}$ state was calculated as a function of the well depth V_0. By extrapolating back into the continuum it was possible to fix V_{so}. The fitted well parameters for O^{17} are given in Table 4.13. The $0d_{3/2}$ binding energy as a function of V_0 is shown in Fig. 4.2a. The curve is not quite linear; however, the extrapolation should be sufficiently accurate for our purposes. In Fig. 4.2b the mean energy shift per unit change in V_0 is plotted vs. the mean of the change in the potential treated as a perturbation. The linear relationship would imply that adding the term $\Delta V(r)$ to the single-particle potential and removing it from the two-body perturbation has no effect on the unperturbed single-particle energy. The calculated neutron single-particle energies, together with the experimental energies are shown in Fig. 4.3. The r.m.s. radius of the O^{16} charge distribution is not well established experimentally. The value quoted in Table 4.1 was obtained using HO wavefunctions. Recently Elton and Swift[45] have fitted WS wavefunctions to elastic electron scattering data and the single-particle energies to the proton separation energies obtained from (p,2p) experiments. They obtained the result $< r^2 >_c^{\frac{1}{2}} = 2.79$ fm. which corresponds to an equivalent uniformly charged sphere of radius $R_u = 3.60$ fm. The

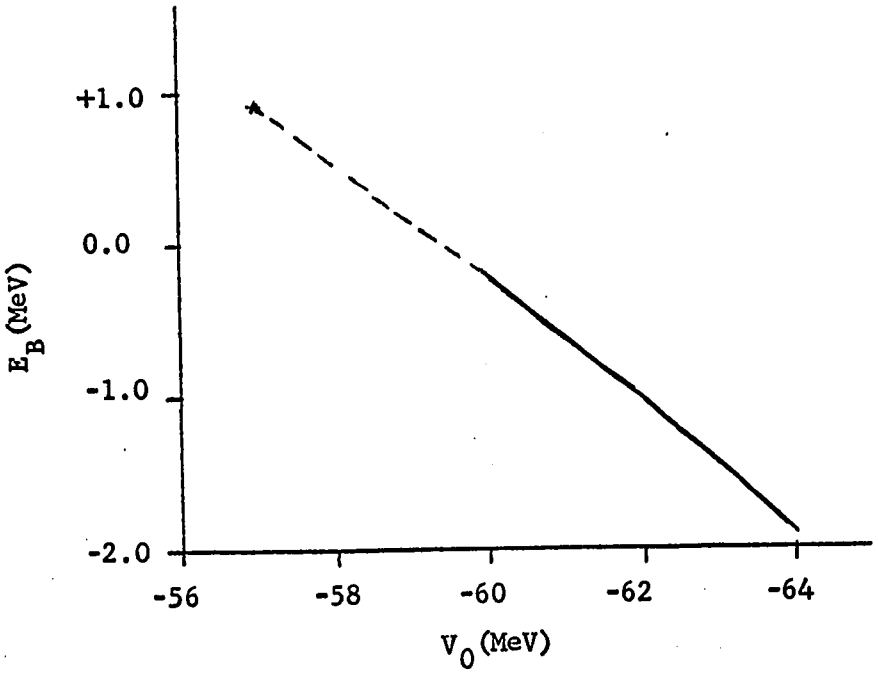

(a)

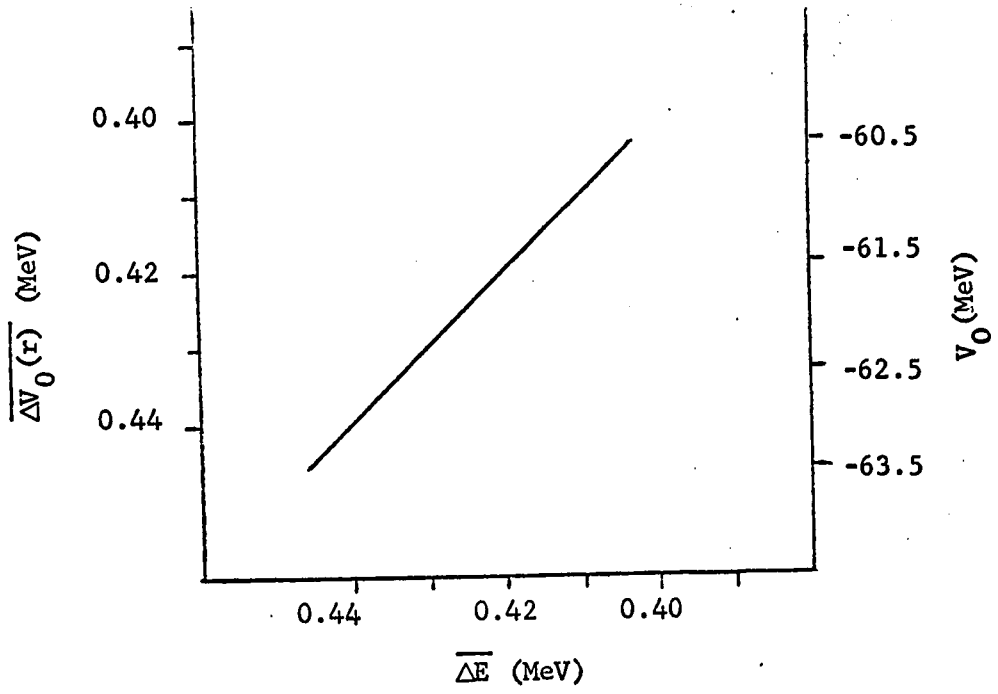

(b)

Fig. 4-2. (a) The $0d_{3/2}$ binding energy as a function of the well depth. (b) The integral of $\Delta V(r)$ and the change in binding energy of the $0d_{3/2}$ state as a function of the well depth.

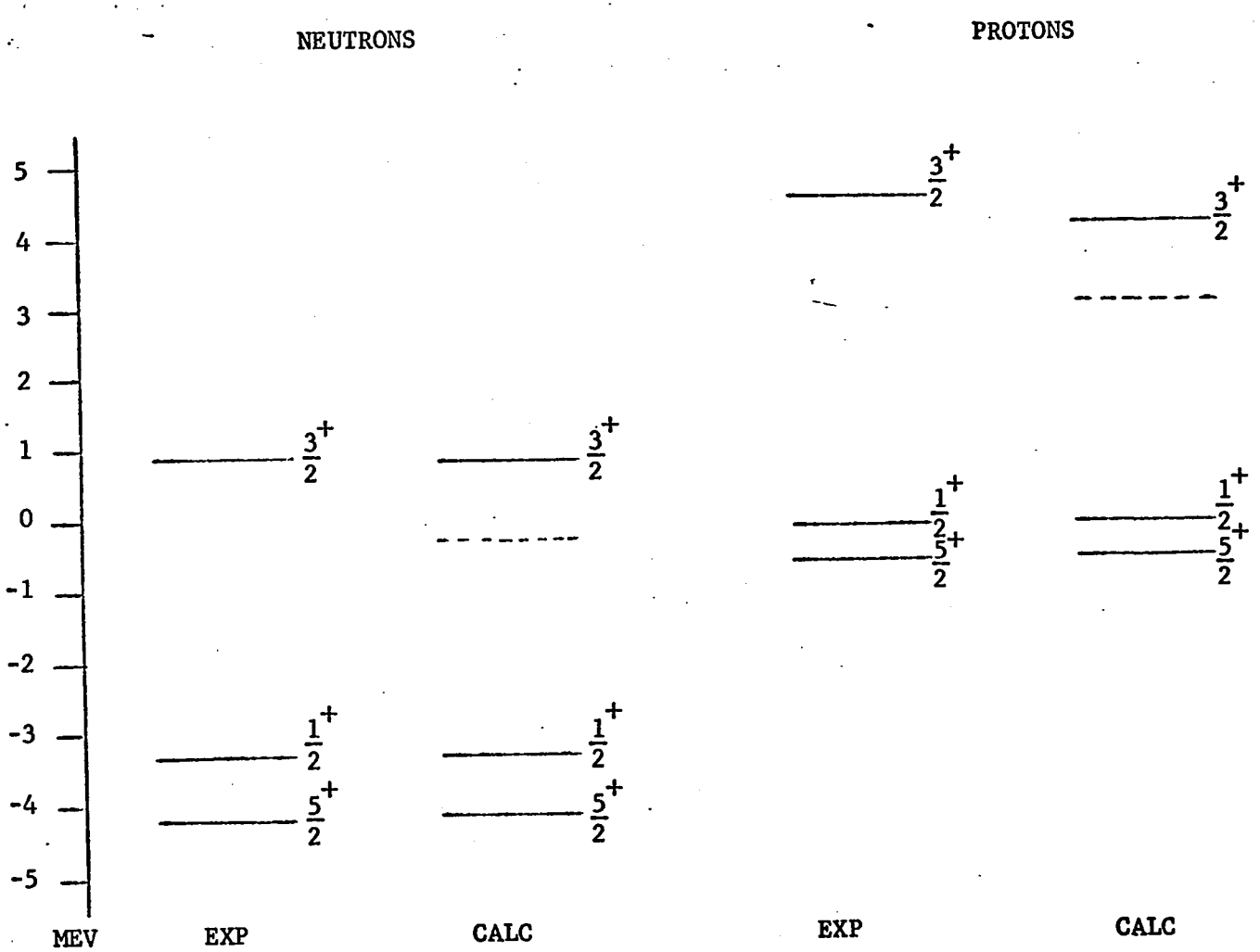

Fig. 4-3. The single-particle spectra of A=17 nuclei. The dashed line is the bound $0d_{3/2}$ state determined for shell model calculations. The theoretical spectrum of proton states is that predicted by adding the calculated value of ΔE_c to the neutron energies.

Table 4.13

Potential parameters for O^{17} and O^{15}

Nucleus	V_0 (MeV)	V_{so} (MeV)	a (fm^{-1})	r_0 (fm)
O^{17}	57.0	5.7	0.63	1.17
O^{15}	61.9	9.2	0.63	1.17

Coulomb displacement energies for the A=17 analogue states calculated in perturbation theory with R_u = 3.60 fm. are given in Table 4.14. With R_u = 3.46 fm. the Coulomb energies were increased by about 2%. Apart from the $0d_{3/2}$ state the calculated numbers are in good agreement with experiment. The Thomas-Ehrman shift of the $1s_{1/2}$ level is reproduced in this model. The calculated $0d_{3/2}$ energy shift is too small; however, with the level bound by 1.9 MeV the shift is only increased to 3.45 MeV. It is obvious that the level would have to be bound nearly as deep as the $0d_{5/2}$ level to give the experimental energy shift. It is very likely that the error is in the quoted experimental value of the displacement energy. The number quoted is the difference in binding energy of the levels in O^{17} and F^{17}. This energy difference is only the Coulomb energy shift if the Coulomb potential does not appreciably distort the wavefunction. An example of the effects of such distortions will be discussed in Chapter 5. In Sec. 4.G exchange energy corrections to the Coulomb displacement energies calculated

Table 4.14

Coulomb displacement energies calculated in perturbation theory with R_u = 3.60 fm

A=17			A=15		
$n\ell j$	ΔE_c (MeV)	Exp (MeV)	$n\ell j$	ΔE_c (MeV)	Exp. (MeV)
$0d_{5/2}$	3.51	3.54	$0p_{1/2}$	3.50	3.54
$1s_{1/2}$	3.14	3.17	$0p_{3/2}$	3.51	3.47
$0d_{3/2}$	3.26†	3.56			

† Calculated with wavefunction for E_B = -0.23 MeV.

above were discussed. To include the corrections would decrease the calculated energy shifts and imply that the nuclear potential should have a smaller radius. The present model is not sufficiently accurate to merit considering this detail.

The wavefunctions for the O^{17} states are tabulated in Table 4.15 as expansions in terms of oscillator functions. The coefficients tabulated are those defined in Eq. (4.17). Two sets of parameters are tabulated; one for the $\hbar\omega$ value that maximizes the overlap with the oscillator function having the same number of nodes while the second is a common $\hbar\omega$ value for the set of states. To compare HO and WS wavefunctions a few of the wavefunctions are plotted

Table 4.15

The coefficients of the expansion of the WS wavefunctions for O^{17} in terms of HO wavefunctions

$\nu\ell j$	$0d_{5/2}$		$1s_{1/2}$		$0d_{3/2}$		$0d_{3/2}$		$0d_{3/2}$	
E_B (MeV)	-4.11		-3.27		-1.93		-1.05		-0.23	
n \ $\hbar\omega$	13.5	13.4	12.0	13.4	13.0	13.4	12.0	13.4	11.0	13.4
0	0.988	0.988	-0.143	-0.079	0.978	0.977	0.971	0.967	0.958	0.949
1	-0.014	-0.008	0.947	0.939	-0.014	-0.033	-0.003	-0.070	0.001	-0.109
2	0.137	0.138	-0.087	-0.163	0.183	0.180	0.206	0.195	0.234	0.214
3	-0.053	-0.051	0.228	0.224	-0.059	-0.065	-0.060	-0.085	-0.067	-0.110
4	0.032	0.032	-0.098	-0.128	0.057	0.058	0.070	0.073	0.091	0.094
5	-0.029	-0.029	0.078	0.088	-0.041	-0.043	-0.048	-0.057	-0.060	-0.077
6	0.014	0.014	-0.061	-0.072	0.027	0.029	0.036	0.041	0.051	0.060
7	-0.014	-0.014	0.038	0.048	-0.024	-0.026	-0.032	-0.036	-0.045	-0.053
8	0.009	0.008	-0.034	-0.040	0.017	0.018	0.023	0.028	0.036	0.044
9	-0.007	-0.007	0.023	0.030	-0.015	-0.016	-0.021	-0.024	-0.033	-0.039
10	0.005	0.005	-0.020	-0.024	0.013	0.012	0.016	0.020	0.028	0.034

in Fig. 4.4. The WS $0d_{5/2}$ state is very similar to an oscillator function while the $1s_{1/2}$ WS wavefunction extends much further beyond the potential than the HO wavefunction. The differences between the wavefunctions are partly understood by considering the $\hbar\omega$ value that maximizes the overlap of the WS and HO wavefunctions. A direct measure of the extent to which the wavefunctions extend beyond the nuclear potential is given by the integrals of r^2 in Table 4.16. In an oscillator potential all states with a shell have the same value of $< r^2 >$. In the WS potential the $< r^2 >$ are 11.62 and 17.79 fm^2 for the $0d_{5/2}$ and $1s_{1/2}$ states respectively. The large $< r^2 >$ for the ℓ=0 state is reflected in the decrease in the Coulomb displacement energy.

The single-hole states in O^{16} were determined by the procedure outlined in the previous section. Changing only the well radius, by the $A^{1/3}$ factor, did not give p states with sufficient binding energy. The well depth and spin-orbit strength were both increased to fit the experimentally observed energies. The well parameters are given in Table 4.13. The wavefunctions are plotted in Fig. 4.4 and tabulated in Table 4.17. Since the p states are deeply bound the WS wavefunctions are very nearly HO wavefunctions; however, they correspond to HO wavefunctions with a considerably larger value of $\hbar\omega$ than required for the valence particles in O^{17}. The integrals of r^2 are given in Table 4.16. The WS wavefunctions have smaller r.m.s. radii for hole states and larger r.m.s. radii for particle states than a common oscillator potential for O^{16} and

Fig. 4-4. Woods-Saxon radial wavefunctions for A=17 and A=15 nuclei. Harmonic oscillator wavefunctions with $\hbar\omega$ = 13.4 MeV are presented for comparison. The figures are

(a) $0p_{1/2}$ and $0p_{3/2}$ neutron states

(b) $0d_{5/2}$ neutron state

(c) $0d_{3/2}$ (E_B = -0.23 MeV) neutron state

(d) $1s_{1/2}$ neutron state

(e) $1s_{1/2}$ proton state

(f) $0d_{5/2}$ proton state

(g) $0p_{1/2}$ proton state

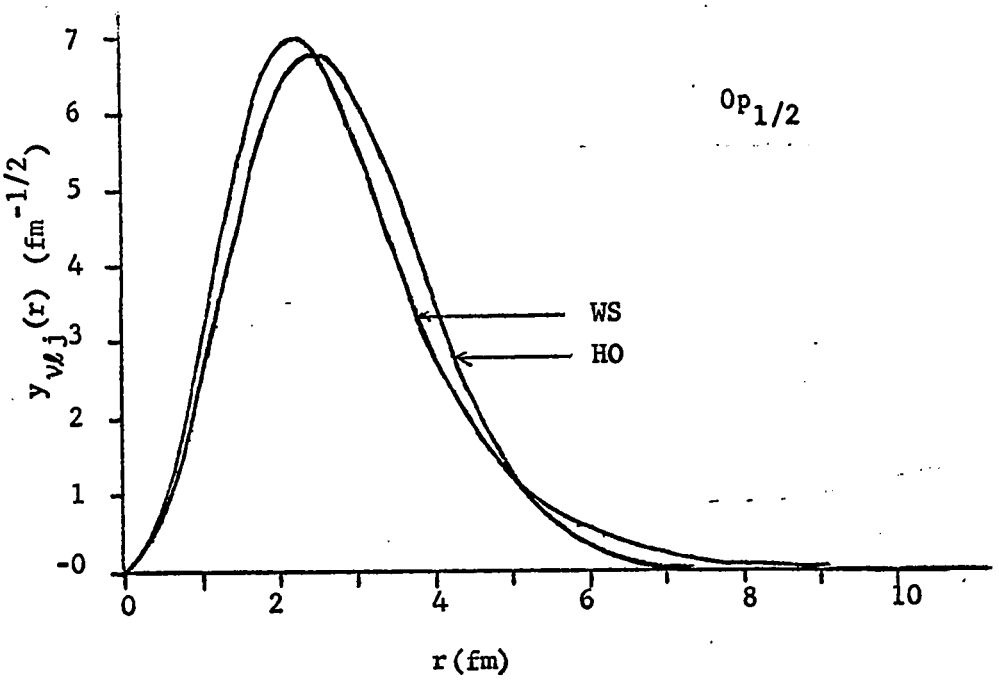

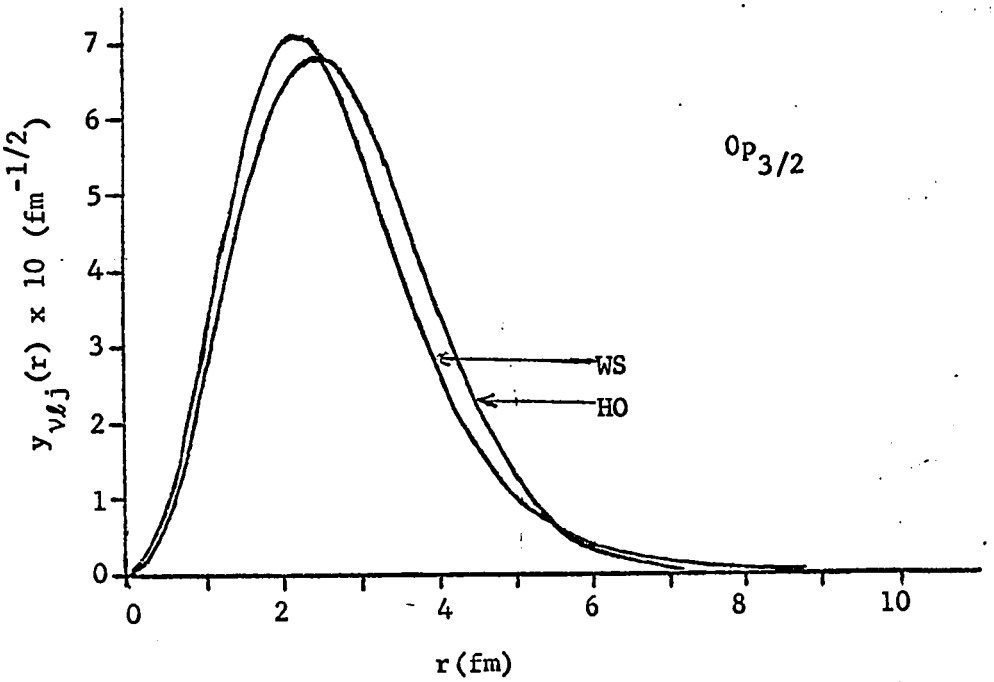

(a)

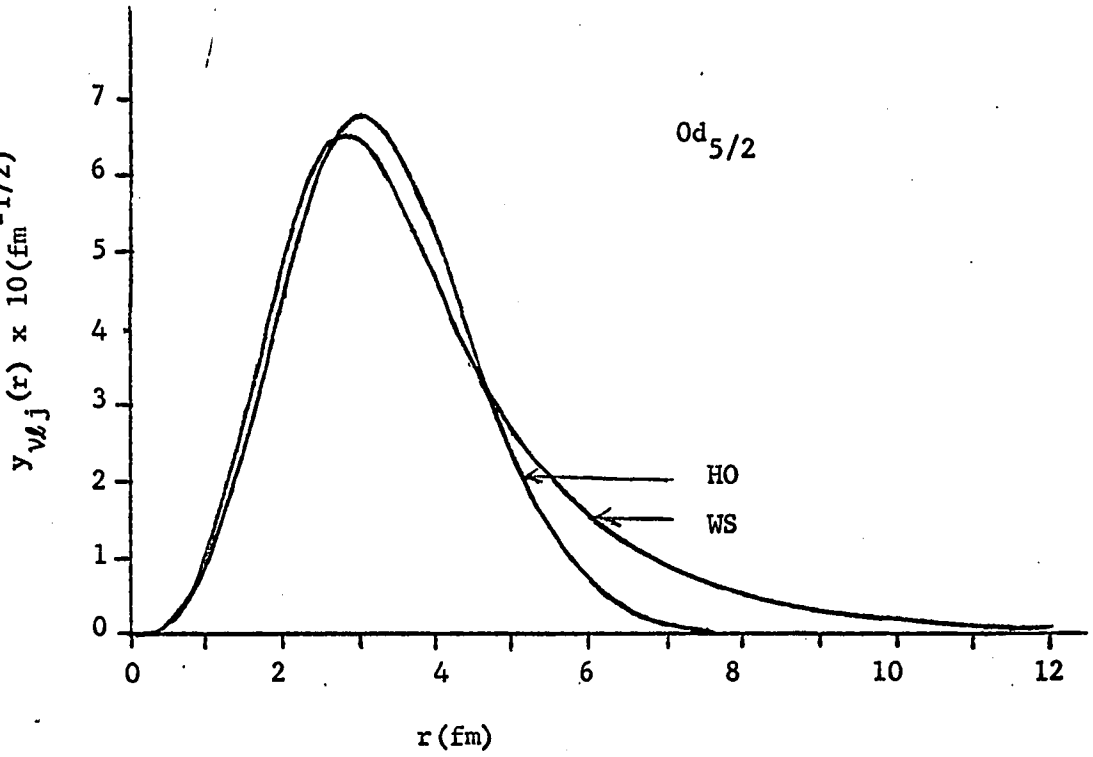
$0d_{5/2}$
HO
WS
$y_{vlj}(r) \times 10(fm^{-1/2})$
r (fm)
0
1
2
3
4
5
6
7
0
2
4
6
8
10
12

(b)

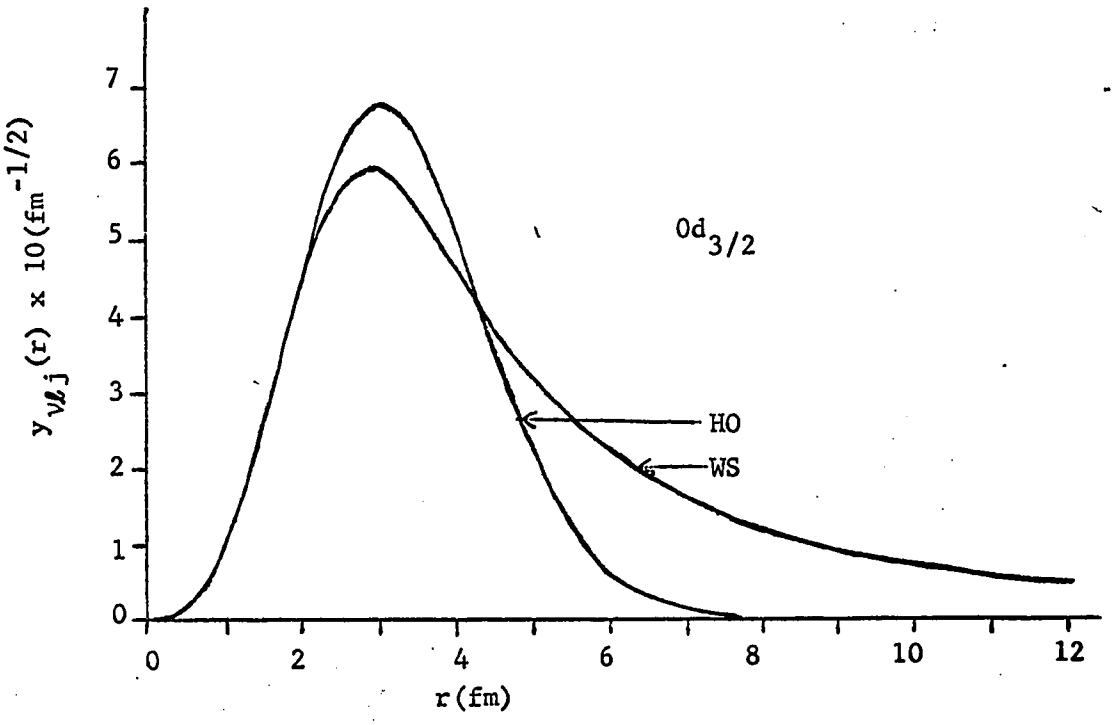
$0d_{3/2}$
HO
WS
$y_{vlj}(r) \times 10(fm^{-1/2})$
r (fm)
0
1
2
3
4
5
6
7
0
2
4
6
8
10
12

(c)

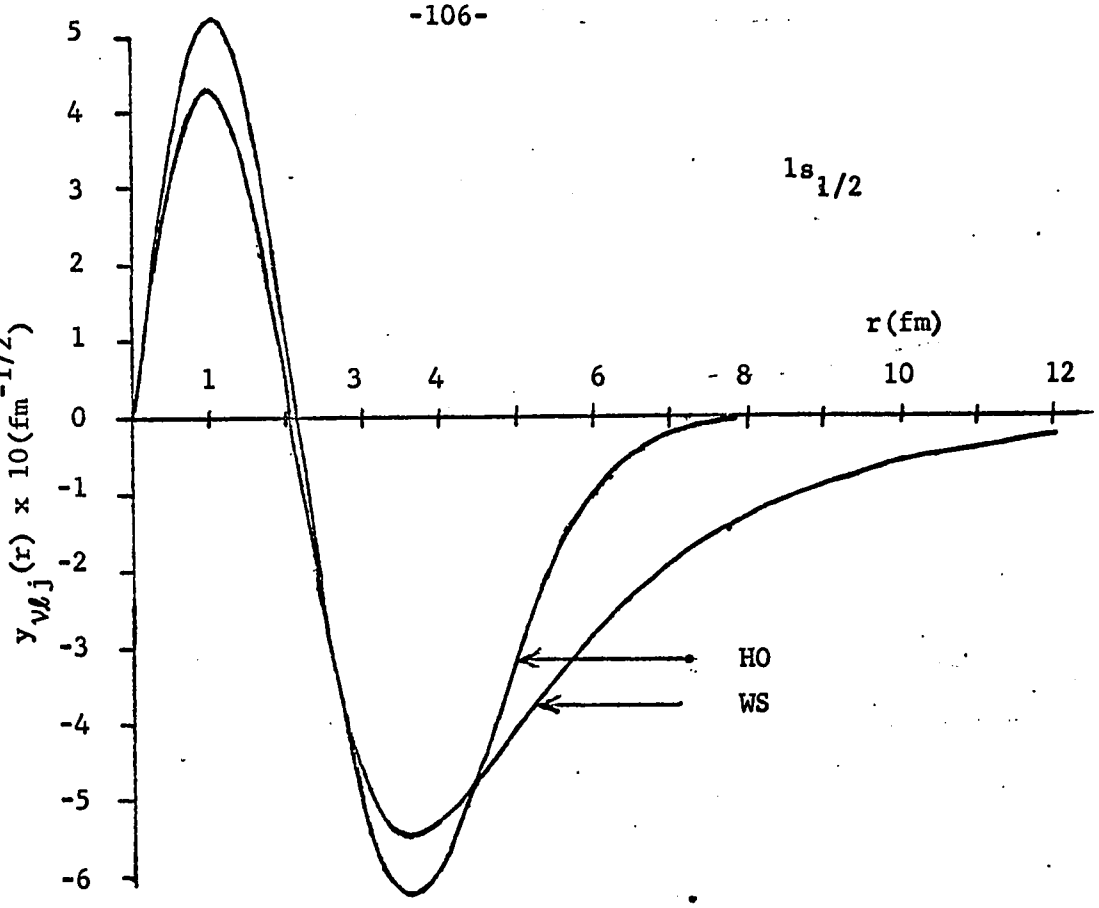
$1s_{1/2}$
r(fm)
$y_{\nu\ell j}(r)$ x $10(fm^{-1/2})$
HO
WS

(d)

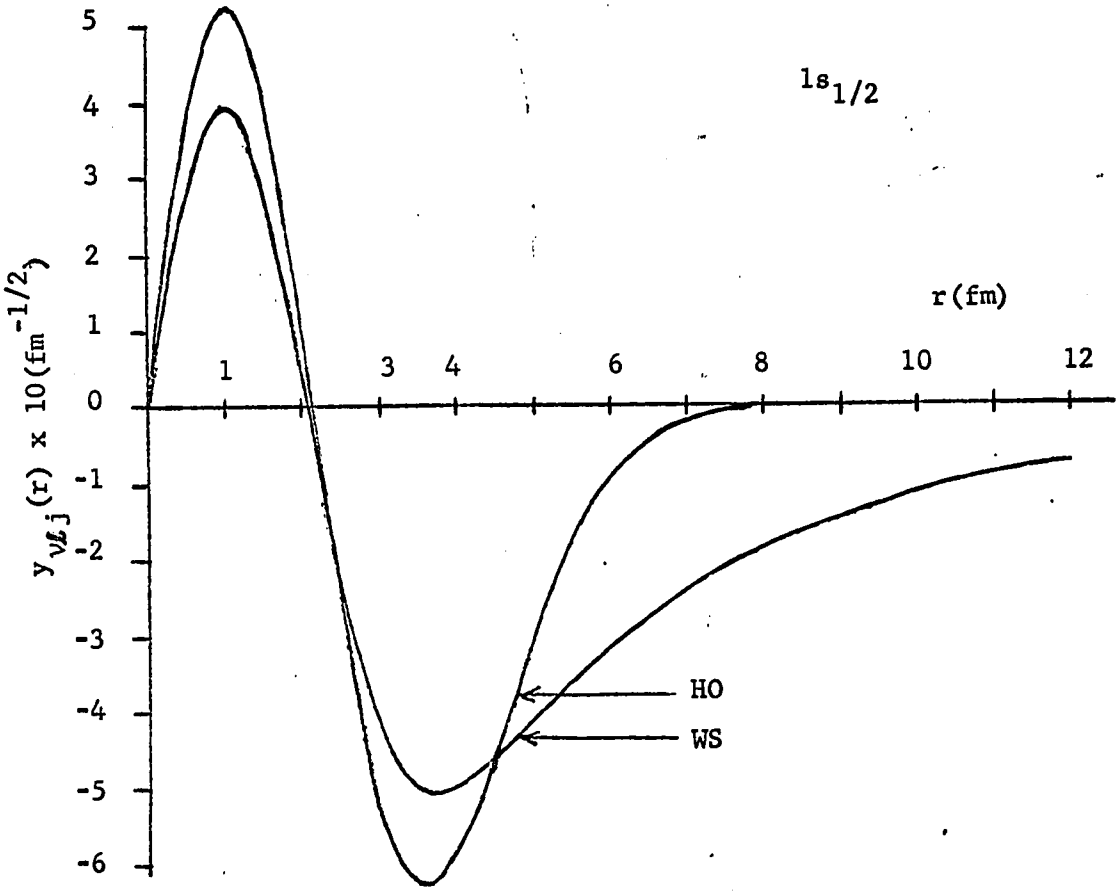
$1s_{1/2}$
r(fm)
$y_{\nu\ell j}(r)$ x $10(fm^{-1/2})$
HO
WS

(e)

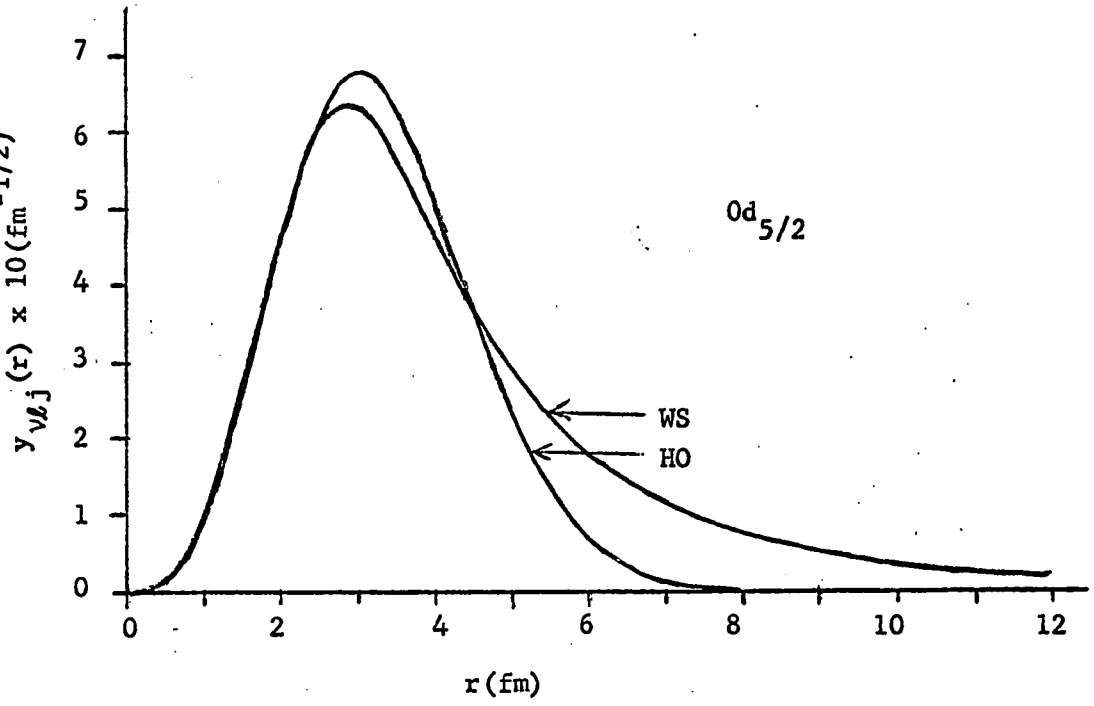
$y_{n\ell j}(r) \times 10(fm^{-1/2})$
$0d_{5/2}$
WS
HO
r(fm)

(f)

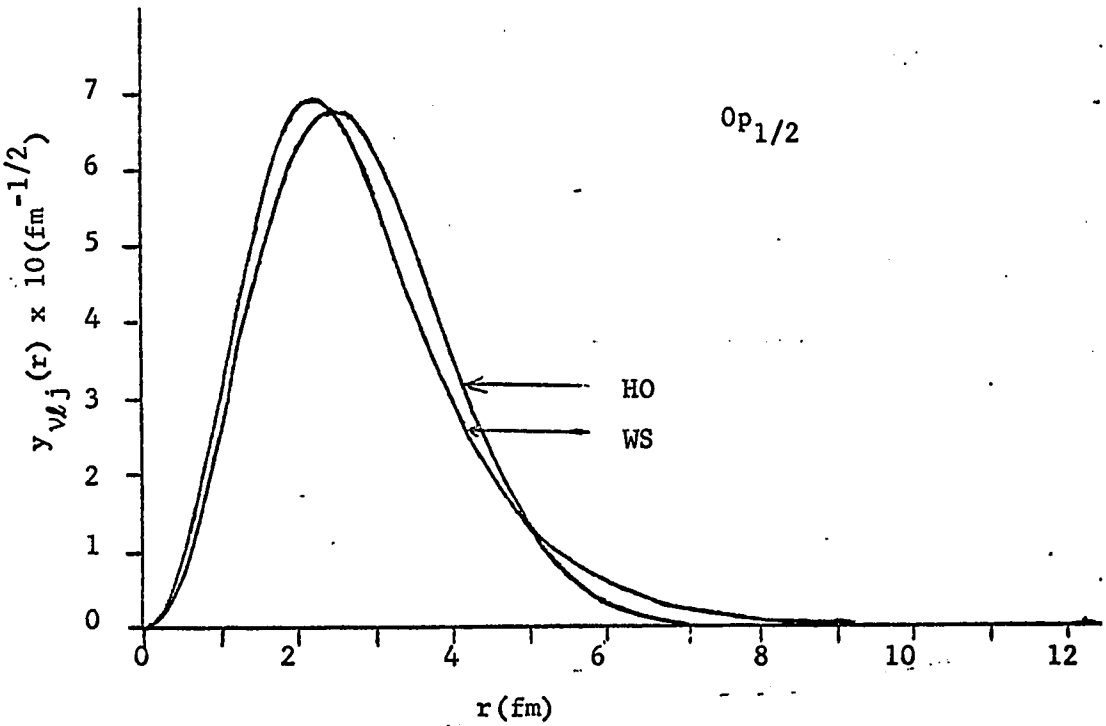
$y_{n\ell j}(r) \times 10(fm^{-1/2})$
$0p_{1/2}$
HO
WS
r(fm)

(g)

Table 4.16

The integrals $< r^2 >$ for A=17 and A=15

$\nu\ell j$	$< r^2 >$ (fm.^{2})		
	HO[a]	WS (neutron)	WS (proton)
$0d_{5/2}$	10.83	11.62	12.98
$1s_{1/2}$	10.83	17.79	25.54
$0d_{3/2}$	10.83	16.90[b]	
$0p_{1/2}$	7.74	6.70	6.92
$0p_{3/2}$	7.74	6.46	

a) HO with $\hbar\omega$ = 13.4 MeV.

b) E_B = -0.2 MeV

Table 4.17

The coefficients of the expansion of WS wavefunctions for O^{15} in terms of oscillator functions

$\nu\ell j$	$0p_{1/2}$		$0p_{3/2}$	
E_B (MeV)	-15.68		-2.179	
n \ $\hbar\omega$ (MeV)	16.0	13.4	16.25	13.4
0	0.997	0.990	0.999	0.989
1	-0.012	0.100	-0.004	0.135
2	0.069	0.086	0.038	0.061
3	-0.026	-0.004	-0.025	-0.007
4	0.008	0.005	0.000	-0.004
5	-0.009	-0.007	-0.006	-0.007
6	0.002	-0.001	0.001	-0.002

O^{17} would have. The common HO potential is taken to have $\hbar\omega$ = 13.4 MeV which is the result obtained from electron scattering data[44] and commonly used in shell model calculations. The Coulomb displacement energies calculated in perturbation theory are in as good agreement with experiment as in the case of O^{17}. If the well radius had been kept the same as that for O^{17} the Coulomb energies would have been decreased by approximately 1%. Clearly the present model cannot detect an $A^{1/3}$ radius change when $\Delta A=1$.

The proton states were calculated using the same WS potentials as for the neutrons but with the Coulomb potential included in the solution of the differential equation. The calculated binding energies of the $0p_{1/2}$ and $0p_{3/2}$ states were -12.20 and -18.30 MeV, respectively. The experimental energies are -12.10 and -18.40 MeV. The calculated binding energies for the $0d_{5/2}$ and $1s_{1/2}$ states were -0.61 and -0.10 MeV. A few of the proton wavefunctions are plotted in Fig. 4.4 and tabulated in Table 4.18. The proton p states have a complete overlap with the neutron states; however, the $0d_{5/2}$ and $1s_{1/2}$ proton-nueotron overlaps are 0.997 and 0.980, respectively. The small binding energy of the $1s_{1/2}$ proton state allows the wavefunction to spread out considerably more than the neutron wavefunction. The integral of r^2 is 25.54 fm^2 for the proton state and 17.79 fm^2 for the neutron state.

The r.m.s. radius of the charge distribution (calculated assuming the neutron and proton matter distributions to be the same) for O^{16} with the present wavefunctions is 2.54 fm. This result is

consistent with the results of Wilkinson and Mafethe[75] and Wilkinson[76]; however it is small compared with the recent result (2.79 fm) of Elton and Swift.[45]

Table 4.18

The coefficients of the expansion of WS wavefunctions for F^{17} and N^{15} in terms of HO wavefunctions

$n\ell j$	$0d_{5/2}$		$1s_{1/2}$		$0p_{1/2}$	
E_B	-0.61		-0.22		-12.16	
$\hbar\omega$ / n	12.5	13.4	11.0	13.4	15.5	13.4
0	0.981	0.979	-0.168	-0.060	0.996	0.992
1	-0.005	-0.052	0.902	0.879	-0.009	0.090
2	0.165	0.158	-0.111	-0.222	0.076	0.089
3	-0.061	-0.075	0.277	0.264	-0.028	-0.009
4	0.048	0.051	-0.135	-0.180	0.010	0.007
5	-0.041	-0.045	0.124	0.138	-0.011	-0.008
6	0.025	0.028	-0.101	-0.120	0.003	0.001
7	-0.024	-0.025	0.078	0.094	-0.004	-0.004
8	+0.017	0.019	-0.071	-0.083	0.002	0.001
9	-0.015	-0.016	0.057	0.070	-0.002	-0.002
10	0.012	-0.014	-0.052	-0.062	0.002	0.002

4-J Results for A=39 and A=41 nuclei

The procedure followed in fitting the A=39 and A=41 single-particle (hole) spectra was identical to that of the previous

section. The fitted well parameters are given in Table 4.19a and the results for the levels are tabulated in Table 4.19b. The fits to the spectra are good except for the $0f_{5/2}$ level which has a binding energy 1.17 MeV less than the experimental value. The experimental value, quoted in Table 4.8, was based on the observation of only 50% of the $0f_{5/2}$ single-particle strength. For that reason it is likely that the unperturbed single-particle position is higher than that given in Table 4.8. The Coulomb displacement energies listed in column 4 of Table 4.19b were calculated in perturbation theory with an equivalent radius $R_u = 4.52$ fm ($< r^2 >^{\frac{1}{2}} = 3.50$ fm). For an r.m.s. radius of 3.41 fm the Coulomb displacement energies were increased by 1% for the particle states and 1.5% for the hole states. The displacement energies are in good agreement with experiment considering the fragmentation of the single-particle strengths. The integrals of r^2 are listed in column 6 of Table 4.19b. The $< r^2 >$ vary considerably compared to a constant value for all states within a HO shell. The neutron wavefunctions are tabulated in Tables 4.20 and 4.21. Except for the p states, the wavefunctions all have good overlaps with corresponding oscillator wave function. The proton states were calculated by including the Coulomb potential in the differential equation. The results for the proton states are listed in the last three columns of Table 4.19b and the wavefunctions are tabulated in Table 4.22. The proton states have larger $< r^2 >$ values but the overlaps with the neutron wavefunctions are very good.

Table 4.19a

Woods-Saxon potential parameters for Ca^{41} and Ca^{39}

Nucleus	V_0 (MeV)	V_{so} (MeV)	a (fm^{-1})	r (fm)
Ca^{41}	61.77	7.0	0.75	1.14
Ca^{39}	62.9	8.5	0.75	1.14

Table 4.19b

Results for A=41 and A=39 nuclei

	neutrons						protons[a]		
$\nu\ell j$	E_B (MeV)	E_B Exp	ΔE_c[a] (MeV)	ΔE_c[b] Exp	$\langle r^2 \rangle$ (fm^2)	$\langle r^2 \rangle$ HO ($\hbar\omega$-11.5)	E_B (MeV)	E_B Exp	$\langle r^2 \rangle$ (fm^2)
$0f_{5/2}$	- 1.69	- 2.86	7.09		17.07	16.23	- 1.00	- 1.08	15.93
$1p_{1/2}$	- 4.34	- 4.23	6.71		20.93	16.23			
$1p_{3/2}$	- 6.31	- 6.29	6.92	7.00	18.73	16.23			
$0f_{7/2}$	- 8.30	- 8.36	7.32	7.28	14.78	16.23	- 1.00	- 1.08	15.93
$0d_{3/2}$	-15.62	-15.64	7.49	7.53	10.87	12.62	- 8.11	- 8.33	11.49
$1s_{1/2}$	-18.03	-18.11	7.43	7.25	11.37	12.62	-10.58	-10.86	12.13
$0d_{5/2}$	-21.54	-21.25	7.49		10.84	12.62	-14.03		11.30

a) Calculated with R_u = 4.52 fm

b) Deduced from Table 4.11

Table 4.20

The coefficients of the expansion of the WS wavefunctions for Ca^{41} in terms of HO wavefunctions

$\nu\ell j$	$0f_{7/2}$		$1p_{3/2}$		$1p_{1/2}$	$0f_{5/2}$	
E_B (MeV)	-8.30		-6.31		-4.34	-1.69	
$\hbar\omega$ / n	12.75	11.5	11.88	11.5	11.5	11.75	11.5
0	0.997	0.991	-0.073	-0.098	-0.111	0.986	0.986
1	0.004	0.100	0.982	0.981	0.968	-0.011	0.006
2	0.068	0.084	-0.056	-0.022	-0.072	0.144	0.147
3	-0.040	-0.024	0.138	0.142	0.179	-0.056	-0.052
4	0.007	0.002	-0.077	-0.069	-0.089	0.038	0.037
5	-0.013	-0.013	0.031	0.028	0.050	-0.033	-0.032
6	0.005	0.001	-0.032	-0.031	-0.045	0.019	0.018
7	-0.003	-0.003	0.016	0.014	0.025	-0.017	-0.016
8	0.003	0.002	-0.012	-0.012	-0.021	0.012	0.011
9	-0.001	0.000	0.009	0.008	0.015	-0.001	-0.009
10	0.001	0.001	-0.006	-0.005	-0.011	0.008	0.007

Table 4.21

The coefficients of the expansion of the WS wavefunctions for Ca^{39} in terms of HO wavefunctions

$n\ell j$	$0d_{3/2}$		$1s_{1/2}$		$0d_{5/2}$	
E_B (MeV)	-15.62		-18.03		-21.54	
$\hbar\omega$ / n	13.5	11.5	12.88	11.5	13.5	11.5
0	0.998	0.989	0.010	-0.059	0.999	0.989
1	-0.003	0.132	0.998	0.990	-0.006	0.138
2	0.048	0.070	-0.005	0.112	0.017	0.040
3	-0.027	-0.009	0.044	0.062	-0.027	-0.016
4	0.003	-0.001	-0.037	-0.024	-0.002	-0.008
5	-0.007	-0.007	0.001	-0.006	-0.004	-0.006
6	0.002	-0.002	-0.008	-0.009	0.002	-0.001
7	-0.001	-0.002	0.002	0.000	0.000	0.000

Table 4.22

The coefficients of the expansion of WS wavefunctions for Sc^{41} and K^{39} in terms of oscillator functions

$\nu\ell j$	$0f_{7/2}$		$0d_{3/2}$		$1s_{1/2}$		$0d_{5/2}$	
E_B (MeV)	-1.00		-8.11		-10.58		-14.03	
n \ $\hbar\omega$	12.0	11.5	13.0	11.5	12.25	11.5	13.0	11.5
0	0.994	0.993	0.997	0.993	0.000	-0.038	0.999	0.994
1	0.002	0.041	-0.013	0.089	0.997	0.995	-0.007	0.102
2	0.091	0.097	0.060	0.074	-0.007	0.057	0.024	0.039
3	-0.050	-0.042	-0.033	-0.018	0.058	0.066	-0.030	-0.021
4	0.016	0.014	0.007	0.003	-0.043	-0.034	-0.001	-0.006
5	-0.021	-0.021	-0.011	-0.010	0.004	0.000	-0.005	-0.007
6	0.010	0.008	0.005	0.002	-0.011	-0.012	0.002	0.000
7	-0.008	-0.008	-0.004	-0.005	0.004	0.002		
8	0.006	0.006	0.004	0.004	-0.002	-0.002		
9	-0.004	-0.003	-0.004	-0.004	0.002	0.002		
10	0.004	0.003	0.004	0.004	0.000	0.000		

The variation in the extension of the neutron wavefunctions is reflected in the Coulomb energy shifts. The $0p_{1/2}$ wavefunction which is considerably more spread out than the $0f_{7/2}$ wavefunction gives a Coulomb energy shift 0.61 MeV smaller than that for the $0f_{7/2}$ state. On this basis one would expect the $1p_{1/2}$ proton state to be unbound by 2.37 MeV. On the other hand, the lowest $\frac{1}{2}^-$ state in Sc^{41} (Table 4.6) has an excitation energy only 0.15 MeV less than that of the lowest $\frac{1}{2}^-$ state in Ca^{41} (Table 4.8). The second $\frac{1}{2}^-$ level in Sc^{41} is depressed by 0.22 MeV relative to the second $\frac{1}{2}^-$ in Ca^{41} which is identified as containing more than 50% of the $p_{\frac{1}{2}}$ single-particle strength. The behaviour of the $p_{\frac{1}{2}}$ state is very similar to that of the $0d_{3/2}$ state in A=17 nuclei.

Certainly the treatment of these levels, the $p_{\frac{1}{2}}$ state in Sc^{41} and the $d_{3/2}$ state in F^{17}, would be improved by recognizing that they lie in the continuum. However, further investigation of this sort is somewhat outside the scope of the present work. We require only a fairly reasonable determination of the single-particle wavefunctions which are later to be used in shell model spectroscopic calculations.

4-K Results for A=207 and A=209 Nuclei

There have been many attempts [77-82] to obtain single-particle potentials that fit the experimental data in the lead region. In the oxygen and calcium isotopes there were sufficient parameters available to fit the experimental spectra. In Pb^{209} and Pb^{208} there are seven particle levels and six hole levels while there are only

three parameters in the potential since the radius is to be fixed by fitting the Coulomb displacement energy. The general feature of WS potentials is that they give single-particle levels spaced too far apart.[79] Recently Rost[82] obtained a reasonable fit to the neutron states in lead with a WS potential. It is a property of the single-particle potential that the levels can be brought closer together by increasing the well radius while decreasing the well depth. At the same time the spin-orbit strength must be increased to keep spin-orbit pairs of states apart. This is essentially what Rost did to improve upon the results of Blomqvist and Wahlborn[79] for neutrons. When fitting the experimental spectrum it is assumed that the states are pure single-particle states; however if there is some fragmentation of the single-particle strength then the unperturbed single-particle energies are not those observed experimentally. In the lead region the residual two-body interaction matrix elements are too small so that the difference between the unperturbed single-particle positions and the observed energies would not be as large as 1 or 2 MeV.[79]

In the present work it has been our approach to remove the well known $V_0 r_0^n$ ambiguity by determining the well radius from a calculation of Coulomb displacement energies. The experimental Coulomb displacement energy of the Bi^{208} analogue of the Pb^{208} ground state is 18.98 MeV.[83] Including the exchange correction of 3.5% estimated by Nolen et al.[71] the present model should predict a Coulomb displacement energy of approximately 19.69 MeV. In the shell model description of the Bi^{208} analogue state, the Coulomb energy shift is

calculated by averaging over the Coulomb energies of the states in the neutron excess as discussed in Sec. 4-E. Another quantity that is determined by the well radius is the r.m.s. radius of the neutron excess. Nolen et al. assumed a form for the neutron density distribution and by adjusting the parameters to give the correct Coulomb displacement energy calculated the r.m.s. radius of the neutron excess to be 5.70 fm. This result is consistent with the total neutron r.m.s. radius being slightly larger than the proton r.m.s. radius ($< r^2 >_n^{\frac{1}{2}} = 1.035 < r^2 >_p^{\frac{1}{2}}$). From an optical modelanalysis of low energy proton on Pb^{208} scattering Greenless, Pyle and Tang[84] have deduced that the neutron radius is larger than the proton radius ($< r^2 >_n^{\frac{1}{2}} = (1.09 \pm 0.05) \times < r^2 >_p^{\frac{1}{2}}$). In view of these results we imposed the condition that the neutron well radius lead to a Coulomb displacement energy of approximately 19.6 MeV and an r.m.s. radius for the neutron excess of approximately 5.70 fm.

Before proceeding to fit potentials to the experimental specta the Blomqvist-Wahlborn (BW) and Rost potentials were checked for conformity to the above criteria. The BW and Rost well parameters used in the calculation are given in Table 4.23. The Rost well gave a Coulomb displacement energy of 18.16 MeV and an r.m.s. radius of 6.53 fm for the neutron excess. The BW well gave a Coulomb displacement energy of 18.73 MeV and an r.m.s. radius of 6.21 fm for the neutron excess. The Coulomb energies were calculated for a uniform charge distribution having an r.m.s. radius of 5.49 fm. (Table 4.1). Rost also fitted the levels by using a different radius for the

Table 4.23

Parameters for the Blomqvist-Wahlborn[79] and Rost[82] neutron potentials

	V_0 (MeV)	V_{so} (MeV)	r_o (fm)	a (fm^{-1})
Rost	40.5	8.30	1.349	0.70
BW	44.0	7.82	1.27	0.67

spin-orbit term than for the central well. Blomqvist and Wahlborn, and Rost, included corrections for pairing energies in the hole states and for collective effects. Neither of these improvements on the model would alter the above results significantly. All of the potentials studied by Rost have a central well radius larger than that of the BW well. Clearly the potential must have a smaller radius than that of the Rost or BW potential in order that the Coulomb energy and r.m.s. radius are correctly predicted.

Rost introduced two additional parameters into the spin-orbit term but found that the neutron data could not be reasonably fitted with $r_0 \approx 1.25$ fm. To fit the Coulomb energy and radius of the neutron excess we considered first only the hole levels in Pb^{208}. It was found that the radius and the energy levels could not be fitted simultaneously. However, by omitting the $0i_{13/2}$ level a good fit was obgained. With the set of parameters the position of the $0i_{13/2}$ level was calculated and the positions of the Pb^{209} particle

levels were calculated. In going from Pb^{208} to Pb^{209} we made the $A^{1/3}$ change as discussed in the previous sections. The results with this set of well parameters are given in column I of Fig. 4.5. All of the levels are above their experimental positions. This is in marked contrast to lighter nuclei where it was found that as the experimental levels became more deeply bound the well depth and spin-orbit strength had to be increased. This phenomenon has been pointed out by Brown, Gunn and Gould.[85] By increasing the well depth and the spin-orbit strength the $0i_{13/2}$ hole level and the particle levels, except for the $0j_{15/2}$ state, come down to give good agreement with experiment. The results are shown in column II of Fig. 4.5. The fact that the $0i_{13/2}$ hole level was fitted with the same parameters as the particle levels and the $0j_{15/2}$ level was not fitted with the second set of parameters indicates a correlation with the oscillator shell degeneracy of $2n+\ell$. Since there was only the $0j_{15/2}$ state remaining to be fitted, both the well depth and spin-orbit strength for this level were increased arbitrarily to fit the experimental position. The final spectrum with the well parameters of Table 4.24bis given in the fourth column of Fig. 4.5. With the wavefunctions for the Pb^{208} hole levels the Coulomb displacement energy of the Bi^{208} analogue state was calculated to be 19.62 MeV. Including the exchange correction of 3.5% we have that ΔE_c = 18.93 MeV to be compared to the experimental value of 18.98 MeV. In addition, the r.m.s. radius of the neutron excess was calculated to be 5.72 fm which is consistent with the value of 5.70 fm obtained by Nolen et al.

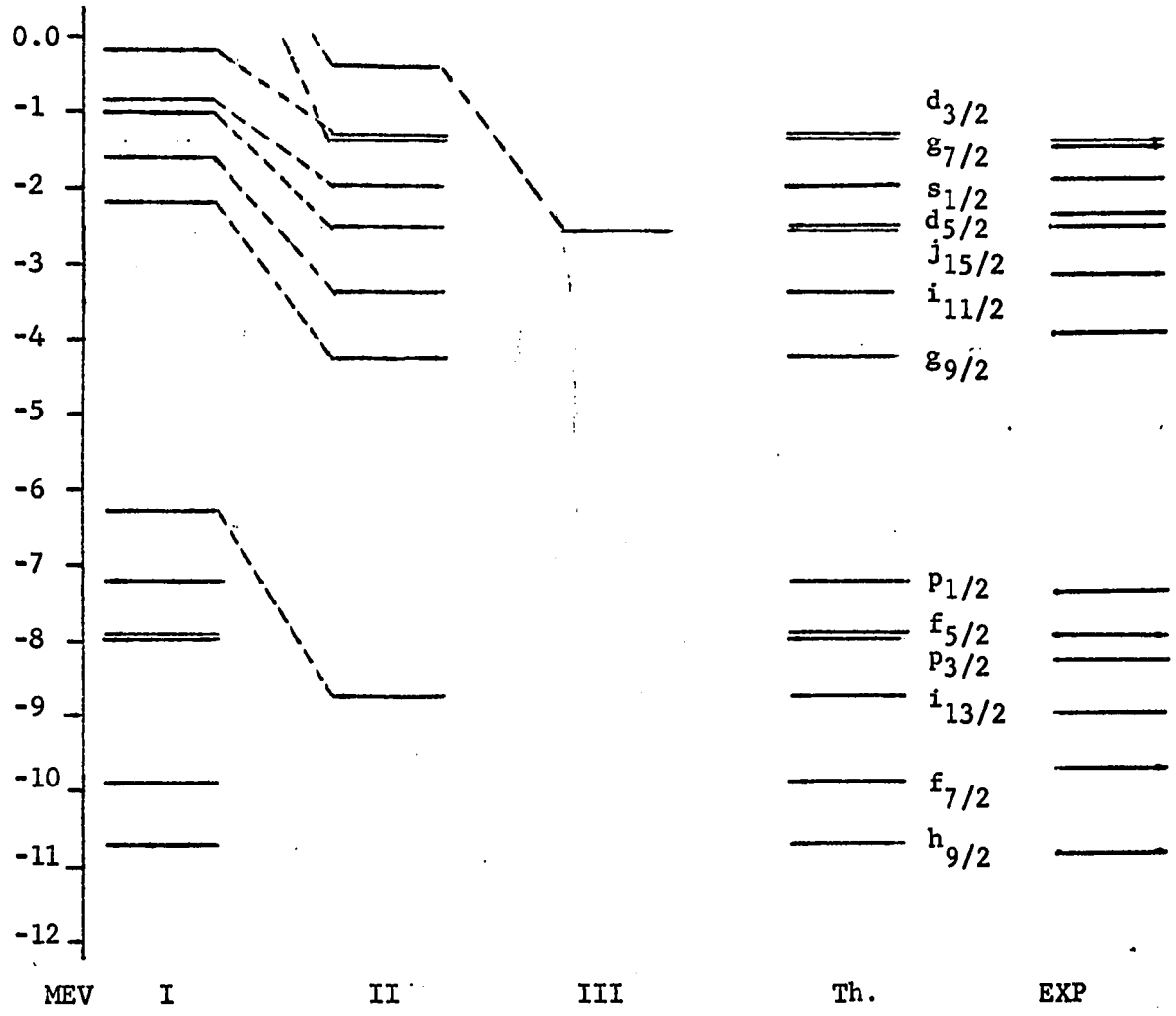

Fig. 4-5. The single-particle and hole spectra of Pb^{209} and Pb^{208}. Columns I, II and III are the spectra with different potentials for states belonging to the same oscillator shell. The parameters are given in Table 4.25b.

Table 4.24

The integrals $< r^2 >$ and Coulomb energy shifts for the Pb^{209} particle states and Pb^{208} hole states

$\nu\ell j$	E_B (MeV)	$< r^2 >$ (fm^2)	ΔE_c † (MeV)	$\nu\ell j$	E_B (MeV)	$< r^2 >$ (fm^2)	ΔE_c † (MeV)
$2d_{3/2}$	-1.34	52.13	17.39	$2p_{1/2}$	- 7.22	34.08	19.52
$1g_{7/2}$	-1.37	39.99	18.65	$1f_{5/2}$	- 7.97	31.79	19.79
$3s_{1/2}$	-1.98	56.18	17.02	$2p_{3/2}$	- 7.94	33.55	19.59
$2d_{5/2}$	-2.52	46.36	17.98	$0i_{13/2}$	- 8.76	34.84	19.23
$0j_{15/2}$	-2.54	37.80	18.76	$1f_{7/2}$	- 9.87	31.58	19.82
$0i_{11/2}$	-3.39	33.37	19.47	$0h_{9/2}$	-10.70	30.47	19.94
$1g_{9/2}$	-4.24	37.39	18.97				

† Calculated for a charge distribution with an r.m.s. radius 5.49 fm

The calculated energies, integrals of r^2 and Coulomb energy shifts, are given in Table 4.24. From the values of the integrals of r^2 it can be seen that wavefunctions vary considerably from those of a HO potential. In particular, the states of low orbital angular momentum and small binding energy have large tails. The wavefunctions are tabulated in Table 4.25 as expansions in HO wavefunctions. In the calculation of the wavefunctions a cutoff of 16.0 fm was used. The (2s,1d,0g) shell hole states were calculated with the same well parameters as for the (2p,1f,0h) shell states. The hole energies are given in Table 4.26.

Table 4.25a

The WS particle and hole neutron wavefunctions for Pb^{209} and Pb^{208} as expansions in terms of HO wavefunctions. For each state the first column is the value of $\hbar\omega$ that maximizes the overlap of the oscillator function with the same number of nodes, the second column is a common $\hbar\omega$ value for all states.

$n\ell j$	$2d_{3/2}$		$1g_{7/2}$		$3s_{1/2}$		$2d_{5/2}$		$0j_{15/2}$		$0i_{11/2}$	
E_B (Mev)	-1.34		-1.37		-1.98		-2.52		-2.54		-3.39	
n \ $\hbar\omega$	7.81	8.00	8.44	8.00	7.56	8.00	7.81	8.00	9.38	8.00	9.38	8.00
0	0.068	0.066	-0.023	-0.085	0.000	0.002	0.072	0.071	0.998	0.973	0.998	0.976
1	-0.082	-0.050	0.988	0.983	0.085	0.082	-0.046	-0.013	-0.006	0.221	-0.004	0.203
2	0.956	0.954	-0.026	0.058	-0.093	-0.012	0.976	0.974	-0.020	0.044	0.002	0.057
3	-0.072	-0.109	0.077	0.096	0.946	0.936	-0.043	-0.084	-0.058	-0.049	-0.055	-0.040
4	0.158	0.151	-0.114	-0.104	-0.083	-0.171	0.104	0.097	0.004	-0.024	0.003	-0.018
5	-0.172	-0.177	0.026	0.012	0.172	0.157	-0.147	-0.151	0.000	-0.012	-0.004	-0.013
6	0.065	0.072	-0.032	-0.034	-0.185	-0.197	0.037	0.045	0.010	0.004	0.009	0.002
7	-0.073	-0.073	0.029	0.024	0.070	0.091	-0.044	-0.044				
8	0.058	0.062	-0.012	-0.009	-0.078	-0.080	0.040	0.043				
9	-0.034	-0.037	0.014	0.013	0.062	0.072	-0.016	-0.019				
10	0.030	+0.032	-0.009	-0.005	-0.034	-0.043	0.017	0.018				

Table 4.25a

$\nu\ell j$	$1g_{9/2}$		$2p_{1/2}$		$1f_{5/2}$		$2p_{3/2}$		$0i_{13/2}$		$1f_{7/2}$	
E_B (Mev)	-4.24		-7.22		-7.97		-7.94		-8.76		-9.87	
n \ $\hbar\omega$	8.25	8.00	7.75	8.00	8.12	8.00	7.75	8.00	9.00	8.00	8.00	8.00
0	0.022	-0.014	0.063	0.064	0.044	0.027	0.065	0.066	0.998	0.986	0.078	0.078
1	0.995	0.993	0.019	0.059	0.996	0.996	0.042	0.082	-0.012	0.155	0.994	0.994
2	0.007	0.061	0.992	0.990	0.018	0.043	0.992	0.988	-0.039	-0.005	0.012	0.012
3	0.016	0.027	0.014	-0.043	-0.002	0.002	0.006	-0.052	-0.048	-0.054	-0.030	-0.030
4	-0.095	-0.093	0.021	0.014	-0.007	-0.077	0.004	-0.002	0.003	-0.018	-0.073	-0.073
5	0.006	-0.003	-0.098	-0.098	-0.001	-0.005	-0.095	-0.094	0.005	-0.002	-0.001	-0.001
6	-0.010	-0.012	0.002	0.011	-0.003	-0.004	0.002	0.011	0.007	0.007	0.003	0.003

Table 4.25a continued

$\nu\ell j$	$0h_{9/2}$	
E_B (MeV)	-10.70	
$\hbar\omega$ / n	8.81	8.00
0	0.998	0.990
1	0.006	0.132
2	-0.028	-0.003
3	-0.045	-0.046
4	-0.001	-0.015
5	0.003	-0.002
6	0.006	0.005

Table 4.25b

The neutron potential parameters for the single-particle and hole states in Pb^{209} and Pb^{208}

$2n+\ell$	V_0 (MeV)	V_{so} (MeV)	r_o (fm)	a (fm^{-1})
5	52.0	5.32	1.135	0.70
6	55.0	6.32	1.135	0.70
7	57.8	6.82	1.135	0.70

Table 4.26

Additional neutron hole state energies in Pb^{208}

$n\ell j$	$0h_{11/2}$	$2s_{1/2}$	$1d_{3/2}$	$1d_{5/2}$	$0g_{7/2}$	$0g_{9/2}$
E_B (MeV)	-14.3	-16.1	-16.6	-17.8	-19.4	-21.9

In light nuclei with N=Z the proton and neutron nuclear potentials are the same. In heavy nuclei with a neutron excess an isospin dependent or "symmetry energy" term is required.[86-91] The isospin dependent term is usually taken to have a volume form factor identical to the isospin independent form factor.[92] With such a volume form factor the neutron and proton well depths are found to differ by a factor proportional to $(\frac{N-Z}{A})$. Surface peaked form factors have been discussed by Terasawa and Satchler.[93] To fit the proton particle and hole spectra of Bi^{209} and Pb^{208} we first assumed that the neutron and proton nuclear potentials differed only in their well depths. It was impossible to fit the experimental spectra with one set of parameters. The proton levels showed an oscillator shell dependence similar to that for the neutron states although it was not as pronounced. A reasonable fit to the data was found using different well depths and spin orbit strengths for states having different values of $2n+\ell$. The fitted well parameters are given in Table 4.27. With the well parameters for the $2p_{3/2}$ state the $2p_{\frac{1}{2}}$ level was unbound. The well depth was increased slightly to obtain

Table 4.27

Wood-Saxon potential parameters for the proton particle and hole states in Bi^{209} and Pb^{208}

$2n+\ell$	V_0 (MeV)	V_{so} (MeV)	r_0 (fm)	a (fm^{-1})
4	67.5	5.32	1.135	0.70
5	69.6	7.82	1.135	0.70
6	71.2	7.82	1.135	0.70
$(2p_{1/2})$	70.85	7.82	1.135	0.70

a bound state wavefunction for shell model calculations. The calculated spectrum is shown in the first column of Fig. 4.6 and the binding energies and integrals of r^2 are given in Table 4.28. The wavefunctions are tabulated as expansions in terms of HO wavefunctions in Table 4.29.

Table 4.28

The proton particle and hole energies and integrals of r^2 for Bi^{209} and Pb^{208} (r_0=1.135 fm)

$n\ell j$	E_B (MeV)	$< r^2 >$ (fm^2)	$n\ell j$	E_B (MeV)	$< r^2 >$ (fm^2)
$2s_{1/2}$	- 7.64	23.81	$2p_{1/2}$	-0.18	28.79
$1d_{3/2}$	- 8.52	24.36	$2p_{3/2}$	-0.34	29.13
$0h_{11/2}$	- 9.29	30.58	$1f_{5/2}$	-0.48	28.49
$1d_{5/2}$	- 9.74	24.64	$0i_{13/2}$	-2.11	33.35
$0g_{7/2}$	-12.40	26.40	$1f_{7/2}$	-3.23	28.78
$0g_{9/2}$	-14.8	27.63	$0h_{9/2}$	-4.21	28.65

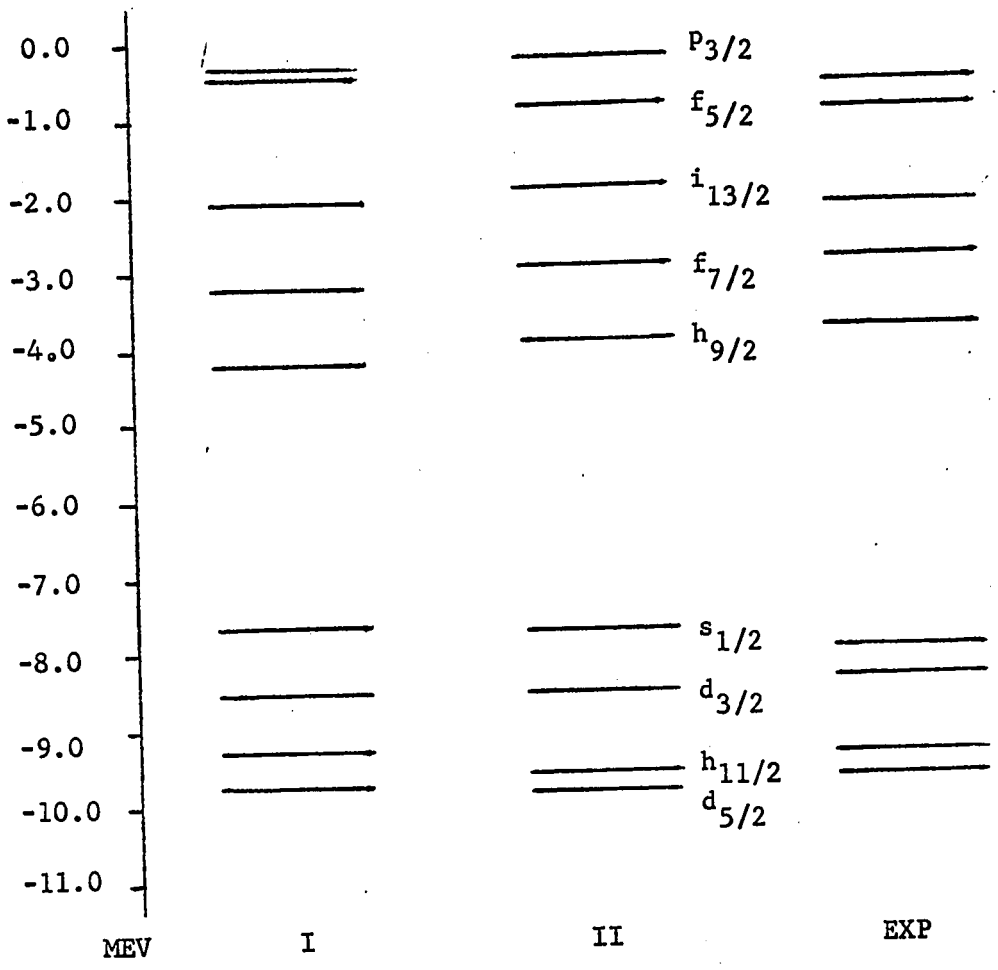

Fig. 4-6. The proton particle and hole spectra for Bi^{209} and Pb^{208}. The spectra I and II are for the potentials with r_o - 1.135 and 1.27 fm respectively.

Table 4.29

The proton WS wavefunctions for Bi^{209} and Pb^{208} as expansions in terms of HO wavefunctions. For each state the first column is the value of $\hbar\omega$ that maximizes the overlap with an oscillator function and the second is a common value for all the states. The wavefunctions are for the WS potentials with $r_0 = 1.135$ fm.

$n\ell j$	$2p_{1/2}$		$2p_{3/2}$		$1f_{5/2}$		$0i_{13/2}$		$1f_{7/2}$		$0h_{9/2}$	
E_B (Mev)	-0.18		-0.34		-0.48		-2.11		-3.23		-4.21	
$\hbar\omega$ / n	8.31	8.00	8.12	8.00	8.62	8.00	9.38	8.00	-8.25	8.00	9.50	8.00
0	0.077	0.076	-0.080	0.080	0.081	0.002	0.997	0.973	0.100	0.068	0.997	0.975
1	0.073	0.025	0.083	0.064	0.992	0.983	-0.008	0.220	0.988	0.986	-0.014	0.215
2	0.988	0.984	0.986	0.986	0.036	0.165	-0.064	-0.006	0.056	0.110	-0.055	0.001
3	0.045	0.118	0.046	0.075	-0.047	-0.014	-0.047	-0.059	-0.070	-0.057	-0.042	-0.050
4	-0.042	-0.024	-0.049	-0.043	-0.076	-0.079	0.003	-0.028	-0.077	-0.082	0.002	-0.025
5	-0.094	-0.096	-0.095	-0.097	-0.005	-0.024	0.009	-0.004	-0.007	-0.016	0.006	-0.005
6	-0.006	-0.018	-0.006	-0.012	0.004	-0.004	0.007	0.007				

Table 4.29 continued

$\nu\ell j$	$2s_{1/2}$		$1d_{3/2}$		$0h_{11/2}$		$1d_{5/2}$		$0g_{7/2}$		$0g_{9/2}$	
E_B (Mev)	-7.64		-8.52		-9.29		-9.74		-12.4		-14.8	
$\hbar\omega$ / n	7.69	8.00	7.94	8.00	8.88	8.00	7.75	8.00	8.62	8.00	8.25	8.00
0	0.007	0.071	0.122	0.130	0.996	0.987	0.134	0.163	0.996	0.992	0.995	0.994
1	0.129	0.171	0.984	0.984	-0.009	0.136	0.982	-.980	-.003	0.100	0.003	0.043
2	:0.979	0.975	0.068	0.055	-0.079	-0.053	0.071	0.019	-0.073	-0.058	-0.086	-0.081
3	0.079	0.009	-0.079	-0.081	-0.042	-0.058	-0.088	-0.096	-0.040	-0.051	-0.041	-0.047
4	-0.083	-0.094	-0.069	-0.067	0.004	-0.016	-0.070	-0.063	0.002	-0.010	0.003	-0.002
5	-0.080	-0.071	-0.009	-0.007	0.011	0.005	-0.008	0.000	0.009	0.006	0.011	0.010

Comparing Tables 4.24 and 4.28 it can be seen that the proton particle states have smaller r.m.s. radii than the corresponding neutron states. Although the proton states have smaller binding energies the Coulomb barrier tends to keep them localized more within the well. The proton states have radii more like the constant radius within a shell for a HO potential. By examining the overlap integrals in Table. 4.29 it can be seen that the proton states differ from HO wavefunctions more in shape in the interior region of the nucleus rather than in extension beyond the well as in the case of neutrons. The r.m.s. radius for the first shell of proton hole states is 5.23 fm. Including the remainder of the core would decrease this and give a proton distribution r.m.s. radius of approximately 5.0 fm. Clearly this is inconsistent with the observed chrage distribution r.m.s. radius of 5.49 fm. To obtain the observed r.m.s. radius for the protons and keep our single-particle description of the nucleus a proton well different from the neutron well is required.

To fit the observed r.m.s. radius for protons the single particle spectra was refitted with WS potentials of larger radius. The final well parameters are given in Table 4.30. All of the bound levels except the 0h levels were reasonably fitted with one set of potential parameters. To fit the experimental positions of the 0h levels a larger spin-orbit splitting was required. To obtain a bound state wavefunction for the $2p_{\frac{1}{2}}$ state the well depth was increased slightly. The calculated spectra are shown in the second

Table 4.30

Potential parameters to fit the proton particle and hole spectra of Bi^{209} and Pb^{208} and the charge distribution radius

$n\ell j$	V_0 (MeV)	V_{so} (MeV)	r_0 (fm)	a (fm^{-1})
$2p_{1/2}$ $2p_{1/2}$	60.6	7.40	1.27	0.70
$2p_{3/2}$, $1f_{5/2}$, $0i_{13/2}$ $1f_{7/2}$, $2s_{1/2}$, $1d_{3/2}$ $1d_{5/2}$, $0g_{7/2}$, $0g_{9/2}$	60.6	7.40	1.27	0.70
$0h_{9/2}$, $0h_{11/2}$	59.6	11.0	1.27	0.70

column of Fig. 4.6. The calculated energies and integrals of r^2 are given in Table 4.31. The r.m.s. radius for the proton distribution was determined using wavefunctions for the remaining states calculated with the well parameters that fitted the first shell of hole states (excluding $0h_{11/2}$). The result was an r.m.s. radius of 5.49 fm for the proton centres and 5.55 fm for the charge distribution which is consistent with the experimental value. The wavefunctions are tabulated in Table 4.32 as expansions in terms of HO wavefunctions. A best oscillator size parameter for all of the levels was taken to be $\hbar\omega$ = 6.75 MeV. For calculations using the neutron and proton wavefunctions together the proton wavefunctions are tabulated in Table 4.33 with $\hbar\omega$ = 8.0 MeV.

Table 4.31

Proton particle and hole energies and integrals of r^2 for Bi^{209} and Pb^{208} (r_0=1.27 fm)

$n\ell j$	E_B (MeV)	$< r^2 >$ (fm^2)	$n\ell j$	E_B (MeV)	$< r^2 >$ (fm^2)
$2s_{1/2}$	- 7.71	27.79	$2p_{1/2}$	-0.14	33.64
$1d_{3/2}$	- 8.52	28.92	$2p_{3/2}$	-0.21	34.07
$0h_{11/2}$	- 9.58	38.59	$1f_{5/2}$	-0.84	33.99
$1d_{5/2}$	- 9.84	29.47	$0i_{13/2}$	-1.92	41.45
$0g_{7/2}$	-12.33	32.50	$1f_{7/2}$	-2.93	34.50
$0g_{9/2}$	-14.9	34.68	$0h_{9/2}$	-3.93	34.95

Table 4.32

The proton WS wavefunctions for Bi^{209} and Pb^{208} as expansions in HO wavefunctions. For each state the first column is the value of $\hbar\omega$ that maximizes the overlap with an oscillator function while the second is a common value for all states. The wavefunctions are for the potentials with $r_0 = 1.27$ fm.

$n\ell j$	$2p_{1/2}$		$2p_{3/2}$		$1f_{5/2}$		$0i_{13/2}$		$1f_{7/2}$		$0h_{9/2}$	
E_B (Mev)	-0.14		-0.21		-0.84		-1.92		-2.93		-3.93	
$\hbar\omega$ / n	6.69	6.75	6.50	6.75	7.00	6.75	7.50	6.75	6.62	6.75	7.75	6.75
0	0.092	0.092	0.094	0.098	0.125	0.087	0.955	0.983	0.132	0.152	0.996	0.980
1	0.108	0.119	0.110	0.156	0.985	0.985	0.001	0.159	0.980	0.979	-0.006	0.183
2	0.979	0.979	0.977	0.973	0.035	0.100	-0.085	-0.050	0.070	0.036	-0.074	-0.031
3	0.065	0.046	0.077	0.002	-0.080	-0.066	-0.053	-0.070	-0.096	-0.102	-0.046	-0.062
4	-0.074	-0.077	-0.077	-0.092	-0.082	-0.088	0.004	-0.021	-0.087	-0.082	0.003	-0.024
5	-0.103	-0.102	-0.106	-0.098	-0.004	-0.015	0.013	0.005	-0.009	-0.002	0.010	0.000
6	-0.010	-0.006	-0.012	0.002	0.012	0.008	0.009	0.012	0.015	0.017	0.007	0.009

Table 4.32 continued

$\nu\ell j$	$2s_{1/2}$		$1d_{3/2}$		$0h_{11/2}$		$1d_{5/2}$		$0g_{7/2}$		$0g_{9/2}$	
E_B (Mev)	-7.71		-8.52		-9.58		-9.84		-12.3		-14.9	
n \ $\hbar\omega$	6.12	6.75	6.38	6.75	7.00	6.75	6.19	6.75	7.06	6.75	6.62	6.75
0	0.079	0.092	0.151	0.204	0.993	0.992	0.170	0.248	0.994	0.993	0.992	0.992
1	0.159	0.258	0.975	0.969	-0.001	0.052	0.971	0.956	-0.006	-0.054	-0.006	-0.031
2	0.966	0.948	0.092	-0.004	-0.106	-0.099	0.089	-0.060	-0.095	-0.088	-0.111	-0.112
3	0.114	-0.063	-0.102	-0.118	-0.049	-0.059	-0.115	-0.133	-0.043	-0.053	-0.045	-0.040
4	-0.107	-0.133	-0.080	-0.065	0.007	-0.001	-0.083	-0.054	0.006	-0.002	0.008	0.012
5	-0.094	-0.063	-0.011	0.005	0.017	0.016	-0.010	0.015	0.013	0.012	0.017	0.016
6	-0.016	0.015	0.015	0.018	0.009	0.011	0.018	0.022	0.007	0.009	0.008	0.007

Table 4.33

The proton wavefunctions of Table 4.32 expanded in terms of HO wavefunctions with $\hbar\omega$ = 8.0 MeV

$\nu\ell j$	$2p_{1/2}$	$2p_{3/2}$	$1f_{5/2}$	$0i_{13/2}$	$1f_{7/2}$	$0h_{9/2}$	$2s_{1/2}$	$1d_{3/2}$	$0h_{11/2}$	$1d_{5/2}$	$0g_{7/2}$	$0g_{9/2}$
E_B (Mev)	-0.14	-0.21	-0.84	-1.92	-2.93	-3.93	-7.71	-8.52	-9.58	-9.84	-12.3	-14.9
n \ $\hbar\omega$	8.0	8.0	8.0	8.0	8.0	8.0	8.0	8.0	8.0	8.0	8.0	8.0
0	0.122	0.132	0.262	0.990	0.323	0.995	0.127	0.352	0.976	0.394	0.981	0.963
1	0.318	0.350	0.938	-0.098	0.902	-0.051	0.417	0.888	-0.196	0.854	-0.172	-0.258
2	0.891	0.865	-0.205	-0.086	-0.271	-0.076	0.825	-0.281	-0.090	-0.331	-0.083	-0.073
3	-0.283	-0.324	-0.078	-0.036	-0.082	-0.040	-0.350	-0.083	-0.007	-0.073	-0.010	0.011
4	-0.066	-0.059	-0.044	0.017	-0.022	0.009	-0.069	-0.005	0.026	0.010	0.020	0.025
5	-0.048	-0.038	0.031	0.013	0.038	0.011	0.004	0.033	0.010	0.035	0.009	0.005
6	0.045	0.050	0.010	0.005	0.010	0.006	0.040	0.009	-0.001	0.005	0.001	-0.004
7	0.007	0.005	0.007	-0.003	0.001	-0.001	0.005	-0.002	-0.005	-0.005	-0.004	-0.004

It is clear from the above results that the present microscopic description of the Pb^{208} single-particle states and size is ambiguous. For this reason we briefly review the validity of the results. It is possible that Woods-Saxon potentials fitted to a few states near the top of the well are not a valid description of the remaining levels that are more deeply bound. For example, in light nuclei the well depth had to be increased for more deeply bound levels; however, this has the effect of decreasing the r.m.s. radius. For the proton well with $r_0 = 1.135$ fm the well was fitted to the states in the shell containing 42 of the 82 protons. For this shell the r.m.s. radius was 5.23 fm and the reminaing levels could not increase the radius. Elton and Swift[45] have checked for Ca^{40} the effect of including the correct charge distribution rather than the uniform distribution used here and found the effect to be small. For the neutron case the present microscopic model gave a Coulomb displacement energy and r.m.s. radius for the neutron excess which were consistent with the results of Nolen et al.[71] who used a macroscopic model with realistic Fermi distributions. In our calculation the Coulomb exchange energy correction used was the same as that of Nolen et al. Increasing the exchange correction would give a larger well radius. In the limit of zero exchange correction the BW potential well, which has $r_0 = 1.27$ fm., gives a Coulomb displacement energy of 18.73 MeV which is consistent with experiment. The corresponding large r.m.s. radius for the neutron excess

would seem to imply the existence of a neutron "halo". In fact, the results are consistent with those of the naive HO potential model of Sec. 4-D. Imposing the condition that the proton and neutron matter distributions have the same r.m.s. radii forced the use of HO potentials of different sizes. The values of $\hbar\omega$ deduced for HO potentials are close to the average values from the WS calculation.

With a charge independent nuclear Hamiltonian the use of single-particle potentials of different radii for neutrons and protons destroys isospin invariance. To regain isospin invariance the single-particle potentials must be coupled through the introduction of ground state correlations.[94] This means that in shell model calculations with these potentials the residual two-body perturbation would have to account for this coupling.

In the single-particle description of the neutron states it was found that the well parameters were oscillator shell dependent. The well depth was larger for states belonging to higher oscillator shells. The necessity of a deeper well near the Fermi surface was pointed out by Brown, Gunn and Gould[85] and was interpreted to imply an effective mass greater than unity. This effect has also been observed by Elton and Swift[95] in Ca^{48}.[96] Recently Bertsch and Kuo have discussed the effect of core-polarization on the single-particle strength and the resultant increase in effective mass for states near the Fermi surface. It is possible that the peculiar behaviour of the levels in the single-particle model can be explained by the

presence of correlations in the ground state. When the proton well was increased in size to give a radius consistent with experiment the shell effect for protons disappeared.

4-L Summary

Woods-Saxon potentials with a Thomas spin-orbit term were used to obtain single-particle wavefunctions for shell model calculations. The wavefunctions were expanded in terms of HO wavefunctions. In the light nuclei the single-particle potentials were consistent with the experimental data. It was found that the value of $\hbar\omega$ that maximized the overlap of an HO wavefunction with the calculated WS wavefunction was state dependent. The state dependence was most pronounced for particle states relative to hole states with hole states requiring a larger average value of $\hbar\omega$ than particle states.[/] To a good approximation deeply bound levels can be represented by a single HO wavefunction. The states that have small binding energies, in particular, states with low orbital angular momentum, tend to extend much further beyong the potential than the corresponding oscillator functions.

In the heavy nuclei of the Pb region it was found that the present single-particle model was inconsistent with the experimental data. Neutron and proton potentials of different radii are required to fit the data which immediately implies the existence of ground state correlations. The analysis of nucleon-transfer experiments discussed in Sec. 4-F are consistent with the shell model description of the Pb^{208} ground state. Recent experiments by Glashausser et al.[97]

[/] This effect has been pointed out by Wong and Wong.[98]

using inelastic proton scattering to excite single-hole states in Pb^{207} indicate that core-polarization is important in describing the single-particle transitions. Furthermore, single-particle electromagnetic properties[97] indicate the presence of significant amounts of core-excitation.

Apart from the validity of the single-particle model it is interesting that the potential parametrization used in this case allows one to fit the neutron spectra with a small well radius. Rost introduced additional parameters into the spin-orbit term but still required a neutron well larger than the proton well which is inconsistent with the matter distributions being nearly the same. Rost obtained his best fit with the large radius using six parameters to fit thirteen single-particle energies. In our fit with the small radius six parameters were used to fit twelve single-particle energies and the r.m.s. radius of the neutron excess. With the additional parameters Rost was able to fit the proton states with one potential of nearly the same radius as the present one whereas we required a larger spin-orbit splitting for the 0h levels. Since the radius of the valence orbitals is a determining factor in two-body interactions we would expect either Rost's or our proton wells to give similar two-particle and two-hole spectra. However, definite differences should arise from replacing Rost's neutron well by ours.

Experimental results obtained by the Los Alamos group after this theoretical analysis was completed indicate that the $0j_{15/2}$ single-particle strength is spread over at least two states. The

state at E_x = 1.41 MeV contains only 50% of the single-particle strength and a state at E_x = 3.56 MeV may contain as little as 30% of the single-particle strength. The splitting of the single-particle strength arising from strong mixing with the $\{g_{9/2}(Pb^{208}, 3^-)\}\ \frac{15}{2}^-$ configuration. Assuming that the 3.56 MeV state contains 50% of the strength the unperturbed position of the $0j_{15/2}$ state would be at E_x = 2.48 MeV or E_B = -1.46 MeV. With this unperturbed energy the $0j_{15/2}$ level is still not predicted with the Woods-Saxon potential for the other Pb^{209} single-particle states. However, if future experiments show further fragmentation of the single-particle strength, it may be possible to fit all of the Pb^{209} states with a single set of potential parameters.

CHAPTER 5

THE EFFECT OF WOODS-SAXON WAVEFUNCTIONS ON SHELL MODEL SPECTRA

5-A Introduction

In this chapter we present several calculations that were performed to examine the effects of using Woods-Saxon wavefunctions in shell model calculations. In these calculation the phenomenological free reaction matrix that was used as an effective interaction in Chapter 3 was used as the residual interaction. This interaction is simple to work with and was determined from the free nucleon scattering data. It also had the added feature that the results for a normal attractive potential and a velocity dependent potential could be studied simultaneously. Since the interactions act only in relative S states, the calculations were confined to light nuclei. The two-particle and two-hole spectra of A=14, 18 and 38 nuclei were calculated using both harmonic oscillator (HO) and Woods-Saxon (WS) wavefunctions. For valence particles with small binding energies the WS wavefunctions are spread out relative to the HO wavefunctions which must lead to smaller two-body matrix elements. For more deeply bound levels which are localized within the potential, the shapes of the WS and HO wavefunctions differ only slightly. The (1s,0d) states are valence particle states in A=17 nuclei and deeply bound hole states in A=39 nuclei; consequently, the two-body matrix

elements for these two cases are convenient for isolating the effects of tails and shape in the WS wavefunctions.

Flowers and Wilmore[10] have studied the A=17 spectra using a phenomenological interaction and Woods-Saxon wavefunctions. Their work differs from the present calculations in the interaction and in the wavefunctions used. The WS wavefunctions were calculated using an effective mass in the solution of the Schrödinger equation and the calculated single-particle energies were depressed from their experimental positions. Stamp and Mayer[11] have examined the effects of using WS wavefunctions to calculate the position of the octupole state in O^{16} and Ca^{40}.

5-B The Model

In Chapter 2 the shell model description of two-particle and two-hole states was discussed. If the residual interaction is not a function of the excitation energy, the spectra are obtained by diagonalizing Hamiltonians of the form

$$H = H_0 + v$$

where H_0 is the unperturbed single-particle Hamiltonian and v is the residual two-body interaction. The calculations were carried out for both HO and WS single-particle potentials. With a HO potential the unperturbed energies used are the experimental single-particle energies. For the WS potentials the wavefunctions given in Tables 4-15, 4-17 and 4-21 were used. In the WS calculations the experimental single-particle energies rather than the calculated energies were used. The effective interactions used were the free reaction

matrices given in Sec. 3-C. Our primary interest in the calculations was to consider the effects of WS wavefunctions on two-body interaction matrix elements. With ϵ = 86 MeV the free reaction matrices give reasonable matrix elements for the nuclei considered and that value was used in all the calculations. Expressions for the two-body interaction matrix elements for two-particle and two-hole states are given in Appendix A. The j-j coupling scheme was used in all the calculations.

A two-body matrix element with HO or WS wavefunctions only differs in the radially dependent part of the matrix element. By expanding the WS wavefunctions for the single-particle states included in a calculation in terms of HO wavefunctions with a common value of $\hbar\omega$ the WS matrix elements become sums over HO matrix elements. With WS wavefunctions radial integrals of the interaction for many values of the HO relative state principal quantum numbers (n,n') are required. To illustrate the dependence of the interaction on the values of n and n' several radial integrals are given in Table 5-1. The attractive terms decrease with increasing n and n' while the velocity dependent repulsive terms increase.

In the diagonalization of the interaction matrices the single-particle energies of the A=15, 17 and 39 ground states were taken to be at zero energy. The single-particle energies used are given in Table 5-2. With this energy scale the experimental binding energies for A=18 and A=14 nuclei are given by

Table 5.1

Oscillator function radial integrals of the phenomenological relative S state free reaction matrix (Chap. 3) with ϵ = 86.0 MeV and $\hbar\omega$ = 13.4 MeV. The attractive and repulsive terms are designated by - and + respectively.

		T=1 (MeV)			T=0 (MeV)		
n	n'	-	+	Total	-	+	Total
0	0	-7.48	0.44	-7.04	-11.40	0.57	-10.83
0	1	-5.04	0.89	-4.15	- 8.75	1.11	-7.64
0	2	-3.42	1.25	-2.17	- 6.55	1.53	- 5.02
0	3	-2.43	1.57	-0.86	- 5.00	1.87	- 3.13
1	1	-5.51	1.38	-4.13	- 9.07	1.68	- 7.39
1	2	-4.45	1.81	-2.64	- 7.80	2.17	- 5.63
1	3	-3.39	2.18	-1.21	- 6.39	2.58	- 3.81
2	2	-4.57	2.28	-2.29	- 7.76	2.70	- 5.06
2	3	-3.95	2.68	-1.27	- 6.98	3.15	- 3.83
2	4	-3.21	3.03	-0.18	- 6.00	3.52	- 2.48
3	3	-3.99	3.11	-0.88	- 6.89	3.62	- 3.27
3	4	-3.57	3.48	-0.09	- 6.35	4.30	- 2.32
4	4	-3.59	3.89	+0.30	- 6.26	4.45	- 1.81
5	5	-3.29	4.62	+1.33	- 5.78	5.22	- 0.56

Table 5.2

The unperturbed neutron single-particle (hole) energies used in the calculations

A=15		A=17		A=39	
$\nu\ell j$	$\epsilon_{\nu\ell j}$ (MeV)	$\nu\ell j$	$\epsilon_{\nu\ell j}$ (MeV)	$\nu\ell j$	$\epsilon_{\nu\ell j}$ (MeV)
$0p_{1/2}$	0.0	$0d_{5/2}$	0.0	$0d_{3/2}$	0.0
$0p_{3/2}$	6.16	$0s_{1/2}$	0.87	$1s_{1/2}$	2.50
		$0d_{3/2}$	5.08	$0d_{5/2}$	6.00

$$BE(2p;O^{18}) = 2BE(O^{17}) - BE(O^{16}) - BE(O^{18})$$
$$= -3.90 \text{ MeV}$$
$$BE(2p,F^{18}) = BE(O^{17}) + BE(F^{17}) - BE(O^{16}) - BE(F^{18})$$
$$= -5.01 \text{ MeV}$$
$$BE(2h;O^{14}) = BE(O^{16}) + BE(O^{14}) - 2BE(O^{15})$$
$$= 2.45 \text{ MeV}$$
$$BE(2h;N^{14}) = BE(O^{16}) + BE(N^{14}) - BE(O^{15}) - BE(N^{15})$$
$$= 4.83 \text{ MeV}.$$

The above binding energies were taken from the 1964 Atomic Mass Table.[100] From neutron separation energies[59] the experimental binding energy for Ca^{38} is

$$BE(2h;Ca^{38}) = 2.34 \text{ MeV}.$$

Using the hole energies given in Table 5.2 the two-hole eigenvalue problem is identical to the two-particle problem; however, the calculated energies are the negative of the experimental energies.

5-C The Spectra of A=14, 18 and 38 Nuclei

The states in A=14 nuclei that arise from p^{-2} configurations were calculated with HO wavefunctions and with the WS wavefunctions given in Table 4.17. In shell model calculations of two-particle and two-hole states using the HO wavefunctions the common practice is to use a HO size parameter determined by the size of the closed shell core. A value commonly used for O^{16} is $\hbar\omega = 13.4$ MeV. From Tables 4.15 and 4.17 is can be seen that $\hbar\omega = 13.4$ MeV lies between the average values of $\hbar\omega$ that maximized the overlap of a HO wavefunction with the WS wavefunctions for the 0p and (1s,0d) shells. For comparison with calculations using WS wavefunctions the A=14 and A=18 spectra were calculated using HO wavefunctions with $\hbar\omega = 13.4$ MeV. The A=14

spectrum was calculated using the WS wavefunctions with five terms of the expansion in HO wavefunctions included.

Recently Mangelson et al.[101] have summarized the experimental and theoretical knowledge of the states in N^{14}. The experimental energies of the states that are identified as being predominatly of p^{-2} configurations are given in Table 5.3. The calculated eigenvalues are given in Table 5.4 and compared with experiment in Fig. 5-1. The WS spectrum is depressed relative to the HO spectrum; that is the WS calculation gives larger binding energies for particles in the p shell. A HO calculation with a larger value of $\hbar\omega$ would reproduce the WS spectrum since the WS wavefunctions have a very good overlap with HO wavefunctions of larger $\hbar\omega$. In the WS calculation the T=0 states are depressed (relative to the HO calculation) more than the T=1 states. This effect arises because the T=0 interaction is more dependent on the oscillator size parameter than the T=1 interaction. However the main point of interest is that hole states require a considerably larger value of $\hbar\omega$ than the particle states. This state dependence has been pointed out previously by Wong and Wong.[98]

The experimental energies of the low-lying positive parity states in O^{18} are given in Table 5.3. The two-particle spectrum was calculated using HO wavefunctions with $\hbar\omega$ = 13.4 MeV and the WS wavefunctions given in Table 4.15. The wavefunctions for the $0d_{3/2}$ state with a binding energy of -0.23 MeV was used. In the calculation five, seven and ten terms of the expansions in HO wavefunctions were included for the $0d_{5/2}$, $0d_{3/2}$ and $1s_{1/2}$ wavefunctions,

Table 5.3

The experimental energies of low-lying positive parity states in A=14, 18 and 38 nuclei

N^{14} (a)		O^{18} (b)		F^{18} (c)		Ca^{38} (d)	
J^π,T	E_B(MeV)	J^π,T	E_B(MeV)	J^π,T	E_B(MeV)	J^π,T	E_B(MeV)
1^+,0	-4.83	0^+,1	-3.90	1^+,0	-5.01	0^+,1	-2.34
0^+,1	-2.52	2^+,1	-1.92	3^+,0	-4.07	2^+,1	-0.14
1^+,0	-0.89	4^+,1	-0.35	5^+,0	-3.88	0^+,1	2.02
2^+,0	2.20	0^+,1	-0.27	1^+,0	-3.31	(2^+)	2.50
1^+,1	8.89	2^+,1	0.02	2^+,0	-2.49		
		2^+,1	1.35	2^+,3^+	-1.65		
		0^+,1	1.43	2^+	-1.17		
		3^+,1	1.47				
		4^+,1	3.22				

a) reference 101

b) references 102, 103, 104

c) reference 105

d) reference 59

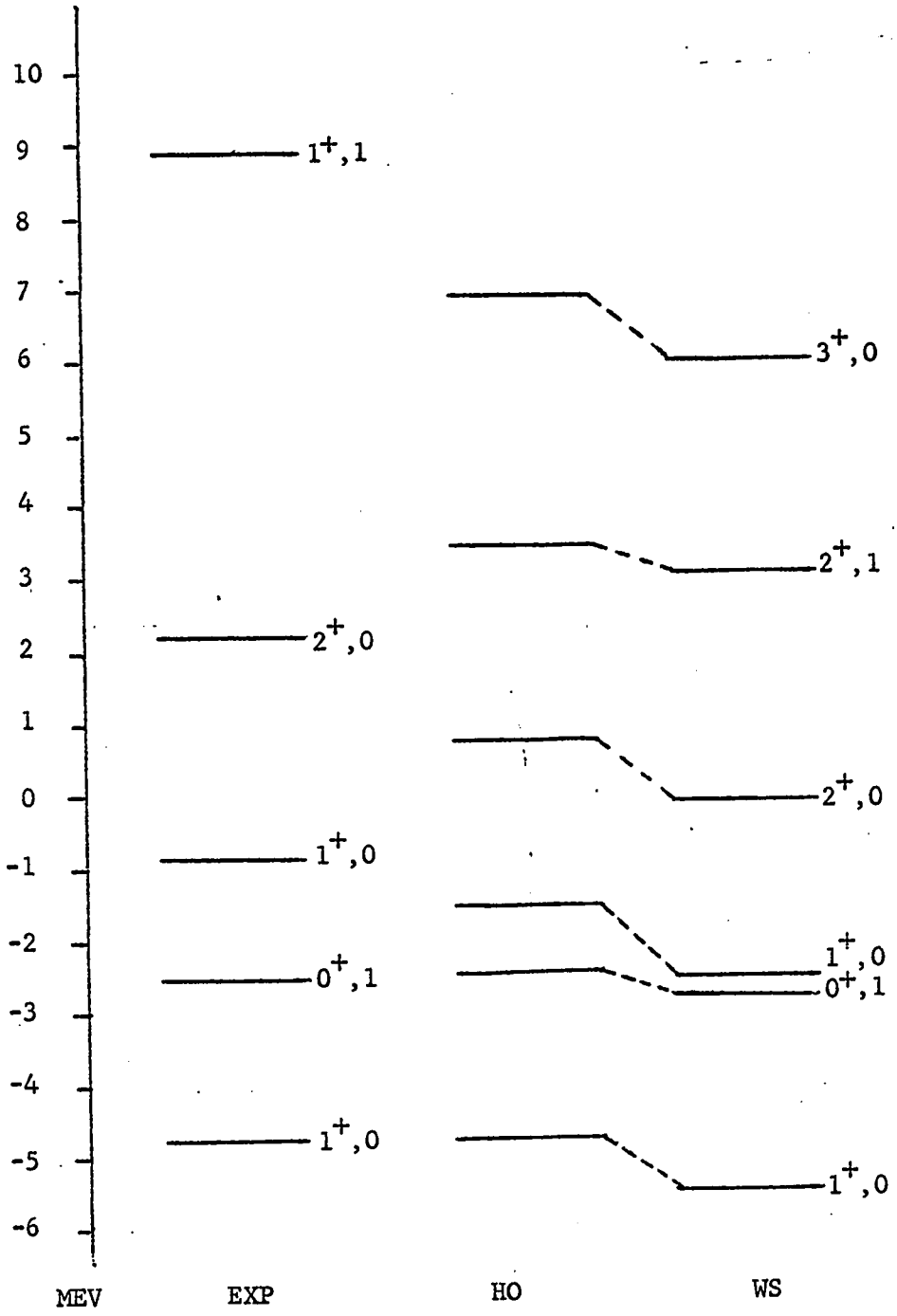

Fig. 5-1. The two-hole spectrum of N^{14}. The theoretical spectra are for harmonic oscillator wavefunctions (HO, $\hbar\omega$ = 13.4 MeV) and Woods-Saxon (WS) wavefunctions.

Table 5.4

The calculated spectra of N^{14}. HO and WS designate calculations with harmonic oscillator ($\hbar\omega$ = 13.4 MeV) and Woods-Saxon wavefunctions respectively.

Calc.	J^π,T	Eigenvalues (MeV)
HO	0^+,1	-2.47, 9.22
	1^+,0	-4.75, -1.54, 10.25
	2^+,0	0.74
	2^+,1	3.46, 11.50
	3^+,0	6.90
WS	0^+,1	-2.70, 9.00
	1^+,0	-5.48, -2.53, 10.10
	2^+,0	-0.11
	2^+,1	3.07, 11.43
	3^+,0	5.98

respectively. The calculated spectra are given in Table 5.5 and compared with experiment in the second and third columns of Fig. 5.2. All of the states in the WS calculation are shifted upwards relative to the states in the HO calculation. The HO calculation is with the value of $\hbar\omega$ that gives a maximum overlap of a HO wavefunction with the WS wavefunction for the $0d_{5/2}$ state. The values of $\hbar\omega$ that maximize the overlap of HO wavefunctions with the WS wavefunctions for the $1s_{1/2}$ and $0d_{3/2}$ states are smaller. This is a reflection of the long tails of the WS wavefunctions. The effect of the spreading out of the $0d_{3/2}$ and $1s_{1/2}$ wavefunctions on two-body matrix

Table 5.5
The calculated spectra for O^{18}. HO and WS designate calculations with harmonic oscillator ($\hbar\omega$ = 13.4 MeV) and Woods-Saxon wavefunctions respectively.

Calc.	J^π,T	Eigenvalues (MeV)
HO	0^+,1	-3.05, 0.06, 8.98
	2^+,1	-1.59, 0.15, 4.68, 5.45, 9.86
	4^+,1	-0.82, 3.26
WS	0^+,1	-2.63, 0.67, 9.23
	2^+,1	-1.33, 0.23, 4.76, 5.52, 9.93
	4^+,1	-0.73, 3.50

elements involving these states is to decrease the matrix elements from their HO values. It should be remembered that all effects are relative to the calculation with HO wavefunctions. The HO calculation is for a single-particle potential that gives a wavefunction most like the WS wavefunction for the $0d_{5/2}$ state. From Table 5.5 and Fig. 5.2 it can be seen that the lowest 0^+ states are affected most. The positions of these states are largely determined by the $(d_{5/2})^2$ and $(s_{1/2})^2$ diagonal and off-diagonal matrix elements. Since the $1s_{1/2}$ state has a poor overlap with a HO wavefunction, the diagonal $(s_{1/2})^2$ matrix element is decreased appreciably. The matrix elements $< (s_{1/2})^2 J=0 | v | (s_{1/2})^2 J=0 >$, $< (s_{1/2})^2 J=0 | v | (d_{5/2})^2 J=0 >$ and $< (d_{5/2})^2 J=0 | v | (d_{5/2})^2 J=0 >$ are decreased by 35%, 10% and 9%, respectively. Matrix elements involving the $d_{3/2}$ state are also decreased. However, most of the low-lying levels shown in Fig. 5.2

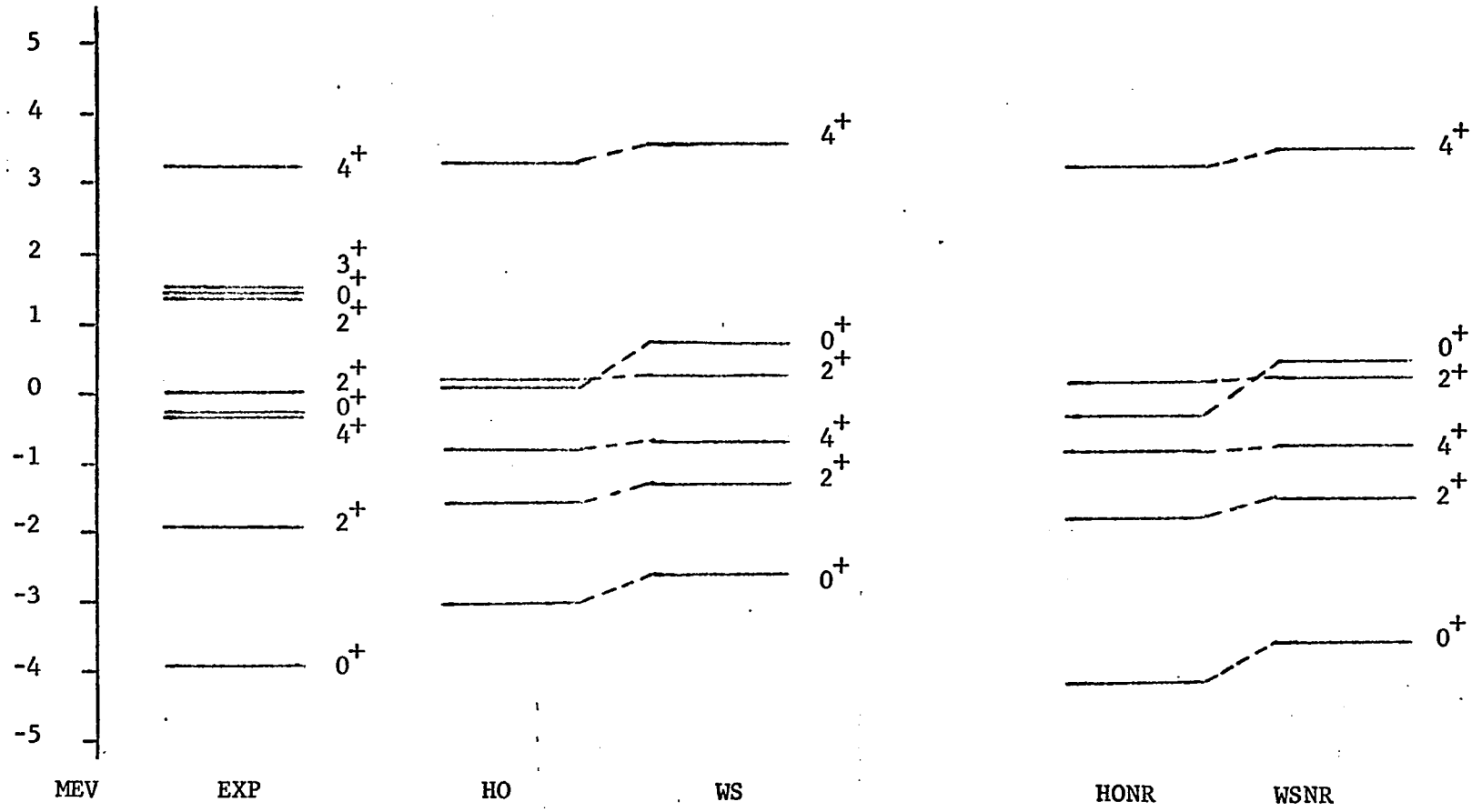

Fig. 5-2. The two-particle spectrum of O^{18}. The theoretical spectra are for harmonic oscillator (HO, $\hbar\omega$ = 13.4 MeV) and Woods-Saxon (WS) wavefunctions. NR denotes the calculations without the repulsive term of the residual interaction.

do not contain appreciable admixtures of this configuration and are not significantly affected. An exception is the second 4^+ state which is shifted upwards more than the first 4^+ state. The second 4^+ state is predominantly the $(d_{5/2}\ d_{3/2})$ configuration while the first is predominantly $(d_{5/2})^2$.

To examine the dependence of the WS calculation in the (n,n') structure of the radial integrals of the interaction the spectrum was calculated neglecting the repulsive term in the interaction. The results of the calculation for the lowest levels are shown in columns four and five of Fig. 5.2. Neglecting the repulsive term gives a more attractive interaction and larger upward shifts of the states in the WS calculation. The upward shifts of the 0^+ states are larger in magnitude than those in the calculation with the full interaction. However, all states are affected in the same way in both calculations.

In O^{18} there are three 0^+ states observed experimentally below 6 MeV excitation energy whereas shell model calculations only predict two states with a third state at about 10 MeV. Furthermore, E2 transition probabilities are much larger than the shell model would predict. The anomalous E2 transition rates have lead to many attempts to describe the states as mixtures of shell model and deformed states.[106-111] The dynamics of transition moments test the structure of the wavefunctions; consequently the calculation of transition probabilities provides important information about the size of the deformed components in the observed states. Shlomo

and Moreh[112] have calculated the electromagnetic transition probabilities in O^{18} using the various calculated admixtures of spherical and deformed states. They found that the Benson-Irvine[109] wavefunctions gave the best overall agreement with experiment. The coexistence of spherical and deformed states leads to difficulties in the interpretation of effective interaction calculations. More precisely, to calculate the structure of O^{18} using an effective interaction one would first calculate the shell model and the deformed state spectra separately and then mix the two types of states with the appropriate effective interaction.[111] By a shell model calculation we generally mean one using spherical valence levels and perhaps involving some core polarization corrections to the effective interaction. In any case the shell model calculations should not reproduce the experimental spectrum. Rather, the experimental spectrum should be reproduced only when the deformed states are included.[4] This has not been the case; as Kuo and Brown pointed out, the shell model calculations usually predict the second 0^+ state to be very near the experimental position while it is believed (on the basis of E2 transiton probabilities) that the state contains a large deformed component. This implies that when the shell model and deformed states are mixed the 0^+ state is not shifted significantly in energy but acquires a large deformed component in the wavefunction.[113] Brown and Green found that the Kuo-Brown effective interaction could not reconcile the energies of the states and the observed transition probabilities.

In the earlier discussion it was seen that the use of WS wavefunctions weakened the $(s_{1/2})^2 J=0$ diagonal matrix element relagive to the $(d_{5/2})^2 J=0$ diagonal matrix element. The result was an upward shift of the first and second 0^+ state relative to the other states in the spectrum. If the 0^+ states contain appreciable deformed state components the calculated energies should be above the experimentally observed energies. WS wavefunctions also have a significant effect on transition probabilties. The longer tails of the WS wavefunctions increase integrals of r^L relative to the values using HO wavefunctions. The radial integrals required for E2 transitions in the (0d,1s) shell are given in Table 5.6. The $(s_{1/2},s_{1/2})$ radial integral is increased by 50% while the $(d_{5/2},d_{5/2})$ radial integral is increased by only 10%. This implies the single-particle effective charge for these levels must be redefined and that changes in transition probabilities might occur. The transitions of particular interest are the E2 transitions $0_2^+ \rightarrow 2_1^+$, and $2_1^+ \rightarrow 0^+$.

The necessary formulae for calculating electromagnetic transition probabilities are given in Appendix A. The spectra calculated with only the attractive term of the interaction were in best agreement with experiment. The wavefunctions for these spectra were used to calculate transition probabilities. For the calculation with HO wavefunctions the theoretical reduced transition probabilities are

$$B(E2;0_2^+ \rightarrow 2_1^+) = 3.61\epsilon_n^2 \; e^2 fm^4$$

and

Table 5.6

Radial integrals $< n\ell \| r^2 \| n'\ell' >$ for HO($\hbar\omega$ = 13.4) and WS wavefunctions.

$n\ell$	$n'\ell'$	HO (fm^2)	WS (fm^2)
$0d_{5/2}$	$0d_{5/2}$	10.83	11.62
$1s_{1/2}$	$1s_{1/2}$	10.83	17.79
$0d_{3/2}$	$0d_{3/2}$	10.83	16.90
$0d_{5/2}$	$1s_{1/2}$	-9.79	-12.59
$0d_{5/2}$	$0d_{3/2}$	10.83	12.59
$1s_{1/2}$	$0d_{3/2}$	-9.79	-16.28

$$B(E2;0_1^+ \rightarrow 2_1^+) = 72.0\epsilon_n^2 \, e^2fm^4$$

where ϵ_n is the effective charge of the neutron in units of e. With the usual effective charge $\epsilon_n = 0.5$ the transition probabilities are

$$B(E2;0_2^+ \rightarrow 2_1^+) = 0.90 \, e^2fm^4$$

and

$$B(E2;0_1^+ \rightarrow 2_1^+) = 18.0 \, e^2fm^4 .$$

The experimental reduced transition probabilities[39] are

$$B(E2;0_2^+ \rightarrow 2_1^+) = 22.2 \, e^2fm^4$$

and

$$B(E2;\ 0_1^+ \rightarrow 2_1^+) = 32.7 \, e^2fm^4 .$$

The above results are typical of all shell model calculations. The $0_1^+ \rightarrow 2_1^+$ theoretical transition probability is about right while

the $0_2^+ \rightarrow 2_1^+$ reduced transition probability is decidedly small. With the wavefunctions from the WS calculation the reduced transition probabilities are

$$B(E2;\ 0_2^+ \rightarrow 2_1^+) = 12.8\epsilon_n^2\ e^2fm^4$$

and

$$B(E2;\ 0_1^+ \rightarrow 2_1^+) = 103.0\epsilon_n^2\ e^2fm^4 \quad .$$

The WS wavefunctions increase the reduced transition probabilities considerably. However, as we noted previously, the effective charge should be consistently defined. In the present model we have assumed that the (0d,1s) neutron states are single-particle states. If the states were pure single-particle states the O^{17} quadrupole moment and transition moments would be zero. Experimentally the quadrupole moment and transition moments are not zero. For the model to be consistent the effective charges required for O^{17} should be used in the calculation of the O^{18} transition probabilities. In O^{17} the $B(E2;s_{1/2} \rightarrow d_{5/2})$ and quadrupole moment are known experimentally.[39,114] With the assumption of pure single-particle states the effective charges are

$$s_{1/2} \rightarrow d_{5/2}: \qquad \epsilon_n^2 = \frac{4\pi}{3} B(E2) \frac{1}{\langle r^2 \rangle^2}$$

and

$$d_{5/2} \rightarrow d_{5/2}: \qquad \epsilon_n^2 = \frac{49}{16} Q^2 \frac{1}{\langle r^2 \rangle^2} \quad .$$

The effective charges for the $s_{1/2} \rightarrow d_{5/2}$ and $d_{5/2} \rightarrow d_{5/2}$ transitions are 0.52 and 0.42, respectively, for HO wavefunctions and 0.41 and 0.39, respectively, for WS wavefunctions. It appears that the WS

wavefunctions provide some evidence for a state independent effective charge. Using an effective charge of 0.4 the transition probabilities in O^{18} with WS wavefunctions are

$$B(E2;0_2^+ \rightarrow 2_1^+) = 2.05\ e^2fm^4$$

and

$$B(E2;0_1^+ \rightarrow 2_1^+) = 16.5\ e^2fm^4 \quad .$$

With the WS wavefunctions there $0_2^+ \rightarrow 2_1^+$ transition acquires more of the transition strength but is still an order of magnitude too small. If the experimental values of the reduced matrix elements for O^{17} were used in the O^{18} calculation with HO wavefunctions the result would be closer to the WS result. Nevertheless, the calculated two-particle amplitudes are different in the WS calculation. The wavefunctions for the states being considered are given in Table 5.7. The main difference between the HO and WS calculations is that in the WS case there is less configuration mixing. This is a result of the weakening of the matrix elements containing the $s_{1/2}$ state.

The T=0 spectrum of F^{18} was calculated using the same wavefunctions and single-particle energies that were used in the O^{18} calculation. The experimental energies of the low-lying positive parity T=0 states are given in Table 5.3. The results of the calculations with HO and WS wavefunctions are given in Table 5.8 and compared with experiment in the second and third columns of Fig. 5.3. The upward shifts of T=0 states in the WS calculation are larger than those in the T=1 calculation. The 5^+ state is shifted very little since only the $(d_{5/2})^2$ configuration is involved. The 1^+ states are

Table 5.7

Two-particle wavefunctions in O^{18} for the calculations with HO and WS single-particle wavefunctions and only the attractive term of the residual interaction

$J^{\pi}, T = 2^{+}, 1$

E (MeV)	Calc.	$(d_{3/2})^2$	$(d_{3/2}\ d_{5/2})$	$(d_{3/2}\ s_{1/2})$	$(d_{5/2})^2$	$(d_{5/2}\ s_{1/2})$
-1.86	HO	0.085	-0.137	-0.185	0.721	0.648
-1.54	WS	0.071	-0.121	-0.152	0.773	0.600

$J^{\pi}, T = 0^{+}, 1$

E (MeV)	Calc	$(d_{3/2})^2$	$(d_{5/2})^2$	$(s_{1/2})^2$
-4.17	HO	0.212	0.893	0.397
-3.60	WS	0.179	0.936	0.302
-0.37	HO	0.012	0.404	-0.915
+0.44	WS	-0.018	0.310	-0.951

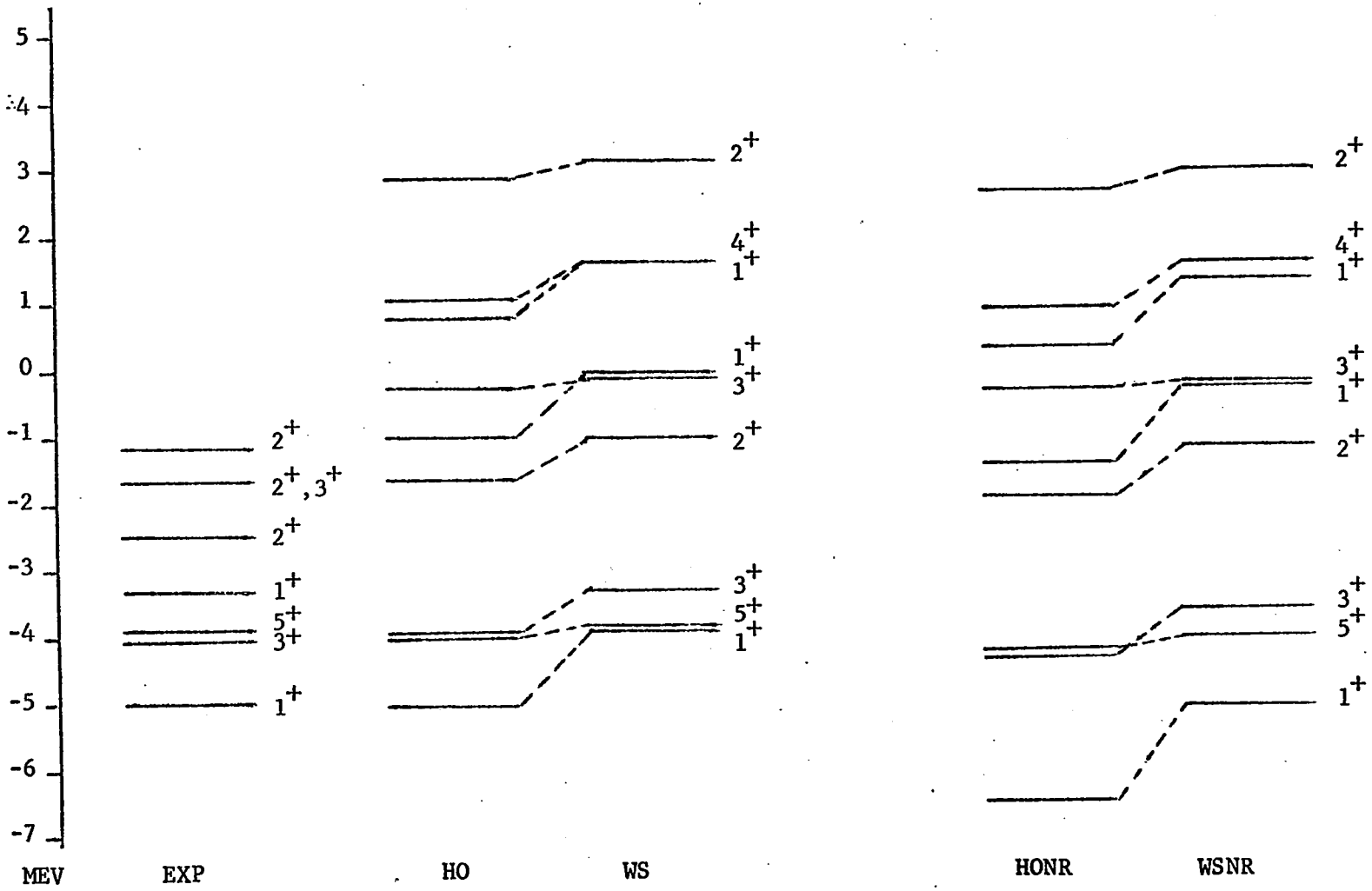

Fig. 5-3. The T=0 spectrum of F^{18}. The theoretical spectra are for harmonic oscillator (HO, $\hbar\omega$ = 13.4 MeV) and Woods-Saxon (WS) wavefunctions. NR denotes the spectra calculated neglecting the repulsive term in the residual interaction.

Table 5.8

The calculated spectra for F^{18}. HO and WS designate the calculations with harmonic oscillator ($\hbar\omega$ = 13.4 MeV) and Woods-Saxon wavefunctions.

Calc.	J^π,T	Eigenvalues (MeV)
HO	1^+,0	-5.05, -1.05, 0.75, 3.47, 8.94
	2^+,0	-1.67, 2.81, 5.16
	3^+,0	-3.97, -0.32, 3.37, 7.37
	4^+,0	1.02
	5^+,0	-4.06
WS	1^+,0	-3.98, -0.12, 1.64, 3.93, 9.22
	2^+,0	-1.06, 3.08, 5.31
	3^+,0	-3.37, -0.20, 3.77, 7.95
	4^+,0	1.64
	5^+,0	-3.90

shifted upwards by approximately 1 MeV. The wavefunction for the ground state is given in Table 5.9. From the wavefunctions it can be seen that both the $(d_{5/2}\ d_{3/2})$ and $(s_{1/2})^2$ configurations are large components in the ground state. The $(s_{1/2})^2_{J=1}$ and $(d_{5/2}\ d_{3/2})$ J=1 diagonal matrix elements are decreased from the values with HO wavefunctions by 40% and 20%, respectively. The even J states are shifted upwards also since the main components in the lowest states are either $(d_{5/2}\ s_{1/2})$ or $(d_{5/2}\ d_{3/2})$.

The T=0 spectrum was calculated with only the attractive term of the free reaction matrix and the results are given in the fourth and fifth column of Fig. 5.3. The shifts of the WS spectrum

Table 5.9

The ground state wavefunction for F^{18} in the calculation with HO and WS wavefunctions.

E (MeV)	Calc.	$(d_{3/2})^2$	$(d_{3/2}\ d_{5/2})$	$(d_{3/2}\ s_{1/2})$	$(d_{5/2}\ d_{5/2})^2$	$(s_{1/2})^2$
-5.05	HO	-0.137	0.489	-0.033	0.702	0.499
-3.98	WS	-0.124	0.446	-0.042	0.792	0.397

are larger in magnitude than for the calculation with the full interaction; however, the effect of using WS wavefunctions is the same.

The two-hole spectrum of Ca^{38} was calculated using HO wavefunctions and the WS wavefunctions given in Table 4.21. The single-particle energies used in the calculations are given in Table 5.2 and the experimental energies of the states in Ca^{38} are given in Table 5.3. The spectrum calculated with WS wavefunctions is given in Table 5.10 and compared with experiment in Fig. 5.4. The spectrum was calculated with HO wavefunctions for $\hbar\omega$ = 11.5 MeV and $\hbar\omega$ = 13.4 MeV. The results of the HO calculations are given in Table 5.10 and Fig. 5.4. The HO calculation with $\hbar\omega$ = 13.4 MeV is nearly identical to the WS calculation while the spectrum for $\hbar\omega$ = 11.5 MeV is only slightly different. The small differences between the two HO calculations reflect the insensitivity of the interaction to changing $\hbar\omega$ from 11.5 to 13.4 MeV. The Ca^{39} hole states are deeply bound and the overlap with HO wavefunctions is maximized for $\hbar\omega \doteqdot$ 13.4 MeV.

Table 5.10

The calculated spectra for Ca^{38}. HO and WS designate calculations with harmonic oscillator and Woods-Saxon wavefunctions. The HO calculations are given for $\hbar\omega$ = 11.5 MeV and 13.5 MeV.

Calc.	J^π,T	Eigenvalues (MeV)
HO	0^+,1	-1.89, 3.13, 10.20
($\hbar\omega$=11.5)	2^+,1	-0.56, 1.65, 5.64, 7.56, 11.52
	4^+,1	4.00, 11.64
WS	0^+,1	-1.96, 2.98, 10.1
	2^+,1	-0.60, 1.57, 5.62, 7.50, 11.5
	4^+,1	3.75, 11.6
HO	0^+,1	-2.02, 3.02, 10.1
($\hbar\omega$=13.5)	2^+,1	-0.64, 1.54, 5.61, 7.47
	4^+,1	3.73, 11.6

The lack of differences between the WS and HO spectra indicates that the small deviations in shape of the WS wavefunctions from HO wavefunctions for deeply bound levels has little effect on the matrix elements. The best value of $\hbar\omega$ for the Ca^{39} hole states is larger than that for the Ca^{41} particle states; however, with the present residual interaction this does not lead to large state dependent effects in matrix elements.

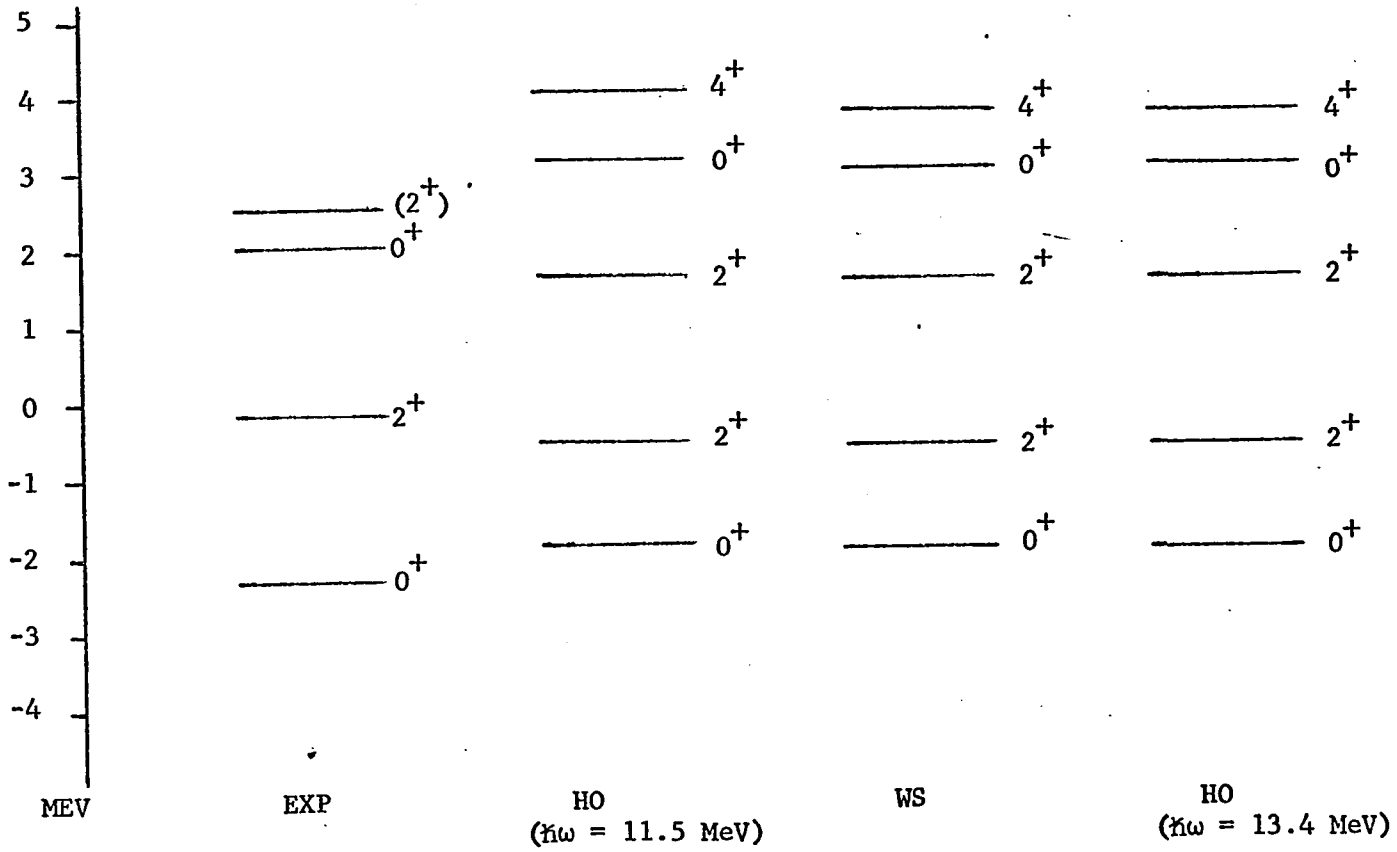

Fig. 5-4. The two-hole spectrum of Ca^{38}. The theoretical spectra are for harmonic oscillator (HO) and Woods-Saxon (WS) wavefunctions.

5-D Remarks About Interaction Matrix Elements with Woods-Saxon Wavefunctions

A few of the residual interaction matrix for the (0p;1s,0d) shells are given in Table 5.11. The matrix elements given are those from the calculation of the A=18 spectra with a few cross shell matrix elements that are required in particle-hole calculations. The matrix elements given illustrate the main effects of using WS wavefunctions to evaluate residual interaction matrix elements. For deeply bound levels such as hole states the WS wavefunctions are very much like HO wavefunctions for an appropriate value of $\hbar\omega$. For particle levels where the binding energy is small the WS wavefunctions have long tails and poor overlaps with HO wavefunctions. In A=18 the $0d_{5/2}$ wavefunction is very much like a HO wavefunction with $\hbar\omega$ = 13.4 MeV. The $(d_{5/2})^2$ diagonal matrix elements are only reduced by 5-10% from their HO values. The matrix elements involving the $d_{3/2}$ and $s_{1/2}$ states are decreased by as much as 40% from their HO values obtained with $\hbar\omega$ = 13.4 MeV. In the case of cross-shell matrix elements such as $< (p_{1/2}\ s_{1/2})^{J=1}|v|(p_{1/2}\ s_{1/2})^{J=1,T=1} >$ and $< (p_{1/2})^{2}{}_{J=0,T=1}|v|(d_{5/2})^{2}{}_{J=0} >$ the effects are different. Although both the $p_{1/2}$ and $d_{5/2}$ wavefunctions may,to a good approximation, be represented by a single HO wavefunction the values of $\hbar\omega$ are different for the two states. The effect of the different $\hbar\omega$ values is to reduce the matrix elements. The $(p_{1/2})^2$, $(d_{5/2})^2$: J=0,T=1 matrix element is decreased from the HO value by the same amount as the $(p_{1/2}\ s_{1/2})$, $(p_{1/2}\ s_{1/2})$: J=1,T=1

Table 5.11

Residual interaction matrix elements evaluated with HO ($\hbar\omega$ = 13.4 MeV) wavefunctions and WS wavefunctions. The WS wavefunctions used were those used in the calculation of the A=14 and A=18 spectra.

Configurations	J^π,T	HO (MeV)	WS (MeV)
$(d_{3/2}\ d_{3/2})(d_{3/2}\ d_{3/2})$	0^+,1	-1.54	-1.18
$(d_{5/2}\ d_{5/2})$	0^+,1	-1.87	-1.57
$(s_{1/2}\ s_{1/2})$	0^+,1	-0.77	-0.70
$(d_{5/2}\ d_{5/2})(d_{5/2}\ d_{5/2})$	0^+,1	-2.31	-2.13
$(s_{1/2}\ s_{1/2})$	0^+,1	-0.95	-0.85
$(s_{1/2}\ s_{1/2})(s_{1/2}\ s_{1/2})$	0^+,1	-2.06	-1.32
$(p_{1/2}\ s_{1/2})(p_{1/2}\ s_{1/2})$	1^-,1	-1.01	-0.83
$(p_{3/2}\ d_{5/2})$	1^-,1	0.94	0.83
$(p_{3/2}\ d_{5/2})(p_{3/2}\ d_{5/2})$	1^-,1	-2.78	-2.67
$(p_{3/2}\ s_{1/2})(p_{3/2}\ s_{1/2})$	1^-,1	-2.03	-1.65
$(p_{12/}\ p_{1/2})(d_{5/2}\ d_{5/2})$	0^+,1	1.32	1.12
$(s_{1/2}\ s_{1/2})$	0^+,1	0.21	0.12
$(p_{3/2}\ p_{3/2})(d_{5/2}\ d_{5/2})$	0^+,1	1.86	1.58
$(d_{3/2}\ d_{3/2})(d_{3/2}\ d_{3/2})$	1^+,0	-1.85	-1.38
$(d_{3/2}\ d_{5/2})$	1^+,0	0.60	0.47
$(d_{3/2}\ s_{1/2})$	1^+,0	-1.55	-1.26
$(d_{5/2}\ d_{5/2})$	1^+,0	1.71	1.41
$(s_{1/2}\ s_{1/2})$	1^+,0	0.58	0.50

Table 5.11 (contd)

$(d_{3/2}\ d_{5/2})$	$(d_{3/2}\ d_{5/2})$	$1^+,0$	-4.98	-4.11
	$(d_{3/2}\ s_{1/2})$	$1^+,0$	-1.10	-0.91
	$(d_{5/2}\ d_{5/2})$	$1^+,0$	-2.36	-2.05
	$(s_{1/2}\ s_{1/2})$	$1^+,0$	-1.63	-1.41
$(d_{3/2}\ s_{1/2})$	$(d_{3/2}\ s_{1/2})$	$1^+,0$	-3.26	-2.53
	$(d_{5/2}\ d_{5/2})$	$1^+,0$	0.83	0.71
	$(s_{1/2}\ s_{1/2})$	$1^+,0$	0.00	0.00
$(d_{5/2}\ d_{5/2})$	$(d_{5/2}\ d_{5/2})$	$1^+,0$	-2.26	-2.10
	$(s_{1/2}\ s_{1/2})$	$1^+,0$	-1.08	-0.94
$(s_{1/2}\ s_{1/2})$	$(s_{1/2}\ s_{1/2})$	$1^+,0$	-3.52	-2.12
$(p_{1/2}\ s_{1/2})$	$(p_{1/2}\ s_{1/2})$	$0^-,0$	-4.72	-3.83
	$(p_{3/2}\ d_{3/2})$	$0^-,0$	3.12	2.54
$(p_{3/2}\ d_{3/2})$	$(p_{3/2}\ d_{3/2})$	$0^-,0$	-7.71	-6.46
$(p_{1/2}\ p_{1/2})$	$(d_{5/2}\ d_{5/2})$	$1^+,0$	-1.40	-1.27
	$(s_{1/2}\ s_{1/2})$	$1^+,0$	-0.18	-0.12

matrix element. On the other hand the $(p_{1/2}\ s_{1/2})$, $(p_{1/2}\ s_{1/2})$: J=0,T=0 matrix element is decreased more than the $(p_{1/2})^2$, $(d_{5/2})^2$: J=1,T=0 matrix element.

A few properties of matrix elements for a general central potential are discussed in Appendix C. One point that should be emphasized is that an overlap of a HO wavefunction and WS wavefunction that is 0.94 is not a good overlap. If the overlap of a WS wavefunction and the corresponding HO wavefunction is 0.94 other coefficients of the expansion in terms of HO wavefunctions can be as large as 0.2. In the previous discussion it was seen that the $(s_{1/2})^2$ diagonal matrix elements were decreased from their HO values by far more than $(0.94)^4$. From (C-5) it can be seen that for interactions where the radial integrals increase with increasing (n,n') the terms arising from small components are more important than in cases where the radial integrals decrease. However, there is a large number of terms from the small amplitudes and there is much cancellation among them.

In the calculation of the T=0 spectrum of F^{18} the WS wavefunctions used were the neutron single-particle wavefunctions. The $0d_{5/2}$ and $1s_{1/2}$ proton states in F^{17} are only bound by 0.6 and 0.1 MeV, respectively. The WS wavefunctions for the proton state were given in Table 4.18. It was found that the overlap of the $0d_{5/2}$ proton and neutron wavefunctions was 0.977 while the overlap for the $1s_{1/2}$ states was 0.980. Although the overlaps of the neutron and proton wavefunctions may be very good it is not a measure of the

validity of isospin invariance of residual interaction matrix elements. The small binding energies of the proton states allows the proton wavefunctions to extend beyond the nuclear well more than the neutron wavefunctions. This is reflected in the smaller values of $\hbar\omega$ that maximize the overlaps of the HO and WS wavefunctions with the same number of nodes. For $\hbar\omega$ = 13.4 MeV the overlaps of a $1s_{1/2}$ HO wavefunction with the neutron and proton WS wavefunctions are 0.939 and 0.879. The overlap integrals are maximized with $\hbar\omega$ = 12.0 MeV for the neutron state and 11.0 for the proton state. The $(s_{1/2})^2$ diagonal matrix element for an interacting neutron and proton pair will be smaller than those for two neutron. This point merits further investigation.

5-E Summary

The two-particle spectra of A=18 nuclei and the two-hole spectra of A=14 and A-38 nuclei were calculated with a realistic effective interaction and WS wavefunctions. The WS wavefunctions for hole states are very much like HO wavefunctions with an appropriate choice of $\hbar\omega$ while the $0d_{3/2}$ and $1s_{1/2}$ wavefunctions differ considerably from HO wavefunctions. The A=14 and A=18 spectra calculated with WS wavefunctions were compared with spectra calculated with HO wavefunctions. The HO size parameter chosen for comparison was the value that maximized the overlap of the $0d_{5/2}$ HO and WS wavefunctions and was an intermediate value for the particle and hole states. This value is commonly used by other authors.[24,111] The two-hole matrix elements were increased by using WS wavefunctions while

the two-particle matrix elements were decreased. Since the hole WS wavefunctions are very much like HO wavefunctions with the same size parameter in all states, HO wavefunctions can be used to reproduce the spectra calculated with WS wavefunctions. By using a smaller value of $\hbar\omega$ in the HO calculation of the two-particle spectra the differences between the HO and WS calculations would be lessened. However, for the particle states the maximizing value of $\hbar\omega$ is much more state dependent than for the hole states. For matrix elements involving both the 0p and (1s,0d) configurations the matrix elements calculated with Woods-Saxon wavefunctions vary considerably in the changes relative to the HO calculations. The F^{18} spectrum was calculated using the neutron wavefunctions; however the $1s_{1/2}$ proton WS wavefunction has a poorer overlap with a HO wavefunction than the neutron WS wavefunction. Using different wavefunctions for the proton and neutron would increase the difference between HO and WS matrix elements.

CHAPTER 6

SHELL MODEL CALCULATIONS WITH A FREE REACTION MATRIX AS AN EFFECTIVE INTERACTION

6-A Introduction

In this chapter we present calculations of the two-particle spectra of A=18, 42 and 210 nuclei and the two-hole spectrum of Pb^{206}. A free reaction matrix is used as the effective shell model interaction and the calculations were performed using both harmonic oscillator and Woods-Saxon wavefunctions. In Chapters 3 and 5 we presented nuclear structure calculations for which a free reaction matrix was used as an effective interaction. In general, the free reaction matrix K_F is non-local. In the earlier calculations a local but velocity dependent representation of K_F was used. Lee[17] has made a more complete study of K_F and the nuclear reaction matrix by using a non-local separable potential to fit the free nucleon-nucleon scattering data. The free reaction matrix obtained from the separable potential is used as the effective interaction in the calculations presented here.

6-B The Free Reaction Matrices

In Chapter 2 we discussed the method for obtaining an effective interaction from the free reaction matrix K_F. The nuclear reaction matrix is defined by the integral equation

$$K(\omega) = K_F(\epsilon)+K_F(\epsilon)[\mathcal{G}(\omega)Q-\mathcal{G}_F(\epsilon)P]K(\omega) \qquad (2.52)$$

and K_F is defined by

$$K_F(\epsilon) = V+V\mathcal{G}_F(\epsilon)PK_F(\epsilon) \quad . \qquad (2.48)$$

In (2.52) and (2.48) the propagators are

$$\mathcal{G}(\omega) = \frac{1}{\omega-H_0}$$

and

$$\mathcal{G}_F(\epsilon) = \frac{1}{\epsilon-t}$$

which are the propagators for nucleons in the nucleus and free space respectively. $K_F(\epsilon)$ is determined by nucleon-nucleon scattering in free space whereas $K(\omega)$ is determined by nucleon-nucleon scattering in bound states. The term in (2.52) containing the difference between the propagators is the correction for going from the free reaction matrix to the nuclear reaction matrix. The interpretation of the correction term becomes more transparent by writing the difference between the propagators as

$$\mathcal{G}(\omega)\{Q-1\} + \{\mathcal{G}(\omega)-\mathcal{G}_F(\epsilon)P\} \quad .$$

The difference between $\mathcal{G}(\omega)$ and $\mathcal{G}_F(\epsilon)P$ is referred to as the spectral correction. The term $\mathcal{G}(\omega)\{Q-1\}$ is referred to as the Pauli correction and arises from the fact that not all of the bound states are available for the nucleons scattering in bound states. In general Q is a projection operator excluding from the intermediate state summation all occupied orbitals. In particular cases Q excludes unoccupied states as well to prevent double counting of nucleon-nucleon interactions. An example of such a case is that of two valence particles

outside a closed shell core which was discussed in Sec. 2-D.

K_F is related to the two-nucleon scattering data through on-the-energy-shell matrix elements. With K_F determined from the free nucleon-nucleon scattering data $K(\omega)$ can be determined from (2.52). To obtain a realistic interaction from the free nucleon-nucleon scattering data a potential is defined for each state of total relative angular momentum by the partial wave expansion

$$\langle \underline{k}|V|\underline{k}' \rangle = \sum_{\ell\ell'SJM} V_{\ell\ell',SJ}(k,k') \mathcal{Y}_{\ell SJ}^{M}(\hat{\underline{k}}') \mathcal{Y}_{\ell'SJ}^{M*}(\hat{\underline{k}}')$$

where

$$\mathcal{Y}_{\ell SJ}^{M}(\hat{\underline{k}}) = \langle \ell S m_\ell m_S | JM \rangle Y_\ell^{m_\ell}(\hat{\underline{k}}) \chi_{m_S}$$

and χ is the intrinsic spin wavefunction. J is the total relative angular momentum for a state of orbital angular momentum ℓ and spin S. To fit the nucleon-nucleon scattering data Lee used separable non-local potentials of the form

$$V_{\ell\ell',SJ}(k,k') = \sum_{i=1}^{2} g_{\ell\ell'SJ}^{i} v_{\ell SJ}^{i}(k) v_{\ell'SJ}^{i}(k'). \quad (6.2)$$

To obtain K_F we define a free reaction matrix for each relative angular momentum state

$$\langle \underline{k}|K_F(\epsilon)|\underline{k}' \rangle = \sum_{\ell\ell'SJM} K_{F\ell\ell'SJ}(k,k';\epsilon) \mathcal{Y}_{\ell SJ}^{M}(\hat{\underline{k}}) \mathcal{Y}_{\ell'SJ}^{M*}(\hat{\underline{k}}') \quad (6.3)$$

Substituting (6.2) and (6.3) into (2.48) we have

$$K_{F\ell\ell',SJ}(k,k';\epsilon) = \sum_i g_{\ell\ell'}{}^i v_{\ell SJ}{}^i(k) v_{\ell' SJ}{}^i(k')$$

$$+ \sum_{i\ell''} g_{\ell\ell''}{}^i v_{\ell SJ}{}^i(k) \left\{ P\int_0^\infty k''^2 dk'' v_{\ell'' SJ}{}^i(k'') \frac{1}{\epsilon-\gamma k''^2} K_{F\ell''\ell SJ}(k'',k';\epsilon) \right\} \quad (6.4)$$

where

$$\gamma = \frac{\hbar^2}{m} .$$

Equation (6.4) has the solution

$$K_{F\ell\ell' SJ}(k,k';\epsilon) = \sum_{ij} \lambda_{\ell\ell' SJ}{}^{ij}(\epsilon) v_{\ell SJ}{}^i(k) v_{\ell' SJ}{}^j(k') \quad (6.5)$$

where

$$\lambda_{\ell\ell' SJ}{}^{ij}(\epsilon) = \delta^{ij} g_{\ell\ell' SJ}{}^i + \sum_{k\ell''} g_{\ell\ell'' SJ}{}^i \pi_{\ell'' SJ}{}^{ik}(\epsilon) \lambda_{\ell'' \ell}{}^{kj}(\epsilon) \quad (6.6)$$

and

$$\pi_{\ell SJ}{}^{ik}(\epsilon) \equiv P\int_0^\infty q^2 dq \frac{v_{\ell SJ}{}^i(q) v_{\ell SJ}{}^k(q)}{\epsilon-\gamma q^2} . \quad (6.7)$$

Lee obtained free reaction matrices for the S,P and D states with S-D tensor coupling. The form factors $v_{\ell SJ}{}^i$ in (6.5) that were used for the $^1S_0$ and $^3S_1$-$^3D_1$ states are

$$v_\ell{}^i(k) = \frac{k^\ell}{\{k^2+(a_\ell{}^i)^2\}^{1+\ell/2}} . \quad (6.8a)$$

For all other partial waves the form factors are

$$v_\ell^{\,i}(k) = \frac{k^{\ell+2i+2}}{(k^2+a_\ell^{\,2})^{i+\ell/2}} \qquad (6.8b)$$

where a_ℓ is the "inverse range". The strengths and "ranges" for the various states were determined by fitting the Yale IV[115] nucleon-nucleon scattering data. The potential parameters determined from the data are given in Table 6.1. The fitted parameters give too small a D-state probability for the deuteron indicating that the tensor force obtained from the fit is too weak. To completely determine $K_F(\epsilon)$ the π-functions (6.7) are required. Lee chose the form factors (6.8) such that (6.7) was analytically integrable. The expressions for the π-functions are given in Table 6.2. On the real axis $\pi(\epsilon)$ is not an analytic function of ϵ. There is a singularity at $\epsilon=0$ and $\pi(\epsilon)$ on the positive real axis is not the analytic continuation of $\pi(\epsilon)$ from the negative real axis. In the present calculations we have only used negative values of ϵ so that we have only listed the π-functions for $\epsilon < 0$. With the parameters given in Table 6.1 and the $\pi(\epsilon)$ functions given in Table 6.2. $K_F(\epsilon)$ is completely determined for negative ϵ.

With $K_F(\epsilon)$ determined the nuclear reaction matrix can be obtained from (2.52). The reaction matrix elements for a given nucleus are determined by the size of the nucleus and by the configurations included in the description of the states being considered. The model dependence of the projection operator Q was discussed in Chapter 2. Lee has determined the nuclear reaction matrix elements for the (1s,0d) shell with an O^{16} core. Both plane

Table 6.1

Parameters of the separable potential

$^{2S+1}\ell_J$	a_1 (fm^{-1})	$g_1/\sqrt{a_1}$ (MeV)	a_2 (fm^{-1})	$g_2/\sqrt{a_2}$ (MeV)
$^3S_1$	1.59	-2.89×10^2	6.23	6.87×10^3
$^3S_1$-$^3D_1$		-7.80×10^1		1.53×10^4
$^3D_1$	1.50	5.44×10^2	6.00	4.86×10^4
$^1P_1$	1.90	4.40×10^2	1.90	4.58×10^5
$^3D_2$	1.29	-2.05×10^2	--	---
$^3D_3$	2.37	-2.56×10^2	--	---
$^1S_0$	1.51	-1.91×10^2	7.29	7.78×10^3
$^3P_0$	1.53	-2.07×10^2	1.53	8.86×10^2
$^3P_1$	1.37	1.14×10^2	1.37	3.11×10^2
$^3P_2$	1.57	-7.38×10^1	1.57	-1.73×10^2
$^1D_2$	1.59	-1.21×10^2	--	---

Table 6.2

The $\pi(\epsilon)$ functions for the separable potential and $\epsilon < 0$. The notation is $\gamma \equiv \frac{\hbar^2}{m}$, $\epsilon_i = \gamma\, a_i^{\,2}$ (MeV) and $\epsilon \equiv -\gamma\alpha^2 < 0$

$^{2S+1}\ell_j$	$v_\ell^{\,1}(k)$	$v_\ell^{\,2}(k)$	$\pi(-\alpha^2)$
$^1S_0, {}^3S_1$	$\frac{1}{(k^2+a_1^{\,2})}$	$\frac{1}{(k^2+a_2^{\,2})}$	$\pi_0^{\,ii} = -\frac{\pi}{4\gamma a_i (a_i+\alpha)^2}$
			$\pi_0^{\,12} = -\frac{\pi}{2\gamma (a_1+a_2)(a_1+\alpha)(a_2+\alpha)}$
$^3D_1$	$\frac{k^2}{(k^2+a_1^{\,2})^2}$	$\frac{k^2}{(k^2+a_2^{\,2})^2}$	$\pi_2^{\,ii} = -\frac{\pi(a_i^{\,2}+4a_i\alpha+5\alpha^2)}{32\gamma a_i (a_i+\alpha)^4}$
			$\pi_2^{\,12} = -\frac{\pi}{4\gamma (a_1+a_2)^3 (a_1+\alpha)^2 (a_2+\alpha)^2} \times$ $\times \{a_1^{\,2}a_2^{\,2}+2a_1a_2(a_1+a_2)\alpha+(a_1^{\,2}+3a_1a_2+a_2^{\,2})\alpha^2\}$

Table 6.2 (contd)

$^1P_1, {}^3P_{0,1,2}$	$\frac{k}{(k^2+a^2)^{3/2}}$	$\frac{k}{(k^2+a^2)^{5/2}}$	$\pi_1^{11} = -\frac{\pi(a+3\alpha)}{16\gamma a(a+\alpha)^3}$
			$\pi_1^{12} = -\frac{\pi(a^2+4a\alpha+5\alpha^2)}{32\gamma a(a+\alpha)^4}$
			$\pi_1^{22} = -\frac{\pi}{256\gamma a(a+\alpha)^5} \times \{5a^3+25a^2\alpha+47a\alpha^2+35\alpha^3\}$
$^1D_2, {}^3D_{2,3}$	$\frac{k^2}{(k^2+a^2)^2}$	$\frac{k^4}{(k^2+a^2)^3}$	$\pi_2^{11} = -\frac{\pi(a^2+4a\alpha+5\alpha^2)}{32\gamma a(a+\alpha)^4}$
			$\pi_2^{12} = -\frac{\pi}{256\gamma a(a+\alpha)^5} \times \{5a^3+25a^2\alpha+47a\alpha^2+35\alpha^3\}$
			$\pi_2^{22} = -\frac{\pi}{512\gamma a(a+\alpha)^6} \times \{7a^4+42a^3\alpha+82a^2\alpha^2+122\alpha^3+63\alpha^4\}$

wave and harmonic oscillator intermediate states were used to evaluate the Pauli and spectral corrections. The two sets of intermediate states give quite different reaction matrix elements and the correct choice of states is still an unsolved problem.

To evaluate effective interaction matrix elements with Woods-Saxon (WS) wavefunctions many nuclear reaction matrix elements are required. In general the nuclear reaction matrix elements are a numerical array. To obtain effective interaction matrix elements with WS wavefunctions one would have to use the WS wavefunctions initially in the detailed determination of $K(\omega)$. Such a calculation would be a very difficult computational problem. The free reaction matrix is a convenient device for obtaining an analytic function which reproduces $K(\omega)$ matrix elements to a good approximation. The matrix elements of $K(\omega)$ in (2.52) are independent of ϵ whereas K_F is a specified function of ϵ given by (6.5). Using HO single-particle states for the (0d,1s) shell Lee found that the matrix elements of $K_F(\epsilon)$ with ϵ = -80 and -200 reproduced (to a good approximation) the $K(\omega)$ matrix elements for harmonic oscillator[/] and plane wave intermediate states respectively. With a functional form for the nuclear reaction matrix elements it is possible to calculate all of the HO matrix elements required to evaluate the two-body matrix elements with WS wavefunctions.

[/] The calculation with harmonic oscillator intermediate states was for no gap between the occupied and unoccupied levels in the oscillator spectrum. Baranger[7] has discussed in detail calculations using harmonic oscillator intermediate states.

Radial integrals of the free reaction matrix elements evaluated with HO wavefunctions are given in Table 6.3. The radial integrals are given for ϵ = -80 MeV and ϵ = -200 MeV. The ϵ = -200 MeV radial integrals are considerably weaker than the ϵ = -80 MeV integrals. Since calculations were performed for both light and heavy nuclei n = n' = 0 radial integrals are given as a function of $\hbar\omega$. The interaction is sensitive to the oscillator potential size parameter; consequently the choice of size parameter for each nucleus is important.

6-C The Models

The two-particle and two-hole spectra were calculated using both HO and WS wavefunctions. The WS wavefunctions used were those given in Tables 4.15, 4.20, and 4.25. For the A=18 nuclei the configurations and energies used were those given in Table 5.2. In the HO wavefunction expansion of the WS wavefunction five and seven terms were included for the 0d and 1s levels respectively. The oscillator size parameter used in the expansion was $\hbar\omega$ = 12.5 MeV. For the other nuclei the configurations included in the calculations are listed in Table 6.4 together with the unperturbed energies and the number of terms included in the WS wavefunction expansion. In the calculation the lowest unperturbed configuration was taken to be at zero energy. With this energy scale the experimental spectra for A=18 nuclei is given in Table 5.3. The experimental spectra for the other nuclei are given in Table 6.5. The ground state binding energies given in the 1964 Atomic Mass Table [100] :

Table 6.3

Radial integrals of the free reaction matrix evaluated with HO wavefunctions. Table 6.3a is for $\hbar\omega$ = 13.4 MeV and ϵ = -80 MeV and Table 6.3b is for $\hbar\omega$ - 13.4 MeV and ϵ = -200 MeV. Table 6.3c gives the n = n' = 0 radial integrals as a function of $\hbar\omega$. The integrals are in units of MeV.

(a)

n	n'	$^3S_1$	$^3D_1$	$^3S_1$-$^3D_1$	$^3D_1$-$^3S_1$	$^1P_1$	$^3D_2$	$^3D_3$
0	0	-12.62	1.90	-1.59	-1.59	1.67	-2.42	-0.12
0	1	-11.76	2.41	-1.91	-1.56	2.14	-2.80	-0.19
0	2	-10.36	2.63	-1.96	-1.45	2.36	-2.91	-0.24
0	3	-9.00	2.72	-1.89	-1.34	2.47	-2.91	-0.27
0	4	-7.80	2.73	-1.74	-1.23	2.50	-2.85	-0.30
0	5	-6.75	2.70	-1.56	-1.13	2.50	-2.77	-0.32
1	1	-10.86	3.06	-1.87	-1.87	3.20	-3.25	-0.29
2	2	-8.16	3.67	-1.77	-1.77	4.98	-3.51	-0.46
3	3	-5.79	3.94	-1.53	-1.53	6.77	-3.50	-0.62
4	4	-3.86	4.01	-1.25	-1.25	8.36	-3.36	-0.75
5	5	-2.33	3.99	-0.97	-0.97	9.68	-3.17	-0.86

(a) continued

n	n'	$^1S_0$	$^3P_0$	$^3P_1$	$^3P_2$	$^1D_2$
0	0	-7.08	-2.08	1.89	-1.00	-0.48
0	1	-6.22	-1.95	2.26	-1.28	-0.64
0	2	-5.16	-1.70	2.36	-1.40	-0.71
0	3	-4.20	-1.46	2.35	-1.45	-0.75
0	4	-3.37	-1.26	2.30	-1.46	-0.76
0	5	-2.65	-1.09	2.23	-1.44	-0.76
1	1	-5.32	-1.49	2.86	-1.70	-0.84
2	2	-3.29	-0.42	3.34	-2.12	-1.05
3	3	-1.61	0.55	3.53	-2.36	-1.16
4	4	-0.28	1.29	3.54	-2.46	-1.20
5	5	0.75	1.82	3.46	-2.49	-1.20

(b)

n	n'	$^3S_1$	$^3D_1$	$^3S_1$-$^3D_1$	$^3D_1$-$^3S_1$	$^3P_1$	$^3D_2$	$^3D_3$
0	0	-10.63	2.08	-1.38	-1.38	1.82	-2.27	-0.12
0	1	-9.92	2.64	-1.66	-1.37	2.43	-2.64	-0.18
0	2	-8.75	2.88	-1.71	-1.29	2.75	-2.74	-0.23
0	3	-7.62	2.98	-1.65	-1.20	2.93	-2.73	-0.27
0	4	-6.62	2.99	-1.53	-1.12	3.02	-2.68	-0.30
0	5	-5.74	2.96	-1.38	-1.05	3.05	-2.60	-0.32
1	1	-9.16	3.35	-1.65	-1.65	3.75	-3.06	-0.28
2	2	-6.85	4.01	-1.57	-1.57	6.03	-3.30	-0.46
3	3	-4.79	4.30	-1.37	-1.37	8.30	-3.29	-0.61
4	4	-3.10	4.38	-1.13	-1.13	10.31	-3.16	-0.74
5	5	-1.74	4.34	-0.88	-0.88	11.96	-2.98	-0.85

(b) continued

n	n'	$^1S_0$	$^3P_0$	$^3P_1$	$^3P_2$	$^1D_2$
0	0	-6.48	-2.03	2.01	-0.96	-0.48
0	1	-5.69	-1.92	2.41	-1.23	-0.62
0	2	-4.72	-1.68	2.52	-1.34	-0.70
0	3	-3.84	-1.46	2.52	-1.38	-0.73
0	4	-3.08	-1.26	2.47	-1.39	-0.75
0	5	-2.42	-1.10	2.40	-1.38	-0.75
1	1	-4.84	-1.46	3.07	-1.62	-0.82
2	2	-2.93	-0.38	3.58	-2.03	-1.02
3	3	-1.32	0.60	3.78	-2.25	-1.13
4	4	-0.04	1.35	3.79	-2.35	-1.17
5	5	0.98	1.89	3.70	-2.38	-1.18

(c)

ϵ (MeV)	-80.0			-200.0		
$\hbar\omega$ (MeV)	5.0	10.0	15.0	5.0	10.0	15.0
$^1S_0$	-2.15	-5.10	-7.98	-1.96	-4.67	-7.30
$^3P_0$	-0.35	-1.31	-2.45	-0.34	-1.27	-2.34
$^3P_1$	0.26	1.08	2.34	0.27	1.14	2.48
$^3P_2$	-0.12	-0.55	-1.26	-0.12	-0.53	-1.21
$^1D_2$	-0.03	-0.23	-0.64	-0.03	-0.22	-0.62
$^3S_1$	-3.67	-8.94	-14.33	-3.08	-7.52	-12.07
$^3S_1$-$^3D_1$	-0.23	-0.94	-1.92	-0.20	-0.81	-1.67
$^3D_1$	0.14	0.92	2.47	0.15	1.01	2.71
$^1P_1$	0.21	0.92	2.10	0.22	0.98	2.31
$^3D_2$	-0.21	-1.24	-3.07	-0.19	-1.17	-2.89
$^3D_3$	-0.006	-0.05	-0.17	-0.006	-0.05	-0.16

Table 6.4

Unperturbed single-particle energies used in the calculation of the spectra of Ca^{42}, Sc^{42}, Pb^{206} and Pb^{210}. The third column for each nucleus is the number of terms included in the expansion of WS wavefunctions in terms of HO wavefunctions.

Ca^{42}			Pb^{206}			Pb^{210}		
$\nu\ell j$	$\epsilon_{\nu\ell j}$ (MeV)	n	$\nu\ell j$	$\epsilon_{\nu\ell j}$ (MeV)	n	$\nu\ell j$	$\epsilon_{\nu\ell j}$ (MeV)	n
$0f_{7/2}$	0.00	5	$2p_{1/2}$	0.00	6	$1g_{9/2}$	0.00	5
$1p_{3/2}$	2.07	5	$1f_{5/2}$	0.57	5	$0i_{11/2}$	0.79	3
$1p_{1/2}$	4.13	5	$2p_{3/2}$	0.89	6	$0j_{15/2}$	1.41	2
$0f_{5/2}$	6.69	5	$0i_{13/2}$	1.63	4	$2d_{5/2}$	1.58	6
			$1f_{7/2}$	2.34	5	$3s_{1/2}$	2.03	7
			$0h_{9/2}$	3.47	2	$1g_{7/2}$	2.49	4
						$2d_{3/2}$	2.52	6

Table 6.5

Experimental energies of low-lying states in Ca^{42}, Sc^{42}, Pb^{206} and Pb^{210}

Ca^{42} (a)		Sc^{42} (b)		Pb^{206} (c)		Pb^{210} (d)	
J^π,T	E_B (MeV)	J^π,T	E_B (MeV)	J^π	E_B (MeV)	J^π	E_B (MeV)
0^+,1	-3.11	0^+,1	-3.20	0^+	-0.64	0^+	-1.24
2^+,1	-1.59	1^+,0	-2.59	2^+	+0.16	2^+	-0.44
0^+,1	-1.28	7^+,0	-2.58	0^+	+0.52	4^+	-0.15
2^+,1	-0.69	5^+,(0)	-1.68	3^+	0.70	6^+	-0.05
4^+,1	-0.36	3^+,0	-1.70	2^+	0.82	8^+	+0.03
6^+,1	+0.08	2^+,1	-1.61	4^+	1.04		
2^+,1	0.28	0^+,1	-1.31	1^+	1.09		
2^+,1	0.54	$(2^+)3^+$,0	-1.00	(2^+)	1.14		
2^+,1	1.34	2^+,1	-0.70	4^+	1.36		
2^+,1	1.75	4^+,1	-0.35	$(1^+\ 2^+)$	1.51		
4^+,1	1.90	$(4^+)5^+$,0	-0.10	7^-	1.56		
2^+,1	2.09	6^+,1	+0.05	6^-	1.74		
0^+,1	2.74	$(3^+)2^+$,0	0.19	3^-	1.89		
0^+,1	2.90	1^+,0	0.49	(9^-)	2.01		
4^+,1	2.99	$(2^+)3^+$,0	0.58	5^-	2.14		
2^+,1	3.16	1^+,0	0.66	4^+	2.28		
(0^+),1	3.40	(2^+),3^+	0.73	5^-	2.37		
0^+,1	3.59	0^+,1	2.51	3^+	2.48		
				(5^-)	2.55		
2^+,1	4.07			(6^+)	2.61		
				(5^-)	2.76		

(a) reference 116

(b) reference 117

(c) reference 118

(d) reference 119

$$BE(2p,Ca^{42}) = 2BE(Ca^{41}) - BE(Ca^{40}) - BE(Ca^{42})$$
$$= -3.11 \text{ MeV}.$$
$$BE(2p,Sc^{42}) = BE(Ca^{41}) + BE(Sc^{41}) - BE(Ca^{40}) - BE(Sc^{42})$$
$$= -3.20 \text{ MeV}.$$
$$BE(2h,Pb^{206}) = BE(Pb^{208}) + BE(Pb^{206}) - 2BE(Pb^{207})$$
$$= 0.64 \text{ MeV}.$$
$$BE(2p,Pb^{210}) = 2BE(Pb^{209}) - BE(Pb^{208}) - BE(Pb^{210}$$
$$= -1.24 \text{ MeV}.$$

The A=18 spectra were calculated with HO wavefunctions using both ϵ = -80 MeV and ϵ = -200 MeV. These two calculations correspond to calculations with nuclear reaction matrices determined using plane wave and HO intermediate states as was discussed earlier. The spectra were also calculated using WS wavefunctions and ϵ = -200 MeV. Exact calculations with WS wavefunctions require large amounts of computational time so only the value ϵ = -200 was used since it yielded matrix elements more in accord with those of Kuo and Brown.[4] The WS calculations were performed retaining terms in the matrix elemtns for which the product of expansion coefficients was greater than or equal to 0.05. This approximation was checked for several matrix elements by including additional terms. It was found that the approximation was worst for the $(s_{1/2})^2$ diagonal matrix elements. With the approximation used the $(s_{1/2})^4$ matrix elements are approximately 10% too small. Errors in other matrix elements were considerably smaller.

Nuclear reaction matrix elements for the separable potential

given in the previous section have only been determined for the A=18 nuclei. In the calculations of A=42, Pb^{206} and Pb^{210} spectra the free reaction matrix with ϵ = -200 MeV was used as an effective interaction. The WS calculations for these nuclei were performed in the same approximation as for the A=18 nuclei.

6-D Results for A=18 Nuclei

The two-particle spectrum of O^{18} was calculated with HO wavefunctions ($\hbar\omega$ = 13.4) for ϵ = -80 MeV and ϵ = -200 MeV. The low-lying levels from both calculations are compared with experiment in columns a and b of Fig. 6.1. The entire spectrum for ϵ = -200 MeV is given in Table 6.6. The free reaction matrix with ϵ = -200 MeV gives 0.4 MeV less binding energy for the ground state than K_F with ϵ = -80 MeV. Apart from the ground state the two calculations give the same level positions to within 0.2 MeV. The spectrum calculated using WS wavefunctions for ϵ = -200 MeV is given in Table 6.6 and compared with experiment in column c of Fig. 6.1. The 0_1^+ and 0_2^+ states are shifted upwards by 0.8 and 1 MeV respectively relative to the HO calculation with $\hbar\omega$ = 13.4 MeV. With the approximation used in the WS calculation the upward shift of the 0^+ states is overestimated by approximately 0.1-0.2 MeV. The other low-lying levels have smaller although significant shifts relative to the HO calculation. The use of WS wavefunctions leads to an overall state dependent weakening of the interaction matrix elements relative to the values in the HO calculation. The spectrum calculated with HO wavefunctions with $\hbar\omega$ - 12.0 MeV and for ϵ = -200 MeV is

Table 6.6

The two-particle spectra of O^{18} calculated with HO and WS wavefunctions for ϵ = -200 MeV.

Calc.	J^π,T	Eigenvalues (MeV)
HO ($\hbar\omega$=13.4)	0^+,1	-2.87, -0.24, 10.88
	1^+,1	4.59, 5.63
	2^+,1	-1.78, -0.10, 4.29, 5.91, 10.16
	3^+,1	0.55, 4.48
	4^+,1	-0.74, 3.34
WS	0^+,1	-2.05, 0.80, 10.63
	1^+,1	4.72, 5.78
	2^+,1	-1.35, 0.09, 4.51, 5.86, 10.14
	3^+,1	0.63, 4.59
	4^+,1	-0.58, 3.68
HO ($\hbar\omega$=12.0)	0^+,1	-2.71, -0.10, 10.55
	1^+,1	4.63, 5.67
	2^+,1	-1.53, 0.02, 4.40, 5.87, 10.11
	3^+,1	0.61, 4.59
	4^+,1	-0.62, 3.51

given in Table 6.6 and compared with the other calculations in column d of Fig. 6.1. As would be expected the HO calculation with $\hbar\omega$ = 12.0 MeV shifts the spectrum upwards relative to the spectrum calculated with HO wavefunctions and $\hbar\omega$ = 13.4 MeV. Nevertheless, a HO calculation with a smaller $\hbar\omega$ value does not reproduce the state dependence of the matrix elements in a WS calculation.

The calculations that were performed for the T=1 states of

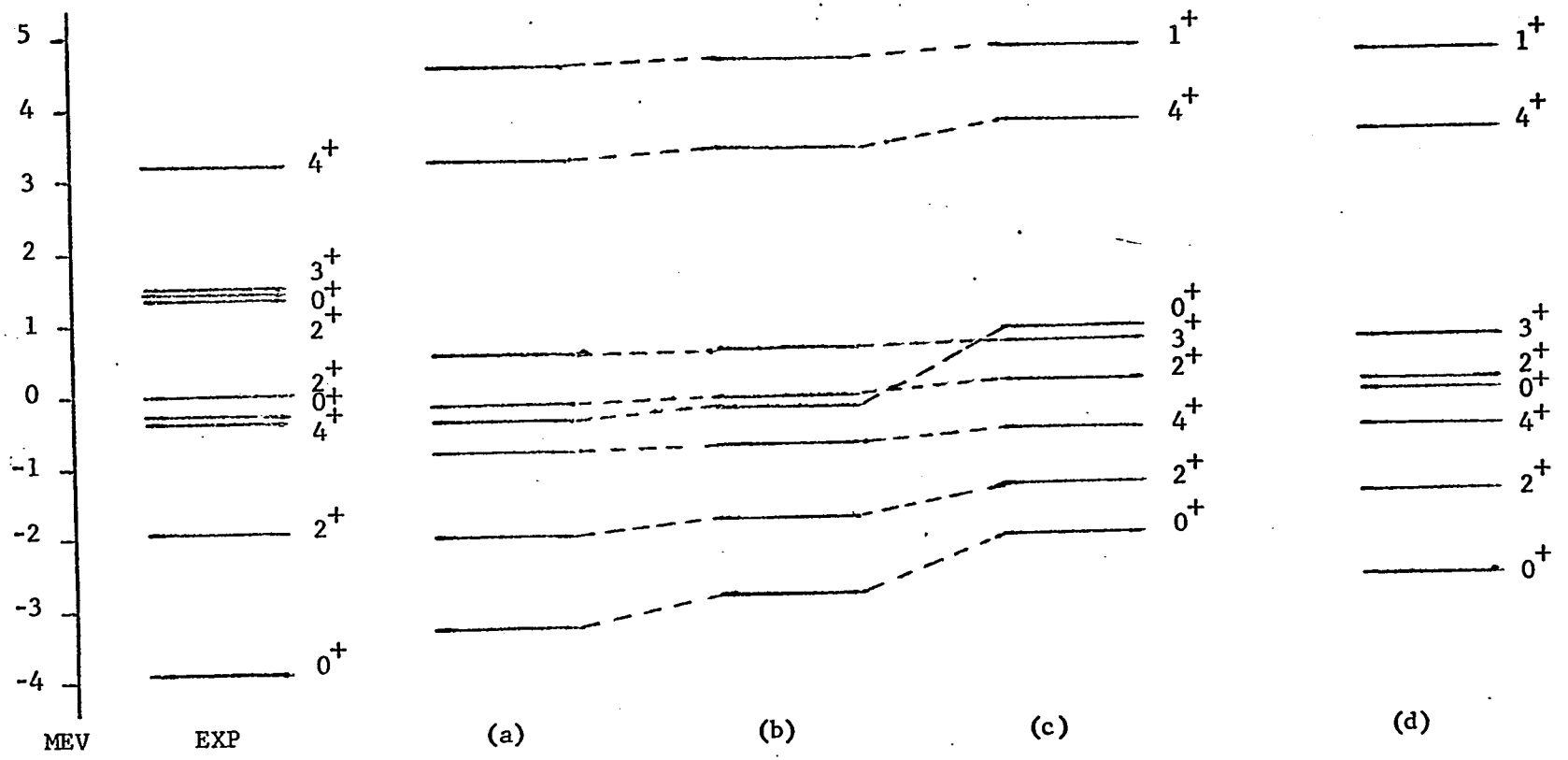

Fig. 6-1. The two-particle spectrum of O^{18} calculated with harmonic oscillator (HO) and Woods-Saxon (WS) wavefunctions. The calculations are for: (a) HO, $\hbar\omega$ = 13.4 MeV, ϵ = -80 MeV; (b) HO, $\hbar\omega$ = 13.4 MeV, ϵ = -200 MeV; (c) WS, ϵ = -200 MeV; (d) HO, $\hbar\omega$ = 12.0 MeV, ϵ = -200 MeV.

O^{18} were repeated for the T=0 states of F^{18}. The results are given in Table 6.7 and compared with experiment in Fig. 6.2. The HO calculation with ϵ = -200 MeV gives 1.5 MeV less binding energy for the F^{18} ground state than the calculation with ϵ = -80 MeV. Except for the 3_1^+ state the remaining low-lying states in the spectrum for ϵ = -200 MeV are shifted upwards by approximately 1 MeV relative to their positions for ϵ = -80 MeV. The spectrum calculated using WS wavefunctions for ϵ = -200 MeV is given in column c of Fig. 6.2. The upward shifts of the levels in the spectrum for the WS calculation relative to those for the HO calculation with $\hbar\omega$ = 13.4 MeV are as large as 2 MeV. The approximation made in the WS calculation is worst for the 1^+ states and the calculated positions of the 1_1^+ and 1_2^+ levels are too high by approximately 0.25 MeV. The spectrum calculated using the HO wavefunctions for $\hbar\omega$ = 12.0 MeV and ϵ = -200 MeV is compared with the other calculations in column c of Fig. 6.2. The calculation using HO wavefunctions and $\hbar\omega$ = 12.0 MeV weakens the interaction matrix elements but does not reproduce the state dependence in the WS calculation.

5-E Results for A=42 Nuclei

The two-particle spectrum of Ca^{42} was calculated using both HO ($\hbar\omega$=11.5 MeV) and WS wavefunctions for ϵ = -200 MeV. The results are given in Table 6.8 and compared with experiment in Fig. 6.3. The HO and WS calculations are very similar except for the 0_1^+ and 0_2^+ states which are shifted upwards by approximately 0.25 MeV in the WS calculation. The agreement between the calculated and experi-

Table 6.7

The two-particle spectra of F^{18} calculated with HO and WS wavefunctions for ϵ = -200 MeV

Calc.	J^π,T	Eigenvalues (MeV)
HO ($\hbar\omega$=13.4)	1^+,0	-5.84, -1.67, 1.78, 4.49, 10.45
	2^+,0	-2.67, 2.47, 5.80
	3^+,0	-4.21, -0.48, 3.40, 8.13
	4^+,0	0.61
	5^+,0	-4.02
WS	1^+,0	-3.81, 0.02, 2.62, 4.78, 10.33
	2^+,0	-1.30, 2.74, 5.71
	3^+,0	-3.18, -0.29, 3.46, 8.61
	4^+,0	1.57
	5^+,0	-3.50
HO ($\hbar\omega$=12.0)	1^+,0	-5.21, -1.38, 1.90, 4.44, 10.13
	2^+,0	-2.00, 2.56, 5.65
	3^+,0	-3.66, -0.37, 3.63, 8.20
	4^+,0	1.20
	5^+,0	-3.53

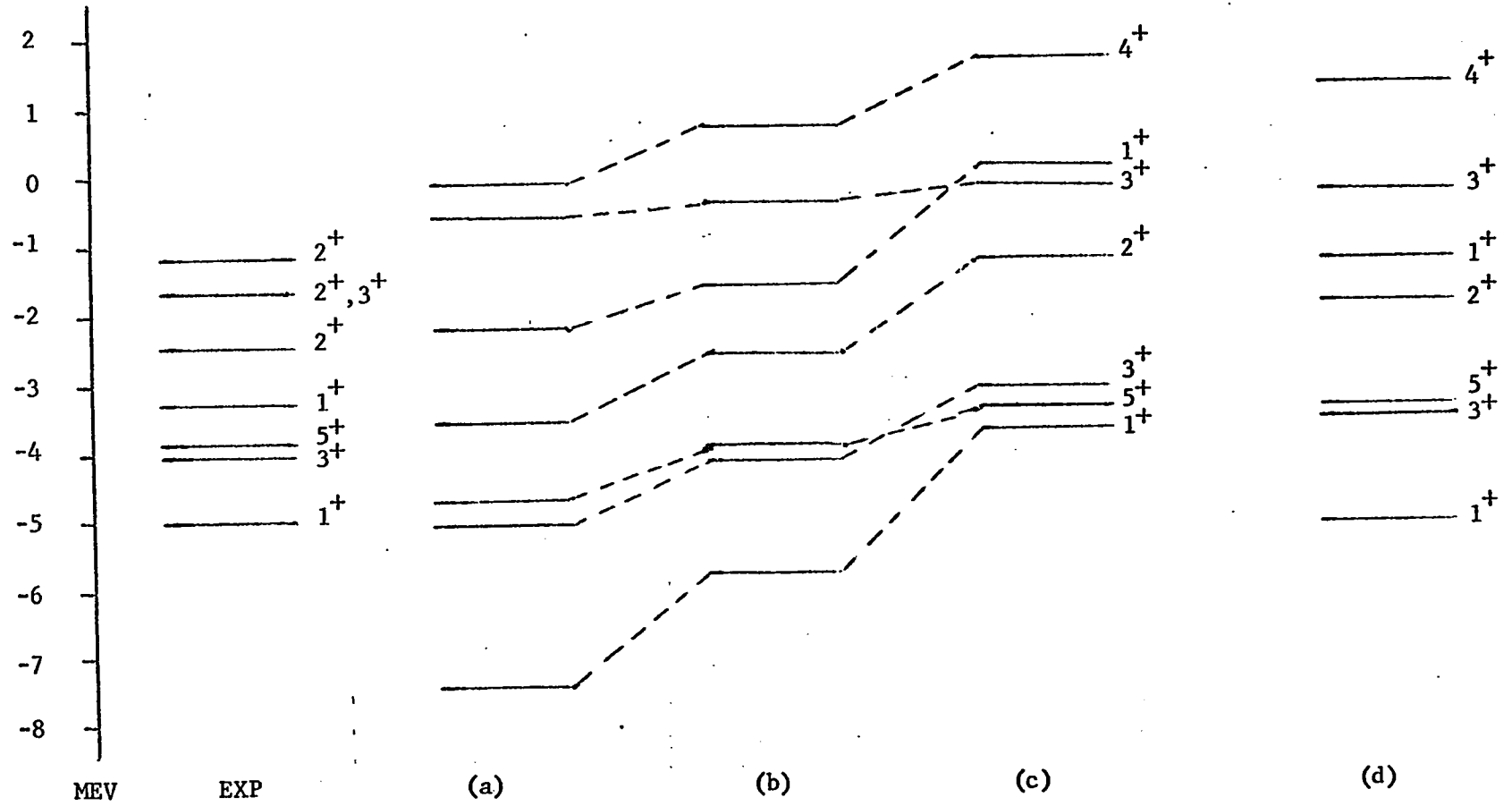

Fig. 6-2. The T=0 two-particle states in F^{18} calculated with harmonic oscillator (HO) and Woods-Saxon (WS) wavefunctions. The calculated spectra are: (a) HO,$\hbar\omega$ = 13.4 MeV, ϵ = -200 MeV; (b) HO,$\hbar\omega$ = 13.4 MeV, ϵ = -200 MeV; (c) WS, ϵ = -200 MeV; (d) HO,$\hbar\omega$ = 12.0 MeV, ϵ = -200 MeV.

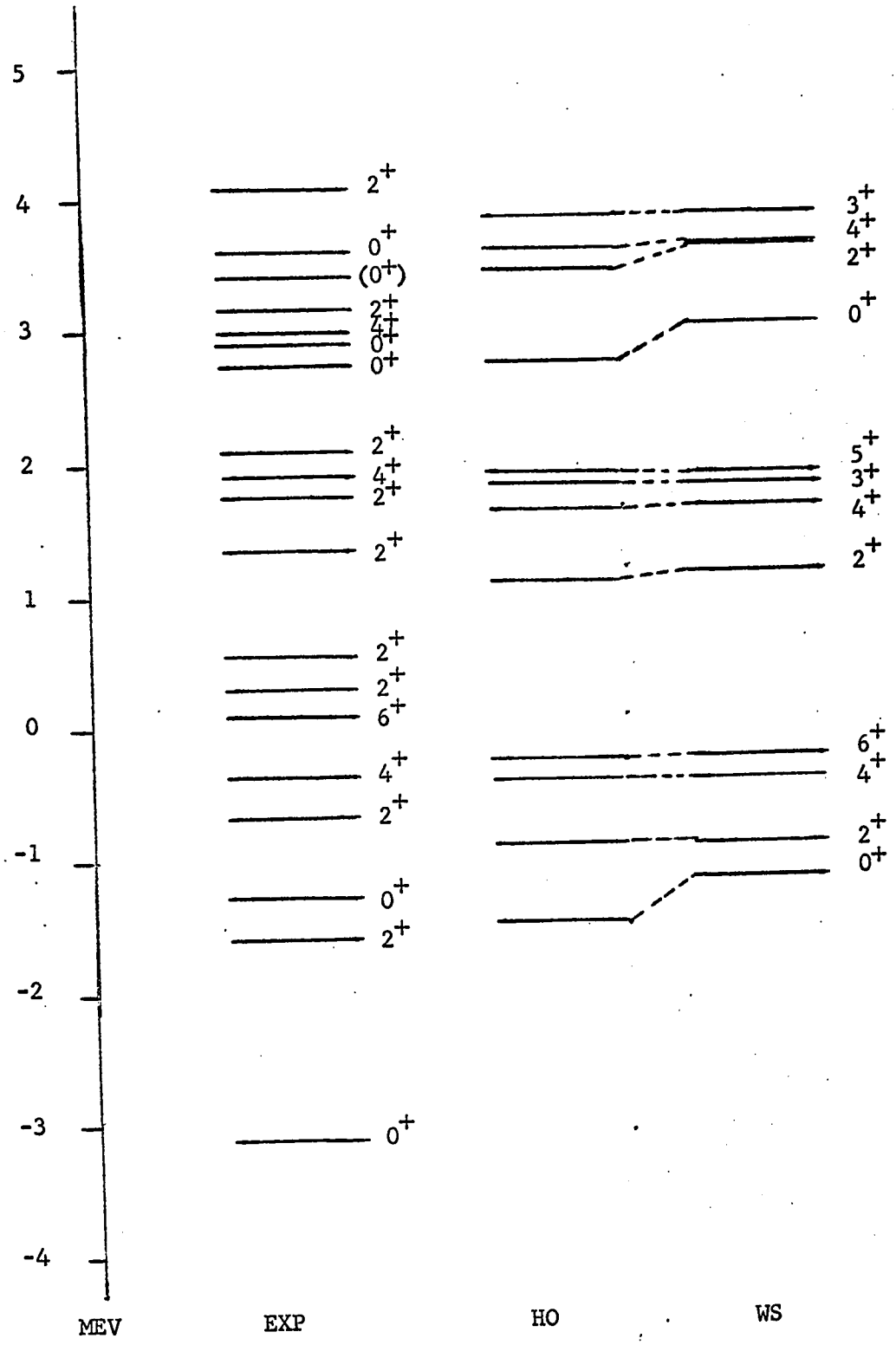

Fig. 6-3. The two-particle spectrum of Ca^{42}. The calculated spectra are for harmonic oscillator wavefunctions (HO, $\hbar\omega$ = 11.5 MeV) and Woods-Saxon wavefunctions (WS).

Table 6.8

The two-particle spectra of Ca^{42} calculated with HO ($\hbar\omega$=11.5 MeV) and WS wavefunctions for ϵ = -200 MeV

Calc.	J^π,T	Eigenvalues (MeV)
HO	0^+,1	-1.47, 2.74, 8.61, 13.81
	1^+,1	6.05, 6.34, 8.52
	2^+,1	-0.90, 1.09, 3.44, 5.37, 6.41, 8.74 10.69, 13.22
	3^+,1	1.83, 3.89, 6.24, 8.47, 10.68
	4^+,1	-0.42, 1.63, 3.59, 6.28, 8.48, 13.38
	5^+,1	1.91, 6.33
	6^+,1	-0.26, 5.26
WS	0^+,1	-1.16, 3.02, 8.38, 13.93
	1^+,1	6.12, 6.42, 8.58
	2^+,1	-0.90, 1.15, 3.61, 5.55, 6.45, 8.76 10.73, 13.25
	3^+,1	1.80, 3.89, 6.23, 8.48, 10.70
	4^+,1	-0.41, 1.65, 3.62, 6.32, 8.50, 13.40
	5^+,1	1.89, 6.29
	6^+,1	-0.27, 5.28

mental spectra is not good. The choice of ϵ = -200 MeV in K_F for the effective interaction was arbitrary; however, one would not expect the Pauli and spectral corrections for the reaction matrix elements in the (f,p) shell to differ greatly from those in the (s,d) shell. On the other hand there is no reason to expect agreement with experiment by using a simple model containing only spherical

two-particle configurations. The model predicts two 0^+ and three 2^+ states below E_B = 5 MeV. Experimentally there are six 0^+ and eight 2^+ states below E_B = 5 MeV. Several authors [120-123] have discussed the structure of the low-lying states in Ca^{42} in terms of a model in which the spherical shell model states are mixed with deformed states.

The T=0 two-particle spectrum of Sc^{42} was calculated using both HO ($\hbar\omega$=11.5 MeV) and WS wavefunctions for ϵ = -200 MeV. The results are given in Table 6.9 and compared with experiment in Fig. 6.4. The calculated spectrum is in reasonable agreement with experiment which is in marked contrast to the T=1 spectra. The 1_1^+, 1_2^+, and 2_2^+ states in the WS calculation are shifted upwards by 0.5 MeV relative to their positions in the HO calculation. The state dependence of the interaction matrix elements in the WS calculation leads to a downward shift of the 5_2^+ and 7_1^+ states relative to their positions in the HO calculation. The downward shift of the 7_1^+ state relative to its position in the HO spectrum is a consequence of the $\hbar\omega$ value used in the HO calculation. The $0f_{7/2}$ WS wavefunction is very much like a HO wavefunction with $\hbar\omega$ = 12.75 MeV (Table 4.21) whereas the HO calculation presented here is for $\hbar\omega$ = 11.5 MeV.

5-F Results for Pb^{206}

In the absence of a calculation of nuclear reaction matrix elements for the Pb region the free reaction matrix was used as the effective interaction with calculations being performed for

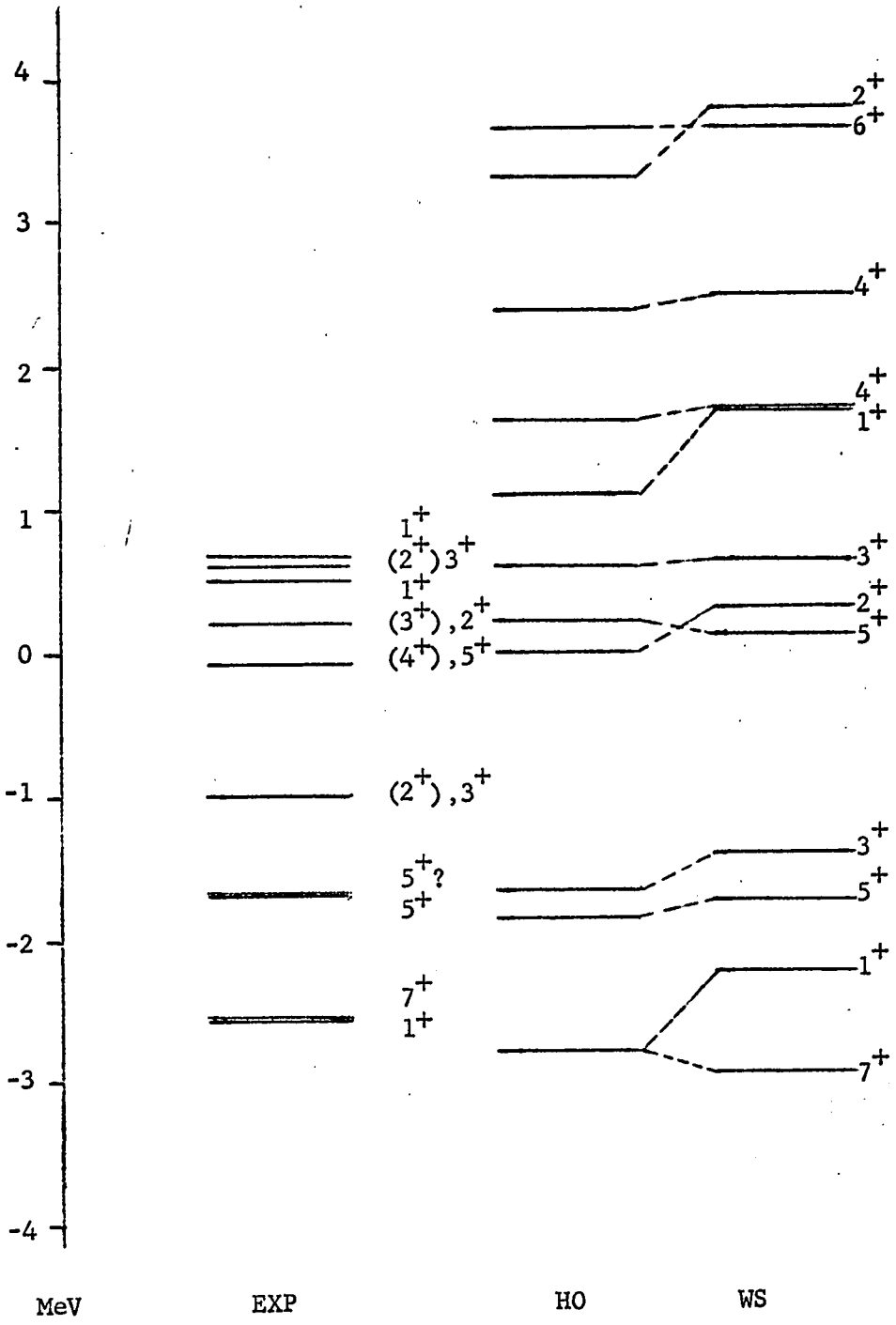

Fig. 6-4.

The T=0 two-particle spectrum of Sc^{42}. The spectra presented are for harmonic oscillator (HO, $\hbar\omega$ = 11.5 MeV) and Woods-Saxon (WS) wavefunctions with ϵ = -200 MeV.

Table 6.9

The two-particle T=0 spectra of Sc^{42} calculated with HO ($\hbar\omega$=11.5 MeV) and WS wavefunctions for ϵ = -200 MeV.

Calc.	J^π,T	Eigenvalues (MeV)
HO	1^+,0	-2.79 1.10, 4.16, 5.57, 7.07, 7.96 13.82
	2^+,0	-0.02, 3.31, 4.86, 8.21, 10.84
	3^+,0	-1.66, 0.58, 2.14, 3.38, 5.35, 7.86, 9.70, 12.97
	4^+,0	1.61, 2.38, 5.33, 8.36
	5^+,0	-1.86, 0.21, 6.04, 11.40
	6^+,0	3.67
	7^+,0	-2.79
WS	1^+,0	-2.24, 1.67, 4.56, 5.90, 7.12, 8.05 13.98
	2^+,0	0.30, 3.80, 5.08, 8.26, 10.90
	3^+,0	-1.42, 0.63, 2.42, 3.51, 5.50, 7.91, 9.79, 13.06
	4^+,0	1.69, 2.49, 5.32, 8.38
	5^+,0	-1.73, 0.12, 6.10, 11.59
	6^+,0	3.65
	7^+,0	-2.95

ϵ = -200 MeV and ϵ = -80 MeV. On the basis of the neutron single-particle potentials deduced in Chap. 4 the best value of $\hbar\omega$ for HO wavefunctions in the Pb region would be approximately 8.0 MeV. On the other hand, the neutron well found by Rost[82] had a much larger radius and the best value of $\hbar\omega$ in a calculation with Rost's HO

wavefunctions would be approximately 6.0 MeV. To study the effect of the nuclear size in determining effective interaction matrix elements and consequently the two-hole spectrum the spectrum was calculated using HO wavefunctions with $\hbar\omega$ = 6.0 MeV and 8.0 MeV. The results of the calculations are given in Table 6.10. From Table 6.10 it can be seen that the positive parity states with even spin are affected most. The 0_1^+, 2_1^+, 4_1^+ and 6_1^+ states are depressed by 0.15, 0.24, 0.12 and 0.19 MeV respectively for $\hbar\omega$ = 8.0 MeV relative to their positions for $\hbar\omega$ = 6.0 MeV. For the Pb region energy shifts of this size are significant since the matrix elements are small. This can be seen by comparing the unperturbed positions of levels with the positions after diagonalizing the shell model Hamiltonian. In Fig. 6.5 the calculated spectra are compared with experiment and the unperturbed positions of the levels.

Decreasing the value of $\hbar\omega$ does not necessarily lead to a decrease in the magnitude of a matrix element. In fact, some matrix elements become larger in magnitude as $\hbar\omega$ is decreased. For example, with HO wavefunctions and ϵ = -200 MeV we have

$$< (h_{9/2})^2 J | K_F | (h_{9/2})^2 J=0 > = -0.083 \text{ MeV} \quad (\hbar\omega=8.0 \text{ MeV})$$
$$= -0.270 \text{ MeV} \quad (\hbar\omega=6.0 \text{ MeV}) \quad .$$

The nuclear size dependence of the matrix elements is complicated by two factors: 1) the different size dependence of the attractive and repulsive terms in the $^1S_0$ interaction; and 2) a cancellation between the singlet-even and triplet-odd components of the interaction.

Table 6.10

Two-hole states in Pb^{206} with $E_B < 4.0$ MeV calculated using HO wavefunctions with $\hbar\omega$ = 6.0 MeV, and $\hbar\omega$ = 8.0 MeV for ϵ = -200 MeV.

$\hbar\omega$	6.0	8.0
J^π	Eigenvalues (MeV)	Eigenvalues (MeV)
0^+	-0.37, 0.62, 1.56, 2.73	-0.52, 0.58, 1.62, 2.78
1^+	0.84, 1.40, 2.83	0.83, 1.38, 2.82
2^+	0.24, 0.59, 1.03, 1.43, 1.63, 2.84, 2.88, 3.07, 3.92	0.00, 0.54, 0.99, 1.42, 1.58, 2.75, 2.83, 3.03, 3.95
3^+	0.54, 1.39, 2.28, 2.82, 3.18, 3.98	0.52, 1.34, 2.24, 2.77, 3.13, 3.93
4^+	1.05, 1.22, 2.21, 2.80, 3.10, 3.19, 3.39, 3.98	0.93, 1.16, 2.18, 2.78, 3.07, 3.18, 3.38, 3.99
5^+	2.84, 3.18, 3.45, 4.02	2.80, 3.16, 3.43, 4.00
6^+	2.48, 3.18, 4.00	2.29, 3.16, 4.00
7^+	4.01	3.98
8^+	3.20	3.18
10^+	3.22	3.21
12^+	3.24	3.23
3^-	3.69	3.63
4^-	2.14, 3.90	2.11, 3.84
5^-	2.13, 2.37	2.09, 2.33, 3.86
6^-	1.60, 2.16, 2.50, 3.94	1.58, 2.14, 2.48, 3.92
7^-	1.50, 2.12, 2.48, 3.90	1.44, 2.10, 2.46, 3.89
8^-	2.16, 2.49, 3.96	2.13, 2.48, 3.94
9^-	1.95, 3.93	1.84, 3.92
10^-	3.94	3.92

Fig. 6-5. The two-hole spectrum of Pb^{206}. Spectra are presented for calculations with both harmonic oscillator (HO) and Woods-Saxon (WS) wavefunctions. For each spin the columns are:

1) experimental spectrum
2) unperturbed spectrum
3) theory, HO, $\hbar\omega$ = 6.0 MeV, ϵ = -200 MeV
4) theory, HO, $\hbar\omega$ = 8.0 MeV, ϵ = -200 MeV
5) theory, WS, ϵ = -200 MeV.

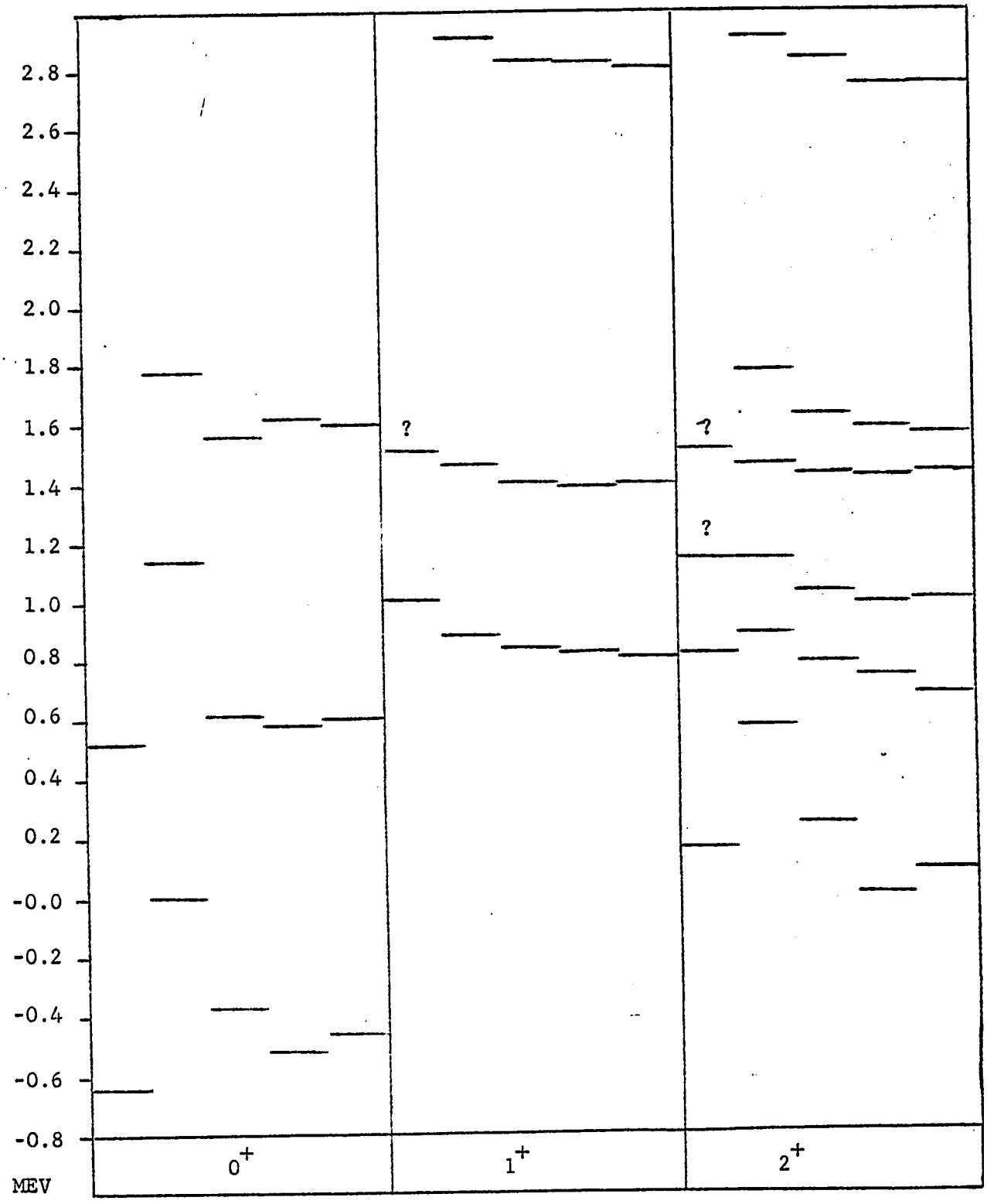
2.8
2.6
2.4
2.2
2.0
1.8
1.6
1.4
1.2
1.0
0.8
0.6
0.4
0.2
-0.0
-0.2
-0.4
-0.6
-0.8
MEV
?
?
?
0+
1+
2+

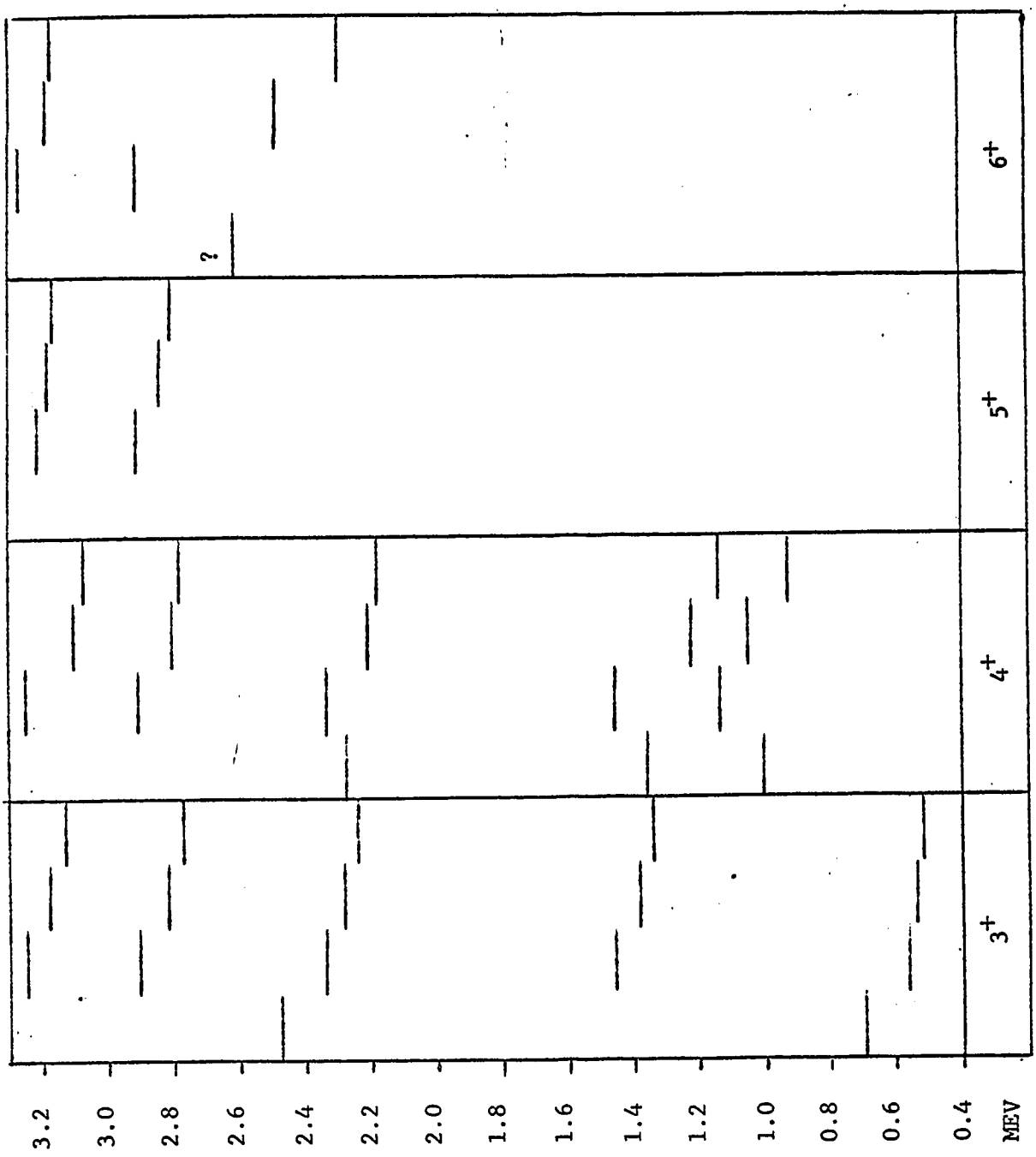
6+
5+
4+
3+
?
3.2
3.0
2.8
2.6
2.4
2.2
2.0
1.8
1.6
1.4
1.2
1.0
0.8
0.6
0.4
MEV

With $\hbar\omega$ = 8.0 MeV the n=n'=0 radial integral of $^1S_0$ is larger than its value when $\hbar\omega$ = 6.0 MeV. However, for increasing (n,n') the radial integrals for $\hbar\omega$ = 8.0 decrease more rapidly than those for $\hbar\omega$ = 6.0 MeV. The result is that for higher values of (n,n') the radial integrals are more attractive with $\hbar\omega$ = 6.0 MeV. For J=0 only the $^1S_0$, $^1D_2$ and $^3P_1$ components of the interaction contribute to the matrix elements. For diagonal matrix elements the $^1S_0$ and $^1D_2$ terms are attractive while the $^3P_1$ term is repulsive. The degree of cancellation is shown in Table 6.11 by the values of the matrix elements with and without the $^3P_1$ interaction. The degree of cancellation is dependent on the value of ϵ. Increasing the value of ϵ makes the $^1S_0$ interaction more attractive and the $^3P_1$ interaction less repulsive. Although the matrix elements do not exhibit a uniform behaviour as a function of $\hbar\omega$ it can be seen from Fig. 6.5 that the overall effect is to increase the binding energies of the levels when $\hbar\omega$ is increased.

The calculated spectrum of negative parity states is compared with experiment in Fig. 6.6. The overall agreement with experiment for both positive and negative parity states is not good. The results given here are very similar to those obtained by Clement and Baranger[124] with the Tabakin potential. It is interesting to note that for the 1^+, 3^+, 6^+ and 6^- states the experimental positions of the levels are above the unperturbed energy of the dominant configuration. Except for the 0^+ and 3^- states the calculated positions of the levels are below the experimental positions. The

Table 6.11

Diagonal J=0 matrix elements calculated with HO wavefunctions for $\hbar\omega$ = 8.0 MeV and ϵ = -80.0 MeV.

Configuration	$^1S_0+^1D_2$	$^1S_0+^1D_2+^3P_1$
$(h_{9/2})^2$	-0.930 (MeV)	-0.215 (MeV)
$(i_{13/2})^2$	-0.934	-0.305
$(f_{5/2})^2$	-0.619	-0.229
$(f_{7/2})^2$	-0.826	-0.533
$(p_{1/2})^2$	-0.359	-0.086
$(p_{3/2})^2$	-0.718	-0.581

discrepancy between theory and experiment for the 3^- state is so large that the 3^- state must arise from configurations other than those of two-holes. Wavefunctions for several of the low-lying levels are given in Table 6.12 from which it can be seen that, in general there is little configuration mixing in the low-lying levels.

A few low-lying states were calculated using WS wavefunctions. The results are given in Table 6.13 and compared with experiment in Fig. 6.5. The only appreciable change in the WS calculation was to move the 0_1^+ one state upward slightly and the 2_1^+ and 2_2^+ states closer together. Wavefunctions for the 0^+ and 2^+ states from the WS calculation are given in Table 6.14. By comparing the wavefunctions in Tables 6.14 and 6.12 it can be seen that although

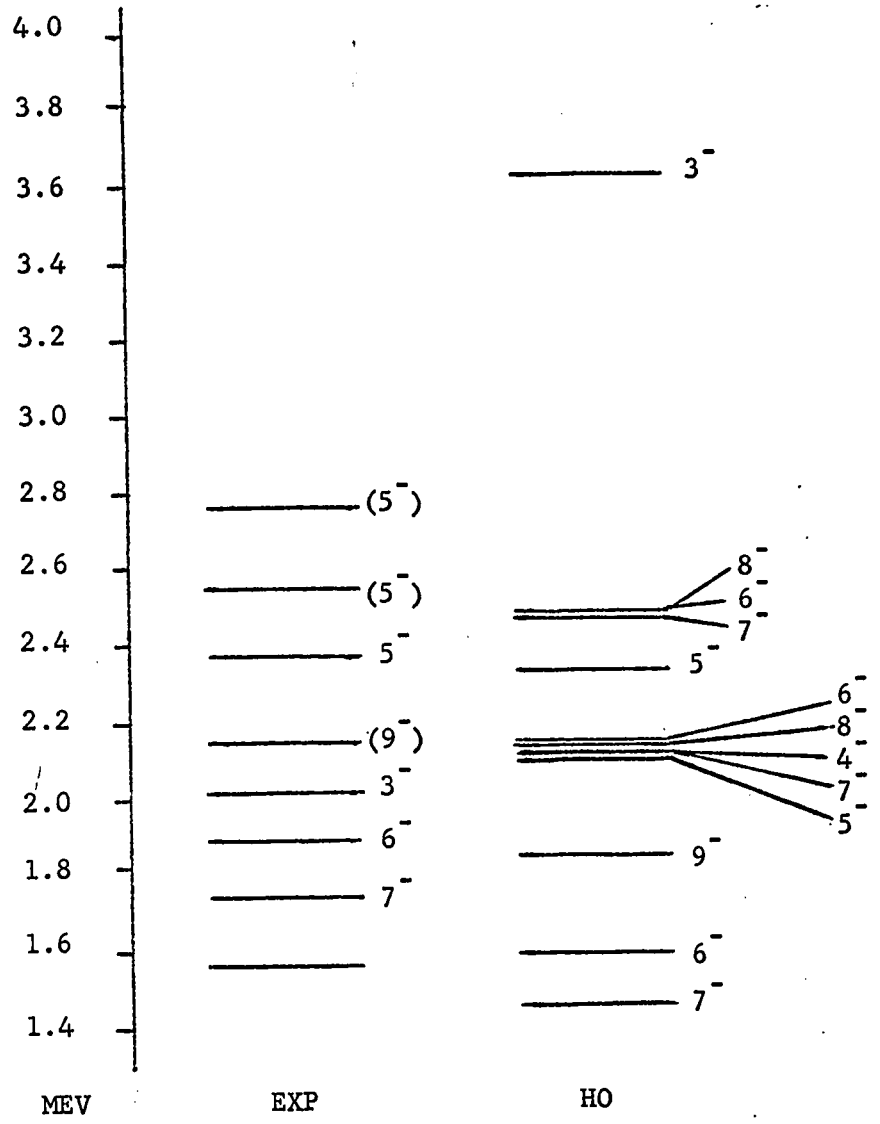

Fig. 6-6. Negative parity states in Pb^{206}. The theoretical spectrum was calculated with harmonic oscillator (HO) wavefunctions for $\hbar\omega$ = 8.0 MeV and ϵ = -200 MeV.

Table 6.12

Wavefunctions for low-lying states in Pb^{206}. The wavefunctions are for the spectrum calculated using HO wavefunctions with $\hbar\omega$ = 8.0 MeV and ϵ = -200 MeV

$J^{\pi}=0^{+}$

E_B (MeV)	$(h_{9/2})^2$	$(i_{13/2})^2$	$(f_{5/2})^2$	$(f_{7/2})^2$	$(p_{1/2})^2$	$(p_{3/2})^2$
-0.52	0.070	-0.164	0.324	0.154	0.819	0.410
0.58	-0.084	0.229	-0.815	-0.227	0.464	-0.093
1.62	-0.017	-0.022	0.274	0.045	0.332	-0.901

$J^{\pi}=1^{+}$

E_B (MeV)	$h_{9/2}f_{7/2}$	$f_{5/2}f_{7/2}$	$f_{5/2}p_{3/2}$	$p_{1/2}p_{3/2}$
0.83	-0.002	-0.001	-0.012	1.00
1.38	0.005	-0.009	1.00	0.012

$J^{\pi}=3^{+}$

E_B (MeV)	$h_{9/2}f_{5/2}$	$h_{9/2}f_{7/2}$	$h_{9/2}p_{3/2}$	$f_{5/2}f_{7/2}$	$f_{5/2}p_{1/2}$	$f_{5/2}p_{3/2}$	$f_{7/2}p_{1/2}$	$f_{7/2}p_{3/2}$
0.52	0.001	0.001	0.001	-0.009	1.00	0.005	0.008	0.015
1.34	-0.002	-0.003	-0.003	-0.016	0.005	1.00	0.017	-0.005

Table 6.12 continued

$J^{\pi}=5^{+}$

E_B (MeV)	$h_{9/2}f_{5/2}$	$h_{9/2}f_{7/2}$	$h_{9/2}p_{1/2}$	$h_{9/2}p_{3/2}$	$f_{5/2}f_{7/2}$	$f_{7/2}p_{3/2}$
2.80	0.001	-0.003	0.023	0.015	0.999	0.017

$J^{\pi}=3^{-}$

E_B (MeV)	$h_{9/2}i_{13/2}$	$i_{13/2}f_{7/2}$
3.63	-0.007	1.00

$J^{\pi}=4^{-}$

E_B (MeV)	$h_{9/2}i_{13/2}$	$i_{13/2}f_{5/2}$	$i_{13/2}f_{7/2}$
2.11	-0.005	1.00	-0.008

$J^{\pi}=5^{-}$

E_B (MeV)	$h_{9/2}i_{13/2}$	$i_{13/2}f_{5/2}$	$i_{13/2}f_{7/2}$	$i_{13/2}p_{3/2}$
2.09	0.005	0.910	0.066	0.410
2.33	-0.006	0.414	-0.063	-0.908

Table 6.12 continued

$J^{\pi}=6^-$

E_B (MeV)	$h_{9/2}i_{13/2}$	$i_{13/2}f_{5/2}$	$i_{13/2}f_{7/2}$	$i_{13/2}p_{1/2}$	$i_{13/2}p_{3/2}$
1.58	0.003	-0.055	0.005	-0.998	0.018
2.14	0.012	0.998	0.013	-0.054	0.035

$J^{\pi}=7^-$

E_B (MeV)	$h_{9/2}i_{13/2}$	$i_{13/2}f_{5/2}$	$i_{13/2}f_{7/2}$	$i_{13/2}p_{1/2}$	$i_{13/2}p_{3/2}$
1.44	-0.002	0.174	0.052	0.976	0.117
2.10	0.011	-0.969	-0.047	0.192	-0.146

$J^{\pi}=8^-$

E_B (MeV)	$h_{9/2}i_{13/2}$	$i_{13/2}f_{5/2}$	$i_{13/2}f_{7/2}$	$i_{13/2}p_{3/2}$
2.13	0.012	0.999	0.003	-0.051

$J^{\pi}=9^-$

E_B (MeV)	$h_{9/2}i_{13/2}$	$i_{13/2}f_{5/2}$	$i_{13/2}f_{7/2}$
1.84	-0.047	0.996	0.072

Table 6.12 continued

$J^{\pi}=2^{+}$

E_B (MeV)	0.00	0.54	0.99	1.42	1.58	2.75
$(h_{9/2})^2$	0.023	-0.003	-0.017	0.004	-0.008	-0.093
$(h_{9/2}f_{5/2})$	0.073	0.007	-0.046	0.032	-0.016	-0.282
$(h_{9/2}f_{7/2})$	-0.010	0.003	0.008	-0.003	0.002	0.048
$(i_{13/2})^2$	-0.088	-0.015	0.062	-0.039	0.030	0.857
$(f_{5/2})^2$	0.216	0.001	0.947	-0.107	0.104	0.133
$(f_{5/2}f_{7/2})$	-0.082	-0.028	0.082	-0.067	-0.008	0.014
$(f_{5/2}p_{1/2})$	0.698	0.637	0.216	-0.153	0.053	0.123
$(f_{5/2}p_{3/2})$	-0.161	-0.023	0.042	0.970	0.020	-0.118
$(f_{7/2})^2$	0.070	0.009	-0.061	0.013	-0.016	-0.093
$(f_{7/2}p_{3/2})$	0.199	0.070	-0.077	0.085	-0.076	-0.331
$(p_{1/2}p_{3/2})$	-0.586	0.751	0.176	0.075	-0.232	-0.039
$(p_{3/2})^2$	0.179	-0.153	-0.038	-0.067	-0.962	0.089

Table 6.12 continued

$J^{\pi}=4^{+}$			
E_B (MeV)	0.93	1.16	2.18
$(h_{9/2})^2$	0.017	-0.002	-0.019
$(h_{9/2}f_{5/2})$	0.046	-0.012	-0.017
$(h_{9/2}f_{7/2})$	-0.014	0.003	0.021
$(h_{9/2}p_{1/2})$	0.055	-0.011	-0.038
$(h_{9/2}p_{3/2})$	-0.025	0.003	0.015
$(i_{13/2})^2$	-0.074	0.010	0.044
$(f_{5/2})^2$	0.598	0.784	0.126
$(f_{5/2}f_{7/2})$	-0.149	0.018	-0.058
$(f_{5/2}p_{3/2})$	-0.699	0.609	-0.310
$(f_{7/2})^2$	0.061	0.006	-0.041
$(f_{7/2}p_{1/2})$	0.302	-0.093	-0.935
$(f_{7/2}p_{3/2})$	0.158	-0.068	-0.057

Table 6.13

Two-hole states in Pb^{206} with $E_B < 4.0$ MeV calculated using WS wavefunctions for $\epsilon = -200$ MeV.

J^π	Eigenvalues (MeV)
0^+	-0.46, 0.60, 1.60, 2.73
1^+	0.81, 1.39, 2.81
2^+	0.08, 0.48, 1.00, 1.43, 1.56, 2.75, 2.80, 3.04, 3.80
3^+	0.53, 1.34, 2.22, 2.77, 3.12, 3.77
3^-	3.66
4^-	2.11, 3.82
5^-	2.12, 2.34, 3.87

Table 6.14

Wavefunctions for low-lying states in Pb^{206}. The wavefunctions are for the spectrum calculated using WS wavefunctions and $\epsilon = -200$ MeV.

Table 6.14 continued

$J^\pi=2^+$						
E_B (MeV)	0.08	0.48	1.00	1.43	1.56	2.75
$(h_{9/2})^2$	0.015	-0.002	-0.016	0.001	-0.006	-0.016
$(h_{9/2}f_{5/2})$	0.054	0.011	-0.045	0.024	-0.010	-0.272
$(h_{9/2}f_{7/2})$	-0.004	0.005	0.009	0.002	-0.002	0.036
$(i_{13/2})^2$	-0.061	-0.018	0.057	-0.023	0.022	0.931
$(f_{5/2})^2$	0.197	0.033	-0.957	-0.082	0.093	0.102
$(f_{5/2}f_{7/2})$	-0.078	-0.031	0.081	-0.078	0.003	0.068
$(f_{5/2}p_{1/2})$	0.687	0.658	0.206	-0.141	0.045	0.076
$(f_{5/2}p_{3/2})$	-0.142	-0.039	0.041	-0.958	0.172	-0.075
$(f_{7/2})^2$	0.058	0.012	-0.062	0.006	-0.015	-0.052
$(f_{7/2}p_{3/2})$	0.174	0.089	-0.061	0.079	-0.089	-0.124
$(p_{1/2}p_{3/2})$	-0.624	0.722	-0.136	0.015	-0.264	-0.020
$(p_{3/2})^2$	0.182	-0.184	-0.031	-0.204	-0.939	0.044

$J^\pi=0^+$			
E_B (MeV)	-0.46	0.60	1.60
$(h_{9/2})^2$	0.046	-0.073	-0.010
$(i_{13/2})^2$	-0.107	0.207	-0.032
$(f_{5/2})^2$	0.267	-0.869	0.205
$(f_{7/2})^2$	0.124	-0.237	0.040
$(p_{1/2})^2$	0.852	0.369	0.369
$(f_{3/2})^2$	0.417	-0.064	-0.905

the binding energies of a state may be nearly the same in both the HO and WS calculations the wavefunction does change appreciably. An example of this is the 0_2^+ state.

5-G Results for Pb^{210}

Calculations of the two-particle spectrum of Pb^{210} were performed using HO wavefunctions with $\hbar\omega$ = 6.0 MeV and $\hbar\omega$ = 8.0 MeV. The results are given in Table 6.15. The states most affected by increasing $\hbar\omega$ from 6.0 to 8.0 MeV are the 0^+, 2^+, 10^+ and 13^- states. It is these states which are initially shifted furthest from their unperturbed positions. As in Pb^{206} the difference in energy between the unperturbed and perturbed positions of a given configuration are not large. As a result a change of 0.1 MeV in the position of a level is significant. In Fig. 6.7 the levels arising from the $(g_{9/2})^2$ and $(g_{9/2},i_{13/2})$ configurations are shown relative to the positions of the unperturbed configurations. Except for the 0_1^+, 2_1^+ and 10_1^+ levels the shifts are less than 0.2 MeV.

In Pb^{210} the matrix elements depend on the relative strengths of the singlet-even and triplet-odd interactions in the same way as the Pb^{206} matrix elements. Decreasing the value of ϵ lessens the cancellation between the $^1S_0$ and $^3P_1$ interactions and gives a more attractive interaction. The spectra calculated with HO wavefunctions for ϵ = -80 MeV and ϵ = -200 MeV are compared with experiment in Fig. 6.8. Wavefunctions for a few of the low-lying states are given in Table 6.16.

Table 6.15

Two-particle spectra of Pb^{210} below E_B = 2.5 MeV calculated using HO wavefunctions for ϵ = -200 MeV

J^π	Eigenvalues (MeV) $\hbar\omega$ = 6.0 MeV	Eigenvalues (MeV) $\hbar\omega$ = 8.0 MeV
0^+	-0.68, 0.91	-0.76, 0.90
1^+	0.68, 2.41	0.66, 2.42
2^+	-0.24, 0.77, 1.15, 1.46, 2.42	-0.34, 0.74, 1.02, 1.38, 2.37, 2.47
3^+	0.70, 1.51, 2.32, 2.40, 2.45	0.65, 1.46, 2.78, 2.36, 2.43
4^+	-0.11, 0.78, 1.37, 1.54, 1.91, 2.34, 2.44, 2.47	-0.15, 0.76, 1.29, 1.52, 1.86, 2.32, 2.41, 2.45
5^+	0.72, 1.56, 2.00, 2.34, 2.42, 2.48	0.68, 1.54, 1.99, 2.31, 2.39, 2.45
6^+	-0.06, 0.76, 1.46, 1.56 2.25, 2.36, 2.40	-0.09, 0.74, 1.41, 1.55, 2.17, 2.33, 2.38
7^+	0.73, 1.54, 2.34, 2.43	0.69, 1.53, 2.32, 2.40
8^+	-0.04, 0.71, 1.55, 2.08, 2.29	-0.06, 0.68, 1.54, 1.96, 2.26
9^+	0.74	0.70
10^+	0.56, 1.57	0.47, 1.58
12^+	2.79	2.79
14^+	2.80	2.80
2^-	2.03	2.00
3^-	1.17, 2.10	1.14, 2.04
4^-	1.32, 2.09	1.25, 2.05
5^-	1.32, 2.16	1.31, 2.14
6^-	1.38, 2.10	1.35, 2.06
7^-	1.34, 2.15	1.32, 2.13
8^-	1.39, 2.12	1.38, 2.07
9^-	1.36, 2.11	1.34, 2.08
10^-	1.40, 2.13	1.39, 2.08
11^-	1.37, 2.03	1.36, 1.97
12^-	1.38, 2.14	1.36, 2.09
13^-	1.71	1.47

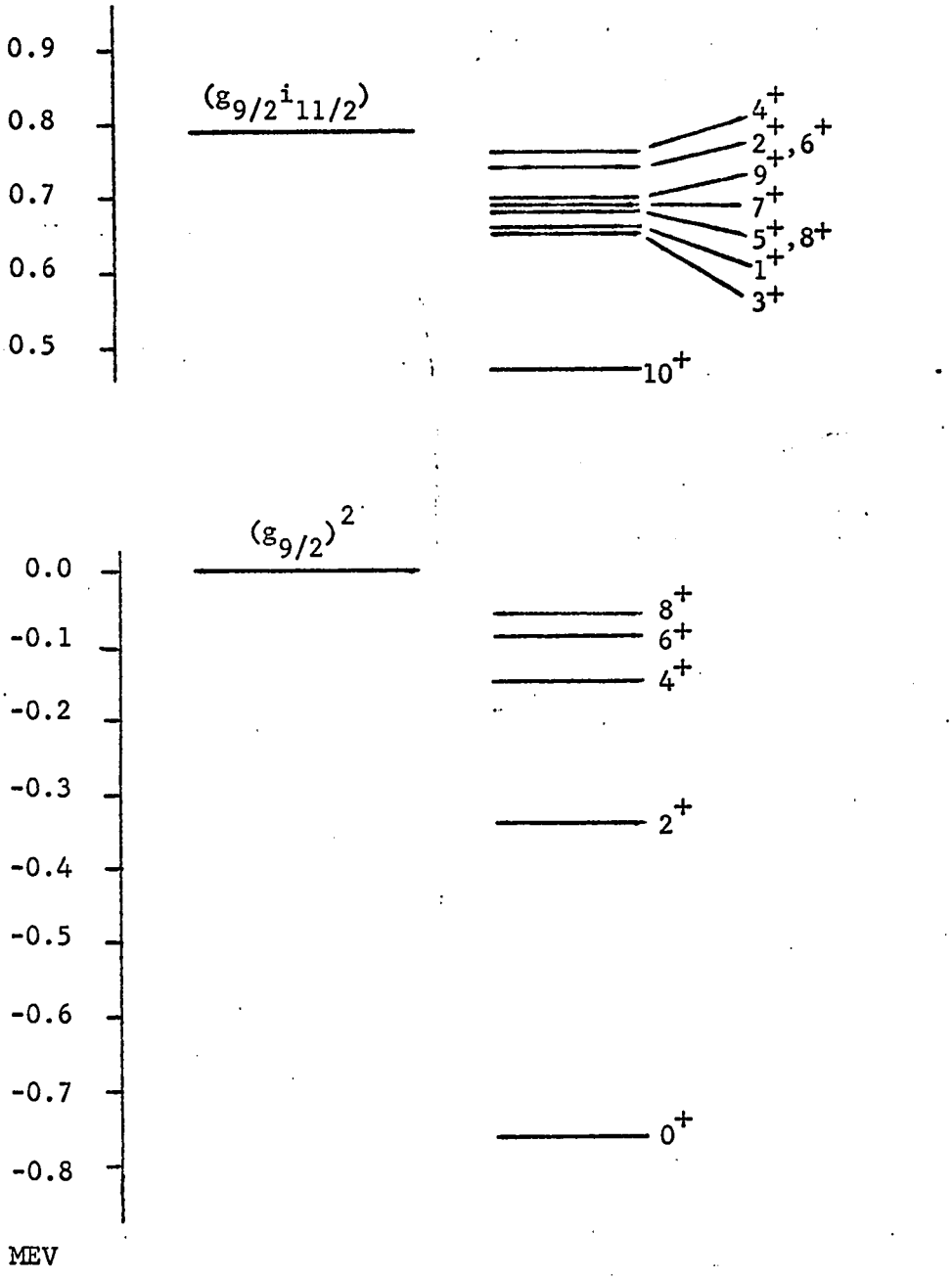

Fig. 6-7. Low-lying states in Pb^{210} relative to their unperturbed positions. The theoretical spectrum was calculated with harmonic oscillator wavefunctions for $\hbar\omega$ = 8.0 MeV and ϵ = -200 MeV.

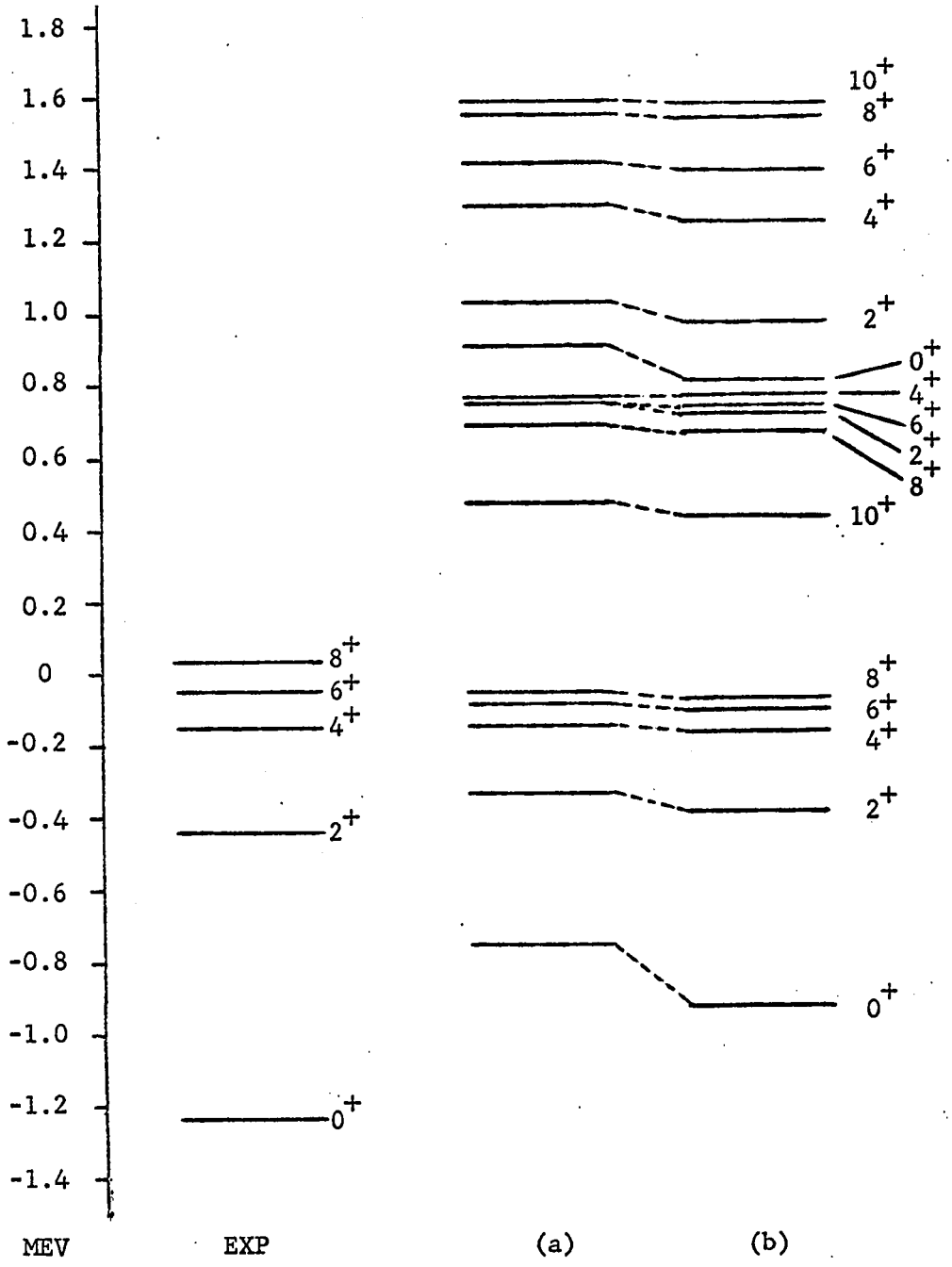

Fig. 6-8. The low-lying two-particle states in Pb^{210} calculated with harmonic oscillator wavefunctions. The theoretical spectra are for (a) $\hbar\omega$ = 8.0 MeV, ϵ = -200 MeV and (b) $\hbar\omega$ = 8.0 MeV, ϵ = -80 MeV.

Table 6.16

Wavefunctions for low-lying two-particle states in Pb^{210}. The wavefunctions are for the spectrum calculated with HO wavefunctions, $\hbar\omega$ = 8.0 MeV and ϵ = -200 MeV.

$J^{\pi}=0^{+}$

E_B (MeV)	$(i_{11/2})^2$	$(j_{15/2})^2$	$(g_{7/2})^2$	$(g_{9/2})^2$	$(d_{3/2})^2$	$(d_{5/2})^2$	$(s_{1/2})^2$
-0.76	0.324	-0.208	0.182	0.892	0.078	0.116	0.053
0.90	-0.745	0.520	0.010	0.406	-0.026	-0.092	-0.031
2.60	-0.180	0.011	0.100	-0.107	0.265	0.908	0.226

$J^{\pi}=8^{+}$

E_B (MeV)	$(i_{11/2})^2$	$i_{11/2}g_{7/2}$	$i_{11/2}g_{9/2}$	$i_{11/2}d_{3/2}(j_{15/2})^2$	$g_{7/2}g_{9/2}$	$(g_{9/2})^2$
-0.06	0.020	0.006	-0.014	-0.037	-0.012	-0.098	0.994
0.68	0.000	-0.034	0.993	0.090	0.029	0.061	0.024
1.54	-0.984	-0.013	-0.013	-0.004	0.087	0.153	0.035

$J^{\pi}=10^{+}$

E_B (MeV)	$(i_{11/2})^2$	$i_{11/2}g_{9/2}$	$(j_{15/2})^2$
0.47	0.013	0.999	0.030
1.58	0.998	-0.012	-0.058

Table 6.16 continued

$J^{\pi}=2^{+}$

E_B (MeV)	-0.34	0.74	1.02	1.38	2.37
$(i_{11/2})^2$	0.096	0.070	-0.516	0.796	-0.204
$(i_{11/2}g_{7/2})$	0.053	0.073	-0.095	-0.016	0.284
$(i_{11/2}g_{9/2})$	-0.024	-0.955	-0.273	-0.062	0.082
$(j_{15/2})^2$	-0.072	-0.085	0.161	-0.205	-0.371
$(g_{7/2})^2$	0.056	0.022	-0.053	-0.013	0.082
$(g_{7/2}g_{9/2})$	-0.011	-0.054	0.024	-0.074	-0.817
$(g_{7/2}d_{3/2})$	0.054	0.034	-0.109	-0.073	0.090
$(g_{7/2}d_{5/2})$	-0.020	-0.014	0.042	0.030	-0.087
$(g_{9/2})^2$	0.971	-0.088	0.207	0.007	-0.037
$(g_{9/2}d_{5/2})$	0.163	0.232	-0.735	-0.553	-0.103
$(d_{3/2})^2$	0.021	0.012	-0.034	-0.012	0.040
$(d_{3/2}d_{5/2})$	-0.018	-0.020	0.036	0.004	-0.053
$(d_{3/2}s_{1/2})$	-0.030	-0.018	0.052	0.022	-0.075
$(d_{5/2})^2$	0.044	0.031	-0.102	-0.046	0.112
$(d_{5/2}s_{1/2})$	0.041	0.037	-0.094	-0.030	0.093

Table 6.16 continued

$J^{\pi}=4^{+}$

E_B (MeV)	0.15	0.78	1.29	1.52	1.86
$(i_{11/2})^2$	0.050	0.029	-0.488	-0.839	0.152
$(i_{11/2}g_{7/2})$	0.020	0.033	-0.056	-0.003	-0.035
$(i_{11/2}g_{9/2})$	-0.025	-0.987	-0.130	0.021	-0.046
$(i_{11/2}d_{3/2})$	0.036	0.047	-0.046	0.008	-0.035
$(i_{11/2}d_{5/2})$	-0.022	-0.027	0.029	-0.020	0.062
$(j_{15/2})^2$	-0.031	-0.041	0.119	0.110	0.011
$(g_{7/2})^2$	0.030	0.008	-0.036	0.008	-0.019
$(g_{7/2}g_{9/2})$	-0.041	-0.037	0.059	0.022	-0.025
$(g_{7/2}d_{3/2})$	0.020	0.011	-0.061	0.025	-0.039
$(g_{7/2}d_{5/2})$	-0.018	-0.012	0.073	-0.035	0.031
$(g_{7/2}s_{1/2})$	-0.017	-0.013	0.078	-0.037	0.063
$(g_{9/2})^2$	0.988	-0.047	0.124	0.000	0.040
$(g_{9/2}d_{3/2})$	0.038	0.043	-0.117	0.001	-0.107
$(g_{9/2}d_{5/2})$	0.077	0.086	-0.756	0.526	0.334
$(g_{9/2}s_{1/2})$	0.068	0.071	-0.309	0.045	-0.912
$(d_{3/2}d_{5/2})$	-0.029	-0.021	0.072	-0.011	0.059
$(d_{5/2})^2$	0.019	0.011	-0.059	0.012	-0.040

Table 6.16 (continued)

$J^{\pi}=6^{+}$

E_B (MeV)	-0.09	0.74	1.41	1.55	2.17
$(i_{11/2})^2$	0.031	-0.014	0.480	0.860	-0.120
$(i_{11/2}g_{7/2})$	0.011	-0.033	0.030	0.004	0.052
$(i_{11/2}g_{9/2})$	-0.022	0.992	0.080	-0.014	0.084
$(i_{11/2}d_{3/2})$	0.017	-0.030	0.021	-0.004	0.071
$(i_{11/2}d_{5/2})$	-0.025	0.040	-0.028	0.026	0.468
$(i_{11/2}s_{1/2})$	-0.030	0.045	-0.037	0.020	-0.172
$(j_{15/2})^2$	-0.018	0.032	-0.085	-0.080	-0.110
$(g_{7/2})^2$	0.019	-0.005	0.024	-0.004	0.047
$(g_{7/2}g_{9/2})$	-0.056	0.041	-0.105	-0.012	-0.369
$(g_{7/2}d_{5/2})$	-0.022	0.020	-0.120	0.048	-0.162
$(g_{9/2})^2$	0.993	0.035	-0.079	-0.003	-0.073
$(g_{9/2}d_{3/2})$	0.062	-0.061	0.219	-0.010	0.694
$(g_{9/2}d_{5/2})$	0.047	-0.052	0.820	-0.501	-0.242

A few of the low-lying states were determined using WS wavefunctions and ϵ = -200 MeV. The calculated energies are given in Table 6.17. Comparing Tables 6.17 and 6.15 it can be seen that the energy shifts resulting from the use of WS wavefunctions are significant. The binding energy of the ground state is decreased by 0.21 MeV relative to its value in the HO calculation with $\hbar\omega$ = 8.0 MeV. In Pb^{209} the WS wavefunction for the $1g_{9/2}$ state is too a good approximation a HO wavefunction for $\hbar\omega$ = 8.0 MeV. The 2_1^+, 4_1^+, 6_1^+ and 8_1^+ states are predominantly $(g_{9/2})^2$ states and are quite near their unperturbed position. As a result one would expect that these levels would not be affected by the use of WS wavefunctions. On the other hand the 2_3^+ state is predominantly $(i_{11/2})^2$ and $(g_{9/2}\ d_{5/2})$ with equal amplitudes. The $0i_{11/2}$, $1g_{9/2}$ and $2d_{5/2}$ states are not well represented by HO wavefunctions with $\hbar\omega$ = 8.0 MeV. In the WS calculation the 2_3^+ state is shifted by 0.12 MeV. Two-particle wavefunctions for the 0^+ states calculated with WS wavefunctions are given in Table 6.18. In the WS calculation there is less configuration mixing in the 0^+ states.

5-H Summary

The two-particle spectra of A=18 nuclei were calculated using the free reaction matrix as an effective interaction. For the A=18 nuclei the nuclear reaction matrix elements had been determined by Lee. The values of the nuclear reaction matrix elements evaluated with harmonic oscillator and plane wave intermediate states

Table 6.17

Two-particle states in Pb^{210} below E_B = 2.5 MeV calculated using WS wavefunctions for ϵ = -200 MeV.

J^π	Eigenvalues (MeV)
0^+	-0.55, 0.98
1^+	0.72, 2.36
2^+	-0.30, 0.79, 1.14, 1.36, 2.36, 2.49
2^-	2.00
3^-	1.16, 2.03
4^-	1.22, 2.05

Table 6.18

Wavefunctions for the 0^+ states calculated with WS wavefunctions and ϵ = -200 MeV.

$J^\pi = 0^+$

E_B	$(i_{11/2})^2$	$(j_{15/2})^2$	$(g_{7/2})^2$	$(g_{9/2})^2$	$(d_{3/2})^2$	$(d_{5/2})^2$	$(s_{1/2})^2$
-0.55	0.235	-0.129	0.171	0.943	0.051	0.078	0.032
0.98	-0.790	0.545	0.008	0.275	-0.007	-0.051	-0.010
2.71	-0.083	0.016	0.075	-0.086	0.223	0.952	0.154

are reproduced by $K_F(\epsilon)$ with ϵ = -80.0 and ϵ = -200 MeV respectively. The matrix elements for ϵ = -80 MeV are considerably stronger than those for ϵ = -200 MeV. There are large differences between the spectra for the two values of ϵ. The correct choice of intermediate states for evaluating reaction matrix elements is not firmly established. Clearly this question needs to be resolved. The A=18 spectra were calculated using WS single-particle wavefunctions. The use of WS matrix elements introduced a pronounced state dependence of the matrix elements. The changes in the spectra introduced by WS wavefunctions are as large as those introduced by corrections arising from core polarization.[4,125-127]

Nuclear reaction matrix elements have not been determined for A=42 nuclei or the Pb region for the interaction used here. Calculations of the A=42 and Pb^{210} two-particle spectra and the two-hole spectrum of Pb^{206} were carried out using $K_F(\epsilon)$ with ϵ = -80 MeV and ϵ = -200 MeV as effective interactions. This arbitrary choice of ϵ did not permit a detailed comparison with experiment. However, the interaction is reasonable and the general effects of nuclear size and WS wavefunctions on effective interaction matrix elements for these nuclei were studied. In Ca^{42} it was found that WS wavefunctions altered the spectrum only slightly while in Sc^{42} the modifications were significant. For Pb^{206} and Pb^{210} it was found that the spectra are sensitive to the choice of Woods-Saxon potential used to fit the single-particle spectra. In the Pb region the effective interaction is very dependent on the relative

strength of the singlet-even and triplet-odd components of the force. Clement and Baranger[124] found that the Tabakin potential had the same behaviour. Using a phenomenological interaction True[118] obtained a better fit to the Pb^{206} spectrum by omitting the triplet-odd interaction. In Pb^{206} it was found that WS wavefunctions did not alter the spectrum except for a few levels. In Pb^{210} WS wavefunctions introduce significant modifications of the two-particle spectrum.

CHAPTER 7

SUMMARY AND CONCLUSIONS

In Chapter 2 Green's functions were used to define the effective shell model Hamiltonians for two-particle, two-hole and particle-hole states. In each case the effective interaction is a nuclear reaction matrix defined self-consistently by the energies of the states under consideration. The nuclear reaction matrices $K(\omega)$ can be evaluated from an expansion in terms of a free reaction matrix $K_F(\epsilon)$ which is determined from the free nucleon-nucleon scattering data. In lowest order the nuclear reaction matrix is the free reaction matrix. The higher order terms correct for the fact that $K_F(\epsilon)$ is determined by nucleons scattering in bound states. From a complete evaluation of $K(\omega)$ one obtains a numerical array of matrix elements. For many shell model calculations it is useful to have an analytic form for $K(\omega)$. By an appropriate state independent choice of ϵ one can hopefully reproduce the array with the simpler free reaction matrix. We have presented a series of calculations of two-particle, two-hole and particle-hole spectra for which $K_F(\epsilon)$ was used as the effective interaction. In general $K_F(\epsilon)$ is non-local. Calculations were performed with both a local but velocity dependent representation of K_F and a K_F determined from a non-local separable potential. For A=18 nuclei the nuclear reaction matrix had been determined for the non-local separable potential. Accordingly the value of ϵ to use in K_F was known for that case. In all other

calculations ϵ was chosen arbitrarily so that the effective interaction matrix elements were reasonable. Our objective was to study model dependence of the nuclear reaction matrix elements; consequently it was sufficient to have reasonable matrix elements.

In Chapter 3 we presented a calculation of the particle-hole states in O^{16}. The local but velocity dependent representation of K_F for only the relative S states was used as the effective interaction. The particle-hole states were constructed in both the Tamm-Dancoff and random phase approximations. The theoretical spectrum was in reasonable agreement with experiment. The positions of the levels that are correctly predicted by the particle-hole model are mainly determined by the unperturbed energies of the dominant configurations. These particle-hole states are fairly insensitive to the structure of the interaction. On the other hand, the collective octupole and giant dipole states are very sensitive to both the interaction and the model used. Only the collective octupole state is sensitive to the higher energy components in K_F. This sensitivity is not unique since the ocutpole state is sensitive to all aspects of the interaction and model.

The modifications of nuclear reaction matrix elements arising from the use of single-particle wavefunctions for a finite single-particle potential with a diffuse surface were studied. To obtain the single-particle wavefunctions a Woods-Saxon potential with a Thomas spin-orbit term was fitted to the experimental single-particle energies for each nucleus considered. The nuclear size is an important

quantity in a determination of nuclear reaction matrix elements. The radii of the Woods-Saxon potentials were determind by requiring the Coulomb displacement energies to be correctly predicted. In the case of Pb, which has a neutron excess, the well radius was fixed by requiring that the wavefunctions predict the observed r.m.s. radius of the charge distribution. When fitting Woods-Saxon potentials to the single-particle states in the Pb region new results were obtained. For the neutron states in Pb it was found that the single-particle energies and the Coulomb displacement energies could not be fitted simultaneously. By using different well depths and spin-orbit strengths for sets of states belonging to different oscillator shells it was possible to obtain a good fit to the experimental data. The proton well did not have the energy dependence required to fit the neutron states. For the proton states it was found that a potential well radius 10% larger than the neutron well radius was required to fit the r.m.s. radius of the charge distribution. The wavefunctions for the proton and neutron wells predict r.m.s. matter radii consistent with the proton and neutron matter radii being nearly identical. The fact that the neutron and proton wells must have different radii to be consistent with the experimental data leads to ambiguities. By fitting the proton-hole and neutron-hole energies with single-particle potentials it was assumed that the Hamiltonian for the Pb^{208} ground state could be written as the sum of a proton single-particle potential and a neutron single-particle potential. The fact that the proton and neutron wells of different radii were required to

fit the data implies that in the absence of the Coulomb interaction the total Hamiltonian does not conserve isospin. Since the nuclear part of the Hamiltonian must conserve isospin an additional term coupling the neutrons and protons must be added to the Hamiltonian so that isospin is conserved. To regain isospin conservation neutron-proton correlations need to be introduced in the ground state. This point requires further investigation.

In Chapter 4 proton and neutron Woods-Saxon wavefunctions for A=15, 17, 39, 41, 207 and 209 nuclei are tabulated as expansions in terms of harmonic oscillator wavefunctions. The expansion of the Woods-Saxon wavefunctions in terms of oscillator wavefunctions is useful for shell model calculations since the mathematical properties of the harmonic oscillator wavefunctions are used to evaluate matrix elements the computational time is greatly increased. In Appendix B results are obtained which can be used to decrease the computational time. New recurrence relations for the Talmi coefficients and relations among radial integrals evaluated with harmonic oscillator wavefunctions are derived. One also obtains in this fashion a simple method for calculating the radial integrals required in calculating electromagnetic moments. With these methods any desired integral of r^L with Woods-Saxon wavefunctions can be obtained from the expansions in terms of harmonic oscillator wavefunctions. The necessary formulae for L = 1,2 and 3 are given in Table B-1.

It was found that the Woods-Saxon wavefunctions deviate from harmonic oscillator wavefunctions in three main respects, which can

be conveniently expressed in terms of the value of $\hbar\omega$ required to maximize the overlap of a Woods-Saxon wavefunction with the main oscillator component. For a set of states belonging to the same oscillator shell the values of $\hbar\omega$ are state dependent. For states with small values of orbital angular momentum and small binding energies the Woods-Saxon wavefunctions have a much greater extension beyond the potential well than harmonic oscillator wavefunctions. For these states even the state dependent $\hbar\omega$ gives a poor overlap of the Woods-Saxon and harmonic oscillator wavefunctions. These characteristics are exhibited by the single-particle states in A=17, 41, and 209 nuclei. In addition to the state dependence for states within an oscillator shell there is a state dependence for states belonging to different oscillator shells. In A=15 and A=39 nuclei the average value of $\hbar\omega$ for the hole states is larger than for the particle states in the A=17 and A=41 nuclei respectively. In the Pb region the state dependence of $\hbar\omega$ within a shell is as great as that between shells.

In Chapter 5 we presented calculations of the A=14,18 and 38 spectra using Woods-Saxon wavefunctions. The local velocity dependent free reaction matrices with only relative S state components included were used as the effective interactions. The Woods-Saxon calculations of the A=14 and A=18 spectra were compared with calculations using harmonic oscillator wavefunctions for an $\hbar\omega$ value averaged over the p and (s,d) shells, For the (s,d) shell matrix elements were decreased considerably whereas the p shell matrix

elements were increased. The Woods-Saxon wavefunctions for the hole states can be well represented by harmonic oscillator wavefunctions with an appropriate value of $\hbar\omega$. As a result the two-hole spectrum calculated with Woods-Saxon wavefunctions can be reproduced by using harmonic oscillator wavefunctions with the appropriate value of $\hbar\omega$. For the A=18 spectra the state dependence of the Woods-Saxon calculation cannot be reproduced by a harmonic oscillator calculation. The Ca^{38} two-hole spectrum was calculated using Woods-Saxon wavefunctions. Since the hole states are deeply bound the Woods-Saxon wavefunctions are well represented by harmonic oscillator wavefunctions. The Woods-Saxon calculation differed only slightly from the harmonic oscillator calculation.

In the calculation of the O^{18} spectrum with Woods-Saxon wavefunctions it was found that the 0_2^+ state was shifted upwards relative to the other states. This shift makes the description of this state as a mixture of spherical shell model and deformed components more consistent. The state dependence of the matrix elements involving configurations from both the p and (s,d) shells indicate that core excitation matrix elements will be significantly affected by using Woods-Saxon wavefunctions. The calculations presented show that single-particle wavefunctions for a finite single-particle potential must be used if a detailed comparison of experiment and theory is to be made.

In Chapter 6 the recently developed $K_F(\epsilon)$, which was obtained from a non-local separable potential, was used as the shell model effective interaction. The spectra of O^{18}, F^{18}, Ca^{42}, Sc^{42}, Pb^{206}

and Pb^{210} were calculated using both harmonic oscillator and Woods-Saxon wavefunctions. The O^{18} and F^{18} spectra were calculated using harmonic oscillator wavefunctions and for ϵ = -200 MeV and ϵ = -80 MeV. These two values of ϵ give matrix elements corresponding to nuclear reaction matrix elements evaluated using plane wave and harmonic oscillator intermediate states. The two sets of matrix elements give significantly different spectra. The question of which method gives the best matrix elements needs to be answered. The O and F^{18} spectra were also calculated using Woods-Saxon wavefunctions. The use of Woods-Saxon wavefunctions introduce changes in the spectra which are as large as those arising from the inclusion of core excitation effects. In Ca^{42} and Sc^{42} the effect of using Woods-Saxon wavefunctions was studied. It was found that for Ca^{42} there were only minor changes in the spectrum whereas for the T=0 states in Sc^{42} the changes were significant.

In the calculations of the Pb^{206} and Pb^{210} spectra the effects of nuclear size and Woods-Saxon wavefunctions were studied. The spectra were calculated using harmonic oscillator wavefunctions for $\hbar\omega$ = 8.0 MeV. These two oscillator potentials corresponds respectively to the Woods-Saxon potentials obtained by Rost[82] and the one obtained in Chapter 4. The two values of $\hbar\omega$ give significantly different spectra. This means that knowledge of the r.m.s. radius of the neutron distributions in Pb is important for the correct determination of nuclear reaction matrix elements. Only a few low-lying states in Pb^{206} and Pb^{210} were calculated with Woods-Saxon wavefunctions.

In Pb^{210} the use of Woods-Saxon wavefunctions produced significant changes in the energies of low-lying states. In the Pb region there is a significant cancellation between the $^1S_0$ and $^3P_1$ components of the interaction. In a determination of the nuclear reaction matrix elements for this region it will be important that both the $^1S_0$ and $^3P_1$ components are accurately determined.

APPENDIX A

SHELL MODEL MATRIX ELEMENTS

The one-particle, one-hole, two-particle, two-hole and particle-hole state vectors are defined in the j-j coupling scheme. With these definitions expressions for the matrix elements of one and two-body operators are given. The phase conventions defined here are used throughout the main text.

A-a State Vectors

The ground state of a closed shell nucleus has total angular momentum zero. We take the ground state to be the shell model vacuum denoted by $|0>$. Then, using the usual fermion creation and annihilation operators, a single-particle state is

$$|jm> = a_{jm}^{+}|0> \qquad \text{(A-1)}$$

where the coupling is

$$|jm> \equiv \sum_{s} <\ell\tfrac{1}{2}m\text{-}ss|jm> u_{\nu\ell j}(r)Y_{\ell m-s}(\theta,\varphi)\chi_{s}^{\frac{1}{2}}. \qquad \text{(A-2)}$$

A single-hole state is formed by removing a particle from the vacuum. For this we define a hole creation operator by

$$|jm>_h = b_{jm}^{+}|0> \ . \qquad \text{(A-3)}$$

The subscript on the ket indicates that the state is a hole state with quantum numbers (j,m) which was formed by removing a particle with the quantum numbers (j,-m). The kets are related by

$$|jm>_h = (-1)^{j-m}a_{j-m}|0> = (-1)^{j-m}|j,-m> . \qquad \text{(A-4)}$$

The phase factor is added so that the hole state transforms as a particle state with angular momentum (j,-m). Then isospin is used as a quantum number in the description of the states we use the notation

$$|\text{proton}> \equiv |\tfrac{1}{2}, +\tfrac{1}{2}>$$

$$|\text{neutron}> \equiv |\tfrac{1}{2}, -\tfrac{1}{2}> \quad . \tag{A-5}$$

The two-particle state of good angular momentum is

$$|(j_a j_b)JM> \equiv \sum_{m_a,m_b} < j_a j_b m_a m_b | JM > |j_a m_a> |j_b m_b> \quad . \tag{A-6a}$$

Including isospin we use the notation

$$|(j_a b_a)JM;TT_Z> = |(j_a j_b)JM>|(\tfrac{1}{2}\tfrac{1}{2})TT_Z>$$

$$= |(j_a j_b)JM> < \tfrac{1}{2}\tfrac{1}{2} t_a t_b | TT_Z > |\tfrac{1}{2}t_a> |\tfrac{1}{2}t_b> \; . \tag{A-6b}$$

The state (A-6b) is not properly antisymmetrized. Denoting the positions of the two nucleons by 1 and 2, the antisymmetrized and normalized two-particle state is

$$|(j_a j_b)JM;TT_Z>_a = \frac{1}{(2)^{\frac{1}{2}}} \frac{1}{[1+\delta(j_a,j_b)]^{\frac{1}{2}}}$$

$$\{|[j_a(1)j_b(2)]JM> + (-1)^T |[j_a(2)j_b(1)]JM>\} \; . \tag{A-7}$$

In (A-7) T+J must be odd if $j_a \equiv j_b$.

The two-hole state vector of good angular momentum is

$$|(j_a j_b)JM>_h \equiv \sum_{m_a,m_b} < j_a j_b m_a m_b | JM > |j_a m_a>_h |j_b m_b>_h \; . \tag{A-8}$$

Using (A-4), (A-8) is

$$|(j_a j_b)JM>_h = (-1)^{J-M}|(j_a j_b)J-M> \quad . \qquad (A\text{-}9)$$

The hole states defined in (A-3) and (A-8) are conjugate to the particle states (A-1) and (A-6). Isospin is included for hole states in the same way as for particle states, except that the third-component of isospin for holes is opposite to that for particles. The normalized and antisymmetrized two-hole state is the conjugate of (A-7).

The particle-hole state vector of good angular momentum is defined to be

$$|(j_p j_h)JM>_{ph} = \sum_{m_p,m_h} < j_p j_h m_p m_h|JM>|j_p m_p>|j_h m_h>_h \qquad (A\text{-}10)$$

where p and h are used to denote the particle and hole quantum numbers, respectively. In terms of particle states the particle-hole state is

$$|(j_p,j_h)JM>_{ph} = \sum_{m_p,m_h} (-1)^{j_n-m_h}< j_p j_h m_p m_h|JM> \times |j_p m_p>|j_h -m_h> \quad . \qquad (A\text{-}11)$$

For states of good isospin we have that

$$|JM;TT_Z>_{ph} = |JM>_{ph} \sum_{t_p,t_h} (-1)^{\frac{1}{2}-t_h}< \tfrac{1}{2}\tfrac{1}{2}t_p t_h|TT_Z> \times |\tfrac{1}{2}t_p>|\tfrac{1}{2}-t_h> \quad . \qquad (A\text{-}12)$$

When the vacuum has non-zero isospin, the isospin formalism is not useful for constructing shell model states.

A-b Particle-Particle Interaction Matrix Elements

In effective interaction calculations the residual interaction has a different form for T=0 and T=1 interactions. To obtain expressions for the matrix elements we assume a residual interaction of the general form

$$V^T(1,2) = \sum_i O_i V_i^T(r) \qquad \text{(A-13)}$$

where O_i designates operators in spin and relative angular momentum and $V_i^T(r)$ is the radial dependence in the relative coordinate. Using (A-7), the antisymmetrized particle-particle interaction matrix elements are

$$\begin{aligned} {}_a\langle (j_c j_d)JM;T|V^T|(j_a j_b)JM;T\rangle_a &= \\ &= \frac{[1-(-1)^{\ell+S+T}]}{[\{1+\delta(c,d)\}\{1+\delta(a,b)\}]^{\frac{1}{2}}} \langle [j_c(1)j_d(2)]JM;T|V^T(1,2)|[j_a(1)j_b(2)]JM;T\rangle \end{aligned} \qquad \text{(A-14)}$$

where ℓ is the relative angular momentum of the pair (a,b). The phase factor occurs because of antisymmetrization. Using shell model transformations and harmonic oscillator single-particle states (A-14) has the final form

$$\begin{aligned} {}_a\langle (j_c j_d)JM;T|V^T|(j_a j_b)JM;T\rangle_a &= \\ &= \frac{1}{[\{1+\delta(c,d)\}\{1+\delta(a,b)\}]^{\frac{1}{2}}} \sum_{L,L',S} \langle (j_c j_d)J|(LS)J\rangle\langle (L'S)J|(j_a j_b)J\rangle (-1)^{L+} \\ &\times \sum_{n\ell n'\ell' N\mathcal{L}} \langle n_c\ell_c, n_d\ell_d; L|n\ell, N\mathcal{L}; L\rangle\langle n'\ell', N\mathcal{L}; L'|n_a\ell_a, n_b\ell_b; L'\rangle \\ &\times (-1)^{\ell+\ell'}\{1-(-1)^{\ell+S+T)}\} \end{aligned} \qquad \text{(A-15)}$$

$$\times \sum_{\mathcal{J}}' [(2L+1)(2L'+1)]^{\frac{1}{2}} (2\mathcal{J}+1) W(L\ell JS;L\mathcal{J}) W(L\ell' JS;L'\mathcal{J}) \times \langle n(\ell S)\mathcal{J};T|V^T|n'(\ell' S)\mathcal{J};T\rangle \quad . \qquad \text{(A-15 contd)}$$

The coefficients

$$\langle (j_c j_d)J|(LS)J\rangle \equiv \langle (\ell_c \tfrac{1}{2}) j_c (\ell_d \tfrac{1}{2}) j_d;J|(\ell_c \ell_d)L(\tfrac{1}{2}\tfrac{1}{2})S;J\rangle$$

are the jj-LS transformation coefficients defined and tabulated by Kennedy and Cliff.[128] The coefficients

$$\langle n_c \ell_c, n_d \ell_d;L|n\ell, N\mathcal{L};L\rangle$$

are the Moshinsky[129] transformation brackets from laboratory to centre-of-mass coordinates of the two particles. The matrix elements

$$\langle n(\ell s)\mathcal{J};T|V^T|n'(\ell' S)\mathcal{J};T\rangle$$

are reduced matrix elements of the interaction where ℓ and ℓ' are the relative orbital angular momenta and $\mathcal{J}$ is the total relative angular momentum. Using (A-13) the reduced matrix element can be written as

$$\langle n(\ell S)\mathcal{J};T|V^T|n'(\ell' S)\mathcal{J};T\rangle = \sum_i \langle (\ell S)\mathcal{J};T|O_i|(\ell' S)\mathcal{J};T\rangle \langle n\ell \|V_i^T(r)\|n'\ell'\rangle \quad . \qquad \text{(A-16)}$$

For scalar, spin-orbit and tensor operators we have that

$$\langle (\ell S)\mathcal{J}|1|(\ell' S)\mathcal{J}\rangle = \delta_{\ell\ell'} \qquad \text{(A-17a)}$$

$$\langle (\ell S)\mathcal{J}|\underline{\ell}\cdot\underline{S}|(\ell' S)\mathcal{J}\rangle = \delta_{\ell\ell'} \; S1 \tfrac{1}{2}[\mathcal{J}(\mathcal{J}+1) - \ell(\ell+1) - 2] \qquad \text{(A-17b)}$$

$$\langle (\ell S)\mathcal{J}|S_{12}|(\ell' S)\mathcal{J}\rangle = \delta_{S1}(-1)^{1-\mathcal{J}}(24)^{\frac{1}{2}}[(2\ell+1)(2\ell'+1)]^{\frac{1}{2}} \times W(\ell S\ell' S;\mathcal{J}2)\langle \ell 0 \ell' 0|20\rangle \quad . \qquad \text{(A-17c)}$$

S_{12} is the usual tensor operator. The radial integrals are

$$\langle n\ell \|V_i^T(r)\|n'\ell'\rangle = \int_0^\infty R_{n\ell}(r) V_i^T(r) R_{n'\ell'}(r) r^2 dr \qquad \text{(A-18)}$$

where the oscillator functions are those defined in Appendix B. In effective interaction calculations the nuclear reaction matrix is usually determined separately for each relative $\mathcal{J}$ value. The various interaction terms are lebelled by $^{2S+1}\ell_{\mathcal{J}}$.

In the above expressions oscillator single-particle wavefunctions were assumed. The generalization to an arbitrary radial single-particle wavefunction expanded in terms of oscillator functions is straightforward. The expansion is

$$u_{\nu\ell j}(r) = \sum_{n=0}^{m} a_n(\nu\ell j) R_{n\ell}(r) \qquad \text{(A-19)}$$

where m is chosen so that the expansion gives a good representation of the wavefunction. Using the radial wavefunction (A-19) the particle-particle matrix element (A-15) is

$$\begin{aligned} &{}_a\langle j_c j_d)JM;T|V^T|(j_a j_b)JM;T\rangle \\ &= \sum_{LL'S} N(LL'S) \sum_{n_c n_d n_a n_b} a_{n_c}(c) a_{n_d}(d) a_{n_a}(a) a_{n_b}(b) \\ &\times \sum_{n\ell n\ell' N\mathcal{L}} \langle n_c\ell_c, n_d\ell_d; L|n\ell, N\mathcal{L}; L\rangle \langle n'\ell'; N\mathcal{L}; L'|n_a\ell_a, n_b\ell_b; L'\rangle \\ &\times M(n\ell, n'\ell', S\mathcal{J}T) \end{aligned} \qquad \text{(A-20)}$$

where N and M denote all the expressions before and after the Moshinsky brackets in (A-15).

A-c Hole-Hole Interaction Matrix Elements

It was shown in Sec. A-a that the two-hole state is related

to the two-particle state by

$$|(j_a j_b)JM;TT_3>_h = (-1)^{J-M+T-T_3}|(j_a j_b J-M;T-T_3> . \quad \text{(A-21)}$$

Since the interaction matrix elements are independent of M and T_3 the hole-hole interaction matrix elements are identical to the particle-particle interaction matrix elements. For interactions which depend on T_3, for example, the Coulomb interaction, the change in sign of T_3 is that required to make proton-hole matrix elements the same as proton-particle matrix elements.

A-d Particle-Hole Interaction Matrix Elements

With the definition (A-12) of particle-hole states the Tamm-Dancoff approximation interaction matrix elements are

$$D^x(J,T) = \sum_{m,t} (-1)^{\varphi} C_{12}C_{34} < j_1 j_4^{-1}|v|j_2^{-1} j_3 > \quad \text{(A-22a)}$$

and

$$E^x(J,T) = \sum_{m,t} (-1)^{\varphi} C_{12}C_{34} < j_1 j_4^{-1}|v|j_3 j_2^{-1} > \quad \text{(A-22b)}$$

where

$$\varphi = j_2+j_4-m_2-m_4+1-t_2-t_4$$

$$C_{12} = < j_1 j_2 m_1 m_2|JM > < \tfrac{1}{2}\tfrac{1}{2} t_1 t_2|TT_3 >$$

and

$$C_{34} = < j_3 j_4 m_3 m_4|JM > < \tfrac{1}{2}\tfrac{1}{2} t_3 t_4|TT_3 > \quad .$$

The subscripts 1 and 3 denote particles while 2 and 4 denote holes. D and E are the direct and exchange matrix elements, respectively. The superscript x denotes the matrix elements of the Tamm-Dancoff

approximation and y will be used to denote the ground state correlation matrix elements of the random phase approximation. For the ground state correlations the matrix elements are

$$D^{y}(J,T) = \sum_{m,t} (-1)^{\varphi} C_{12} C_{34} < j_1 j_3 | v | j_2^{-1} j_4^{-1} > \quad \text{(A-22c)}$$

and

$$E^{y}(J,T) = \sum_{m,t} (-1)^{\varphi} C_{12} C_{34} < j_1 j_3 | v | j_4^{-1} j_2^{-1} > . \quad \text{(A-22d)}$$

Using Racah algebra the particle-hole matrix elements can be expressed in terms of particle-particle matrix elements

$$D^{x}(J,T) = \sum_{J'T'} (-1)^{j_1+j_4+J'+T'+1} (2J'+1)(2T'+1)$$

$$\times W(j_1 j_4 j_3 j_2; J'J) W(\tfrac{1}{2}\tfrac{1}{2}\tfrac{1}{2}\tfrac{1}{2}; T'T)$$

$$\times < (j_1 j_4) J'T' | v^{T'} | (j_2 j_3) J'T' > \quad \text{(A-23a)}$$

$$E^{x}(J,T) = \sum_{J'T'} (-1)^{j_1+j_4+j_2+j_3} (2J'+1)(2T'+1)$$

$$\times W(j_1 j_4 j_3 j_2; J'J) W(\tfrac{1}{2}\tfrac{1}{2}\tfrac{1}{2}\tfrac{1}{2}; T'T)$$

$$\times < (j_1 j_4) J'T' | v^{T'} | (j_3 j_2) J'T' > \quad \text{(A-23b)}$$

$$D^{y}(J,T) = \sum_{J'T'} (-1)^{j_1+j_4+J'+T'+1} (2J'+1)(2T'+1)$$

$$\times W(j_1 j_3 j_2 j_4; J'J) W(\tfrac{1}{2}\tfrac{1}{2}\tfrac{1}{2}\tfrac{1}{2}; T'T)$$

$$\times < (j_1 j_3) J'T' | v^{T'} | (j_2 j_4) J'T' > \quad \text{(A-23c)}$$

$$E^y(J,T) = \sum_{J'T'} (-1)^{j_1+j_2+1} (2J'+1)(2T'+1)$$
$$\times W(j_1 j_3 j_2 j_4; J'J) W(\tfrac{1}{2}\tfrac{1}{2}\tfrac{1}{2}\tfrac{1}{2}; T'T)$$
$$\times < (j_1 j_3) J'T' | v^{T'} | (j_4 j_2) J'T' > \quad . \qquad \text{(A-23d)}$$

Performing the isospin summation in (A-23) we have

$$\sum_{T'} (-1)^{T'+1} (2T'+1) W(\tfrac{1}{2}\tfrac{1}{2}\tfrac{1}{2}\tfrac{1}{2}; T'T) < (j_1 j_4 | J'T' | v^{T'} | (j_2 j_3) J'T' >$$
$$= \tfrac{1}{2} < (j_1 j_4) J' | \{3v^{T'} \delta_{T'1} + v^{T'} \delta_{T'0}\} | (j_2 j_3) J' > \delta_{T0}$$
$$+ \tfrac{1}{2} < (j_1 j_4) J' | \{v^{T'} \delta_{T'1} - v^{T'} \delta_{T'0}\} | (j_2 j_3) J' > \delta_{T1} \qquad \text{(A-24a)}$$

and

$$\sum_{T'} (2T'+1) W(\tfrac{1}{2}\tfrac{1}{2}\tfrac{1}{2}\tfrac{1}{2}; T'T) < (j_1 j_4) J'T' | v^{T'} | (j_3 j_2) J'T' >$$
$$= \tfrac{1}{2} < (j_1 j_4) J'1 \{3v^{T'} \delta_{T'1} - v^{T'} \delta_{T'0}\} | (j_3 j_2) > \delta_{T0}$$
$$+ \tfrac{1}{2} < (j_1 j_4) J' | \{v^{T'} \delta_{T'1} + v^{T'} \delta_{T'0}\} | (j_3 j_2) > \delta_{T1} \quad . \qquad \text{(A-24b)}$$

The isotopic spin coupling in (A-23c) and (A-23d) is the same as that in (A-24).

A-e One-body Operator Matrix Elements

The matrix element of a one-body operator T_{kq} between two-particle states (A-6) is

$$< (j_c j_d) J'M' | T_{kq} | (j_a j_b) JM >$$
$$= < JkMq | J'M' > < (j_a j_d) J' \| T_k \| (j_a j_b) J > . \qquad \text{(A-25)}$$

The reduced matrix can be evaluated in a straightforward manner by making use of the reduction formula

$$< [j_c(1)j_d(2)]J' \| T_k(1)+T_k(2) \| [j_a(1)j_b(2)]J >$$

$$= \hat{J}(-1)^{j_a-j_d}\{\delta(j_dj_b)(-1)^{J'}\hat{j}_c W(j_cj_aJ'J;kj_d) < j_c \| T_k(1) \| j_a >$$

$$+ \quad \delta(j_cj_a)(-1)^{J}\hat{j}_d W(j_dj_bJ'J;kj_c) < j_d \| T_k(2) \| j_b > \} \qquad \text{(A-26a)}$$

where

$$< j_c \| T_k \| j_a > = < (\ell_c \tfrac{1}{2}) j_c \| T_k \| (\ell_a \tfrac{1}{2}) j_a >$$

$$= (-1)^{j_c-\frac{1}{2}-k}\hat{j}_a < j_c j_a \tfrac{1}{2}-\tfrac{1}{2} | k0 >$$

$$x \quad < T_k(r) > \left\{ \frac{1+(-1)^{\ell_a+\ell_c+k}}{2} \right\} \qquad \text{(A-26b)}$$

$$< T_k(r) > = \int u_c(r) T_k(r) u_a(r) r^2 dr \qquad \text{(A-26c)}$$

and

$$\hat{J} = (2J+1)^{\frac{1}{2}} \quad .$$

Equation (A-26b) is the reduced matrix element for single-particle states. With the antisymmetrized state vector (A-9), and (A-26) the reduced matrix element in (A-25) is

$$
\begin{aligned}
{}_a\langle (j_c j_d)J'T' \| T_k(1)+T_k(2) \| (j_a j_b)JT \rangle_a
&= \frac{1}{(2)^{\frac{1}{2}}} \frac{1}{[(1+\delta_{cd})(1+\delta_{ab})]^{\frac{1}{2}}} \times \hat{J}(-1)^{k+j_a-j_d} \\
&\times \{(-1)^{J'} \delta(j_d j_b)\hat{j}_c W(j_c j_a J'J; k j_d) M(j_c, j_a) \\
&+ (-1)^{J+T+T'} \delta(j_c j_a)\hat{j}_d W(j_d j_b J'J; k j_c) M(j_d j_b) \\
&+ (-1)^{T+J+J'+1} \delta(j_d j_a)\hat{j}_c W(j_c j_d J'J; k j_d) M(j_c, j_b) \\
&+ (-1)^{T'+1} \delta(j_c j_b)\hat{j}_d W(j_d j_a J'J; k j_c) M(j_d j_a)\}
\end{aligned}
\qquad \text{(A-27)}
$$

where

$$M(j_c j_a) = \langle j_c \| T_k(1) \| j_a \rangle + (-1)^{T+T'} \langle j_c \| T_k(2) \| j_a \rangle \ .$$

If both particles are neutrons or protons, then

$$M(j_c, j_a) = 2 \langle j_c \| T_k^{n,p} \| j_a \rangle \ .$$

If the particles are different, $M(j_c, j_a)$ will be the sum or difference of the two operators depending on the value of T+T'.

For the case of a scalar operator (A-25) is

$$
\begin{aligned}
&\langle (j_c j_d)J'T' | f(r) | (j_a j_b)J,T \rangle \\
&= \delta(J,J')\delta(T,T')\tfrac{1}{2}[M(j_c, j_a)\delta(j_c j_a) + M(j_d, j_b)\delta(j_d, j_b)]
\end{aligned}
\qquad \text{(A-28)}
$$

where

$$M(j_a, j_a) = \langle j_a \| f(1) \| j_a \rangle + \langle j_a \| f(2) \| j_a \rangle$$

and

$$\langle j_a \| f(r) \| j_a \rangle = \int u_a(r)\ f(r)\ u_a(r) r^2 dr \ .$$

The matrix element of a one body operator between two-hole states (A-9) is

$$
\begin{aligned}
&{}_h\langle (j_c j_d)J'M' | T_{kq} | (j_a j_b)JM \rangle \\
&= (-1)^{J+J'-M-M'} \langle (j_c j_d)J'-M' | T_{kq} | (j_a j_b)J-M \rangle \\
&= (-1)^{J+J'-M-M'} \langle Jk-Mq | J'-M' \rangle \langle (j_c j_d)J' \| T_k \| (j_a j_b) \rangle \, . \qquad \text{(A-29)}
\end{aligned}
$$

The reduced matrix element in (A-29) is independent of (M,M') and is the same for both particles and holes.

The matrix element of a one-body operator between particle-hole states (A-11) is

$$
\begin{aligned}
&\langle (j_3 j_4)J'M' | T_{kq} | (j_1 j_2)JM \rangle \\
&= \langle JkMq | J'M' \rangle \langle (j_3 j_4)J' \| T_k \| (j_1 j_2)J \rangle \, . \qquad \text{(A-30)}
\end{aligned}
$$

The subscripts 1 and 3 denote particles while 2 and 4 denote holes. The reduced matrix element in (A-30) is

$$
\begin{aligned}
&\langle (j_3 j_4)J' \| T_k(p) + T_k(h) \| (j_1 j_2)J \rangle \\
&= (-1)^{k+j_1-j_4} \hat{J} \{ (-1)^{J'} \hat{j}_3 W(j_3 j_1 J' J; k j_2) \langle j_3 \| T_k(p) \| j_1 \rangle \delta(j_2, j_4) \\
&- (-1)^{J} \hat{j}_4 W(j_4 j_2 J' J; k j_1) \langle j_4 \| T_k(p) \| j_2 \rangle \delta(j_1, j_3) \} \, . \qquad \text{(A-31)}
\end{aligned}
$$

Equation (A-31) is analogous to (A-26). Since "particles" and "holes" are distinct, there are no additional terms in (A-31) similar to those in (A-27).

The matrix element of a one body operator between a particle-hole

state (A-11) and the ground state is

$$< 0|T_{kq}|(j_1 j_2)JM > = < JkMq|00 >< 0\|T_k\|(j_1 j_2)J > \qquad \text{(A-32)}$$

where the reduced matrix element is

$$< 0\|T_k\|(j_1 j_2)J > = (-1)^{L+j_1-j_2}\hat{j}_2 < j_2\|T_k\|j_1 > \quad . \qquad \text{(A-33)}$$

A-f Electromagnetic Transitions

The partial width of a gamma ray transition (with angular momentum L, energy E_γ and parity π) from an initial state of spin J_i and final state of spin J_f is given by

$$\Gamma_{L,\pi} = \frac{8\pi(L+1)}{L[(2L+1)!!]^2}\left(\frac{E_\gamma}{\hbar c}\right)^{2L+1} B(L\,\pi) \quad . \qquad \text{(A-34)}$$

The reduced transition probability is

$$B(L,\pi;i \to f) = \frac{1}{(2J_i+1)} \sum_{m_i,m_f} |< f|T_{kq}|i >|^2 = \frac{(2J_f+1)}{(2J_i+1)} |< f\|T_k\|i >|^2 \qquad \text{(A-35)}$$

where the reduced matrix element is defined by

$$< J_f M_f|T_{kq}|J_i M_i > = < J_i k M_i q|J_f M_f >< f\|T_k\|i > \quad . \qquad \text{(A-36)}$$

The operators T_{kq} are the appropriate multipole operators (see below). It follows from (A-35) and (A-36) that

$$B(L,\pi;f \to i) = \frac{(2J_i+1)}{(2J_f+1)} B(L,\pi;i \to f) \quad . \qquad \text{(A-37)}$$

Convenient units for the reduced transition probabilities are

$$[B(L\pi)] = e^2 fm^{2L} \qquad \text{electric}$$

$$[BL\pi] = \mu_0{}^2 fm^{2L-2} \qquad \text{magnetic} \quad .$$

For electric transitions the multipole operator in (A-35) is

$$\mathcal{E}_L^M = \sum_k e(\tfrac{1}{2}+t_3{}^k) r_k{}^L Y_L{}^M(\theta_k,\varphi_k) \qquad \text{(A-38)}$$

where t_3 is the third component of isospin. The operator (A-38) has zero matrix elements between neutron single-particle states. In shell model calculations it is necessary to use an effective charge for neutrons and protons. Introducing effective charges, (A-38) becomes

$$\mathcal{E}_L^M = \sum_k e[(\epsilon_p+\epsilon_n)\tfrac{1}{2} + (\epsilon_p-\epsilon_n) t_3{}^k] r_k{}^L Y_L{}^M(\theta_k,\varphi_k) \qquad \text{(A-39)}$$

where ϵ_p and ϵ_n are the proton and neutron charges in units of e. It is most convenient in calculations to perform the isospin reduction separately, consequently we write (A-39) in the form

$$\mathcal{E}_L^M = \sum_k I\, r_k{}^L Y_L{}^M(\theta_k,\varphi_k) \qquad \text{(A-40)}$$

where I is the isospin factor in units of e. With the single-particle states (A-2), the reduced matrix element of the electric multipole operator is

$$< (\ell_f \tfrac{1}{2}) j_f \| \mathcal{E}_L \| (\ell_i \tfrac{1}{2}) j_i >$$
$$= I\ (-1)^{j_f - \frac{1}{2} - L}\ \frac{\hat{j}_i}{(4\pi)^{\frac{1}{2}}} < j_f j_i \tfrac{1}{2} - \tfrac{1}{2} | LO > < r^L > \left\{ \frac{1+(-1)^{\ell_f + \ell_i + L}}{2} \right\} \qquad \text{(A-41)}$$

where

$$< r^L > = \int u_f(r) r^L u_i(r) r^2 dr \quad .$$

When the radial wavefunctions are harmonic oscillator wavefunctions the radial integrals in (A-41) may be evaluated analytically. A table of several of the integrals are given in Appendix B.

For magnetic transitions the multipole operator in units of Bohr nuclear magnetons is

$$M_L^M = \sum_k \nabla_k (r_k^L Y_L^M(\theta_k, \varphi_k)) \{ \frac{2}{L+1} I\underline{\ell} + \mu\underline{\sigma} \} \quad . \qquad \text{(A-42)}$$

I is the isospin reduction factor defined previously and μ is a magnetic reduction factor. The magnetic reduction factor is identical to I with ϵ_p and ϵ_n replaced by $\mu_p (=2.79)$ and $\mu_n (=-1.91)$, respectively. It is convenient to separate (A-42) into an orbital and a spin part,

$$M_M^L = M_L^M(\ell) + M_L^M(\sigma) \qquad \text{(A-43)}$$

with

$$M_L^M(\ell) = \sum_k \nabla_k (r_k^L Y_L^M(\theta_k, \varphi_k)) \frac{2}{L+1} I\underline{\ell}$$

and

$$M_L^M(\sigma) = \sum_k \nabla_k (r_k^L Y_L^M(\theta_k, \varphi_k)) \mu\underline{\sigma} \quad .$$

For the single-particle states (A-2) the reduced matrix elements of the magnetic multipole operators are

$$< (\ell_f \tfrac{1}{2}) j_f \| M_L(\ell) \| (\ell_i \tfrac{1}{2}) j_i >$$
$$= 2I(-1)^{j_f+\frac{1}{2}-L} \hat{j}_i \hat{\ell}_f \hat{\ell}_i \left[\frac{\ell_i(\ell_i+1)L}{L+1}\right]^{\frac{1}{2}} W(j_f \ell_f j_i \ell_i \tfrac{1}{2} L)$$
$$\times < \ell_f \ell_i 01 | L1 > \frac{< r^{L-1} >}{(4\pi)^{\frac{1}{2}}} \left\{ \frac{1+(-1)^{\ell_i+\ell_f+L+1}}{2} \right\} \qquad \text{(A-44a)}$$

and

$$< (\ell_f \tfrac{1}{2}) j_f \| M_L(\sigma) \| (\ell_i \tfrac{1}{2}) j_i > = \mu(-1)^{j_f-\frac{1}{2}-L} \hat{j}_i < j_f j_i \tfrac{1}{2} -\tfrac{1}{2} | L0 >$$
$$\times \{L-(\ell_i-j_i)(2j_i+1)-(\ell_f-j_f)(2j_f+1)\}$$
$$\times \frac{< r^{L-1} >}{(4\pi)^{\frac{1}{2}}} \left\{ \frac{1+(-1)^{\ell_i+\ell_f+L+1}}{2} \right\} \qquad \text{(A-44b)}$$

where

$$< r^{L-1} > = \int u_f(r) r^{L-1} u_i r^2 dr \quad .$$

The reduced single-particle matrix elements (A-41) and (A-44), combined with the one-body operator matrix elements of Sec. A-e, can be used to evaluate electromagnetic transition rates for the various shell model states considered.

APPENDIX B

RECURRENCE RELATIONS FOR TALMI COEFFICIENTS AND SHELL MODEL RADIAL INTEGRALS

Harmonic oscillator functions are used as the unperturbed single-particle wave functions in most nuclear shell model calculations. Apart from being a good representation of the single-particle wave functions in most cases, the oscillator functions have convenient mathematical properties. The best known properties are the Talmi transformation[132] from laboratory coorindates and the Talmi method[132] for evaluating radial integrals. Brody, Jacob and Moshinsky[133] have discussed the evaluation of shell model matrix elements using the above methods. Since any radial wave function can be expanded in terms of oscillator functions, the transformation properties of the oscillator functions can always be used to simplify calculations. As shell model calculations become increasingly complex the methods used to evaluate matrix elements become more important. For example, the calculation of oscillator brackets required in Hartree-Fock calculations.[134]

We have found that radial oscillator function recurrence relations provide a convenient method for obtaining recurrence relations for radial integrals and Talmi coefficients. These relations are particularly useful when a large number of radial integrals are required. For instance, the case of radial wave functions which

have been expanded in terms of oscillator functions. Several authors[133,135,136] have obtained various expressions for the Talmi coefficients. The recurrence relations given here are more general and have the advantage that all possible coefficients may be generated.

The methods discussed are applied to the simple case of evaluating radial integrals required in calculations of electromagnetic multipole moments.

B-a The Radial Integrals

The various matrix elements required in nuclear shell model calculations have been discussed in detail by Moshinsky[129] and Brody, Jacob and Moshinsky.[133] In Moshinsky's notation the radial integrals required for the matrix elements are

$$< n'\ell' \| V(r) \| n\ell > = \int R_{n'\ell'}(x) V(r) R_{n\ell}(x) x^2 dx \ . \qquad \text{(B-1)}$$

$V(r)$ is the radial dependence of the potential in the relative coordinate and (n,ℓ) are the usual quantum numbers of relative motion. The radial oscillator function is

$$R_{n\ell}(x) = \left[\frac{2n!}{\Gamma(n+\ell+3/2)}\right]^{\frac{1}{2}} x^{\ell} \ e^{-x^2/2} L_n^{\ell+\frac{1}{2}}(x^2) \qquad \text{(B-2)}$$

where

$$x = \alpha r \quad , \quad \alpha = \left(\frac{M\omega}{\hbar}\right)^{\frac{1}{2}}$$

and

$$n,\ell = 0,1,2,\ldots \ .$$

The Laguerre polynomials $L_n^{\ell+\frac{1}{2}}(x^2)$ are those defined by Erdelyi, et al.[137] The radial oscillator functions, as defined in (B-2), are normalized such that

$$\int R_{m\ell}(x) R_{n\ell}(x) x^2 dx = \delta_{mn} \quad . \tag{B-3}$$

For central, spin-orbit and tensor forces the radial integrals required satisfy the condition $\ell' = \ell, \ell \pm 2$. The values of n and n' are determined by energy conservation in the Moshinsky transformation. If the radial wave function being used has been expanded in terms of radial oscillator functions, n and n' can vary over a wide range in a given matrix element.

Using the Talmi transformation the radial integrals (B-1) can be expressed as the sum of Talmi integrals, i.e.

$$< n'\ell' \| V(r) \| n\ell > = \sum_{p=\lambda}^{\lambda+n+n'} B(n'\ell', n\ell; p) I_p \tag{B-4}$$

where $\lambda = \frac{\ell+\ell'}{2}$ and is an integer. The Talmi integrals are

$$I_p = \frac{2}{\Gamma(\frac{1}{2}+3/2)} \int x^{2p+2} e^{-x^2} V(r) dx \tag{B-5}$$

and the coefficients $B(n'\ell, n\ell; p)$ are the Talmi coefficients. Expressions for the Talmi coefficients can be obtained by using the explicit form of the Laguerre polynomials.

B-b Recurrence Relations for the Oscillator Functions

It is convenient in the following discussion to use the notation

$$|n\ell .> \equiv R_{n\ell}(x) \quad . \tag{B-6}$$

The recurrence relations for the Laguerre polynomials can be used to write down the following recurrence relations for the radial oscillator functions:

$$x|n,\ell > = (n+\ell+\tfrac{1}{2})^{\frac{1}{2}}|n,\ell-1 > - (n+1)^{\frac{1}{2}}|n+1,\ell-1 > \tag{B-7}$$

$$x|n,\ell > = (n+\ell+3/2)^{\frac{1}{2}}|n,\ell+1 > - n^{\frac{1}{2}}|n-1,\ell+1 > \tag{B-8}$$

and

$$x^2|n,\ell > = -[(n+1)(n+\ell+3/2)]^{\frac{1}{2}}|n+1,\ell > + (2n+\ell+3/2)|n,\ell > - [n(n+\ell+\tfrac{1}{2})]^{\frac{1}{2}}|n-1,\ell >. \tag{B-9}$$

From (B-8) and (B-9) we have the useful relation

$$(n+\ell+5/2)^{\frac{1}{2}}|n,\ell+2 > = n^{\frac{1}{2}}|n-1,\ell+2 > + (n+\ell+3/2)^{\frac{1}{2}}|n,\ell > - (n+1)^{\frac{1}{2}}|n+1,\ell > . \tag{B-10}$$

B-c Recurrence Relations for Radial Integrals

The oscillator function recurrence relations can be used to

obtain recurrence relations for the radial integrals $< n'\ell' \| V(r) \| n\ell >$. From (B-10) we have immediately that

$$(n+\ell+5/2)^{\frac{1}{2}} < n',\ell' \| V(r) \| n,\ell+2 > = n^{\frac{1}{2}} < n',\ell' \| V(r) \| n-1,\ell+2 > + (n+\ell+3/2)^{\frac{1}{2}} < n',\ell' \| V(r) \| n,\ell > - (n+1)^{\frac{1}{2}} < n'\ell' \| V(r) \| n+1,\ell > . \qquad (B-11)$$

Equation (B-12) may be used to obtain the set of integrals $< n',\ell' \| V(r) \| n,\ell+2 >$ from the set $< n',\ell' \| V(r) \| n+1,\ell >$. It is obvious that both sets of integrals must require the same set of Talmi integrals, that is, moments of the potential V(r).

For potentials that commute with x equations (B-7), (B-8), and (B-9) may be used to obtain relations among the radial integrals of the potentials. Using (B-10) and the relation

$$< n'\ell' \| x^2 V(r) \| n\ell > = < n'\ell' \| V(r) x^2 \| n\ell > \qquad (B-12)$$

we have that

$$\begin{aligned}[(n'+1)(n'+\ell'+3/2)]^{\frac{1}{2}} < n'+1,\ell' \| V(r) \| n,\ell > = \\ -[n'(n'+\ell'+\tfrac{1}{2})]^{\frac{1}{2}} < n'-1,\ell' \| V(r) \| n,\ell > + \\ +[n(n+\ell+\tfrac{1}{2})]^{\frac{1}{2}} < n',\ell' \| V(r) \| n-1,\ell > + \\ +(2n'+\ell'-2n-\ell) < n',\ell' \| V(r) \| n,\ell > + \\ +[(n+1)(n+\ell+3/2)]^{\frac{1}{2}} < n',\ell' \| V(r) \| n+1,\ell > . \qquad (B-13)\end{aligned}$$

From the relation

$$< n',\ell \| xV(r)x \| n\ell > = < n'\ell' \| V(r)x^2 \| n\ell > \qquad \text{(B-14)}$$

and (B-8) and B-9) we have that

$$\begin{aligned}
&[(n'+\ell'+3/2)(n+\ell+3/2)]^{\frac{1}{2}} < n',\ell'+1 \| V(r) \| n,\ell+1 > = \\
&[n(n'+\ell+3/2)]^{\frac{1}{2}} < n',\ell'+1 \| V(r) \| n-1,\ell+1 > + \\
&+[n'(n+\ell+3/2)]^{\frac{1}{2}} < n'-1,\ell'+1 \| V(r) \| n,\ell+1 > - [n,n']^{\frac{1}{2}} \ x \\
&< n'-1,\ell'+1 \| V(r) \| n-1,\ell+1 > - [(n+1)(n+\ell+3/2)]^{\frac{1}{2}} \ x \\
&< n',\ell' \| V(r) \| n+1,\ell > + (2n+\ell+3/2) < n',\ell' \| V(r) \| n,\ell > \\
&-[n(n+\ell+\tfrac{1}{2})]^{\frac{1}{2}} < n',\ell \| V(r) \| n-1,\ell > \ . \qquad \text{(B-15)}
\end{aligned}$$

Equation (B-13) is a relation among integrals of the same ℓ and ℓ' while (B-15) gives the set of integrals $< n',\ell'+1 \| V(r) \| n,\ell+1 >$ in terms of the set $< n',\ell' \| V(r) \| n+1,\ell >$. Other relations may be obtained in a similar manner.

Although (B-13) and (B-15) are only valid for potentials that commute with x, a simple velocity dependent potential of the form

$$W(p,r) = \frac{p^2}{2M} \ V(r) + V(r) \ \frac{p^2}{2M} \qquad \text{(B-16)}$$

(where p is the relative radial momentum operator) can be handled conveniently by these methods. The oscillator potential for relative motion is

$$H_{rel} = \frac{p^2}{2M} + \frac{1}{2}\hbar\omega\, x^2 \quad . \qquad \text{(B-17)}$$

Using (B-17) and (B-9) the radial integrals of W(p,r) are

$$\begin{aligned} \langle n',\ell' \| W(p,r) \| n,\ell \rangle = {} & [(n+1)(n+\ell+3/2)]^{\frac{1}{2}} \hbar\omega \langle n',\ell' \| V(r) \| n+1,\ell \rangle \\ & + (2n+\ell+3/2)\hbar\omega \langle n',\ell' \| V(r) \| n,\ell \rangle \\ & + [n(n+\ell+\tfrac{1}{2})]^{\frac{1}{2}} \hbar\omega \langle n',\ell' \| V(r) \| n-1,\ell \rangle \quad . \end{aligned} \qquad \text{(B-18)}$$

B-d Recurrence Realtions for the Talmi Coefficients

To obtain a recurrence relation for the coefficients $B(n'\ell',n\ell;p)$ we use (B-9) and the equation

$$\begin{aligned} \langle n',\ell' \| V(r)x^2 \| n,\ell \rangle = {} & (2n+\ell+3/2) \langle n',\ell' \| V(r) \| n,\ell \rangle \\ & -[(n+1)(n+\ell+3/2)]^{\frac{1}{2}} \langle n',\ell' \| V(r) \| n+1,\ell \rangle \\ & -[n(n+\ell+\tfrac{1}{2})]^{\frac{1}{2}} \langle n',\ell \| V(r) \| n-1,\ell \rangle \quad . \end{aligned} \qquad \text{(B-19)}$$

Expanding both sides of (B-19) in terms of Talmi integrals, using the result

$$I_p(Vx^2) = (p+3/2)\, I_{p+1}(V) \qquad \text{(B-20)}$$

and equating the coefficients of the integrals we have that

$$B(n'\ell',n+1,\ell'p) = \alpha B(n'\ell',n\ell;p) + \beta B(n'\ell',n\ell;p-1) + \gamma B(n'\ell',n-1\ell;p) \qquad \text{(B-21)}$$

where

$$\lambda \leq p \leq \lambda+n'+n+1, \quad \lambda = \frac{\ell'+\ell}{2} \quad .$$

The coefficients in (B-21) are given by

$$\begin{aligned} &[(n+1)(n+\ell+3/2)]^{\frac{1}{2}} && \alpha = 2n+\ell+3/2 \\ &[(n+1)(n+\ell+3/2)]^{\frac{1}{2}} && \beta = -(p+\tfrac{1}{2}) \\ &[(n+1)(n+\ell+3/2)]^{\frac{1}{2}} && \gamma = -[n(n+\ell+\tfrac{1}{2})]^{\frac{1}{2}} \quad . \end{aligned} \qquad \text{(B-22)}$$

In (B-21) it is to be understood that a Talmi coefficient is zero, if the value of p is outside the range allowed for that coefficient.

To obtain a recurrence formula for the coefficients $B(n'\ell'+1,n\ell+1;p)$ we use the relation

$$< n'\ell' \| V(r)x^2 \| n\ell > = < n'\ell' \| xV(r)x \| n\ell > . \qquad \text{(B-23)}$$

Using (B-8), (B-23) can be written as

$$\begin{aligned} < n',\ell' \| V(r)x^2 \| n,\ell > = \alpha_1 < n',\ell'+1 \| V(r) \| n-1,\ell+1 > + \\ + \alpha_2 < n'-1,\ell'+1 \| V(r) \| n,\ell+1 > + \alpha_3 < n'-1,\ell'+1 \| V(r) \| n-1,\ell+1 > \\ + \alpha_4 < n',\ell' \| V(r)x^2 \| n,\ell > \end{aligned} \qquad \text{(B-24)}$$

where

$$\alpha_1 = \left[\frac{n}{(n+\ell+3/2)} \right]^{\frac{1}{2}}$$

$$\alpha_2 = \left[\frac{n'}{(n'+\ell'+3/2)} \right]^{\frac{1}{2}}$$

$$\alpha_3 = -\left[\frac{nn'}{(n+\ell+3/2)(n'+\ell'+3/2)} \right]^{\frac{1}{2}}$$

$$\alpha_4 = \left[\frac{1}{(n+\ell+3/2)(n'+\ell'+3/2)} \right]^{\frac{1}{2}} \quad . \qquad \text{(B-25)}$$

In the same manner that (B-21) was obtained we have from (B-24) that

$$B(n'\ell'+1,n\ell+1;p) = \alpha_1 B(n'\ell'+1,n-1\ell+1;p) + \alpha_2 B(n'-1\ell'+1,n\ell+1;p) + \alpha_3 B(n'-1\ell'+1,n-1\ell+1;p) + \alpha_4 (p+\tfrac{1}{2}) B(n'\ell',n\ell;p-1) \qquad \text{(B-26)}$$

where

$$\frac{\ell'+\ell+2}{2} = \lambda \leq p \leq \lambda+n+n' \quad .$$

Expanding both sides of (B-11) in terms of Talmi integrals and equation the coefficients we have that

$$(n+\ell+5/2)^{\frac{1}{2}} B(n'\ell',n\ell+2;p) = n^{\frac{1}{2}} B(n'\ell',n-1\ell+2;p) + (n+\ell+3/2)^{\frac{1}{2}} B(n'\ell',n\ell;p) - (n+1)^{\frac{1}{2}} B(n'\ell',n+1\ell;p) \qquad \text{(B-27)}$$

where

$$\frac{\ell'+\ell+2}{2} = \lambda \leq p \leq \lambda+n+n' \quad .$$

Since the range of p for the two sets of coefficients in (B-27) is

different we have that

$$(n+1)^{\frac{1}{2}}B(n'\ell',n+1\ell;\tfrac{\ell'+\ell}{2}) = (n+\ell+3/2)^{\frac{1}{2}}B(n'\ell',n\ell;\tfrac{\ell'+\ell}{2}) \quad . \quad \text{(B-28)}$$

Equations (B-21), (B-26) and (B-27), combined with the symmetry

$$B(n'\ell',n\ell;p) = B(n\ell;n'\ell';p) \quad \text{(B-29)}$$

and the normalization

$$B(00,00;0) = 1 \quad , \quad \text{(B-30)}$$

can be used to generate all of the Talmi coefficients.

B-e The Radial Integrals $< n'\ell' \| x^{\lambda} \| n\ell >$

The calculation of transition moments involves radial integrals of the form

$$I(\lambda;\Delta\ell,\Delta n) = < n'\ell' \| x^{\lambda} \| n\ell > \quad \text{(B-31)}$$

where λ is the multipole order of the transition and $\Delta\ell = \ell'-\ell$; $\Delta n = n'-n$. From (B-31) it is obvious that

$$I(\lambda;\Delta\ell,\ell n) = I(\lambda;-\Delta\ell,-\Delta n) \quad . \quad \text{(B-32)}$$

The radial integrals $I(\lambda;\Delta\ell,\ell n)$ can be evaluated analytically when oscillator function basis states are used. A formula involving a finite sum has been given by Nilsson.[138] However, the oscillator

function recurrence relations may be used to generate the desired integrals without recourse to a summation. Consider the case of a dipole transition. From angular momentum considerations the desired integrals are $< n'\ell-1\|x\|n\ell >$ and $< n'\ell+1\|x\|n\ell >$.

Using (B-3), (B-7) and (B-8), the non-zero integrals are

$$\begin{aligned} < n,\ell-1\|x\|n\ell > &= (n+\ell+\tfrac{1}{2})^{\frac{1}{2}} \\ < n,\ell+1\|x\|n\ell > &= (n+\ell+3/2)^{\frac{1}{2}} \\ < n-1,\ell+1\|x\|n\ell > &= -n^{\frac{1}{2}} \\ < n+1,\ell-1\|x\|n\ell > &= -(n+1)^{\frac{1}{2}} \quad . \end{aligned} \tag{B-33}$$

Any desired integral may be obtained by repeated application of (B-7), (B-8) and (B-9). The integrals for $\lambda = 1,2$ and 3 are tabulated in Table B-1.

Inspection of the recurrence relations for the oscillator functions leads to selection rules for the radial quantum numbers as well. The result is

$$I(2t; \pm 2m, \Delta n) = 0 \quad \text{if} \quad \Delta n > +t+m \quad \text{or} \quad \Delta n < -t+m \tag{B-34a}$$

$$I(2t; \pm 2m+1, \Delta n) = 0 \quad \text{if} \quad \Delta n > +t+m \tag{B-34b}$$

and

$$I(2t+1; \pm 2m-1, \Delta n) = 0 \quad \text{if} \quad \Delta n > +t+m+1 \quad \text{or} \quad \Delta n < -t+m \tag{B-34c}$$

where

$$t = 0,1,2,\ldots.$$
$$m = 0,1,\ldots \leq t \quad .$$

Table B-1 The integrals of X^{λ} where $X = r(\frac{m\omega}{\hbar})^{\frac{1}{2}}$.

λ	n'	ℓ'	$< n'\ell' \|\| X^{\lambda} \|\| n\ell >$
1	n	$\ell-1$	$(n+\ell+\frac{1}{2})^{\frac{1}{2}}$
1	n	$\ell+1$	$(n+\ell+3/2)^{\frac{1}{2}}$
1	n+1	$\ell-1$	$-(n+1)^{\frac{1}{2}}$
1	n-1	$\ell+1$	$-n^{\frac{1}{2}}$
2	n+1	ℓ	$-[(n+1)(n+\ell+3/2)]^{\frac{1}{2}}$
2	n	ℓ	$(2n+\ell+3/2)$
2	n-1	ℓ	$-[n(n+\ell+\frac{1}{2})]^{\frac{1}{2}}$
2	n	$\ell-2$	$[(n+\ell+\frac{1}{2})(n+\ell-\frac{1}{2})]^{\frac{1}{2}}$
2	n+1	$\ell-2$	$-2[(n+1)(n+\ell+\frac{1}{2})]^{\frac{1}{2}}$
2	n+2	$\ell-2$	$[(n+1)(n+2)]^{\frac{1}{2}}$
2	n	$\ell+2$	$[(n+\ell+3/2)(n+\ell+5/2)]^{\frac{1}{2}}$
2	n-1	$\ell+2$	$-2[n(n+\ell+3/2)]^{\frac{1}{2}}$
2	n-2	$\ell+2$	$[n(n-1)]^{\frac{1}{2}}$
3	n-1	$\ell-1$	$-[n(n+\ell-\frac{1}{2})(n+\ell+\frac{1}{2})]^{\frac{1}{2}}$
3	n	$\ell-1$	$(n+\ell+\frac{1}{2})^{\frac{1}{2}}(3n+\ell+3/2)$
3	n+1	$\ell-1$	$-(n+1)^{\frac{1}{2}}(3n+2\ell+3)$
3	n+2	$\ell-1$	$[(n+1)(n+2)(n+\ell+3/2)]^{\frac{1}{2}}$
3	n+1	$\ell+1$	$-[(n+1)(n+\ell+3/2)(n+\ell+5/2)]^{\frac{1}{2}}$
3	n	$\ell+1$	$(n+\ell+3/2)^{\frac{1}{2}}(3n+\ell+5/2)$
3	n-1	$\ell+1$	$-n^{\frac{1}{2}}(3n+2\ell+2)$
3	n-2	$\ell+1$	$[n(n-1)(n+\ell+\frac{1}{2})]^{\frac{1}{2}}$
3	n	$\ell-3$	$[(n+\ell-3/2)(n+\ell-\frac{1}{2})(n+\ell+\frac{1}{2})]^{\frac{1}{2}}$

Table B-1 (continued)

λ	n'	ℓ'	$< n'\ell' \|\|X^{\lambda}\|\| n\ell >$
3	n+1	ℓ-3	$-3[(n+1)(n+\ell+\frac{1}{2})(n+\ell-\frac{1}{2})]^{\frac{1}{2}}$
3	n+2	ℓ-3	$+3[(n+1)(n+2)(n+\ell+\frac{1}{2})]^{\frac{1}{2}}$
3	n+3	ℓ-3	$-[(n+1)(n+2)(n+3)]^{\frac{1}{2}}$
3	n	ℓ+3	$[(n+\ell+3/2)(n+\ell+5/2)(n+\ell+7/2)]^{\frac{1}{2}}$
3	n-1	ℓ+3	$-3[n(n+\ell+3/2)(n+\ell+5/2)]^{\frac{1}{2}}$
3	n-2	ℓ+3	$+3[n(n-1)(n+\ell+3/2)]^{\frac{1}{2}}$
3	n-3	ℓ+3	$-[n(n-1)(n-2)]^{\frac{1}{2}}$

APPENDIX C

WOODS-SAXON RADIAL MATRIX ELEMENTS

Radial matrix elements with Woods-Saxon (WS) single-particle wavefunctions are a series in terms of the same reduced integrals that are required when harmonic oscillator (HO) wavefunctions are used as basis states. Special cases of matrix elements with WS wavefunctions are examined to illustrate the effects of using WS wavefunctions as opposed to harmonic oscillator functions.

It is convenient to write the radially dependent part of the particle-particle interaction matrix element (A-20) in the form

$$\begin{aligned} RME = & \sum_{n_a,n_b,n_c,n_d} \alpha_{n_a}(a)\alpha_{n_b}(b)\alpha_{n_c}(c)\alpha_{n_d}(d) \\ & \times \sum_{n\ell,n'\ell'N\mathcal{L}} \langle n_c\ell_c, n_d\ell_d; L | n\ell, N\mathcal{L}; L \rangle \langle n'\ell', N\mathcal{L}; L' | n_a\ell_a, n_b\ell_b; L' \rangle \\ & \times RI(n\ell, n'\ell') \quad . \end{aligned} \tag{C-1}$$

RI includes both the coupling and the radial integrals. Only the $(n\ell, n'\ell')$ dependence is retained explicitly since it contains all of the information required in the following discussion. To obtain the desired expressions for RME we utilize the properties of Moshinsky brackets that are derived in Appendix D.

For the case $\ell_a = \ell_b$ we use the symmetry (D-3) to write (C-1) in the form

$$\text{RME} = \sum_{\substack{n_c,n_d,n_a \\ n_b > n_a}} \sum'_{\substack{n\ell n'\ell' \\ N\mathcal{L}}} \alpha_{n_c}(c)\alpha_{n_d}(d)$$

$$\times \langle n_c\ell_c, n_d\ell_d; L | n\ell, N\mathcal{L}; L \rangle$$

$$\times \frac{[\alpha_{n_a}(a)\alpha_{n_b}(b) + (-1)^{L-L'}\alpha_{n_b}(a)\alpha_{n_a}(b)]}{[1+\delta(n_a,n_b)]} \langle n'\ell', N\mathcal{L}; L' | n_a\ell_a, n_b\ell_a; L' \rangle$$

$$\times \text{RI}(n\ell, n'\ell') \quad . \qquad \text{(C-2)}$$

For the case of HO wavefunctions with $n_a = n_b$ and $\ell_a = \ell_b$ the Moshinsky bracket vanishes unless L-L' is even. However, for WS wavefunctions the terms in the summation over n_a and n_b add or subtract if L-L' is even or odd.

Equation (C-2) can be reduced further to compare with a matrix element evaluated using HO wavefunctions. In the following we adopt the notation

$$[n_b - n_a] \equiv \frac{\left[\alpha_{n_a}(a)\alpha_{n_b}(b) + (-1)^{L-L'}\alpha_{n_b}(a)\alpha_{n_a}(b)\right]}{[1+\delta(n_a,n_b)]} \quad . \qquad \text{(C-3)}$$

For a central force, performing the summation over n_b in (C-2) leads to

$$\text{RME} = \sum_{n_c,n_d,n_a} \sum_{n\ell n' N\mathcal{L}} \alpha_{n_c}(c)\alpha_{n_d}(d)$$

$$\times \langle n_c\ell_c, n_d\ell_d; L | n\mathcal{L}, N\mathcal{L}; L \rangle \times \Big\{ [0] \langle n'\ell, N\mathcal{L}; L' | n_a\ell_a, n_a\ell_a; L' \rangle$$

$$+ [1] \frac{\text{RI}(n\ell, n'+1\ell)}{\text{RI}(n\ell, n'\ell)} \langle n'+1\ell, N\mathcal{L}; L' | n_a\ell_a, n_a+1\ell_a; L' \rangle$$

$$+ [2] \frac{\text{RI}(n\ell, n'+2\ell)}{\text{RI}(n\ell, n'\ell)} \langle n'+2\ell, N\mathcal{L}; L' | n_a\ell_a, n_a+2\ell_a; L' \rangle$$

$$+ [3] \ldots$$

$$+ \ldots\ldots \Big\} \quad \times \text{RI}(n\ell, n'\ell) \quad . \qquad \text{(C-4)}$$

When L-L' is odd the coefficients $[n_d - n_b]$ tend to cancel making the contributions to the matrix element small.

For the case that L-L' is even (C-4) can be reduced further by using Eq. (D=6). The result is

$$\begin{aligned} RME = \sum_{n_c, n_d, n_a} \sum_{n\ell' n' N\mathcal{L}} \alpha_{n_c}(c)\alpha_{n_d}(d) \times & < n_c\ell_c, n_d\ell_d; L | n\ell, N\mathcal{L}; L > \\ \times \{ & C_1 < n'\ell, N\mathcal{L}; L' | n_a\ell_a, n_a\ell_a; L' > + C_2 < n'+\ell, N-1\mathcal{L}; L' | n_a\ell_a, n_a\ell_a; L' > \\ & + C_3 < n'+2\ell, N-2\mathcal{L}; L' | n_a\ell_a, n_a\ell_a; L' > + C_4 < n'+2\ell, N\mathcal{L} L' | n_a+1\ell_a, n_a+1\ell_a; L' > \\ & + [3] \ldots . \\ & + \ldots\ldots\ldots \} \times RI(n\ell, n'\ell) \end{aligned} \qquad \text{(C-5)}$$

where

$$C_1 = [0] + [1] \frac{RI(n\ell, n'+1\ell)}{RI(n\ell\ n'\ell)} \frac{1}{2} \left[\frac{(n'+1)(n'+\ell+3/2)}{(n_a+1)(n_a+\ell_a+3/2)} \right]^{\frac{1}{2}}$$

$$+ [2] \frac{RI(n\ell; n'+2\ell)}{RI(n\ell, n'\ell)} \frac{1}{2} \left[\frac{(n'+2)(n'+\ell+5/2)(n'+1)(n'+\ell+3/2)}{(n_a+1)(n_a+\ell_a+3/2)} \right]^{\frac{1}{2}}$$

$$C_2 = [1] \frac{RI(n\ell, n'+1\ell)}{RI(n\ell, n'\ell)} \frac{1}{2} \left[\frac{N(N+\mathcal{L}+1/2)}{(n_a+1)(n_a+\ell_a+3/2)} \right]^{\frac{1}{2}}$$

$$+ [2] \frac{RI(n\ell, n'+2\ell)}{RI(n\ell, n'\ell)} [(n'+2)(n'+\ell+5/2)]^{\frac{1}{2}} \left[\frac{N(N+\mathcal{L}+1/2)}{(n_a+1)(n_a+\ell_a+3/2)} \right]^{\frac{1}{2}}$$

$$C_3 = [2] \frac{RI(n\ell, n'+2\ell)}{RI(n\ell, n'\ell)} \frac{1}{2} [(N-1)(N+\mathcal{L}-1/2)]^{\frac{1}{2}} \left[\frac{N(N+\mathcal{L}+1/2)}{(n_a+1)(n_a+\ell_a+1/2)} \right]^{\frac{1}{2}}$$

and

$$C_4 = -[2]\ \frac{RI(n\ell,n'+2\ell)}{RI(n\ell,n'\ell)}\ \left[\frac{(n_a+1)(n_a+\ell_a+3/2)}{(n_a+2)(n_a+\ell_a+5/2)}\right]^{\frac{1}{2}}$$

For the special case $n_a = 0$ (D-14) and (D-15) can be used to write (C-5) as

$$\begin{aligned}
RME = \sum_{n_c,n_d}\ \sum_{n\ell n'N\mathcal{L}} & \alpha_{n_c}(c)\alpha_{n_d}(d)\ x < n_c\ell_c, n_d\ell_d; L | n\ell, N\mathcal{L}; L > \\
& x \left\{ \left[C_1 - C_2 \left[\frac{N(N+\mathcal{L}+1/2)}{(n'+1)(n'+\ell+3/2)}\right]^{\frac{1}{2}} \right.\right. \\
& \qquad \left.\left. + C_3 \left[\frac{(N-1)(N+\mathcal{L}-1/2)N(N+\mathcal{L}+1/2)}{(n'+2)(n'+\ell+5/2)(n'+1)(n'+\ell+3/2)}\right]^{\frac{1}{2}} \right] \right. \\
& x < n'\ell, N\mathcal{L}, L' | 0\ell_a, 0\ell_a; L' > \\
& x\ C_4 < n'+2\ell, N\mathcal{L}; L' | 1\ell_a, 1\ell_a; L' > \\
& + \ldots\ldots \\
& \left. + \ldots\ldots \right\}\ x\ RI(n\ell, n'\ell) \qquad . \qquad (C\text{-}6)
\end{aligned}$$

In many cases for wavefunctions with zero nodes the WS wavefunction can be represented as mainly one HO wavefunction with n=0 plus small amplitudes of n=1 and 2. For these cases (C-6) gives the dependence of the matrix element on the (n,n') structure of the interaction.

APPENDIX D

PROPERTIES OF MOSHINSKY BRACKETS

The oscillator function recurrence relations (Appendix B) are used to obtain relations among Moshinsky brackets for states having the same total energy.

[129]

The Moshinsky transformation

$$(2)^{\frac{1}{2}}\underline{X}_R = \underline{x}_1 - \underline{x}_2 \qquad \text{(relative)}$$
$$(2)^{\frac{1}{2}}\underline{X}_{cm} = \underline{x}_1 + \underline{x}_2 \qquad \text{(centre-of-mass)} \qquad \text{(D-1)}$$

for the oscillator functions (B-2) introduces the transformation brackets $< n\ell, N\mathcal{L}; L | n_1\ell_1, n_2\ell_2; L >$. Energy and momentum conservation impose the restrictions

$$2n_1+\ell_1+2n_2+\ell_2 = 2n+\ell+2N+\mathcal{L}$$
$$\underline{\ell}_1+\underline{\ell}_2 = \underline{\ell}+\underline{\mathcal{L}}$$
$$(-1)^{\ell_1+\ell_2} = (-1)^{\ell+\mathcal{L}} \quad . \qquad \text{(D-2)}$$

Furthermore, the brackets have the symmetries

$$< n\ell, N\mathcal{L}; L | n_1\ell_1, n_2\ell_2; L > = (-1)^{\mathcal{L}-L} < n\ell, N\mathcal{L}; L | n_2\ell_2, n_1\ell_1; L >$$
$$= (-1)^{\ell_1-L} < N\mathcal{L}, n\ell; L | n_1\ell_1, n_2\ell_2; L >$$
$$= (-1)^{\ell_1+\ell} < N\mathcal{L}, n\ell; L | n_2\ell_2, n_1\ell_1; L > . \qquad \text{(D-3)}$$

Since the recurrence relation (B-9) only changes the radial quantum number of the oscillator function, the two-particle states of the Moshinsky transformation satisfy the same equation. For example,

$$X_1^2|n_1\ell_1,n_2\ell_2;L> = -[(n_1+1)(n_1+\ell_1+3/2)]^{\frac{1}{2}}|n_1+1\ell_1,n_2\ell_2;L>$$
$$+(2n_1+\ell_1+3/2)|n_1\ell_1,n_2\ell_2;L>$$
$$-[n_1(n_1+\ell_1+\tfrac{1}{2})]^{\frac{1}{2}}|n_1-1\ell_1,n_2\ell_2;L>. \qquad (D\text{-}4)$$

Similar relations may be obtained for the relative and centre-of-mass coordinate eigenfunctions. If both sides of (D-4) are multiplied by $<n\ell,N\mathcal{L};L|$ only one bracket on the right hand side will be non-zero by energy conservation. Using the equality

$$<n\ell,N\mathcal{L};L|(X_R^2+X_{cm}^2)|n_1\ell_1,n_2\ell_2;L> =$$
$$<n\ell,N\mathcal{L};L|(X_1^2+X_2^2)|n_1\ell_1,n_2\ell_2;L> \qquad (D\text{-}5)$$

and the expansions analogous to (D-4). We obtain the relations:

$$[(n_1+1)(n_1+\ell_1+3/2)]^{\frac{1}{2}}<n\ell,N\mathcal{L};L|n_1+L\ell_1,n_2\ell_2;L>$$
$$+[(n_2+1)(n_2+\ell_2+3/2)]^{\frac{1}{2}}<n\ell,N\mathcal{L};L|n_1\ell_1,n_2+1\ell_2;L>$$
$$=[n(n+\ell+\tfrac{1}{2})]^{\frac{1}{2}}<n-1\ell,N\mathcal{L};L|n_1\ell_1,n_2\ell_2;L>$$
$$+[N(N+\mathcal{L}+\tfrac{1}{2})]^{\frac{1}{2}}<n\ell,N-1\mathcal{L};L|n_1\ell_1,n_2\ell_2;L> \qquad (D\text{-}6)$$

and

$$[(n+1)(n+\ell+3/2)]^{\frac{1}{2}}<n+1\ell,N\mathcal{L};L|n_1\ell_1,n_2\ell_2;L>$$
$$+[(N+1)(N+\mathcal{L}+3/2)]^{\frac{1}{2}}<n\ell,N+1\mathcal{L};L|n_1\ell_1,n_2\ell_2;L>$$
$$=[n_1(n_1+\ell_1+\tfrac{1}{2})]^{\frac{1}{2}}<n\ell,N\mathcal{L};L|n_1-1\ell_1,n_2\ell_2;L>$$
$$+[n_2(n_2+\ell_2+\tfrac{1}{2})]^{\frac{1}{2}}<n\ell,N\mathcal{L};L|n_1\ell_1,n_2-1\ell_2;L> . \qquad (D\text{-}7$$

In a similar manner the integrals of

$$X_1^4-X_2^4 = (X_1^2+X_2^2)(X_1^2-X_2^2) = (X_R^2+X_{cm}^2)(X_1^2-X_2^2) \qquad (D\text{-}8)$$

and

$$X_R^4-X_{cm}^4 = (X_R^2+X_{cm}^2)(X_R^2-X_{cm}^2) = (X_1^2+X_2^2)(X_R^2-X_{cm}^2) \qquad (D\text{-}9)$$

may be used to obtain several relationships among transformation brackets. Two such relations are

$$\beta_1 < n\ell, N\mathcal{L}; L | n_1+2\ell_1, n_2\ell_2; L > + \beta_2 < n\ell, N\mathcal{L}; L | n_1\ell_1, n_2\ell_2; L > =$$
$$\beta_3 < n-1\ell, n\mathcal{L}:1 | n_1+1\ell_1, n_2\ell_2; L > + \beta_4 < n\ell, N-1\mathcal{L}; L | n_1+1\ell_1, n_2\ell_2; L > +$$
$$\beta_5 < n-1\ell, N\mathcal{L}; L | n_1\ell_1, n_2+1\ell_2; L > + \beta_6 < n\ell, N-1\mathcal{L}; L | n_1\ell_1, n_2+1\ell_2; L > \qquad \text{(D-10)}$$

and

$$\gamma_1 < n+2\ell, N\mathcal{L}; L | n_1\ell_1, n_2\ell_2; L > + \gamma_2 < n\ell, N+2\mathcal{L}; L | n_1\ell_1, n_2\ell_2; L > =$$
$$\gamma_3 < n+1\ell, N\mathcal{L}; L | n_1-1\ell_1, n_2\ell_2; L > + \gamma_4 < n+1\ell, N\mathcal{L}; L | n_1\ell_1, n_2-1\ell_2; L > +$$
$$\gamma_5 < n\ell, N+1\mathcal{L}; L | n_1-1\ell_1, n_2\ell_2; L > + \gamma_6 < n\ell, N+1\mathcal{L}; L | n_1\ell_1, n_2-1\ell_2; L > \qquad \text{(D-11)}$$

where

$$\beta_1 = [(n_1+1)(n_1+\ell_1+3/2)(n_1+2)(n_1+\ell_1+5/2)]^{\frac{1}{2}}$$
$$\beta_2 = -[(n_2+1)(n_2+\ell_2+3/2)(n_2+2)(n_2+\ell_2+5/2)]^{\frac{1}{2}}$$
$$\beta_3 = [n(n+\ell+\tfrac{1}{2})(n_1+1)(n_1+\ell_1+3/2)]^{\frac{1}{2}}$$
$$\beta_4 = [N(N+\mathcal{L}+\tfrac{1}{2})(n_1+1)(n_1+\ell_1+3/2)]^{\frac{1}{2}}$$
$$\beta_5 = -[n(n+\ell+\tfrac{1}{2})(n_2+1)(n_2+\ell_2+3/2)]^{\frac{1}{2}}$$
$$\beta_6 = -[N(N+\mathcal{L}+\tfrac{1}{2})(n_2+1)(n_2+\ell_2+3/2)]^{\frac{1}{2}} \qquad \text{(D-12)}$$

and

$$\gamma_1 = [(n+1)(n+\ell+3/2)(n+2)(n+\ell+5/2)]^{\frac{1}{2}}$$
$$\gamma_2 = -[(N+1)(N+\mathcal{L}+3/2)(N+2)(N+\mathcal{L}+5/2)]^{\frac{1}{2}}$$
$$\gamma_3 = [(n+1)(n+\ell+3/2)n_1(n_1+\ell_1+\tfrac{1}{2})]^{\frac{1}{2}}$$
$$\gamma_4 = [(n+1)(n+\ell+3/2)n_2(n_2+\ell_2+\tfrac{1}{2})]^{\frac{1}{2}}$$
$$\gamma_5 = -[(N+1)(N+\mathcal{L}+3/2)n_1(n_1+\ell_1+\tfrac{1}{2})]^{\frac{1}{2}}$$
$$\gamma_6 = -[(N+1)(N+\mathcal{L}+3/2)n_2(n_2+\ell_2+\tfrac{1}{2})]^{\frac{1}{2}} . \qquad \text{(D-13)}$$

The same method can be used to obtain relations for the unequal mass transformation brackets.[139]

The preceding relations give useful results for special cases:

$n_1=0,\ n_2=0$

$$[(n+1)(n+\ell+3/2)]^{\frac{1}{2}} < n+1\ell, N\mathcal{L}; L|0\ell_1, 0\ell_2; L > =$$
$$-[(N+1)(N+\mathcal{L}+3/2) < n\ell, N+1\mathcal{L}; L|0\ell_1, 0\ell_2; L > \qquad \text{(D-14)}$$

$$\gamma_1 < n+2\ell, N\mathcal{L}; L|0\ell_1, 0\ell_2; L > = -\gamma_2 < n\ell, N+2\mathcal{L}; L|0\ell_1, 0\ell_2; L > \qquad \text{(D-15)}$$

$n=0, N=0$

$$[(n_1+1)(n_1+\ell_1+3/2)]^{\frac{1}{2}} < 0\ell, 0\mathcal{L}; L|n_1+1\ell_1, n_2\ell_2; L > =$$
$$-[(n_2+1)(n_2+\ell_2+3/2)]^{\frac{1}{2}} < 0\ell, 0\mathcal{L}; L|n_1\ell_1, n_2+1\ell_2; L > \qquad \text{(D-16)}$$

$$\beta_1 < 0\ell, 0\mathcal{L}: 1|n_1+2\ell_1, n_2\ell_2; L > = -\beta_2 < 0\ell, 0\mathcal{L}; L|n_1\ell_1, n_2+2\ell_2; L > \qquad \text{(D-17)}$$

$(\mathcal{L}-L)$ is even

$$2[(n_1+1)(n_1+\ell_1+3/2)]^{\frac{1}{2}} < n\ell_1, N\mathcal{L}; L|n_1+1\ell_1, n_1\ell_1; L > =$$
$$[n(n+\ell+\tfrac{1}{2})]^{\frac{1}{2}} < n-1\ell, N\mathcal{L}; L|n_1\ell_1, n_1\ell_1; L > +$$
$$[N(N+\mathcal{L}+\tfrac{1}{2})]^{\frac{1}{2}} < n\ell, N-1\mathcal{L}; L|n_1\ell_1, n_1\ell_1; L > \qquad \text{(D-18)}$$

$(\mathcal{L}-L)$ is odd

$$[(n_1+2)(n_1+\ell_1+5/2)]^{\frac{1}{2}} < n\ell, N\mathcal{L}; L|n_1+2\ell_1, n_1\ell_1; L > =$$
$$[n(n+\ell+\tfrac{1}{2})]^{\frac{1}{2}} < n-1\ell, N\mathcal{L}; L|n_1+1\ell_1, n_1\ell_1; L > +$$
$$[N(N+\mathcal{L}+\tfrac{1}{2})]^{\frac{1}{2}} < n\ell, N-1\mathcal{L}; L|n_1+1\ell_1, n_1\ell_1; L > \qquad \text{(D-19)}$$

$(\ell_1$-L) is even

$$2[(n+1)(n+\ell+3/2)]^{\frac{1}{2}} < n+1\ell, n\ell; L | n_1\ell_1, n_2\ell_2; L > =$$
$$[n_1(n_1+\ell_1+\tfrac{1}{2})]^{\frac{1}{2}} < n\ell, n\ell; L | n_1-1\ell_1, n_2\ell_2; L > +$$
$$[n_2(n_2+\ell_2+\tfrac{1}{2})]^{\frac{1}{2}} < n\ell, n\ell; L | n_1\ell_1, n_2-1\ell_2; L > \qquad \text{(D-20)}$$

$(\ell_1$-L) is odd

$$[(n+2)(n+\ell+5/2)]^{\frac{1}{2}} < n+2\ell, n\ell; L | n_1\ell_1, n_2\ell_2; L > =$$
$$[n_1(n_1+\ell_1+\tfrac{1}{2})]^{\frac{1}{2}} < n+1\ell, n\ell; L | n_1-1\ell_1, n_2\ell_2; L > +$$
$$[n_2(n_2+\ell_2+\tfrac{1}{2})]^{\frac{1}{2}} < n+1\ell, n\ell; L | n_1\ell_1, n_2-1\ell_2; L > \qquad \text{(D-21)}$$

REFERENCES

1. M.G. Mayer and J.D. Jensen, Elementary Theory of Nuclear Structure (John Wiley and Sons, 1955).
2. A. de Shalit and I. Talmi, Nuclear Shell Theory (Academic Press New York, 1963).
3. A. Kallio and K. Kolltveit, Nucl. Phys. 53, 87 (1964).
4. T.T.S. Kuo and G.E. Brown, Nucl. Phys. 85, 40 (1966).
5. T.T.S. Kuo, Nucl. Phys. A103, 71 (1967).
6. F. Tabakin, Ann. Phys. (N.Y.) 30, 51 (1964).
7. M. Baranger, Lectures given at the International School of Physics Enrico Fermi, Varenna, 1967.
8. R.D. Woods and D.S. Saxon, Phys. Rev. 95, 577 (1954).
9. A.A. Ross, H. Mark and R.D. Lawson, Phys. Rev. 102, 1613 (1956).
10. B.H. Flowers and D. Wilmore, Proc. Roy. Soc. 83, 683 (1964).
11. A.P. Stamp and D.F. Mayers, Nucl. Phys. 82, 296 (1966).
12. S. Kahana and E. Tomusiak, Nucl. Phys. 71, 402 (1965).
13. E. Tomusiak, Ph.D. Thesis, McGill University (1964).
14. H.C. Lee, M.Sc. Thesis McGill University (1967).
15. C.K. Scott, M.Sc. Thesis McGill University (1967).
16. S. Kahana, Nuclear and Particle Physics, ed. B. Margolis and C.S. Lam (W.A. Benjamin, Inc. 1968).
17. H.C. Lee, Ph.D. Thesis, McGill University (1968).
18. D.J. Thouless, Report on Progress in Physics XXVII 53 (1964).
19. K.A. Brueckner, The Many Body Problem, ed. C. DeWitt (Dunod, 1959).

REFERENCES

20. G.E. Brown, Unified Theory of Nuclear Models and Forces (North-Holland Publishing Company, 1967).

21. D.J. Thouless, Nucl. Phys. 22, 78 (1961).

22. H.A. Bethe, B.H. Brandow and A.G. Petschek, Phys. Rev. 129, 225 (1963).

23. J.P. Elliott and B.H. Flowers, Proc. Phys. Soc. (London), A242, 57 (1957).

24. V. Gillet and N. Vinh Mau, Nucl. Phys. 54, 321 (1964); Erratum, 57, 698 (1964).

25. A. Kallio and A.M. Green, Nucl. Phys. 84, 161 (1966).

26. A.M. Green, A. Kallio and K. Kolltveit, Physics Letters 14, 142 (1965).

27. H.A. Mavromatis, W. Markiewicz and A.M. Green, Nucl. Phys. A90, 101 (1967).

28. B.L. Scott and S.A. Moszkowski, Nucl. Phys. 29, 665 (1962).

29. T. Hamada and I.D. Johnston, Nucl. Phys. 34, 382 (1962).

30. A.M. Green, Report on Progress in Physics XXVIII 113 (1965).

31. G.E. Brown and A.M. Green, Physics Letters 15, 168 (1965).

32. A.P. Zuker, B. Buck and J.B. McGrory, Phys. Rev. Letters 21, 39 (1968).

33. R.K. Bhaduri and E.L. Tomusiak, Proc. Phys. Soc. 86, 451 (1965).

34. E.K. Warburton, Isobaric Spin in Nuclear Physics, ed. J.D. Fox and D. Robson (Academic Press, 1966).

35. E. Hayward, Nuclear Structure and Electromagnetic Interactions, ed. N. MacDonald (Plenum Press, N.Y. 1965).

36. J. Da Providencia and C.M. Shakin, Nucl. Phys. A108, 609 (1968).

REFERENCES

37. T. Deforest Jr., J.D. Walecka, G. Vanpraet and W.C. Barber, Physics Letters 16, 311 (1965).

38. T.E. Drake, R.M. Hutcheon, V. Stobie, G.A. Beer and H.S. Caplan, Phys. Rev. 163, 947 (1967).

39. S.J. Skorka, J. Hertel and T.W. Retz-Schmidt, Nuclear Data A, 2, No. 4 November, 1966).

40. R.D. Gill, O. Hausser, J.S. Lopes and H.J. Rose, Nucl. Phys. A98, 129 (1967).

41. D. Hasselgren, P.U. Renberg, O. Sundberg and G. Tibell, Nucl. Phys. 69, 81 (1965).

42. T.A. Tombrello, Physics Letters 23, 134 (1966).

43. J.A. Nolen, Jr., J.P. Shiffer, N. Williams and D. Von Ehrenstein, Phys. Rev. Letters 18, 1140 (1967).

44. L.R.B. Elton, Nuclear Sizes (Oxford, 1961).

45. L.R.B. Elton and A. Swift, Nucl. Phys. A94, 52 (1967).

46. L.R.B. Elton, Phys. Rev. 158, 970 (1967).

47. F.G. Perey and J.P. Schiffer, Phys. Rev. Letters 17, 324 (1966).

48. E.M. Henley, Isobaric Spin in Nuclear Physics ed. J.D. Fox and D. Robson (Academix Press, 1966).

49. D. Robson, Ann. Rev. Nucl. Sci. Vol. 16, 119 (1966)

50. D.H. Wilkinson, Isobaric Spin in Nuclear Physics, ed. J.D. Fox and D. Robson (Academic Press, 1966).

51. W.M. MacDonald, ibid.

REFERENCES

52. I.M. Naquib and L.L. Green, Nucl. Phys. A112, 76 (1968).

53. A.P. Shukla, Ph.D. Thesis, Princeton University (1967); Technical Report PUC-937-262.

54. D.H. Youngblood, B.H. Wildenthal and C.M. Class, Phys. Rev. 169, 859 (1968).

55. R. Bock, H.H. Duhm and R. Stock, Physics Letters 18, 61 (1965).

56. T.A. Belote, A. Sperduto and W.W. Buechner, Phys. Rev. 139, B80 (1965).

57. S. Hinds and R. Middleton, Nucl. Phys. 84, 651 (1966).

58. R.L. Kozub, Phys. Rev. 172, 1078 (1968).

59. P.M. Endt and C. Van der Leun, Nucl. Phys. A105, 1 (1967).

60. G. Muehllehner, A.S. Poltorak, W.C. Parkinson and R.H. Bassel, Phys. Rev. 159, 1039 (1967).

61. R. Woods, P.D. Barnes, E.R. Flynn and G.J. Igo, Phys. Rev. Letters 19, 453 (1967).

62. B.H. Wildenthal, B.M. Preedom, E. Newman and M.R. Cates, Phys. Rev. Letters 19, 960 (1967).

63. J.S. Lilley and N. Stein, Phys. Rev. Letters 19, 709 (1967).

64. J. Bardwick and R. Tickle, Phys. Rev. 171, 1305 (1968).

65. S. Hinds, R. Middleton, J.H. Bjerregaard, O. Hansen and O. Nathan, Nucl. Phys. 83, 17 (1967).

66. J.D. Anderson, C. Wong and J.W. McClure, Phys. Rev. 138, B615 (1965).

67. R.G. Thomas, Phys. Rev. 81, 148 (1951).

68. S.B. Ehrman, Phys. Rev. 81, 412 (1951).

REFERENCES

69. M. Harchol, A.A. Jaffe, J. Miron, I. Unna and J. Zioni, Nucl. Phys. A90, 459 (1966).

70. P.C. Sood and A.E.S. Green, Nucl. Phys. 5, 274 (1958).

71. J.A. Nolen, Jr., J.P. Schiffer and N. Williams, Physics Letters 27B, 1 (1968).

72. B.C. Carlson and I. Talmi, Phys. Rev. 96, 436 (1954).

73. E.H. Auerbach, Preprint BNL 6562.

74. K.A. Brueckner, J.L. Gammel and H. Weitzner, Phys. Rev. 110, 431 (1958).

75. D.H. Wilkinson and M.E. Mafethe, Nucl. Phys. 85, 97 (1966).

76. D.H. Wilkinson, Nucl. Phys. 85, 114 (1966).

77. L.A. Sliv and B.A. Volchok, Journ. Exp. Theor. Phys. 36, 539 (1959).

78. A. Schoeder, Nuovo Cimento 7, 460 (1958).

79. J. Blomqvist and S. Wahlborn, Ark. f. Fys. 16, 545 (1960).

80. A. Sobiczewski, F.A. Gareev and B.N. Kalinkin, Physics Letters 22, 500 (1966).

81. V.L. Korotkikh, V.M. Moskovkin and N.P. Yudin, Bull. Acad. Sci. USSR, Phys. Ser. 30, 324 (1966).

82. E. Rost, Physics Letters 26B, 184 (1968).

83. D.J. Bredin, O. Hansen, G. Lentz and G.M. Temmer, Physics Letters 21, 677 (1966).

84. G.W. Greenless, G.J. Pyle and Y.C. Tang, Phys. Rev. 171, 1115 (1968).

85. G.E. Brown, J.H. Gunn and P. Gould, Nucl. Phys. 46, 598 (1963).

86. A.M. Lane, Rev. Mod. Phys. 29, 193 (1957).

REFERENCES

87. G.R. Satchler, Phys. Rev. 109, 429 (1958).

88. A.E.S. Green and P.C. Sood, Phys. Rev. 111, 1147 (1958).

89. A.M. Lane, Phys. Rev. Letters 8, 161 (1962).

90. A.M. Lane, Nucl. Phys. 35, 676 (1962).

91. A.M. Lane and J.M. Soper, Nucl. Phys. 37, 506 (1962).

92. S.A.A. Zaidi and S. Darmodjo, Phys. Rev. Letters 19, 1446 (1967).

93. T. Terasawa and G.R. Satchler, Physics Letters 7, 265 (1963).

94. J.N. Ginocchio and J. Weneser, Phys. Rev. 170, 859 (1968).

95. A. Swift and L.R.B. Elton, Phys. Rev. Letters 17, 484 (1966).

96. G.F. Bertsch and T.T.S. Kuo, Nucl. Phys. A112, 204 (1968).

97. C. Glashausser, B.G. Harvey, D.L. Hendrie and J. Mahoney, Phys. Rev. Letters 21, 918 (1968).

98. C.W. Wong and C-Y. Wong, Nucl. Phys. A91, 433 (1967).

99. G.J. Igo, private communication.

100. J.H.E. Mattauch, W. Thiele and A.H. Wapstra, Nucl. Phys. 67, 1 (1965).

101. N.F. Mangelson, B.G. Harvey and N.K. Glendenning, Nucl. Phys. A117, 161 (1968).

102. J.S. Lopes, O. Huasser, R. D. Gill and H.J. Rose, Nucl. Phys. 89, 127 (1966).

103. F.D. Lee, R.W. Krone and F.W. Prosser, Jr., Nucl. Phys. A96, 209 (1967).

104. R. Moreh, Nucl. Phys. A97, 106 (1967).

105. J.W. Olness and E.K. Warburton, Phys. Rev. 156, 1145 (1967).

106. G.E. Brown, Compt. Rend. Intern. Phys. Nucl. Vol. 1, 129 (1964).

REFERENCES

107. P. Federman and I. Talmi, Physics Letters 15,165 (1965).

108. P. Federman and I. Talmi, Physics Letters 19,490 (1965).

109. H.G. Benson and I. Irvine, Proc. Phys. Soc. 89,249 (1966).

110. P. Federman, Nucl. Phys. A95, 443 (1967).

111. T. Engeland, Nucl. Phys. 72, 68 (1965).

112. S. Shlomo and R. Moreh, Nucl. Phys. A110, 204 (1968).

113. G.E. Brown and A.M. Green, Nucl. Phys. 85,87 (1966).

114. G.H. Fuller and V.W. Cohen, Nuclear Moments, Appendix 1 to Nuclear Data Sheets (1965).

115. R.E. Seamon, K.A. Friedman, G. Breit, R.D. Haracz, J.M. Holt, and A. Prakash, Phys. Rev. 165, 1579 (1968).

116. J.H. Bjerregaard, O. Hansen, O. Nathan, R. Chapman, S. Hinds and R. Middleton, Nucl. Phys. A103, 33 (1967).

117. F. Puehlhoffer, Nucl. Phys. A116, 516 (1968).

118. W.W. True, Phys. Rev. 168, 1388 (1968).

119. C. Riedel, R.A. Broglia and A. Miranda, Nucl. Phys. A113, 503 (1968).

120. P. Federman and I. Talmi, Physics Letters 22, 469 (1966).

121. G.F. Bertsch, Nucl. Phys. 89, 673 (1966).

122. W.J. Gerace and A.M. Green, Nucl. Phys. 93, 110 (1967).

123. B.H. Flowers and L.D. Skouras, Nucl. Phys. A116, 529 (1968).

124. D.M. Clement and E.U. Baranger, Nucl. Phys. 89, 145 (1966).

125. G.F. Bertsch, Nucl. Phys. 74, 234 (1965).

126. G.E. Brown and T.T.S. Kuo, Nucl. Phys. A92, 481 (1967).

127. N. de Takacsy, Can. Journ. Phys. (To be published).

REFERENCES

128. J.M. Kennedy and M.J. Cliff, Transformation Coefficients between LS and jj Coupling CRT-609 (Atomic Energy of Canada, Ltd. AECL No. 224).

129. M. Moshinsky, Nucl. Phys. 13, 104 (1959); T.A. Brody and M. Moshinsky, Tables of Transformation Brackets (Monografias del Instituto de Fisica, Mexico, 1960).

130. D.M. Brink and G.R. Satchler, Angular Momentum (Oxford, 1962).

131. M.A. Preston, Physics of the Nucleus, (Addison-Wesley Publishing Co., 1962).

132. I. Talmi, Helv. Physica Acta 25, 185 (1952).

133. T.A. Brody, G. Jacob and M. Moshinsky, Nucl. Phys. 17,16 (1960).

134. M. Baranger and K.T.R. Davies, Nucl. Phys. 79, 403 (1966).

135. K.W. Ford and E.J. Konopinski, Nucl. Phys. 9, 218 (1958).

136. H. Horie and K. Saski, Prog. Theor. Phys. 25, 475 (1961).

137. A. Erdelyi, W. Magnus, F. Oberhettinger and F.G. Tricomi, Higher Transcendental Functions Vol. 2 (McGraw-Hill, 1954).

138. S.G. Nilsson, Kgl. Danske, Videnskab, Selskab, Mat. Fys. Medd. 29, No. 16 (1955).

139. Yu.F. Smirnov, Nucl. Phys. 27, 177 (1961).